UNITED NATIONS EDUCATIONAL, SCIENTIFIC AND CULTURAL ORGANIZATION
INTERNATIONAL ATOMIC ENERGY AGENCY
INTERNATIONAL CENTRE FOR THEORETICAL PHYSICS
I.C.T.P., P.O. BOX 586, 34100 TRIESTE, ITALY, CABLE: CENTRATOM TRIESTE

H4.SMR/1058-2

WINTER COLLEGE ON OPTICS

9 - 27 February 1998

Solitons in Optical Fibres and Ultra Long Distance Transmission

Lecture 1: The Nonlinear Schrödinger Equation and the Soliton

Lecture 2: Rate Limiting of Amplifier Spontaneous Emission and Amelioration with "Guiding" Filters

Lecture 3: Wavelength Division Multiplexing

L. F. Mollenauer

Bell Labs, Holmdel, USA

Chapter 12 Solitons in High Bit-Rate, Long-Distance Transmission

L. F. Mollenauer
J. P. Gordon
P. V. Mamyshev

Lucent Technologies, Bell Laboratories, Holmdel, New Jersey

1. Introduction

In the development of the long-distance transmission technologies made possible by the invention of the erbium fiber amplifier, there have been two very different philosophies on how best to deal with the effects of fiber nonlinearity. The first one attempts, by various means, such as the use of special dispersion maps, and by holding signal intensities to the lowest possible level, to make nonlinear penalties acceptably small. The result is the non-return-to-zero (NRZ) transmission mode reported in Chapters 8, 9, and 10 of Volume IIIA. The second philosophy, by contrast, embraces the fiber's nonlinearity and attempts to extract the maximum possible benefits from it. It is this second approach, based on the uniquely stable and nondispersive pulse known as the *soliton*, that is the proper subject of this chapter.

Soliton transmission makes positive use of the fiber's nonlinearity in a number of ways: First, as is well known, the soliton owes its existence to the fiber nonlinearity. That is, as we shall detail shortly, for the soliton, the effects of the nonlinearity more or less continuously cancel the usual pulse-broadening effect of chromatic dispersion. Second, it makes use of the fact that solitons can regenerate themselves, from the nonlinear effect, while traversing a transmission line containing narrow band optical filters, even when the peaks of such guiding filters gradually shift frequency with distance along the line. That amenability to passive regeneration, again unique to solitons, enables a great reduction of the error-producing effects of noise

and a further stabilization of the transmission. Third, it makes use of the nearly perfect transparency of solitons to one another in the collisions that occur between pulses of different channels in wavelength-division multiplexing (WDM). Fourth, the interaction between the guiding filters and the fiber nonlinearity engenders a powerful, automatic regulation of the relative signal strengths among the various channels in WDM. Fifth, with solitons, the fiber nonlinearity effectively counteracts the dispersive effects, or polarization mode dispersion, of the residual birefringence of the fiber.

Thus, it should come as no surprise that solitons are the undisputed long-distance champions for both single-channel (Fig. 12.1) and WDM transmission (Fig. 12.2), or that certain modes, such as single-channel rates greater than 10 Gb/s or massive WDM at a per-channel rate of 10 Gb/s, are their exclusive domains.

Beyond this leadership in sheer performance, however, soliton transmission has certain other properties that make it highly attractive. For example, in contrast to NRZ, which tends to require lumped dispersion compensation specific to each distance and each wavelength, the continuous dispersion compensation of soliton transmission renders the data immediately readable and/or injectable at any node of a network. The extreme return-to-zero (RZ) format of the soliton transmission further enhances this compatibility with networking, because it enables all-optical manipulation of the data, with attendant high speed, simplicity, convenience, and low cost.

Finally, as we shall attempt to show, the basic physics of solition transmission is straightforward, highly predictable, and easy to understand. One

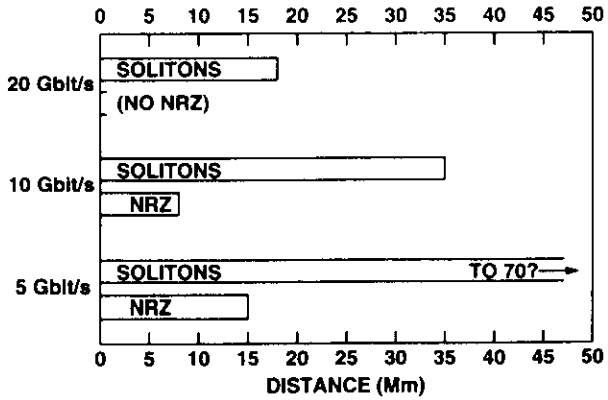

Fig. 12.1 Achieved error-free distances in a single channel, for soliton transmission using sliding frequency guiding filters and for the non-return-to-zero (NRZ) mode.

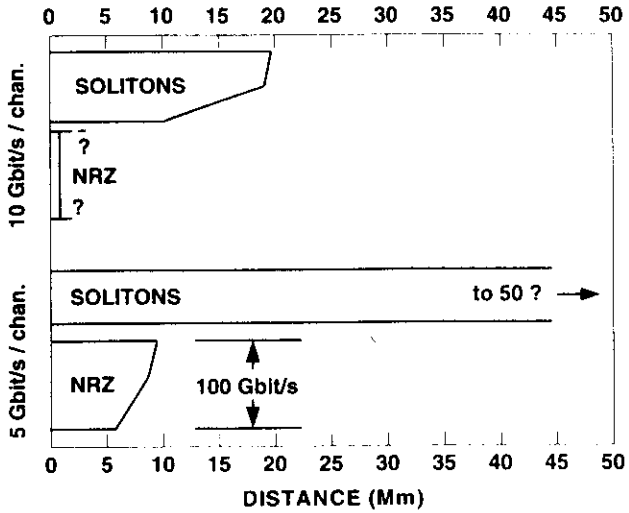

Fig. 12.2 Achieved error-free distances in massive wavelength-division multiplexing (WDM), for solitons and for NRZ. The vertical width of each band is directly proportional to the total achieved capacity in gigabits per second.

consequence of this understanding and ease of analysis is that optimum system designs can be quickly established, and their performance reliably predicted, with a minimum of time-consuming numerical simulation. In this age of rapidly shifting expectations and demands, that is no small advantage.

2. Pulse Propagation and Solitons in Optical Fibers: A Tutorial

2.1 APOLOGIA

This section constitutes a brief tutorial on the theory of pulse propagation in optical fibers. In it, we discuss the fundamental dispersive and nonlinear properties of fiber, and from these we derive the fundamental propagation equation (the nonlinear Schrödinger equation). We then discuss not only the origin and fundamental properties of the soliton, but also other closely related issues such as soliton units and path-average solitons. Because the material in this section is fundamental to all that follows, a careful reading is urged, unless one is already thoroughly familiar with the concepts.

2.2 DISPERSION RELATIONS AND RELATED VELOCITIES

If weak monochromatic light at some angular frequency ω enters a fiber, the wavelength λ_{fiber} of the resulting lightwave in the fiber is determined by the refractive index of the fiber and to a lesser extent by its guiding properties. The phase ϕ of the lightwave has the form $\phi(z, t) = kz - \omega t$, where the wave number k is equal to $2\pi/\lambda_{fiber}$, and z is the distance along the fiber. Central to the problem of lightwave propagation in the fiber is the dependence of the wave number on the frequency. This is the dispersion relation $k = k(\omega)$. For plane waves in vacuum, it is simply $k = \omega/c$. For plane waves in an isotropic transparent medium, it is $k = n\omega/c$, where n is the refractive index at frequency ω. For a single-mode transmission line consisting of a fiber core and cladding, we can also use the same form, $k = n\omega/c$, with the caveat that n now has an effective value intermediate between the values for core and cladding, depending on the transverse mode shape.

An observer moving with velocity $v = dz/dt$ will observe the phase ϕ to change with time according to

$$\frac{d\phi(z, t)}{dt} = kv - \omega. \tag{2.1}$$

If we require the phase to be constant in Eq. (2.1), the needed velocity is $v = \omega/k$. This is the velocity with which any point of constant phase on the wave travels down the fiber. It is called the phase velocity v_p, and its value is just c/n. If we add a second wave at a slightly different frequency, the combined wave will be modulated, with greater amplitude where the two frequency components are in phase and add, and lesser where they are out of phase and subtract. To follow the modulation envelope, our observer must travel at a velocity such that the rate of change of the phase difference between the two waves is zero. From Eq. (2.1) we thus require $k_1 v - \omega_1 = k_2 v - \omega_2$, where the indices 1 and 2 refer to the two waves. The required velocity is $v = (\omega_1 - \omega_2)/(k_1 - k_2)$. The group velocity $v_g(\omega)$ is this velocity in the limit of a small-frequency difference. It satisfies

$$v_g^{-1}(\omega) = \frac{dk}{d\omega}. \tag{2.2}$$

The phase and group velocities usually differ, hence one will generally observe the phase moving with respect to the envelope of a modulated wave. Finally, consider a pulse having a continuous band of frequency components. Such a pulse is most highly peaked if all of its frequency components have the same phase at some common time and place. The pulse envelope will tend to move with its average group velocity, but if the group velocity varies with frequency — i.e., there is some group velocity dispersion — then the pulse will spread as it propagates, becoming chirped as its various frequency components separate in time. We shall see this behavior in more detail later.

In dealing with lightwave propagation in fibers, it is natural to observe the wave as a function of time at various locations along the fiber. To record the progress of a pulse, we therefore plot power versus t for a succession of values of z. In order to keep the pulse in sight, one's time window must be moved as z is varied. However, we can easily manage this movement. A pulse traveling with the group velocity v_g will appear to be stationary in a retarded time frame t' such that $t' = t - v_g^{-1}z$. This is a standard trick used to simplify the analysis.

2.3 FIBER NONLINEARITY

The induced polarization in a nonlinear dielectric takes the form

$$\mathbf{P} = \varepsilon_0[\chi^{(1)} \cdot \mathbf{E} + \chi^{(2)} : \mathbf{EE} + \chi^{(3)} \cdot \mathbf{EEE} + \cdots],$$

where $\mathbf{P}$ and $\mathbf{E}$ are the polarization and electric field vectors, respectively, and the susceptibilities $\chi^{(n)}$ are nth rank tensors. Because the glass of optical fibers is isotropic, one has simply $\chi^{(1)} = n^2 - 1$, where n is the index of refraction, while $\chi^{(2)} = 0$. The effects of $\chi^{(3)}$ of interest here are nonlinear refraction and four-wave mixing. Raman scattering becomes important for shorter pulses than we consider here; third harmonic generation is negligibly small.

In silica glass fibers, because of their isotropy, and because of the relatively small value of $\chi^{(3)}$, the index can be written with great accuracy as

$$n(\omega, |\mathbf{E}|^2) = n(\omega) + n_2|\mathbf{E}|^2, \tag{2.3}$$

where n_2 is related to $\chi^{(3)}$ by

$$n_2 = \frac{3}{8n}\chi^{(3)}_{xxxx}, \tag{2.4}$$

where $\chi^{(3)}_{xxxx}$ is a scalar component of $\chi^{(3)}$, appropriate to whatever polarization state the light may have at the moment.

Even the highest quality transmission fibers are mildly birefringent, however, so that the polarization states of the light tend to change significantly

on a scale of no more than a few meters. In contrast, the nonlinear effects of interest in long-distance transmission tend to require many kilometers of path for their development. Thus, in general, with optical fibers we are usually interested only in n_2 as suitably averaged over all possible polarization states. In silica glass fibers, if we write the nonlinear index as $n_2 I$, where I is the intensity in W/cm^2, then the lastest measurements of n_2 yield such a polarization-averaged value of about 2.6×10^{-16} cm^2/W.

2.4 FUNDAMENTAL PROPAGATION EQUATION

2.4.1 Derivation

We now consider lightwave propagation in a fiber that has both group velocity dispersion and index nonlinearity. Let the lightwave in the line be represented by a scalar function $U(z, t)$ proportional to the complex field amplitude, such that the power P in the line is given by

$$P = P_c|U|^2. \tag{2.5}$$

The proportionality constant P_c can be considered as a power unit. For frequencies near some central frequency ω_0, the generic dispersion relation $k = n\omega/c$ can be expanded to the approximate form

$$k = k_0 + k'(\omega - \omega_0) + \tfrac{1}{2}k''(\omega - \omega_0)^2 + k_2 P, \tag{2.6}$$

where we have used Eq. (2.3). This equation has the form of a Taylor series expansion of $k(\omega, P)$ in the neighborhood of $(\omega_0, 0)$. It adequately describes the propagation of monochromatic waves $U = u_0 \exp(ikz - i\omega t)$ in the line so long as the frequency does not stray too far from ω_0. It leads directly to the nonlinear Schrödinger (NLS) equation. For solitons in fibers, the last two terms of Eq. (2.6) are of comparable importance; k_2 is positive, k'' is negative, and succeeding higher order terms (e.g., $k'''[\omega - \omega_0]^3$, $k_2'[\omega - \omega_0]P$, etc.) can be neglected or adequately treated as perturbations. For the moment, we assume that the line has no loss or gain — i.e., that the constants k_0, k', k'', and k_2 are all real.

The expression for the reciprocal group velocity, namely,

$$v_g^{-1} = \frac{\partial k}{\partial \omega} = k' + k''(\omega - \omega_0), \tag{2.7}$$

identifies k' as the reciprocal group velocity at frequency ω_0 and k'' as its frequency dispersion constant. The dispersion parameter D used widely to

describe fibers is the wavelength derivative of v_g^{-1}, and so is related to k'' or the refractive index by

$$D = \frac{d}{d\lambda}(v_g^{-1}) = -\frac{2\pi c}{\lambda^2}k'' = -\frac{\lambda}{c}\frac{d^2 n}{d\lambda^2}. \tag{2.7a}$$

The term $k_2 P$ in Eq. (2.6) represents the primary nonlinear effect, self-phase modulation, resulting from the intensity dependence of the refractive index of the fiber. Note from Eq. (2.7) that the dependence of the group velocity on power is among the higher order terms not included in Eq. (2.6).

If we now remove the central frequency and wave number from U by defining

$$u(z, t) = Ue^{i(\omega_0 t - k_0 z)} \tag{2.8}$$

so that when U is written out explicitly, $u(z, t)$ becomes

$$u(z, t) = u_0 e^{i[(k - k_0)z - (\omega - \omega_0)t]}, \tag{2.8a}$$

then the wave equation for u that is necessary and sufficient to reproduce exactly our initial dispersion relation (Eq. [2.6]) is

$$-i\frac{\partial u}{\partial z} = ik'\frac{\partial u}{\partial t} - \frac{1}{2}k''\frac{\partial^2 u}{\partial t^2} + k_2 P_c|u|^2 u. \tag{2.9}$$

This can be shown by inserting Eq. (2.8a) in Eq. (2.9).

The standard form of the propagation equation is generated from Eq. (2.9) by transforming to the retarded time frame (this eliminates the k' term) and by choosing unit values of time and distance such that $k'' = -1$ and $k_2 = 1$ when measured in those units, and the power unit already mentioned. The appropriate new variables are

$$\begin{aligned} t' &= (t - k'z)/t_c \\ z' &= z/z_c, \end{aligned} \tag{2.10}$$

where the unit values t_c, z_c, and P_c satisfy the relations

$$\begin{aligned} t_c^2/z_c &= -k'' = \lambda^2 D/(2\pi c) \\ z_c P_c &= 1/k_2. \end{aligned} \tag{2.11}$$

The resulting propagation equation (after we drop the primes on z and t) is the NLS equation

$$-i\frac{\partial u}{\partial z} = \frac{1}{2}\frac{\partial^2 u}{\partial t^2} + |u|^2 u. \tag{2.12}$$

Clearly, the first term on the right-hand side of Eq. (2.12) is the dispersive term, whereas the second term is the nonlinear one.

As its name suggests, Eq. (2.12) has a form similar to the well-known Schrödinger equation of quantum mechanics. Here, of course, it is based instead on Maxwell's classical field equations.

There is an important arbitrariness left in the definitions of the three unit values z_c, t_c, and P_c, because there are only two relations (Eq. [2.11]) that they must satisfy. One unit value may be chosen freely, and thus different real-world fields can be represented by the same solution of Eq. (2.12), and vice versa. In particular, if one solution of Eq. (2.12) is $u(t, z)$, then different scalings of the same real-world field give other solutions of the form $Au(At, A^2z)$, where A is the ratio of the values of t_c. This scaling transformation of the solutions of Eq. (2.12) can be verified by direct substitution.

Broadband gain and/or loss can be accommodated by adding a third term, $-i(\alpha/2)u$, to the right side of Eq. (2.12), where α is the coefficient of energy gain per z_c (negative values of α represent loss). In that case, Eq. (2.12) becomes

$$-i\frac{\partial u}{\partial z} = \frac{1}{2}\frac{\partial^2 u}{\partial t^2} + |u|^2 u - i(\alpha/2)u. \tag{2.12a}$$

2.4.2 Soliton Units

Equation (2.12) is often referred to as a *dimensionless* form of the NLS equation. It is more useful to think of it as having specific dimensions, with z, for example, being a distance always measured in units of z_c rather than in meters or kilometers or any other standard unit. Thus, $z = 2$ means a distance of 2 times z_c. Similarly, t_c and P_c become the units of time and power, respectively. Because here we are primarily interested in solitons, it is convenient to tie these three units (which so far are very general in meaning) to the specific requirements of solitons. The canonical single-soliton solution of the NLS equation, Eq. (2.12), is

$$u(z, t) = \operatorname{sech}(t)\exp(iz/2). \tag{2.13}$$

This soliton has a full width at half maximum (FWHM) power of $\Delta t = 2\cosh^{-1}\sqrt{2} = 1.7627\ldots$. In order for this form to represent some soliton whose FWHM power is τ (in picoseconds, for example), we need simply to take

$$t_c = \frac{\tau}{1.7627\ldots}. \tag{2.14}$$

The unit distance, z_c, is a characteristic length for effects of the dispersive term and is given by

$$z_c = \frac{1}{(1.7627\ldots)^2}\frac{2\pi c}{\lambda^2}\frac{\tau^2}{D}, \tag{2.15}$$

where c and λ are the light velocity and wavelength in vacuum, respectively, and where D is the dispersion constant, as already described (in Section 2.4). (D is often expressed as picoseconds of change in transit time, per nanometer change in wavelength, per kilometer of fiber length. Also, note that $D > 0$ corresponds to anomalous dispersion.) When D is expressed in those units, τ in picoseconds, and for $\lambda = 1557$ nm (corresponding to the longer wavelength erbium amplifier gain peak), Eq. (2.15) becomes

$$z_c \approx 0.25\ \tau^2/D, \tag{2.15a}$$

where z_c is in kilometers. Note that for the pulse widths ($\tau \sim 15$–50 ps) and dispersion parameters ($D \sim 0.3$–1 ps/nm-km) most desirable for long-distance soliton transmission, z_c is hundreds of kilometers. Finally, the unit of power, P_c, is just the soliton peak power, and is given by the formula

$$P_c = \frac{A_{eff}}{2\pi n_2}\frac{\lambda}{z_c} = \left(\frac{1.7627\ldots}{2\pi}\right)^2 \frac{A_{eff}\lambda^3}{n_2 c}\frac{D}{\tau^2}, \tag{2.16}$$

where A_{eff} is the effective area of the fiber core, and where n_2, the nonlinear coefficient, has the polarization-averaged value already cited (see Section 2.3). Thus, for $A_{eff} \sim 50\ \mu m^2$ and $\lambda = 1557$ nm, one has $P_c \approx 0.476/z_c$, where P_c is in watts, and z_c is in kilometers. Note that for a z_c of hundreds of kilometers, the peak soliton power is just a few milliwatts.

2.4.3 Pulse Motion in the Retarded Time Frame

Another important transformation of the solutions of Eq. (2.12) is that produced by a carrier frequency shift. Because the inverse group velocity dispersion constant has the value -1 in the soliton unit system, a frequency shift produces an inverse group velocity shift of equal magnitude. Thus, for the same solution $u(t, z)$ as mentioned previously, one finds yet other solutions, frequency shifted by Ω (in units of t_c^{-1}), of the form

$$u(t + \Omega z, z)e^{-i(\Omega t + \Omega^2 z/2)}. \tag{2.17}$$

This transformation also applies to *any* solution of Eq. (2.12)

2.4.4 A Useful Property of Fourier Transforms

Shortly, we shall have need of the following simple relation between the Fourier transforms of $u(t)$ and those of its time derivatives. Let $u(t)$ and $\tilde{u}(\omega)$ be Fourier transforms of each other, i.e.,

$$u(t) = \frac{1}{\sqrt{2\pi}} \int_{-\infty}^{+\infty} \tilde{u}(\omega) e^{-i\omega t} d\omega. \tag{2.18}$$

We are using the tilde symbol to imply a function of frequency. Successive time differentiations of Eq. (2.18) show that $\partial u(t)/\partial t$ and $-i\omega\tilde{u}(\omega)$ are also Fourier transforms of each other, as are $\partial^2 u(t)/\partial t^2$ and $-\omega^2\tilde{u}(\omega)$, and so on.

2.4.5 Action of the Dispersive Term in the NLS Equation

To obtain the action of the dispersive term alone, we temporarily turn off the nonlinear term, so that Eq. (2.12) becomes

$$\frac{\partial u}{\partial z} = \frac{i}{2} \frac{\partial^2 u}{\partial t^2}. \tag{2.19}$$

The problem is most easily solved in the frequency domain. The Fourier transform of this last equation yields

$$\frac{\partial \tilde{u}}{\partial z} = -\frac{i}{2} \omega^2 \tilde{u}, \tag{2.20}$$

and its solution is

$$\tilde{u}(z, \omega) = \tilde{u}(0, \omega) e^{i\omega^2 z/2}. \tag{2.21}$$

From the form of this general solution, it should be clear that the dispersive term merely rearranges the phase relations among existing frequency components; it adds no new ones. To find how the dispersion affects a pulse, we must transform back to the time domain. An example that has an instructive analytic solution is the Gaussian pulse. Taking $u(0, t) = e^{-t^2/2}$, we have $\tilde{u}(0, \omega) = e^{-\omega^2/2}$, and upon turning the crank we get

$$u(z, t) = \frac{1}{\sqrt{1 + iz}} \exp\left(\frac{-t^2}{2(1 + z^2)} (1 - iz)\right). \tag{2.22}$$

In the near field ($z \ll 1$), the field gets some chirp but the pulse shape does not change (see Fig. 12.3). In the far field ($z^2 \gg 1$), the field approaches what can be shown to be a general relation for an initially narrow pulse

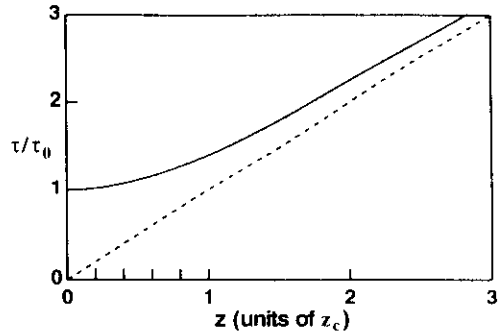

Fig. 12.3 Dispersive broadening of a Gaussian pulse with distance.

$$u(z \gg 1, t) \approx \frac{1}{\sqrt{iz}} \tilde{u}(0, \omega = -t/z) \exp\left(i \frac{t^2}{2z}\right), \tag{2.22a}$$

which shows how dispersion fans the field out into a spectrum of its various frequency components. As depicted in Fig. 12.3, the intensity envelope $|u|^2 \propto \exp(-t^2/(1 + z^2))$. Thus the pulse width grows as

$$\tau = \tau_0 \sqrt{1 + z^2}, \tag{2.23}$$

where τ_0 is the initial, minimum pulse width. We see that the change in τ is only to second order in z at the origin. This may also be seen directly from the differential equation, where we note that if $u(t)$ has a constant phase, then $\partial u/\partial z$ is everywhere in quadrature with u.

2.4.6 Action of the Nonlinear Term in the NLS Equation

To observe the action of the nonlinear term of Eq. (2.12) alone, we turn off the dispersive term, so the equation becomes simply

$$\frac{\partial u}{\partial z} = i|u|^2 u. \tag{2.24}$$

The problem is most naturally solved in the time domain, where the general solution is

$$u(z, t) = u(0, t) e^{i|u(0,t)|^2 z}. \tag{2.25}$$

The nonlinear term modifies $\phi(t)$, but not the intensity envelope. Thus, it adds only new frequency components. To get the spectral spreading, we must transform back to the frequency domain. Once again, for example, let $u(0, t) = e^{-t^2/2}$. In that case, one has

$$\tilde{u}(z, \omega) = \frac{1}{\sqrt{2\pi}} \int_{-\infty}^{\infty} u(0, t) e^{iz|u|^2} e^{i\omega t}\, dt$$

$$= \frac{1}{\sqrt{2\pi}} \int_{-\infty}^{\infty} e^{-t^2/2} e^{iz e^{-t^2}} e^{i\omega t}\, d\omega. \quad (2.26)$$

For $z \gg 1$, this integral produces a multipeaked spectrum, where the number of peaks and the overall spectral width increase directly with z (see Fig. 12.4). However, for $z \ll 1$, the integral is approximately

$$\frac{1}{\sqrt{2\pi}} \int_{-\infty}^{\infty} e^{-t^2/2}(1 + iz e^{-t^2}) e^{i\omega t}\, dt = \tilde{u}(0, \omega) + \frac{iz}{\sqrt{3}} \tilde{u}(0, \omega)^3. \quad (2.27)$$

Note that once again the new component is in quadrature with the original pulse, so the increase in net spectral width scales only as z^2. Thus, the initial increase, here in bandwidth, is also only to second order in z. *This behavior is equally important to the creation of the soliton as was the increase in pulse width from the dispersive term.*

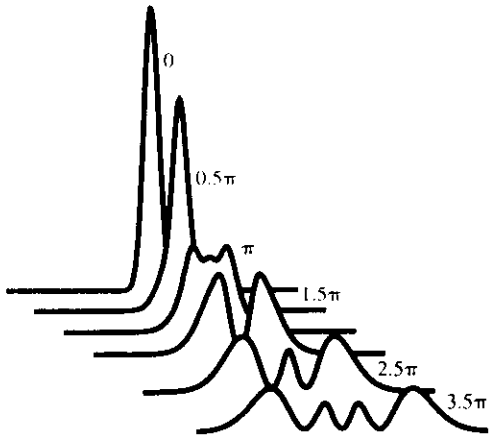

Fig. 12.4 Spectral broadening of a Gaussian pulse at zero dispersion. The numbers

2.5 THE SOLITON

2.5.1 Origin of the Soliton

We are now finally in a position to discuss the origin of the soliton. In Section 1, we stated that the soliton is that pulse for which the nonlinear and dispersive terms of the NLS equation cancel each other's effects. At first, it may seem mysterious that the tendencies to spectral and temporal broadening can cancel each other. As we have just taken pains to show, however, whenever one starts from a transform-limited pulse, such as sech(t), there is no broadening of either kind to first order in z (to be thought of as dz). Instead, the first order effects of both terms are just complementary phase shifts $d\phi(t)$. We have already seen how the nonlinear term generates $d\phi(t) = |u(t)|^2 dz$. For the dispersive effect, first we recognize that if $f(z, t)$ is real, then the general equation

$$\frac{\partial u}{\partial z} = if(z, t)u \quad (2.28)$$

simply generates the phase change $d\phi(t) = f(0, t)\, dz$ in the distance dz. We then write the reduced NLS equation in the form

$$\frac{\partial u}{\partial z} = \left(\frac{i}{2u} \frac{\partial^2 u}{\partial t^2}\right) u. \quad (2.29)$$

Thus, the dispersive term generates

$$d\phi = \left(\frac{1}{2u} \frac{\partial^2 u}{\partial t^2}\right) dz. \quad (2.30)$$

For $u = \text{sech}(t)$, these terms are, respectively,

$$d\phi_{NL} = \text{sech}^2(t)\, dz \quad \text{and} \quad d\phi_{disp.} = [\tfrac{1}{2} - \text{sech}^2(t)]\, dz. \quad (2.31)$$

Note that these differentials sum to a constant (see Fig. 12.5), which, when integrated, simply yields a phase shift of $z/2$ common to the entire pulse. In this way, we arrive at the simplest form for the soliton, already displayed in Eq. (2.13).

It should also be noted that a common phase shift does nothing to change the temporal or spectral shapes of a pulse. Thus, as already advertised, the soliton remains completely nondispersive in both the temporal and frequency domains. Nevertheless, the associated wave-number shift of $(2z_c)^{-1}$, or simply $\frac{1}{2}$ in soliton units, is important in understanding the interaction of the solition with perturbing nonsoliton field components

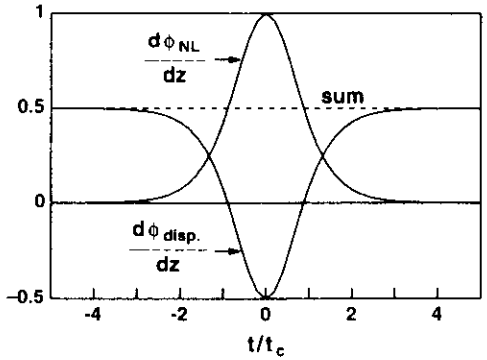

Fig. 12.5 Dispersive and nonlinear phase shifts of a soliton pulse, and their sum.

2.5.2 Path-Average Solitons

For reasons of economy, the loss-canceling optical fiber amplifiers of a long fiber transmission line are usually spaced apart by a distance, which we shall call the *amplifier span*, or L_{amp}, of several tens of kilometers. This spacing results in a large periodic variation in the signal intensity, as illustrated in Fig. 12.6. In addition, the dispersion parameter D may vary significantly within each amplifier span (again, see Fig. 12.6). Clearly, in that case, the differential phase shifts of the dispersive and nonlinear terms (see Eq.

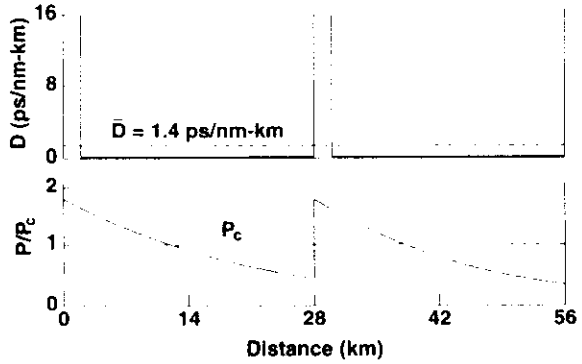

Fig. 12.6 Sample of a transmission line used for numerical testing of the path-average soliton concept. As in certain real-world experiments, the desired $\overline{D}$ is obtained by combining short lengths of high D fiber with dispersion-shifted fiber (for which $D \sim 0$), so there are large variations in D, periodic with the amplifier spacing, as well as in the pulse power.

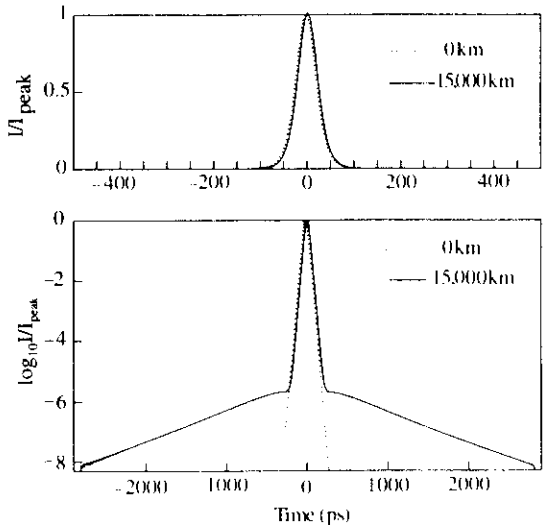

Fig. 12.7 Solitons, for which $z_c \sim 440$ km, at input and after traversing 15,000 km of the transmission line of Fig. 12.6. Note that the defects (dispersive tails on the pulse) are extremely small. The defects have also been computed analytically.

[2.31]) do not cancel in every element dz of the fiber. Nevertheless, if the condition

$$z_c \gg L_{amp} \tag{2.32}$$

is satisfied, and if, furthermore, the path-average values, $\bar{I}$ and $\overline{D}$ of the intensity and dispersion, respectively, are the same for every amplifier span, then one can still have, at least in a practical sense, perfectly good solitons. The reason is that when the inequality of Eq. (2.32) is well satisfied, as already shown, neither the temporal nor the spectral shapes of the soliton are significantly affected within each span. Thus, all that matters is that, over each amplifier span, the path-average dispersive and nonlinear phase shifts cancel (sum to a standard constant). Figure 12.7 illustrates how very well this concept of *path-average solitons** can work [1–5]. Through numerical simulation, it shows $\tau = 50$ ps solitions before and after traversal of 15,000 km of transmission line whose spans are those of Fig. 12.6. For this

* Although the name tends to be obscure, the "guiding center solitons" of Ref. 5 are essentially path-average solitons. The latter name is preferred, however, because it is more accurately descriptive, is better known, and avoids confusion with the more apt use of the word *guiding* in connection with jitter-reducing filters (see Section 4).

case, $z_c/L_{amp} \approx 16$. The difference between the output and input solitions, which can be seen only on the logarithmic plot, appears in the form of very low-intensity tails on the pulse. This defect, usually known as *dispersive wave radiation*, represents the nonsolition component of the pulse. When it is as small as shown here, it is usually of no practical import. Even when z_c/L_{amp} is as small as 3 or 4, the path-average solition concept still works fairly well.

There is another complementary, insightful way of understanding the behavior of path-average solitons, wherein the periodic fluctuations of the amplifier spans are seen as a perturbation to provide phase matching between the solitons on the one hand, and the linear, or dispersive, waves on the other. As we have just seen in the foregoing, the dispersion relation for solitons is just $k_{sol.} = \frac{1}{2}$ (in soliton units), whereas that for the linear waves is $k_{lin.} = -\frac{1}{2}\omega^2$. Clearly, the amplifier spans provide $k_{pert.} = z_c/L_{amp}$. The phase matching condition is

$$k_{pert} = k_{sol.} - k_{lin.}. \tag{2.33}$$

If, as illustrated in Fig. 12.8, k_{pert} is so large that the phase matching occurs only where the spectral density of the soliton is small, then the path-average

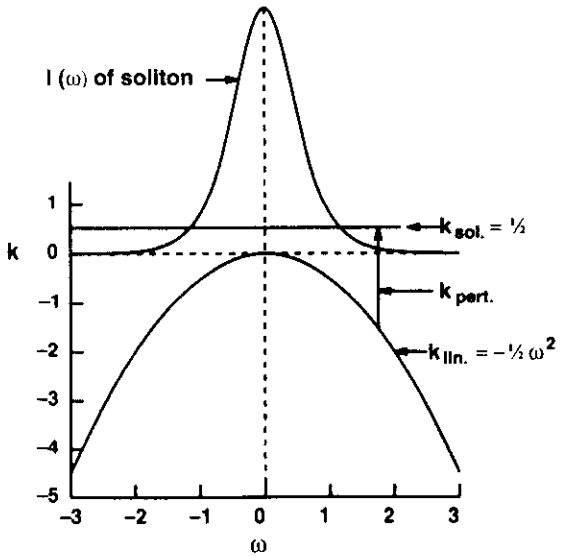

Fig. 12.8 Dispersion relations, $k(\omega)$, for the soliton and for linear waves, and the spectral density of the soliton. A perturbation of wave vector $k_{pert.}$ phase matches

solitons work well. On the other hand, if $k_{pert.}$ is small enough, then the phase matching will be to a region of high spectral density, where a large fraction of the soliton's energy will drain away into dispersive (linear) waves, and the path-average soliton will not work well. It is interesting that, historically, the concept of path-average solitons and the associated resonance condition for disaster ($k_{pert.} = \frac{1}{2}$) were first encountered in these terms of phase matching [1].

2.5.3 Soliton Transmission in Dispersion-Tapered Fiber

With an ever-increasing bit rate, eventually the soliton pulse width and hence z_c become so short that it is no longer possible to satisfy the inequality of Eq. (2.21) in a satisfactory way. Nevertheless, in principle at least, there is still a way to have perfect soliton transmission with lumped amplifiers, and that is to taper the fiber's dispersion parameter $D(z)$ to the same exponential decay curve as that of the intensity itself. That is, $D(z)$ should be given by

$$D(z) = \frac{\alpha L_{amp} \bar{D}}{1 - \exp(-\alpha L_{amp})} e^{-\alpha z} = D_0 e^{-\alpha z}, \tag{2.34}$$

so that Eq. (2.12a) becomes

$$-i\frac{\partial u}{\partial z} = \frac{D_0}{2\bar{D}} e^{-\alpha z} \frac{\partial^2 u}{\partial t^2} + |u|^2 u - i(\alpha/2)u. \tag{2.35}$$

Clearly, the phase shifts generated by the dispersive and nonlinear terms of Eq. (2.12b) will cancel in each and every segment dz of the amplifier span, so the solitons will be without perturbation. It is also easily understood that an N-step approximation to the ideal dispersion taper of Eq. (2.34) can be tremendously helpful, even when N is as small as two or three. Later, in Section 5, we shall show that tapered dispersion is perhaps of even greater importance to avoid excessive growth of four-wave mixing components.

2.5.4 More General Forms for the Soliton

Any single real-world soliton can be expressed in the simple form of Eq. (2.13) by the appropriate choice of scale and frequency. Alternatively, application to Eq. (2.13) of the scale and frequency transformations discussed in Sections 2.4.1 and 2.4.3, respectively, yields the more general form

$$u = A \operatorname{sech}(A(t + \Omega z))e^{i(\phi - \Omega t)}, \tag{2.36}$$

where

$$\phi = (A^2 - \Omega^2)z/2.$$

The form given by Eq. (2.36) is necessary to the consideration of perturbation or multisoliton problems, such as soliton–soliton collisions in WDM, for example.

2.6 *NUMERICAL SOLUTION OF THE NLS EQUATION: THE SPLIT-STEP FOURIER METHOD*

The NLS equation is generally difficult to solve analytically. Numerical solution, however, can be remarkably efficient, when it is based on the split-step Fourier method shown in Fig. 12.9. The method is based on the fact that the effects of the dispersive term are most naturally dealt with in the frequency domain, whereas those of the nonlinear term are best handled in the time domain. Thus, each increment h in z is treated in two consecutive steps, as follows:

Step 1: $u(z, t) \longrightarrow \tilde{u}(z, \omega)$; $\quad \tilde{u}(z, \omega)e^{i(\omega^2/2)h} = \tilde{u}(z + h, \omega)$

and

Step 2: $\tilde{u}(z + h, \omega) \longrightarrow u_{new}(z, t)$; $\quad u_{new}(z, t)e^{i|u|^2 h} = u(z + h, t)$.

That is, in Step 1, $u(z, t)$ is Fourier transformed to $\tilde{u}(z, \omega)$, and then, to reflect the dispersive effects of the element h, $\tilde{u}(z + h, \omega)$ is computed from $\tilde{u}(z, \omega)$ according to the *analytic* solution of Eq. (2.20). In Step 2, $\tilde{u}(z + h, \omega)$ is first Fourier transformed back to make a "new" version of $u(z, t)$. Then, from that new $u(z, t)$, $u(z + h, t)$ is computed according to the *analytic* solution of Eq. (2.24), so that it now reflects the nonlinear effect of the element h as well. On the basis of the ideas just discussed with respect to path-average solitons, one can easily see that reasonable accuracy can often be obtained with relatively large step sizes. Finally, note that fiber loss, amplifier gain, filter response functions, and other linear

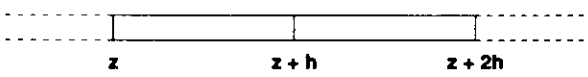

Fig. 12.9 Scheme of the split-step Fourier method.

frequency-dependent factors are most easily applied in the frequency domain.

3. Spontaneous Emission and Other Noise Effects

3.1 *GROWTH OF SPONTANEOUS EMISSION NOISE IN A BROADBAND TRANSMISSION LINE*

In long-distance fiber optic transmission systems, limits to the bit rate and distance for error-free transmission are set mainly by the various effects of noise fields in the line [6, 7]. Although we shall later show how the proper use of narrow band filters can greatly reduce those noise fields and their effects, it is nevertheless instructive to first consider a broadband system in which the response of the transmission line is essentially flat over the entire bandwidth of the soliton. The prototypical system (see Fig. 12.10) consists of single-mode fiber segments of length L_{amp} and loss coefficient α, so that the power loss per segment is $\exp(-\alpha L_{amp})$, connected by amplifiers whose gain $G = \exp(\alpha L_{amp})$ offsets this loss. The path-average signal is thus maintained at the same high level, from the transmitter right through to the receiver. Detector noise is overwhelmed, and the most important noise is the accumulated, or "amplified," spontaneous emission (ASE) created by the amplifiers. In some cases, dispersive-wave radiation created by path-average solitons (Section 2.5.2), and residual four-wave mixing fields from soliton–soliton collisions in WDM, can also make a significant contribution to the noise. Here, however, we shall concentrate on the inevitable ASE noise.

In the system of Fig. 12.10, each amplifier contributes to its output an additive Gaussian ASE noise field whose mean power per unit bandwidth is

$$P_{amp}(\nu) = (G - 1)n_{sp}h\nu, \tag{3.1}$$

where $n_{sp} \geq 1$ is the excess spontaneous emission factor (close to unity if the amplifier populations are highly inverted), and $h\nu$ is the photon energy.

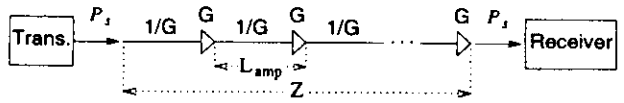

Fig. 12.10 Prototypical all-optical transmission line containing amplifiers of power gain G interleaved with fiber spans of loss $1/G$.

One may note that $P_{amp}(\nu)$ has units of energy. In general, if $P(\nu)$ is the power per unit bandwidth of an effectively white-noise field, then it is also the noise energy emitted (or received) in any time T (e.g., the bit period) and in a corresponding bandwidth $\delta\nu = 1/T$. It is independent of one's choice of time unit and is known as the *equipartition energy*. (Note that we are invoking only classical transmission line theory — i.e., no mention of discrete photons, etc. This is always adequate when the equipartition noise energy is much greater than the photon energy, as it is in systems that use in-line coherent amplifiers. A more sophisticated semiclassic theory involving zero-point fields is conceptually better, but in the present context it is unnecessary.)

Because there is unity gain from the output of each amplifier in Fig. 12.10 to the receiver, the accumulated ASE noise at the receiver is just the value given by Eq. (3.1) multiplied by N, the total number of amplifiers in the chain. To compare the noise with the soliton signal, we must use the path-average value for the noise, just as we do for the solitons. The path-average power is equal to the power at the output of an amplifier multiplied by the average from 0 to L_{amp} of $\exp(-\alpha z)$, which can be expressed as $(G - 1)/(G \ln G)$. If we also write N as $\alpha Z/\ln G$, then the path-average noise at system output takes the form

$$\overline{P}_N(\nu) = \alpha Z h\nu n_{sp} F(G), \tag{3.2}$$

where the overbar on $\overline{P}$ symbolizes the path average, Z is the system length, and the function

$$F(G) = \frac{1}{G}\left[\frac{(G-1)}{\ln G}\right]^2 \tag{3.3}$$

(see Fig. 12.11) represents an important noise penalty incurred simply by using long spans and high gain amplifiers [6]. Systems designers, accustomed to the economics of regenerated systems, would like to place amplifiers no closer together than about 100 km. For systems of transoceanic length, however, the more than 7-dB ASE noise penalty one must pay for such large spacing is excessive, and smaller spacings are usually needed.

3.2 ENERGY ERRORS

There are two main sources of error that affect the soliton system; fluctuations of the pulse energies and of their arrival times. At each amplifier, the addition of the ASE noise changes the energy, central frequency, mean

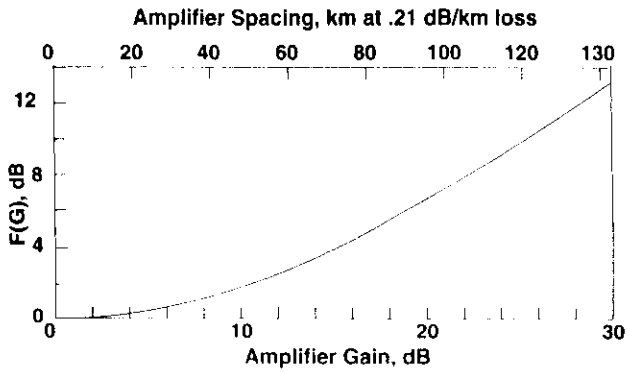

Fig. 12.11 Penalty function, $F(G)$, as a function of amplifier gain.

time, and phase of the solitons in statistically random ways. The changes in mean time and phase are of little importance in the present context. The other two changes can be analyzed separately. We shall focus on the energy fluctuations in this section and on the frequency changes and the resultant jitter in arrival times in the next.

The energy fluctuations are similar to those that occur in a linear system. The argument is as follows: The system is effectively linear over short distances, so there is no difference in the way the noise field is injected into the system. The only difference in the soliton system is that the energy changes of first order in the noise field (the so-called signal–spontaneous noise) are captured by the solitons, which then reshape themselves as they propagate. This reshaping is done with no significant change in energy. Thus, the energy fluctuations at the receiver at like those that would occur if the system were linear and dispersion free.

To evaluate the errors incurred by the energy fluctuations, some model detector must be chosen. For simplicity we shall assume that the detector consists first of an optical filter of bandwidth B_0, followed by a photodetector, followed by an integrator, so that in effect the total energy that passes the optical filter in each time slot T is measured. The detectors actually used in most systems do not work this way, but the good ones give similar results. Let $m = KB_0T$, where $K = 1$ or 2 is the number of polarization states to which the receiver is sensitive. The sampling theorem says that the detected optical field has approximately $2m$ independent degrees of freedom (DOFs), and without loss of generality the soliton may be considered to occupy just one of these. The mean ASE noise energy per DOF

is one-half the equipartition energy, or $\overline{P}_N(\nu_0)/2$. Thus, if we let S be the ratio of the total energy in a bit period to the equipartition energy $\overline{P}_N(\nu_0)$, then S becomes the sum of the squares of $2m$ independent Gaussian random field variables, each with variance equal to one-half. All but one of these have zero mean values. The exception has a mean value that is the square root of the normalized unperturbed soliton energy. One can think of S as the square of the radius to a point in a $2m$-dimensional Euclidean space whose coordinates are the real amplitudes of the normalized DOF field components. On the basis of this picture, we get the following results. The mean and variance of the distribution of S for a zero (soliton absent) are both equal to m, and for a one (soliton present) are equal, respectively, to $S_1 + m$ and $2S_1 + m$, where S_1 is the ratio of the unperturbed soliton energy to the noise equipartition energy. In the variances, the term m represents what is often called the *spontaneous–spontaneous beat noise*, whereas the term $2S_1$ represents the *signal–spontaneous beat noise*.

It is standard practice to characterize error rates using the quantity Q, which is related to the bit error rate (BER) through the complementary error function

$$\text{BER} = (\tfrac{1}{2}\operatorname{erfc}[Q/\sqrt{(2)}] \approx [2\pi(Q^2 + 2)]^{-1/2}\exp(-Q^2/2). \qquad (3.4)$$

The approximate form can be used when $Q \geq 3$. If the energy distributions are assumed Gaussian and the optimum decision level is chosen, then the value of Q is related to the means, μ, and variances, σ^2, of the distributions of ones and zeros by $Q = (\mu_1 - \mu_0)/(\sigma_1 + \sigma_0)$. On this heuristic assumption of Gaussian energy distributions, one gets error rates as a function of the signal to equipartition noise ratio S, as shown by the dashed line in Fig. 12.12.

In more detail, the true probability distributions for S are given by [6]

$$Prob(S) = \frac{S^{m-1}}{(m-1)!}\exp(-S) \qquad (3.5)$$

for a zero, and

$$\begin{aligned} Prob(s) &= 2s(s/s_1)^{m-1}\exp[-(s^2 + s_1^2)]I_{m-1}(2ss_1)^* \\ &\approx \pi^{-1/2}(s/s_1)^{m-1/2}\exp[-(s - s_1)^2] \end{aligned} \qquad (3.6)$$

for a one, where s and s_1 are, respectively, the square roots of S and S_1, whereas I_{m-1} signifies a modified Bessel function of the first kind. The approximate asymptotic form is valid in the tail of the distribution needed for the calculation of errors. Using these probability distributions, one determines error rates by choosing a decision level S_d that equates the probability that $S > S_d$ for a zero with the probability that $s < \sqrt{S_d}$ for a one. The results of this computation are also plotted in Fig. 12.12. Note that the more accurate computation of error rates gives fewer errors than the Gaussian approximation does. For a larger value of m (larger optical bandwidth), the difference would be smaller.

* We thank Curtis Menyuk for pointing out the exact form.

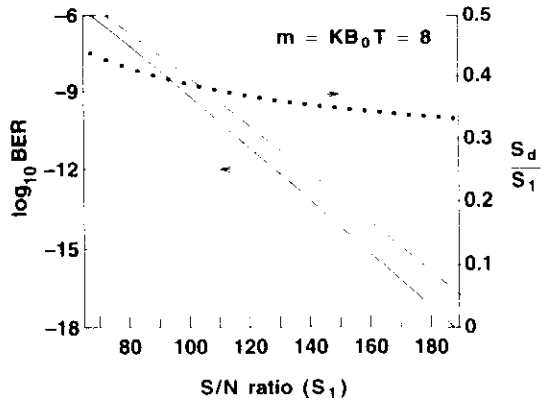

Fig. 12.12 Bit error rate (BER) for amplitude or energy errors, and the optimum decision energy level, as functions of the signal-to-noise ratio, for $m = 8$. (S_d is the decision energy level.) Also shown is the error rate estimate using the Gaussian approximation (*dashed line*).

3.3 GORDON–HAUS EFFECT

The ASE noise also acts to produce random variations of the solitons' central frequencies. The fiber's chromatic dispersion then converts these variations in frequency to a jitter in pulse arrival times, known as the *Gordon–Haus effect* [8]. Such timing jitter can move some pulses out of their proper time slots. Thus, the Gordon–Haus effect is a fundamental and potentially serious cause of errors in soliton transmission.

The calculation of the jitter can be summarized as follows: Recall that each DOF of the noise field produced by an amplifier has a mean path-average energy of $(\frac{1}{2})\overline{P}_{amp}(\nu)$. The field of one such DOF shifts the frequency of the soliton. From perturbation theory, one can deduce that the effective noise-field component has the form $\delta u = iau_{sol}\tanh(t)$ (see Fig. 12.13), and that it shifts the soliton's frequency by an amount $\delta\Omega = 2a/3$. Here, a is a

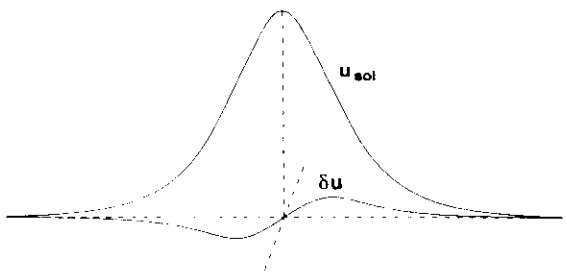

Fig. 12.13 Noise component that modifies the frequency of a soliton, in relation to the field envelope of the soliton. The two field components are in quadrature.

real random Gaussian variable whose variance $(\frac{3}{4})\overline{P}_{amp}(\nu)$ is determined by the DOF's mean energy requirement. The soliton's random frequency shift therefore has a variance of

$$\langle \delta\Omega^2 \rangle_{amp} = \tfrac{1}{3}\,\overline{P}_{amp}(\nu). \tag{3.7}$$

Because in soliton units (see Section 2.4.3) the inverse velocity shift is numerically just -1 times the frequency shift, the net time shift of a given pulse is

$$\delta t = -\sum_{amps} \delta\Omega_n z_n, \tag{3.8}$$

where z_n is the distance from nth amplifier to the end. On the right side of Eq. (3.8) we have the sum of N independent variables, each of which has a Gaussian distribution. In such a case, the sum also has a Gaussian distribution whose variance is the sum of the variances of the individual terms. Thus, the variance of δt is

$$\langle \delta t^2 \rangle = \langle \delta\Omega^2 \rangle_{amp} \sum_{amps} z_n^2 = \frac{\overline{P}_{amp}(\nu)}{3}\frac{Z^3}{3L_{amp}}, \tag{3.9}$$

where, for the second step in Eq. (3.9), Z represents the total system length, and we have approximated the discrete sum over the (many) amplifiers by an integral. Now substituting $\ln G/\alpha$ for L_{amp} and using the path average form of Eq. (3.1), we obtain

$$\langle \delta t^2 \rangle = \tfrac{1}{9}\,\alpha n_{sp} F(G) h\nu Z^3. \tag{3.10}$$

(From now on in this chapter, we shall write the variance in arrival times, $\langle \delta t^2 \rangle$, as σ^2, so σ then becomes the corresponding standard deviation.)

Translated from soliton units into practical units (see Eqs. [2.14] and [2.15], Eq. (3.10) becomes

$$\sigma_{gh}^2 = 3600\, n_{sp} F(G)\frac{\alpha}{A_{eff}}\frac{D}{\tau} Z^3, \tag{3.11}$$

where σ_{gh} is in picoseconds, n_{sp} and $F(G)$ are as defined previously, the fiber loss factor α is in inverse kilometers, the effective fiber core area A_{eff} is in square microns, the group delay dispersion D is in picoseconds per nanometer per kilometer, τ is the soliton FWHM intensity in picoseconds, and Z is the total system length in megameters (1 Mm = 1000 km). (The numerical constant in Eq. (3.11) is not dimensionless.) We can deduce from Eq. (3.11) that σ_{gh}^2 is proportional to the energy of the solitons because the latter is also proportional to D/τ.

To get a feeling for the size of the effect, consider the example $Z = 9$ Mm (trans-Pacific distance), $\tau = 20$ ps, $D = 0.5$ ps/nm-km, $A_{eff} = 50\ \mu m^2$, $\alpha = 0.048\ km^{-1}$, $n_{sp} = 1.4$, and $F = 1.19$ (~30-km amplifier spacing). Equation (3.11) then yields $\sigma_{gh} = 11$ ps.

The BER from the Gordon–Haus effect is the probability that a pulse will arrive outside the acceptance window of the detection system. If the window width is $2w$ and we assume that these errors affect only the ones, then the BER has a Q value of w/σ (see Eq. [3.4]. For example, this implies that for an error rate no greater than 1×10^{-9}, $2w \geq 12\sigma_{gh}$. Now, the upper bound on $2w$ is just the bit period, although practical considerations may make the effective value of $2w$ somewhat smaller. Note, therefore, that for the previous example, where $\sigma_{gh} = 11$ ps, the quantity $12\sigma_{gh}$ corresponds to a maximum allowable bit rate of about 7.5 Gb/s.

3.4 THE ACOUSTIC EFFECT

Traditionally, the Gordon–Haus effect is considered to be the dominant source of timing jitter. There is, however, another contribution, one arising from an acoustic interaction among the pulses. Unlike the bit-rate-independent Gordon–Haus jitter, the acoustic jitter increases with bit rate, and as we shall soon see, it also increases as a higher power of the distance. Thus, the acoustic jitter tends to become important for the combination of great distance and high bit rate. In this section, we briefly review what is known about the acoustic effect.

The acoustic effect appeared in the earliest long-distance soliton transmission experiments [9] as an unpredicted "long-range" interaction: one

that enabled pairs of solitons separated by at least several nanoseconds (and which were thus far beyond the reach of direct nonlinear interaction) to significantly alter each other's optical frequencies, and hence to displace each other in time. Shortly thereafter, Dianov *et al.* [10] correctly identified the source of the interaction as an acoustic wave, generated through electrostriction as the soliton propagates down the fiber (see Fig. 12.14). Other pulses, following in the wake of the soliton, experience effects of the index change induced by the acoustic wave. In particular, they suffer a steady acceleration, or rate of change of inverse group velocity with distance, dv_g^{-1}/dz, proportional to the local slope of the induced index change (again, see Fig. 12.14). In a broadband transmission line, when this steady acceleration is integrated over z, it yields $\delta v_g^{-1} \propto z$, and a second such integration yields a time displacement $\delta t \propto z^2$. It can be shown that the standard deviation of the acoustic effect for a fiber with $A_{\text{eff}} = 50\ \mu\text{m}^2$ is approximately [11, 12]

$$\sigma_a \approx 8.6 \frac{D^2}{\tau} \sqrt{R - 0.99} \frac{Z^2}{2}, \tag{3.12}$$

where σ_a is in picoseconds, D is in picoseconds per nanometer per kilometer, τ is in picoseconds, R is in gigabits per second, and Z is in megameters. Comparing Eq. (3.12) with the square root of Eq. (3.11), note the different

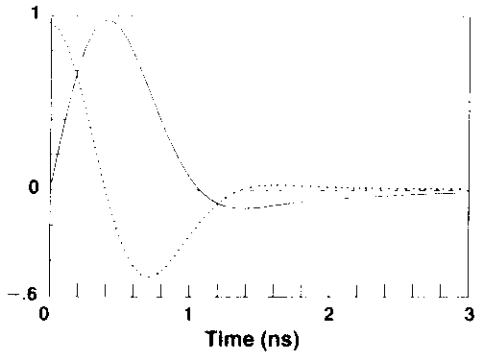

Fig. 12.14 *Solid curve:* Relative index change due to the acoustic effect following passage of a soliton at $t = 0$. *Dotted curve:* Relative force acting on the following soliton at t; this curve is proportional to the time derivative of the relative index curve. For these curves, the interacting solitons are assumed to have a common state of polarization. The effect is only weakly dependent on their relative polarizations, however.

power dependencies on D, τ, R, and Z, most of which have already been discussed for both the Gordon–Haus and the acoustic effects. For the acoustic jitter, the scaling of σ_a as D^2/τ is easily understood, because it is clearly in direct proportion to the soliton energy, or D/τ, and the extra factor in D is required for the conversion of frequency shifts into timing shifts.

3.5 OPTIMIZATION OF THE SOLITON ENERGY FOR BEST BER PERFORMANCE

It should be clear from the discussion in Sections 3.2 and 3.3 that energy errors decrease, whereas errors from the Gordon–Haus jitter increase, with increasing soliton pulse energy W_{sol}. Thus, there will be an optimum value of W_{sol} for which the combined error rates are a minimum. Because $W_{sol} \propto D/\tau$, one can hope to attain that optimum value of W_{sol} by adjusting D and τ. There are, of course, certain limitations on the practical ranges for both parameters. For example, lack of perfect uniformity of fiber preforms and other factors tend to limit the smallest values of D that can be produced reliably. To avoid significant interaction between nearest-neighbor soliton pulses, τ can be no more than about 20–25% of the bit period. Nevertheless, D/τ can usually be adjusted over a considerable range.

The optimum value of W_{sol} can be most efficiently found from a diagram [6] like that shown in Fig. 12.15, where, for a fixed value of the transmission distance, the rates for both energy and timing errors are plotted as a function of the parameter τ/D. Proceeding from the far right, where W_{sol} is smallest, note that at first, only energy errors are significant, but as W_{sol} increases, those errors fall off exponentially. Eventually, timing errors become significant and then dominate. Also note that although the energy errors are bit-rate independent, the timing errors are not, because the allowable size of the acceptance window in time is determined by the bit period. Note that for transmission at 5 Gb/s, the optimum value of $\tau/D \approx 70$ nm-km. If we choose $D = 0.5$ ps/nm-km, a value large enough to be reproducible, then we have $\tau = 35$ ps, a value short enough relative to the (200-ps) bit period to allow for negligible pulse interactions.

The curves of Fig. 12.15 would seem to imply a maximum allowable bit rate not much greater than 5 Gb/s for trans-Pacific soliton transmission over a broadband transmission line (at least not for the specific choice of parameters reflected there). As already noted in Section 1, and as will soon be thoroughly explored in the following section, the technique of passive regeneration known as *guiding filters* has enabled that limit to be surpassed

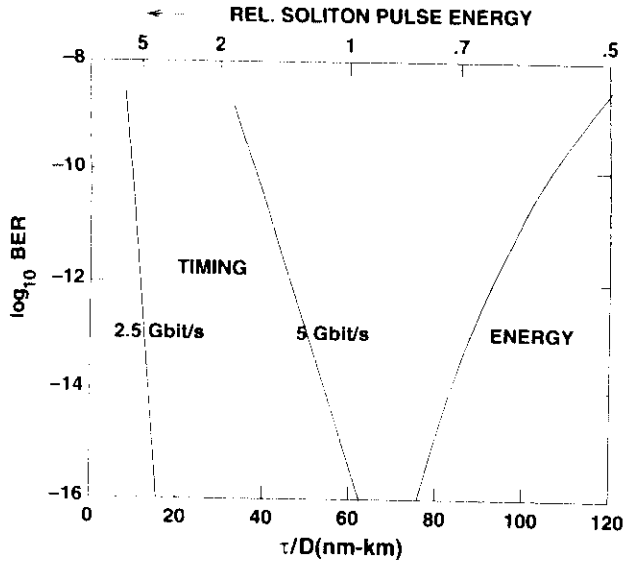

Fig. 12.15 BER, for energy and timing errors, as a function of the parameter τ/D, for a transmission distance of 9 Mm (the trans-Pacific distance). The other assumed parameters are as follows: fiber loss rate, 0.21 dB/km; L_{amp} = 30 km; n_{sp} = 1.5; A_{eff} = 50 μm^2; m = 8 (see Section 3.2).

by a large factor. Thus, the theory in this section, and its predictions, are largely of interest as background for the understanding of transmission using filters. Nevertheless, for the record, we close this section by citing the results of an experimental test of single-channel transmission at 5 Gb/s that was made a number of years ago [13]. Although made with guiding filters, the filters were only of the weak, fixed tuned type, so the results that would have been obtained without filters may reasonably be projected from them. See Fig. 12.16.

4. Frequency Guiding Filters

4.1 INTRODUCTION

In mid-1991, two groups independently suggested the idea that the Gordon–Haus jitter and other noise effects could be significantly suppressed in soliton transmission systems simply through a narrowing of the amplifier

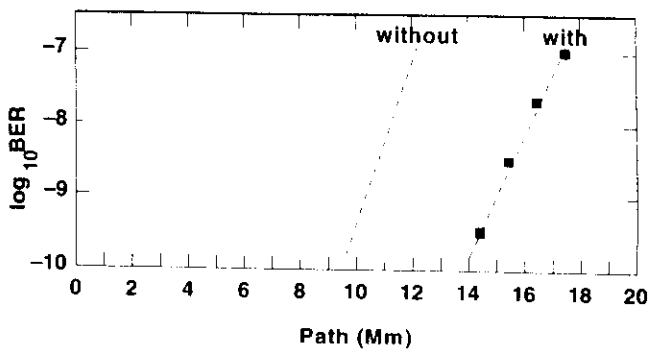

Fig. 12.16 Experimentally measured BER for a single-channel rate of 5 Gb/s, as a function of transmission distance, and with a 2^{15}-bit-long random sequence. *Curve labeled "with"*: Weak, fixed-frequency guiding filters used. *Curve labeled "without"*: Scaled back projection with no filters. The other parameters are as follows: fiber loss rate, 0.21 dB/km; L_{amp} = 28 km; D = 0.7 ps/nm-km; n_{sp} = 1.6; τ = 40 ps; A_{eff} = 35 μm^2. At the receiver, the effective window width was about 170 ps.

gain bandwidth [14, 15]. In practice, this means the use of narrow band filters, typically one per amplifier. Figure 12.17 shows appropriate filter response curves in comparison with the spectrum of a 20-ps-wide soliton. The fundamental idea is that any soliton whose central frequency has

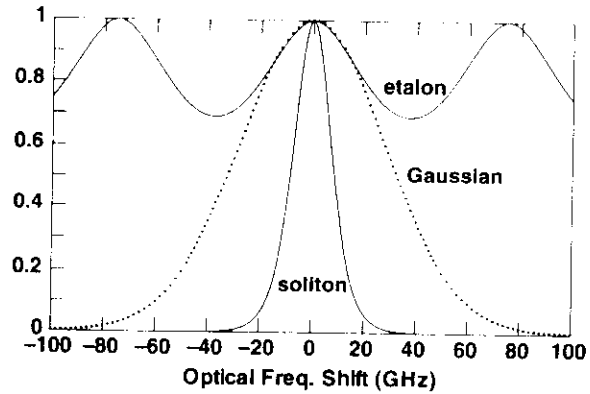

Fig. 12.17 Intensity response curves of a practical etalon guiding filter and a Gaussian filter with the same peak curvature, compared with the spectrum of a 20-ps soliton. The etalon mirrors have R = 9%, and their 2.0-mm spacing creates

strayed from the filter peak will be returned to the peak, in a characteristic damping length delta (Δ), by virtue of the differential loss that the filters induce across its spectrum. The resultant damping of the frequency jitter leads in turn to a corresponding damping of the jitter in pulse arrival times. For example, in Eq. (3.9) for the variance of the Gordon–Haus jitter, when guiding filters are used, the quantities z_n^2 in the sum are all replaced with the common factor Δ^2. Thus, the factor $Z^3/3$ in the final expression is replaced by the (potentially much smaller) factor $Z \times \Delta^2$.

The filters also cause a reduction in amplitude jitter. Consider, for example, a pulse with greater than normal power; that pulse will be narrower in time, have a greater bandwidth, and hence experience greater loss from passage through the filter than the normal pulse. The opposite will occur for a pulse of less than standard power. Thus, amplitude jitter also tends to be dampened out, as is detailed later, in essentially the same characteristic length Δ as is the frequency jitter.

Because the major benefit comes from the filter response in the neighborhood of its peak, the etalon filter whose shallow response is shown in Fig. 12.17 provides almost as much benefit as the Gaussian filter of the simplest theory [14, 15]. But the etalon, with its multiple peaks, has the great fundamental advantage that it is compatible with extensive WDM. The etalons also have the practical advantage that they are simple, are low in cost, and can be easily made in a rugged and highly stable form.

It should be understood that linear pulses cannot traverse a long chain of such filters: after a sufficient distance, their spectra will be greatly narrowed, and the pulses correspondingly spread out in time. The solitons survive because they can regenerate the lost frequency components, more or less continuously, from the nonlinear term of the NLS equation. On the other hand, the amplifiers must supply a certain excess gain to compensate for the net loss that the solitons suffer from passage through the filters. As a result, noise components at or near the filter peak grow exponentially with distance. To keep the noise growth under control, the filters can be made only so strong, so the maximum possible benefit from them is limited. For example, Fig. 12.18 shows the standard deviation of timing jitter, as a function of distance, for systems with the optimum strength filters (those experimentally observed [13] to produce the best BER performance), and for those with no filters. Note that at the trans-Pacific distance of 9 Mm, the filters reduce the standard deviation of the jitter by a factor somewhat less than two times.

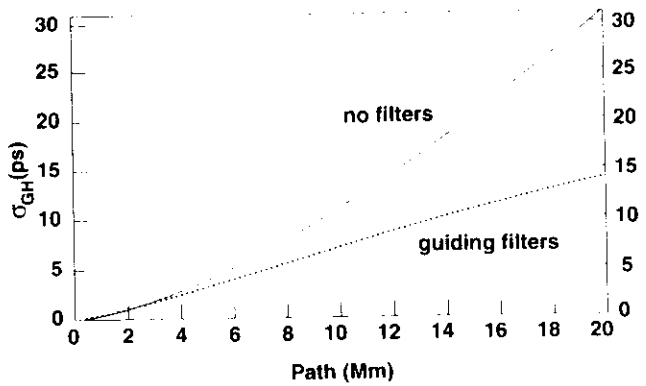

Fig. 12.18 Computed standard deviation, σ_{GH}, of pure Gordon–Haus jitter as a function of total path, for a broadband transmission line ("no filters") and for one having optimum strength, fixed-frequency guiding filters. The optimum filter strength, determined experimentally, corresponds to one uncoated, 1.5-mm-thick solid quartz etalon filter every 78 km. The other pertinent transmission line and soliton parameters in the strength-determining experiment were as follows: D = 0.7 ps/nm-km, n_{sp} = 1.4, and τ = 40 ps. (The BER data of a Fig. 12.16 were obtained in the same expriments [13].)

4.2 *SLIDING-FREQUENCY GUIDING FILTERS*

There is a simple and elegant way [16] to overcome the noise growth, and hence the limited performance, of a system of fixed-frequency filters. The trick is to "slide," i.e., translate, the peak frequency of the filters with distance along the transmission line (see Fig. 12.19). As long as the sliding is gradual enough, the solitons will follow, in accord with the same "guiding" principle that dampens the jitter. On the other hand, the noise, being

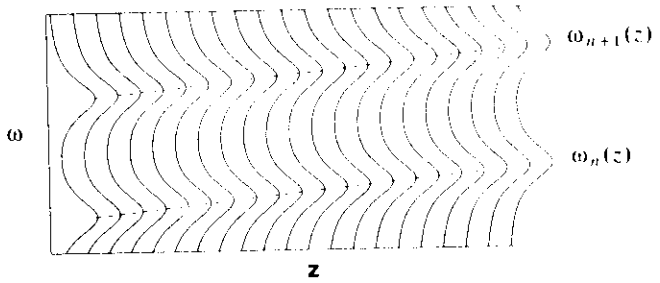

Fig. 12.19 Transmission of sliding-frequency guiding filters versus z.

essentially linear, can follow only the horizontal path in Fig. 12.19. Thus, the sliding creates a transmission line that is opaque to noise for all but a small, final fraction of its length, yet remains transparent to solitons. In consequence, the filters can be made many times stronger, and the jitter reduced by a corresponding factor, with the final result that the maximum bit rate can be increased at least several-fold over that possible without sliding.

The sliding-frequency filters provide many other important benefits beyond the simple suppression of timing and amplitude jitter. Note, for example, that they suppress all noiselike fields, whatever the source, such as dispersive-wave radiation from imperfect input pulses or other perturbations. They provide tight regulation of all the fundamental soliton properties, such as energy, pulse width, and optical frequency. As is detailed later, in WDM the filters suppress timing shifts and other defects from soliton–soliton collisions, and they provide a powerful regulation of the relative signal strengths among the channels in the face of wavelength-dependent amplifier gain. Thus, in short, the sliding-frequency guiding filters can be regarded as an effective form of passive, all-optical regeneration, and one that is uniquely compatible with WDM.

Finally, it should be noted that the required set of hundreds of sliding-frequency filters can be supplied more easily and at less cost than the corresponding set of fixed-frequency filters. That is, unlike the fixed-frequency mode, in which all filters must be carefully tuned to a common standard, the sliding-frequency mode does not require any tuning. Rather, only a statistically uniform distribution of frequencies is needed. Provided the distribution is over at least one or more free spectral ranges, simple ordering of the filters should be able to provide any reasonable desired sliding rate.

4.3 ANALYTIC THEORY OF GUIDING FILTERS

In the mathematical representation of a transmission line with filters, in general, only numerical solutions are possible when the exact response functions of real filters are used. Nevertheless, analytic solutions are possible when the filter response is approximated by a truncated series expansion [16]. When expanded in a Taylor series, the logarithm of the filter response function F takes the general form

$$\ln F(\omega - \omega_f) = i\zeta_1(\omega - \omega_f) - \zeta_2(\omega - \omega_f)^2 - i\zeta_e(\omega - \omega_f)^3 + \cdots, \quad (4.1)$$

where ω_f is the filter peak frequency and the constants ζ are all real and positive. The first-order term can be ignored because the linear phase shift

that it provides serves only to translate the pulses in time. Although higher order filter terms can have important effects, the most fundamental features are revealed by analytic solutions to the simplified propagation equation employing only the second-order term:

$$\frac{\partial u}{\partial z} = i\left[\frac{1}{2}\frac{\partial^2 u}{\partial t^2} + u^* u^2\right] + \frac{1}{2}\left[\alpha - \eta\left(i\frac{\partial}{\partial t} - \omega_f\right)^2\right]u, \quad (4.2)$$

where α is the gain required to overcome the loss imposed on the solitons by the filters and $\eta = 2\zeta_2$. (Both continuously distributed quantities α and η are easily converted into lumped, periodic equivalents.) Without filter sliding ($d\omega_f/dz = \omega_f' = 0$), and where, for convenience, we set $\omega_f = 0$, the exact stationary solution is

$$u = \sqrt{P}\,\mathrm{sech}(t)\exp(i\phi)$$
$$\text{where} \quad \phi = Kz - \nu \ln\cosh(t), \quad (4.3)$$

and the parameters (α, η, P, ν, K) must satisfy

$$\nu = \frac{3}{2\eta}\left[\left(1 + \frac{8\eta^2}{9}\right)^{1/2} - 1\right] = \frac{2}{3}\eta - \frac{4}{27}\eta^3 + \cdots \quad (4.4a)$$

$$\alpha = (\eta/3)(1 + \nu^2) \quad (4.4b)$$

$$P = (1 + \eta^2)(1 - \nu^2/2) \quad (4.4c)$$

$$K = (\tfrac{1}{2})(1 - \nu^2) + (\nu^2/3)(2 - \nu^2). \quad (4.4d)$$

Note from Eq. (4.3) that the pulse's frequency is chirped — i.e., $\partial\phi/\partial t = -\nu\tanh(t)$. Because of this chirp, the root mean square (rms) bandwidth is increased by the factor $(1 + \nu^2)^{1/2}$.

Numerical simulation involving real filters shows that the principal features (the chirp, extra bandwidth, and increased peak power) of the previous solution are approximately preserved. The major differences lie in slight asymmetries induced in $u(t)$ and in its spectrum by the third-order filter term, and in the fact that, through a complex chain of events, those asymmetries cause the soliton mean frequency to come to rest somewhat above the filter peak.

Numerical simulation has also shown that sliding (within certain limits given subsequently) does not significantly alter this solution. Sliding does, however, have the potential to alter the damping of amplitude and frequency fluctuations. To get some notion of the effects of sliding on damping

we introduce the general unperturbed form for the soliton (Eq. [2.36]) into Eq. (4.2). We then obtain the following pair of coupled, first-order perturbation equations:

$$\frac{1}{A}\frac{dA}{dz} = \alpha - \eta[(\Omega - \omega_f)^2 + \tfrac{1}{3}A^2] \tag{4.5a}$$

$$\frac{d\Omega}{dz} = -\frac{2}{3}\eta(\Omega - \omega_f)A^2. \tag{4.5b}$$

According to Eq. (4.5b), equilibrium at $A = 1$ and at constant ω_f' requires that $d\Omega/dz = \omega_f'$, and hence that the lag $\Delta\Omega \equiv (\Omega - \omega_f)$ of the soliton mean frequency behind the filter frequencies is

$$\Delta\Omega = -\frac{3}{2\eta}\omega_f'. \tag{4.6}$$

Equation (4.6), as written, correctly predicts the difference in lag frequencies for up- versus down-sliding, $\Delta\Omega_u - \Delta\Omega_d$. To acount for the offset in $\Delta\Omega$ produced by the third-order filter term (mentioned previously for the case of no sliding), one must add a positive constant (as determined empirically from numerical simulation) to the right-hand side of Eq. (4.6). Equation (4.6) then correctly predicts $\Delta\Omega$ for all sliding rates. For etalon filters, the offset in $\Delta\Omega$ has been estimated from the third-order filter term [17]. That is, it has been shown from perturbation theory that

$$\Delta\Omega_{offset} \approx \tfrac{6}{5}\zeta_3, \tag{4.7}$$

where ζ_3 is computed as

$$\zeta_3 = \frac{1.762\ldots}{6}\frac{(1+R)}{(1-R)}\frac{\eta}{\tau F} \tag{4.7a}$$

where F is the free spectral range of the etalon filters. Combining Eqs. (4.6), (4.7), and (4.7a), one obtains

$$\Delta\Omega = \left(\frac{1.762\ldots}{5}\frac{(1+R)}{(1-R)}\frac{\eta}{\tau F}\right) - \frac{3}{2\eta}\omega_f'. \tag{4.6a}$$

Note that the two terms in Eq. (4.6a) tend to cancel for up-sliding ($\omega_f' > 0$), whereas they add for down-sliding. Because the damping of the filters is best for the smallest $|\Delta\Omega|$ (see Eq. [4.8]), up-sliding is definitely preferable to down-sliding.*

* *Note:* In the original article on sliding-frequency guiding filters (Ref. 16), because of an improper combination of sign conventions, the numerical simulations reported on there incorrectly yielded the offset $\delta\omega < 0$. As a further result of that error, the article incorrectly

Equations (4.5a) and (4.5b), when linearized in small soliton frequency and amplitude displacements δ and a, respectively, yield two eigenvalues (damping constants):

$$\gamma_1 = \tfrac{2}{3}\eta(1 + \sqrt{6}\,\Delta\Omega) \quad \text{and} \quad \gamma_2 = \tfrac{2}{3}\eta(1 - \sqrt{6}\,\Delta\Omega), \tag{4.8}$$

with corresponding normal modes $x_1 = \delta + \sqrt{\tfrac{2}{3}}a$ and $x_2 = \delta - \sqrt{\tfrac{2}{3}}a$. This implies a monotonic decrease of damping for both frequency and amplitude fluctuations with increasing $|\Delta\Omega|$, and, through Eq. (4.6), the existence of maximum allowable sliding rates for stability. The numerical simulations we have done to date with real filters are at least qualitatively consistent with these predictions.

In principle, on the basis of the damping constants of Eq. (4.8), one can go on to write expressions for the variances in soliton energy and arrival time. It is not at all clear, however, how accurate such expressions would be in predicting the effects of strong, real filters. Nevertheless, because we are primarily interested in the behavior for $\gamma z \gg 1$, where the energy fluctuations have come to equilibrium with the noise, the energy variance can be written as

$$\frac{\langle \delta E_{sol}^2 \rangle}{E_{sol}^2} \approx \frac{N}{\gamma_E E_{sol}} = \frac{N\Delta_E}{E_{sol}}, \tag{4.9}$$

where N is the spontaneous emission noise spectral density generated per unit length of the transmission line, E_{sol} is the soliton pulse energy, and the effective damping length, $\Delta_E \equiv 1/\gamma_E$, is expected to increase monotonically with increasing $|\Delta\Omega|$. Note that Eq. (4.9) implies that as far as the noise growth of ones is concerned, the system is never effectively longer than Δ_E. Because the characteristic damping lengths with sliding-frequency filters are typically about 600 km or less, this means a very large reduction of amplitude jitter in transoceanic systems.

As far as the variance in timing jitter is concerned, we have already seen that, for $\gamma z \gg 1$, the factor $Z^3/3$ is replaced by $Z\Delta_t^2$. In other words, the variance in timing jitter is subject to a reduction factor

$$f(\gamma_t, z) \approx \frac{3}{(\gamma_t Z)^2} = 3\left(\frac{\Delta_t}{Z}\right)^2, \tag{4.10}$$

where Δ_t is also expected to increase monotonically with increasing $|\Delta\Omega|$. Although Δ_E and Δ_t are in general different, nevertheless, for Gaussian filters, both are expected to be approximately equal to $3/(2\eta)$ in the neigh-

For a transmission line using Fabry–Perot etalon filters with mirror spacing d and reflectivity R, the parameters η, ω_f', and α, in soliton units, are computed from the corresponding real-world quantities as follows [18]:

$$\eta = \frac{8\pi R}{(1-R)^2}\left(\frac{d}{\lambda}\right)^2 \frac{1}{cDL_f} \tag{4.11a}$$

$$\omega_f' = 4\pi^2 f' c t_c^3/(\lambda^2 D) \tag{4.11b}$$

$$\alpha = \alpha_R t_c^2 2\pi c/(\lambda^2 D). \tag{4.11c}$$

Here, f' and α_R are just $\omega_f'/2\pi$ and α, respectively, but as expressed in "real" units (such as GHz/Mm, for example); $t_c \equiv \tau/1.763$ (Eq. [2.14]); and L_f is the filter spacing.

We can now illustrate the power of sliding-frequency filters through a specific numerical example. Anticipating a bit from the next section, where we discuss the optimum choice of filter parameters, we choose the following soliton and fiber parameters: $D = 0.5$ ps/nm-km, $\tau = 16$ ps, so $z_c = 128$ km. The sliding rate will be 13 GHz/Mm (note that this means that the total sliding will be just about 1 nm in the trans-Pacific distance), so by Eq. (4.11b), $\omega_f' = 0.095$. For the filters, we choose $R = 8\%$, 2-mm air-gap etalons, with $L_f = 50$ km. By Eq. (4.11a), $\eta = 0.52$. Thus, we have $\alpha = 0.185$, and by Eq. (4.11c), $\alpha_R = 1.4$/Mm. For the damping constants of shallow etalons, however, η has a certain functional dependence on τ and must be degraded to about $\eta_{eff} = 0.4$ for the 16-ps pulses to be used in this case.

The relative noise growth with sliding-frequency filters is easily simulated. Figure 12.20 shows the results of such a simulation for the conditions of our example. Note that the sliding keeps the peak spectral density clamped to a value less than that which would be obtained at 10 Mm without filtering, whereas without the sliding, the noise would potentially grow by e^{14}, or about 1.2 million times, in the same distance! (Long before that could happen, however, the amplifiers would saturate.) Also note the spectral narrowness of the noise.

In Fig. 12.21, normalized standard deviations of the soliton energy (ones) and of the noise energy in empty bit periods (zeros) are shown as functions of distance [16]. These curves are obtained from Eq. (4.9), and the estimate $\Delta_E \approx 600$ km derived from $\eta_{eff} \approx 0.4$ and Eq. (4.8), the data of Fig. 12.20, and the analysis of Section 3.2. Note that with the filtering, both standard deviations soon become clamped to small, indefinitely maintained values, corresponding to immeasurably small BERs.

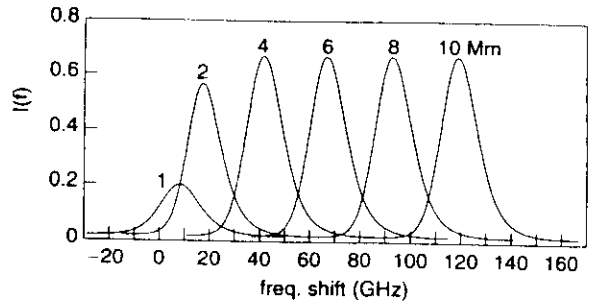

Fig. 12.20 Noise spectral density, normalized to value at 10 Mm with no filtering, as a function of frequency and distance, for the conditions of our example (one R = 8%, 75-GHz free spectral range (FSR) etalon filter per 50 km; sliding rate = 13 GHz/Mm; α_R = 1.4/Mm).

Finally, in Fig. 12.22, the standard deviation of the Gordon–Haus jitter is plotted versus distance, both for when the sliding filters are used and for when there are no filters. Note the nearly 10× reduction in $\sigma_{G/H}$ at 10 Mm, and compare it with the same factor from Fig. 12.18.

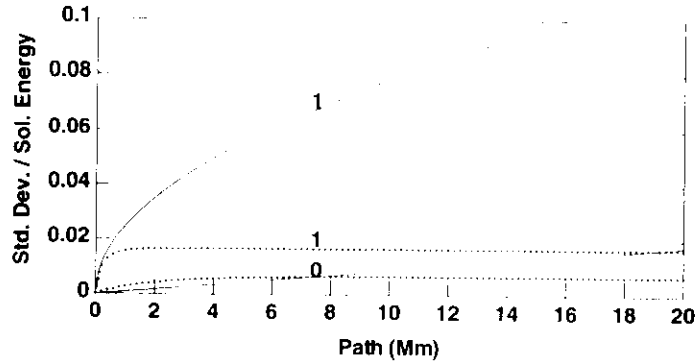

Fig. 12.21 Standard deviations of the soliton energy (ones) and of the noise in empty bit periods (zeros) versus distance, both normalized to the soliton energy itself, for the sliding-filter scheme of Fig. 12.20 (*dotted curves*), and with no filtering save for a single filter at z, passing only eight noise modes (*solid curves*). The assumed fiber loss rate and effective core area are 0.21 dB/km and 50 μm^2, respectively; the amplifier spacing and the excess spontaneous emission factor are ~30 km and 1.4,

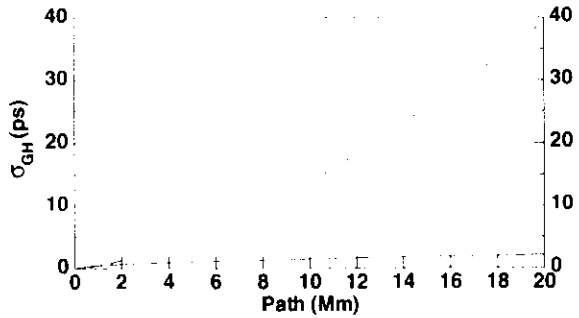

Fig. 12.22 Standard deviation of the Gordon–Haus jitter, σ_{GH}, as a function of total path. *Solid curve:* With strong, sliding-frequency guiding filters. *Dashed curve:* No filters. Conditions: τ = 16 ps; D = 0.5 ps/nm-km; n_{sp} = 1.4; $F(G)$ = 1.1; filter strength parameter η = 0.5; damping length $\Delta \approx 600$ km.

4.4 EXPERIMENTAL CONFIRMATION

4.4.1 Measurement of Noise and Amplitude Jitter

Figures 12.23 and 12.24 refer to experimental transmission with sliding-frequency guiding filters, where the parameters are at least similar, if not identical, to those in the example cited in Section 4.2. Figure 12.23 shows the signal and noise levels during a 15-Mm-long transmission, where the signal train was purposely made not quite long enough to fill the recirculating loop. Thus, once each round-trip, for a period too brief (a few microseconds) for the amplifier populations to change significantly, one sees only

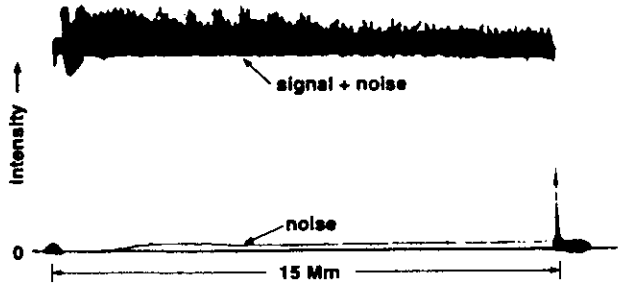

Fig. 12.23 Noise and signal levels during a transmission using strong, sliding-frequency filters. The signal level is represented by the *thick, upper line*, whereas the noise level is represented by the *fine line* immediately above the zero signal level.

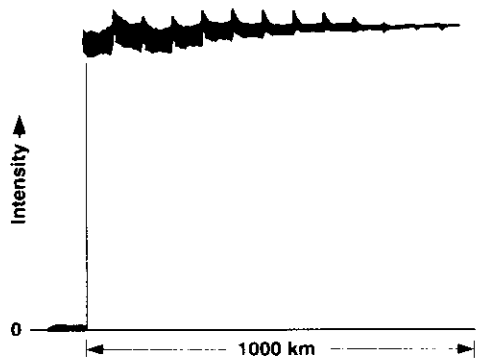

Fig. 12.24 Observed amplitude jitter reduction with successive round-trips in a transmission using sliding-frequency filters.

the noise. Note that, just as in the theoretical model (Fig. 12.20), the noise grows for only a few megameters and then saturates at a steady, low value.

In another early experiment with sliding-frequency filters, the pulse source was a mode-locked, erbium fiber ring laser, which had been purposely maladjusted to produce a substantial amplitude jitter at a few tens of kilohertz. Figure 12.24 shows the very rapid reduction in that amplitude jitter with successive round-trips in the recirculating loop. The data shown in this figure imply a damping length of about 400 km, which is consistent with the filter strength parameter of $\eta \approx 0.6$ and the known dispersion length z_c = 160 km (see Eq. [4.8]).

4.4.2 Measurement of Timing Jitter

The timing jitter in a transmission using sliding-frequency filters has been measured accurately by observing the dependence of the BER on the position, with respect to the expected pulse arrival times, of a nearly square acceptance window in time [19]. The scheme, which involved time-division demultiplexing, is shown in Fig. 12.25. The fundamental measurement is of the time span (inferred from the precision phase shifter in Fig. 12.25), for which the BER is 10^{-10} or less for each distance. The resultant spans, or time-phase margins, are plotted in Fig. 12.26, as a function of distance, for three cases: (1) a 2.5-Gb/s data stream (which, because it also passes through the loop mirror, can be thought of as a 10-Gb/s data stream for which only every fourth 2.5-Gb/s subchannel is occupied); (2) a true

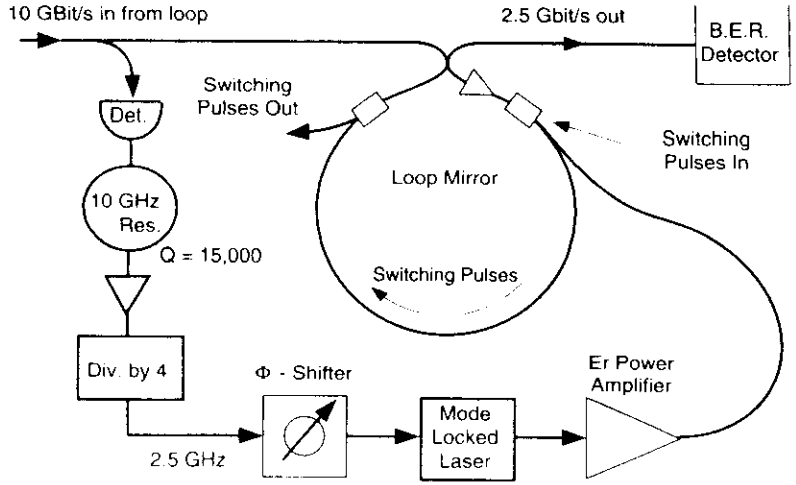

Fig. 12.25 Scheme for the pulse timing measurements. The main elements of the clock recovery are the detector; the high-Q, 10-GHz resonator; and the divide-by-4 chip. The wavelength-dependent couplers in the loop mirror (*small rectangular boxes*) each contain an interference filter that transmits at the signal wavelength (~1557 nm) and reflects the $\lambda = 1534$ nm switching pulses.

10-Gb/s data stream with adjacent pulses orthogonally polarized; (3) a 10-Gb/s data stream with all pulses copolarized. Note that the error-free distances (for which the phase margin first becomes zero) are 48, 35, and 24 Mm, respectively.

From the known properties of the error function, the difference between the effective width (here 82 ps) of the acceptance window and the measured

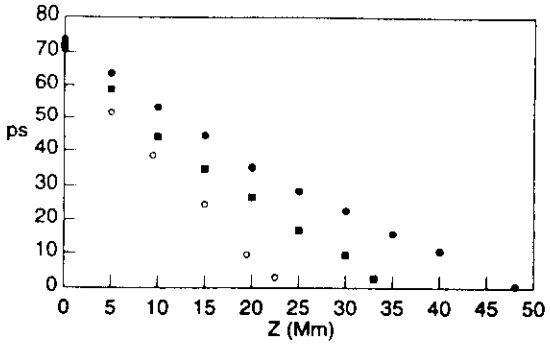

Fig. 12.26 Time-phase margin versus distance. *Bullets:* 2.5 Gb/s; *squares:* 10 Gb/s,

time-phase margin at a 10^{-10} BER should be about 13 σ of the Gaussian distribution in pulse arrival times. From this fact, one can then obtain the plots of σ shown in Fig. 12.27. Note that in all three cases shown there, the data makes a good fit to a curve of the form

$$\sigma = \sqrt{\sigma_0^2 + \sigma_{GH}^2 + \sigma_{lin}^2}, \tag{4.12}$$

where σ_0, σ_{GH}, and σ_{lin} represent the standard deviations of the source jitter (a constant), filter-damped Grodon–Haus jitter (varies as $z^{1/2}$), and jitter whose σ varies linearly with z, respectively.

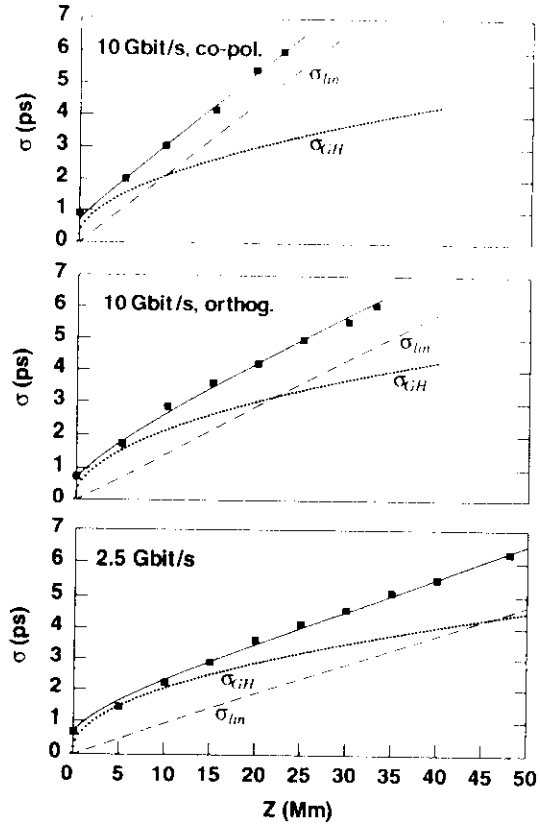

Fig. 12.27 Standard deviation of jitter versus distance for (bottom to top) 2.5 Gb/s, 10 Gb/s with adjacent pulses orthogonally polarized, and 10 Gb/s with adjacent pulses copolarized. *Squares:* Experimental points, as extrapolated from the data of Fig. 12.25; *solid curve:* best fit to theoretical curve of form $\sigma =$

The best-fit Gordon–Haus term (σ_{GH}) is always about two times greater than expected for the known parameters of the experiment, and for the damping length of approximately 400 km as calculated, and as confirmed by the independent measurement of the damping of amplitude jitter (Fig. 12.24). The frequency offset of the pulse spectra from the filter peaks is very small and can thus at best account for only a small part of the discrepancy, despite speculation to the contrary [20]. Thus, the only likely explanation here is in terms of the noiselike fields of dispersive-wave radiation. Among the perturbations that may be responsible for significant amounts of such noise are the fiber's birefringence (see Section 6) and the periodic intensity associated with the use of lumped amplifiers (Section 2.5.2).

There are two contributions to the linear term; polarization jitter and the acoustic effect (Section 3.4). (The polarization jitter arises from a noise-induced spread in the polarization states of the solitons and the conversion of that spread by the fiber's birefringence into a timing jitter. This effect discussed further in Section 6.) Because both contributions have essentially Gaussian distributions, the effects add as $\sigma_{lin} = \sqrt{\sigma_{pol}^2 + \sigma_a^2}$. For a filtered transmission line, the factor $Z^2/2$ in Eq. (3.12) is replaced with $Z \times \Delta$. Thus modified, Eq. (3.12) becomes:

$$\sigma_a \approx 8.6 \frac{D^2}{\tau} Z\Delta \sqrt{R - 0.99}. \tag{3.12a}$$

Using the bit-rate dependence of σ_a and the slopes of σ_{lin} from the two lower plots of Fig. 12.27, one can easily extract values for σ_{pol} and σ_a. At $Z = 10$ Mm, those values are as follows: $\sigma_{pol} = 0.80$ ps, $\sigma_{a,2.5} = 0.50$ ps, and $\sigma_{a,10} = 1.21$ ps. The experimental values for σ_a are just 7% less than predicted by Eq. (3.12a), a remarkable degree of agreement.

BER measurements have been made at 12.5 and 15 Gb/s, as well as at the 10 Gb/s already cited [19]. Figure 12.28 summarizes those results. Finally, it should be noted that by using sliding-frequency guiding filters, LeGuen *et al.* [21] achieved error-free transmission at 20 Gb/s over more than 14 Mm.

4.5 STABILITY RANGE

The range of soliton pulse energies for which the transmission with sliding-frequency filters is stable and error free will henceforth be simply referred to as the *stability range*. It is important for the stability range to be large enough (at least several decibels) to allow for the aging of amplifier pump lasers, and other factors that may tend to degrade the signal strength with

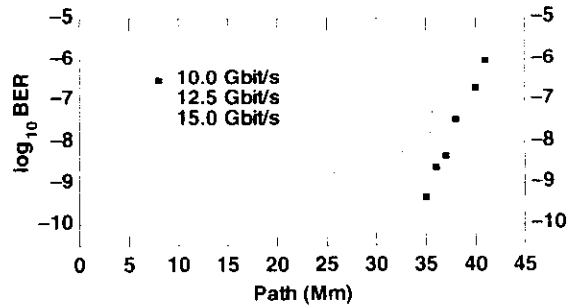

Fig. 12.28 Measured BER as a function of distance, at 10, 12.5, and 15 Gb/s. In all cases, adjacent pulses were orthogonally polarized, and the data stream was a repeated, 2^{14}-bit random word.

time, in real systems. Perhaps not surprisingly, the stability range is a function of both the filter strength parameter (η) and the sliding rate (ω_f'). The following is a brief summary of an experimental determination of that dependence, and of the optimum values for those parameters [18].

The experiment was carried out in a small recirculating loop with piezo-driven etalon sliding-frequency filters having fixed reflectivity ($R = 9\%$) and fixed mirror spacing ($d = 1.5$ mm), and where $L_f = 39$ km. Because of the fact that η is inversely proportional to D (see Eq. [4.11a]), the fiber's third-order dispersion ($\partial D/\partial\lambda = 0.7$ ps/km^2-nm) enabled η to be varied simply through change of the signal wavelength itself. At the same time, the signal power at equilibrium, hence the soliton pulse energies, could be controlled by means of the pump power supplied to the loop amplifiers. Thus, the experiment consisted simply of measuring, for each signal wavelength, and for a fixed sliding rate, the maximum and minimum signal power levels for which a transmission over 10 Mm was stable and error free. The results are shown in Fig. 12.29. Note that although error-free propagation ceases for $\eta \geq 0.8$, the stability range reaches a maximum of nearly two to one for $\eta \approx 0.4$. Figure 12.30 shows the complementary data — i.e., the measured stability range as a function of sliding rate — for fixed $\eta = 0.4$. Note that in this case, too, there is an optimum rate of about 13 GHz/Mm. Essentially the same results as in Figs. 12.29 and 12.30 were obtained for two other values of L_f (26 and 50 km, respectively) and for etalons having an FSR of 75 GHz (as opposed to 100 GHz).

The existence of E_{min} is easily predicted from the analysis of Section 4.3. That is, for stability, neither of the damping constants can be negative,

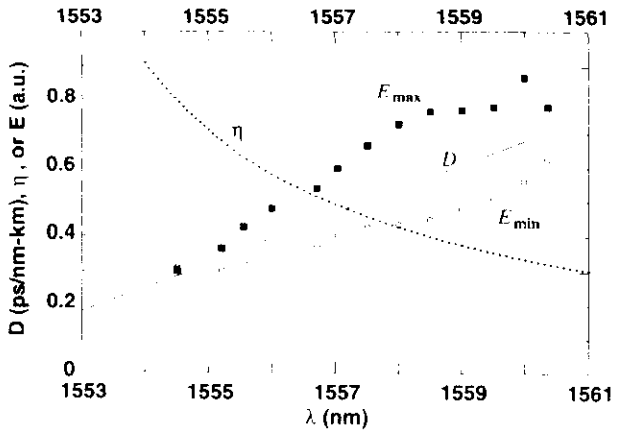

Fig. 12.29 Fiber dispersion D (*solid line*), filter strength parameter η (*dotted line*), and experimentally determined allowable soliton pulse energy limits E_{max} and E_{min} (*filled squares* and *open circles*, respectively), as functions of the signal wavelength λ, for a fixed sliding rate of 13 GHz/Mm.

so from Eq. (4.8), one has $|\Delta\Omega| \leq 1/\sqrt{6}$. From Eq. (4.6) or (4.6a), one then gets a maximum allowed sliding rate, ω_f', in soliton units. Finally, from Eq. (4.11b), one sees that, for fixed real sliding rate f' and for fixed D, ω_f' increases as the third power of the pulse width, and hence inversely as the third power of the pulse energy. Perhaps less abstractly, one can easily see that as the pulse energy is lowered, the rate at which the nonlinear term can alter the soliton's frequency will eventually become so low that it can no longer keep up with the filter sliding.

The existence of the upper limit, E_{max}, may be somewhat less obvious, but it has to do with the fact that eventually, as its energy is raised, the soliton's bandwidth, hence its loss from the filters, becomes too great. In this example, numerical simulation was helpful in elucidating the precise failure mechanism. Figure 12.31 shows the simulated pulse intensity evolution at $\eta = 0.4$ for different values of α_R. Note that for α_R below some critical value (here, ≈1.45/Mm), there is no stable solution, and the pulse disappears after some distance of propagation; this corresponds to the lower energy limit already discussed. Above this lower limit, there is a range of allowable values of α_R (between 1.5/Mm and 3.5/Mm in Fig. 12.31). Nevertheless, one can see nondecaying oscillations in the pulse intensity

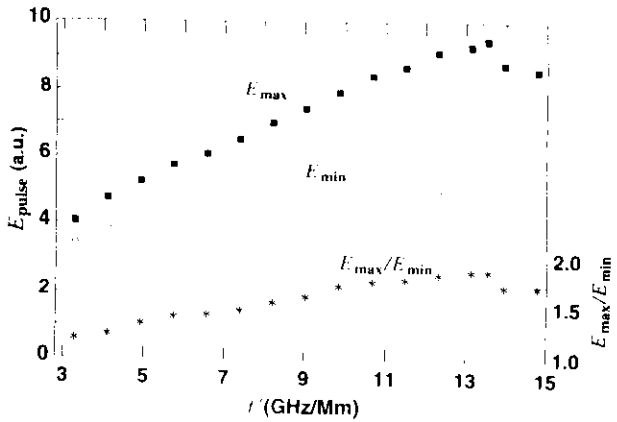

Fig. 12.30 Experimentally determined allowable soliton pulse energy limits E_{max} and E_{min} (*filled squares* and *open circles*, respectively), and their ratio (*asterisks*), as functions of the frequency-sliding rate f', for fixed, optimum filter strength parameter $\eta = 0.4$.

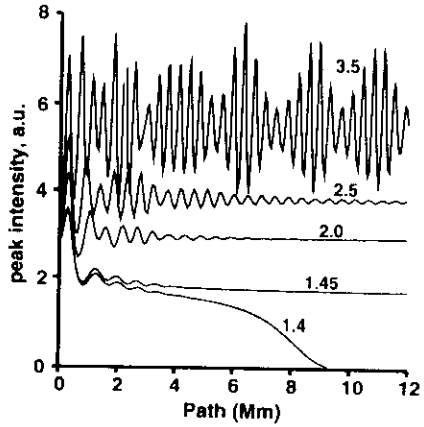

Fig. 12.31 Soliton peak intensities as a function of distance, as determined by numerical simulation, for filter strength $\eta = 0.4$ and for various of excess gain. The number next to each curve represents the excess gain parameter, α_R, in units of Mm^{-1}.

evolution for the higher values of α_R. These oscillations are due to a nonsoliton component, not completely removed by the sliding, and generated by the perturbing effects of the filtering and sliding themselves. If the excess gain is further increased, this nonsoliton component evolves into a second soliton. Clearly, this process determines the upper limit of the excess gain and of the soliton energy.

4.6 FILTERING IN TIME

Another form of optical regeneration for solitons involves the use of intensity modulators periodically placed along the transmission line and timed to open only during the middle of each bit period. The mean position in time of a pulse that is either early or late is thus guided back to the center of its bit period in a manner that is analogous to the guiding in the frequency domain provided by the etalon filters. Note, for example, that like frequency filtering, this "filtering in time" requires excess gain to overcome the loss imposed by the modulators, even to those arriving exactly on time. Unlike frequency filtering, however, filtering in time is not stable by itself; rather, it must always be accompanied by a proportional amount of frequency filtering. The principal advantage of filtering in time is that it corrects timing jitter directly, rather than indirectly as the frequency filtering does. When combined with filtering in the frequency domain, it can offer error-free transmission over an indefinitely long distance, at least in principle [22, 23].

Unfortunately, however, filtering in time shares several of the most fundamental disadvantages of electronic regeneration. First, it is incompatible with WDM. (To do WDM, at each regenerator the N channels must be demultiplexed, separately regenerated, and then remultiplexed, in a process that is at once extremely expensive and an engineering nightmare.) Second, each regenerator requires a quantity of active, failure-prone hardware, including clock recovery, adjustable delay lines, and modulator drive, in addition to the modulator itself. (Compare this with the extremely simple, inexpensive, stable, and strictly passive etalon filters of the pure frequency filtering.) At present, there are serious technical difficulties as well, such as the fact that nonchirping intensity modulators, whose insertion loss is polarization independent, simply do not exist. Combine all that with the fact that through massive WDM the sliding-frequency filters have already enabled a net capacity of nearly 100 Gb/s, whereas single-channel transmission at anything like that rate is at best formidably difficult, and filtering in time no longer looks economically or technically competitive for transmission. On the other hand, filtering in time might be useful in enabling long-term, fast-access data storage in large recirculating fiber loops.

4.7 LUMPED DISPERSION COMPENSATION AND FILTERING

From the discussion in Section 3.3 on the Gordon–Haus effect, we have seen how the fiber's dispersion converts the frequency displacements of the solitons into corresponding timing displacements (see Eq. [3.9]). Thus, to the extent that the accompanying pulse broadening can be tolerated, one might be tempted to consider using dispersion-compensating elements (either fiber having $D < 0$ or some equivalent lumped device) to reduce the net timing jitter. In principle, at least, postransmission dispersion compensation of $-\frac{1}{2}$ the total dispersion of the transmission line itself can reduce the standard deviation of timing jitter by a factor of 2 [24]. As the system length grows beyond a few times z_0, however, to prevent pulse broadening from exceeding the bit period, the compensating element must become weaker, and the jitter reduction correspondingly small. Because in most cases of interest the system is many times z_0 long, such dispersion compensation does not buy much improvement.

Very recently, however, Suzuki *et al.* [25] have shown how to make much better use of dispersion compensation. In their experiments, periodically along the transmission line, these researchers insert elements that compensate for 90–100% of the dispersion. In a system N amplifier spans long, and where there is complete compensation after each set of n amplifiers, one can easily show (again, see Eq. [3.9]) that the standard deviation of Gordon–Haus jitter should be reduced by a factor of n/N. In the experiments of Suzuki *et al.*, where $N \approx 300$ and $n = 10$, the Gordon–Haus jitter is thus greatly reduced. To the extent that timing jitter is the dominant source of errors, it is thus not surprising that transmission at 20 Gb/s was error free over as much as 14 Mm. What is surprising is that the pulses were apparently able to tolerate the huge periodic perturbation caused by the dispersion compensation. One would expect that perturbation to generate copious amounts of nonsoliton components. Indeed, apparently it is necessary to use filters as well [25], in order to suppress the growth of such nonsoliton fields. Because the optimum filter strength in this case is much weaker than with sliding-frequency filters, it is not surprising that the decrease in the Q factor with distance is primarily from amplitude jitter [25].

Because of third-order dispersion, any technique involving dispersion compensation tends to work only over a rather narrow wavelength band.

In addition, the discontinuity in D at each point of compensation would tend to wreak havoc with soliton–soliton collisions centered there. Thus, Suzuki *et al.*'s dispersion-compensation technique is likely not suitable for WDM. For single-channel transmission, however, it represents an intriguing concept, and one that may be of practical interest.

5. Wavelength-Division Multiplexing

5.1 SOLITON–SOLITON COLLISIONS IN WDM

In WDM, solitons of different channels gradually overtake and pass through each other. Because the solitons interact with each other then, the time of overlap is known as a *collision* (Fig. 12.32). An important parameter here is the collision length, L_{coll}, or the distance that the solitons must travel down the fiber together in the act of passing through each other. If L_{coll} is defined to begin and end with overlap at the half-power points, then transparently

$$L_{coll} = \frac{2\tau}{D\Delta\lambda}, \tag{5.1}$$

where $\Delta\lambda = \lambda_1 - \lambda_2$. For example, for $\tau = 20$ ps, $D = 0.5$ ps/nm-km, and $\Delta\lambda = 0.6$ nm, $L_{coll} = 133$ km.

The interaction stems, of course, from the nonlinear susceptibility, $\chi^{(3)}$ (see Section 2.3), or equivalently, from the nonlinear term in the NLS equation (Eq. [2.12a]). In a single-channel transmission, the only significant effect of that term is the *self-phase modulation* resulting from the self-induced index change at each pulse. During collisions, however, each pulse experiences an additional nonlinear index change as induced by the other pulse or pulses; as is detailed shortly, the resultant *cross-phase modulation* tends to produce shifts in the mean frequency, or group velocity, of the

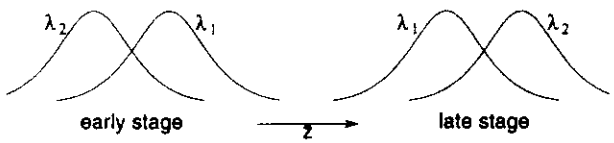

Fig. 12.32 Two stages of a soliton–soliton collision. Because of the anomalous group velocity dispersion, the shorter wavelength soliton (λ_2) gradually overtakes and passes through the longer wavelength one (λ_1).

affected pulse. Finally, the nonlinear term enables the colliding pulses to produce fields at the frequencies $\omega_S = 2\omega_1 - \omega_2$ and $\omega_A = 2\omega_2 - \omega_1$ (the Stokes and anti-Stokes frequencies, respectively) in the process known as *four-wave mixing*. In general, these effects have the potential to bring about a significant exchange of energy and momentum between the pulses and hence to create serious timing and amplitude jitter. Under the right conditions, however, with solitons the nonlinear effects are only transient — i.e., the solitons emerge from a collision with pulse shapes, widths, energies, and momenta completely unchanged. It is this potential for nearly perfect transparency to each other that makes solitons so well adapted for WDM.

5.2 COLLISIONS IN LOSSLESS AND CONSTANT-DISPERSION FIBER

It is useful first to consider the ideal case of lossless and constant-dispersion fiber. It is the simplest example of perfect transparency, and it is the easiest to analyze. It is of more than academic interest, however, because it can also serve as the paradigm for a number of practically realizable situations with real fibers and lumped amplifiers. In particular, it is the exact mathematical equivalent of the (at least approximately) realizable and practically important case of dispersion-tapered fiber spans (see Section 2.5.3).

The colliding solitions are written in the general form of Eq. (2.36), where, for simplicity, we set $A = 1$:

$$u_1 = \operatorname{sech}(t + \Omega_1 z)e^{i\Omega_1 t}e^{i(1-\Omega_1^2)z/2} \tag{5.2a}$$

$$u_2 = \operatorname{sech}(t + \Omega_2 z)e^{i\Omega_2 t}e^{i(1-\Omega_2^2)z/2}. \tag{5.2b}$$

Although the solitons' frequencies will change during the actual collision, and the difference between them is determined by their relative velocities, we are perfectly free to choose the zero of frequency. For convenience then, let us set $\Omega_2(-\infty) = -\Omega_1(-\infty) = \Omega \gg 1$; note that this makes the solitons move with equal but opposite velocities in the retarded time frame. Also note that this makes $L_{coll} = 1/\Omega$ ($= 1.762\ldots \times z_0/\Omega$ in ordinary units).

Now let us insert $u = u_1 + u_2$ into the NLS equation for lossless fiber, expand, and group the terms according to their frequency dependencies. As long as $\Omega \gg 1$, the various frequency terms are independent. Thus, we get four equations: one for each soliton and one each for the terms in $\pm 3\Omega$. The latter correspond to the aforementioned four-wave mixing components. Because for the special case under consideration these components are weak and disappear completely after the collision, they are neglected for

now. Assuming, for the moment, that the pulses are copolarized, the equation for u_1 is

$$\frac{\partial u_1}{\partial z} = i\frac{1}{2}\frac{\partial^2 u_1}{\partial t^2} + i|u_1|^2 u_1 + 2i|u_2|^2 u_1. \tag{5.3}$$

The first two terms on the right in Eq. (5.3) correspond to the NLS equation for the isolated pulse, u_1. The last term in Eq. (5.3) corresponds to the cross-phase modulation and is zero except when the pulses overlap. It produces a transient phase shift in u_1 at the rate

$$\frac{d\phi_1(z, t)}{dz} = 2|u_2(z, t)|^2.$$

The corresponding frequency shift $\omega_1(z, t) = \partial\phi_1/\partial t$ in u_1 is thus induced at the rate

$$\frac{\partial\omega_1}{\partial z} = \frac{\partial}{\partial z}\frac{\partial\phi_1}{\partial t} = \frac{\partial}{\partial t}\frac{\partial\phi_1}{\partial z} = \frac{\partial}{\partial t}(2|u_2|^2). \tag{5.4}$$

Note that this induced frequency shift is not uniform across the pulse. Nevertheless, the soliton retains its shape, and we want the shift in its inverse group velocity. Now it can be shown rigorously that the inverse group velocity is given by (-1 times) the mean frequency of the pulse. Thus, we really want $\delta\Omega_1 = \langle\omega_1\rangle$, the time-averaged frequency of u_1.

Using the weighting factor $|u_a(t)|^2$, and using the fact that $\int_{-\infty}^{\infty} \operatorname{sech}^2(x)\, dx = 2$, one obtains

$$\begin{aligned}\frac{\partial\Omega_1}{\partial z} &= 2\int_{-\infty}^{\infty} |u_1|^2 \frac{\partial}{\partial t}|u_2|^2\, dt \\ &= \int_{-\infty}^{\infty} \operatorname{sech}^2(t + \Omega_1 z)\frac{\partial}{\partial t}\operatorname{sech}^2(t + \Omega_2 z)\, dt.\end{aligned} \tag{5.5}$$

(Interchanging subscripts in Eq. (5.5) yields a similar expression for $\partial\Omega_2/\partial z$.)

Equation (5.5) (multiplied by -1) represents the "acceleration" — i.e., the rate of change of inverse group velocity with distance into the collision. All that remains now is to evaluate Eq. (5.5) and the corresponding inverse velocity shift. Because for $\Omega \gg 1$, $\delta\Omega/\Omega \ll 1$, in the integrals, we can replace Ω_1 and Ω_2 by their initial values. Equation (5.5) can then be rewritten as

$$\frac{\partial\Omega_{(1,2)}}{\partial z} = (-, +)\frac{1}{2\Omega}\frac{d}{dz}\int_{-\infty}^{\infty} \operatorname{sech}^2(t - \Omega z)\operatorname{sech}^2(t + \Omega z)\, dt. \tag{5.5a}$$

Equation (5.5a) is now easily integrated to yield the inverse velocity shift:

$$\delta\Omega_{(1,2)} = (-, +)\frac{1}{2\Omega}\int_{-\infty}^{\infty} \operatorname{sech}^2(t - \Omega z)\operatorname{sech}^2(t + \Omega z)\, dt \tag{5.6}$$

$$= (-, +)\frac{2}{\Omega}\frac{[2\Omega z\cosh(2\Omega z) - \sinh(2\Omega z)]}{\sinh^3(2\Omega z)}. \tag{5.6a}$$

Finally, Eq. (5.6) can be integrated over z to yield the net time displacements:

$$\delta t_{(1,2)} = (+, -)\,\Omega^{-2}. \tag{5.7}$$

The preceding expressions for the acceleration and the inverse velocity shift (Eqs. [5.5] and [5.6]) may not be particularly transparent. When numerically evaluated and graphed, however, they are seen to be simply behaved (see Fig. 12.33). Note, either from the graph in Fig. 12.33 or from the pertinent equations, that the pulses attract each other, whereas their frequencies repel each other. Also note that, as purported, the completed collision leaves the soliton intact, with the same velocity and other properties that it had before the collision. Thus, the only change is the time shift, δt. As is shown later, however, the guiding filters tend to remove even that defect.

The discussion in this section has thus far been almost entirely in terms of soliton units. For convenient future reference, however, we now list formulas for the principal quantities in practical units. First, in terms of the full-channel separation Δf and the pulse width τ, the half-channel separation in soliton units is

$$\Omega = 1.783\,\tau\Delta f. \tag{5.8a}$$

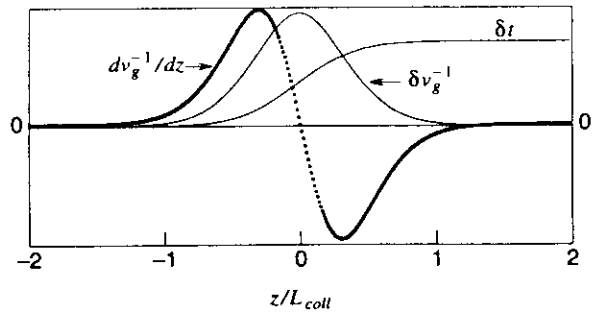

Fig. 12.33 Acceleration (dv_g^{-1}/dz), velocity shift ($\delta v_g^{-1} = -\delta\Omega$), and time shift ($\delta t$) of the slower pulse, during a soliton–soliton collision in a lossless fiber. (For the faster [higher frequency] pulse, turn this graph upside down.) The maximum inverse group velocity shift $(\delta v_g^{-1})_{max} = 2/(3\Omega)$, and $\delta t_{max} = \Omega^{-2}$.

The maximum frequency shift during the collision, δf, and the net time displacement, δt, when expressed in practical units, are, respectively,

$$\delta f = \pm \frac{0.105}{\tau^2 \Delta f} \tag{5.8b}$$

and

$$\delta t = \pm \frac{0.1786}{\tau \Delta f^2}. \tag{5.8c}$$

(In this case, the numerical coefficients are all dimensionless and represent various combinations of $\tau/t_c = 1.762\ldots$ and π.) For example, consider a collision between 20-ps solitons in channels separated by 75 GHz (0.6 nm). Then Eqs. (5.8a) through (5.8c) yield, respectively, $\Omega = 2.67$ (more than large enough for effective separation of the soliton spectra), $\delta f = \pm 3.5$ GHz, and $\delta t = \pm 1.59$ ps.

5.3 EFFECTS OF PERIODIC LOSS AND VARIABLE DISPERSION

The periodic intensity fluctuations in a system with real fiber and lumped amplifiers can serve to destroy the perfect asymmetry of the acceleration curve of Fig. 12.33, and hence result in a net residual velocity shift and associated timing displacement [26]. For the purposes of illustration, Fig. 12.34 shows an extreme case, where the collision length is short relative to the amplifier spacing, and where the collision is centered at an amplifier. Note that just prior to the amplifier, where the intensity is low, the acceleration curve is correspondingly attenuated, whereas just the opposite happens in the space immediately following the amplifier. Thus, most of the integral of the acceleration curve comes from the right half of the graph, and, as a result, there is a large residual velocity (frequency) shift. The residual frequency shift in this example (~4 GHz) is large. Note that when its wavelength equivalent is multiplied by $D = 0.8$ ps/nm-km and by a characteristic filter damping length of say, 600 km, the resultant time shift is approximately 15 ps. When further magnified by the typical spread of nearly zero to at least several tens of collisions in a transoceanic length, that time shift would result in a completely disastrous timing jitter.

On the other extreme, where the collision length is large relative to the amplifier spacing, one might reasonably expect the velocity curve to look much like that of Fig. 12.33. For example, Fig. 12.35 shows what happens

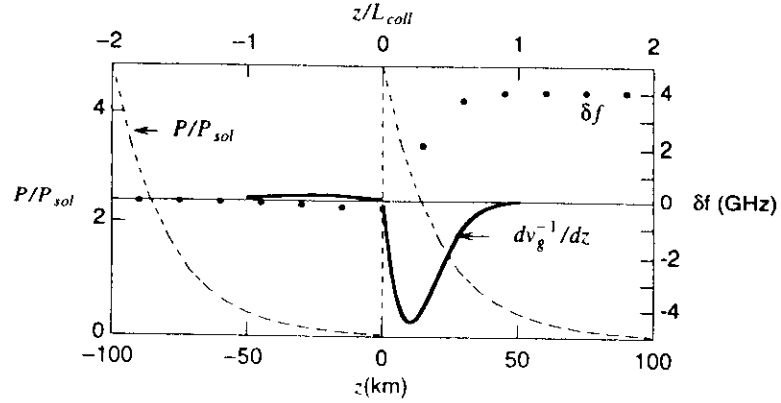

Fig. 12.34 Acceleration (*heavy curve*) and frequency shift ($\propto dv_g^{-1}$) (*dots*) for a collision centered at an amplifier, and where $L_{coll} \ll L_{amp}$ (i.e., 50 vs. 100 km). The *dashed lines* show the relative intensities in each span. The other pertinent parameters here are: $\tau = 16$ ps, $D = 0.8$ ps/nm-km, and $\Delta\lambda = 0.8$ nm ($\Delta f = 100$ GHz). Note the severe asymmetry of the acceleration curve and the resultant large residual velocity shift.

when L_{coll} is just $2.5L_{amp}$. Although the acceleration curve in Fig. 12.35 contains large discontinuities at each amplifier, its integral looks remarkably close to the ideal velocity curve (Fig. 12.33). Most important, the velocity returns almost exactly to zero following the collision. Extensive numerical

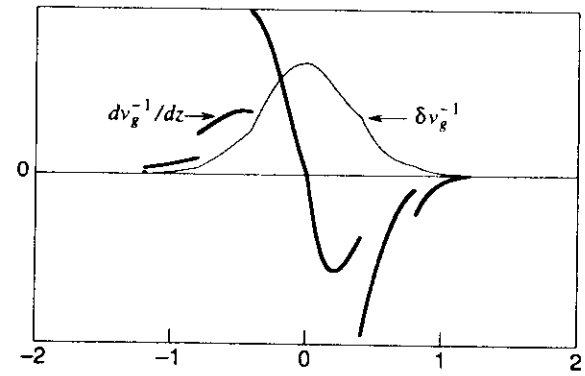

Fig. 12.35 Acceleration and velocity shift for a collision centered at an amplifier, in constant D fiber, and where $L_{coll} = 2.5L_{amp}$. Note how the velocity curve here closely approximates the ideal of lossless fiber (Fig. 12.33).

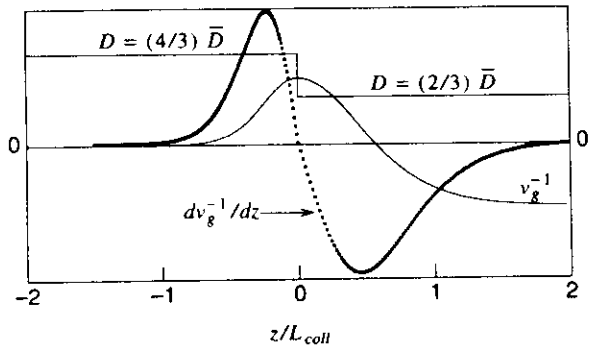

Fig. 12.36 Acceleration and velocity curves for a collision centered at an discontinuity in D, and where, for simplicity, the fiber is lossless.

simulation and related analysis [26] both show that the residual velocity is essentially zero as long as the condition

$$L_{coll} \geq 2L_{amp} \tag{5.9}$$

is satisfied. Note that this condition, combined with Eq. (5.1), puts an upper bound on the maximum allowable channel spacing:

$$\Delta\lambda_{\max} = \frac{\tau}{DL_{amp}}. \tag{5.10}$$

For example, let $\tau = 20$ ps, $D = 0.5$ ps/nm-km, and $L_{amp} = 33$ km. Equation (5.10) then yields $\Delta\lambda_{\max} \approx 1.2$ nm; with a nearest channel wavelength spacing of 0.6 nm, the maximum allowable number of channels is just three. As is shown later, however, this limit can be circumvented.

Variation in the fiber's chromatic dispersion can also upset the symmetry of the collision. For example, Fig. 12.36 illustrates what happens when the collision is centered at a discontinuity in D. To keep the example pure, the fiber is lossless. Note the different length scales on either side of the discontinuity in D. These occur, of course, because the length scale for the collision, or for any part of it, is L_{coll}, which is in turn inversely proportional to D (see Eq. [5.1]).

5.4 DISPERSION-TAPERED FIBER SPANS

From the discussion in Section 5.3, note that a decrease in the acceleration, from decreasing intensity, can be compensated for by a corresponding increase in L_{coll}, hence by a decrease in D. Thus, if the dispersion-tapered

fiber spans discussed in Section 2.5.3 were used, it should be clear that the resultant curves of acceleration and velocity (as plotted in soliton units) will look exactly like the symmetrical ideal of Fig. 12.33. Formally, the NLS equation for real fiber with dispersion tapering can be transformed into that for lossless fiber with constant dispersion (see Ref. 26, Appendix). Thus, with that one transformation, it can be seen that the use of dispersion-tapered fiber spans removes *all* perturbing effects stemming from the use of lumped amplifiers. This idea is extremely important for the achievement of massive WDM with solitons.

Fiber spans having the ideal exponential taper in D are not yet available commercially. Thus, at present it is usually necessary to use a stepwise approximation. Figure 12.37 illustrates the optimum three-step approximation to the ideal taper. The length of each step is inversely proportional to the D value of the step. Note that this makes the steps all have equal lengths, as measured in soliton units. Also note that using such an N-step approximation to the ideal dispersion taper increases the limit on maximum channel spacing imposed by Eq. (5.10) by a factor of N. That is, one now has

$$\Delta\lambda_{\max} = \frac{N\tau}{DL_{amp}}. \tag{5.10a}$$

In practice, once N is large enough, the intensity variation over each step becomes so small that the perturbations become acceptably small in any event. In that case, the "limit" of Eq. (5.10a) is no longer significant.

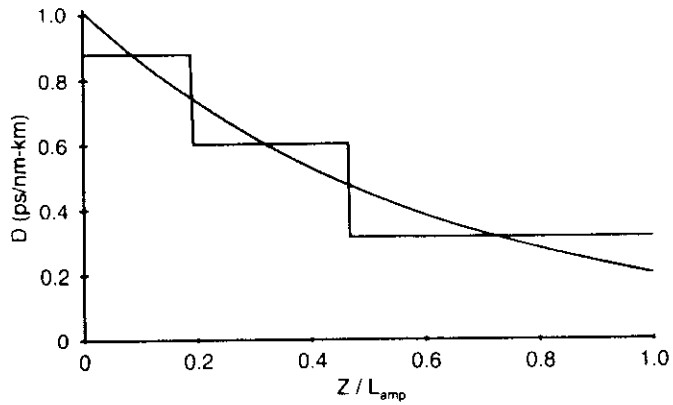

Fig. 12.37 Ideal exponential taper of D and the best three-step approximation to it for a fiber span with $L_{amp} = 33.3$ km and a loss rate of 0.21 dB/km.

5.5 FOUR-WAVE MIXING IN WDM

In Section 5.2, we were able to ignore the terms (in $\pm 3\Omega$) that result from four-wave mixing. In general, however, pseudo phase matching from the periodic intensity fluctuations associated with the use of lumped amplifiers can enable the four-wave mixing products to grow to high levels [27]. Very serious timing and amplitude jitter can then result. Thus, it is necessary to consider four-wave mixing carefully.

There are three possible four-wave mixing processes:

$$2\Omega_1 - \Omega_2 \rightarrow \Omega_S \tag{5.11a}$$

$$2\Omega_2 - \Omega_1 \rightarrow \Omega_A \tag{5.11b}$$

$$\Omega_1 + \Omega_2 - \Omega_S \rightarrow \Omega_A. \tag{5.11c}$$

The spectrum associated with these processes is shown in Fig. 12.38. In the first two processes, two photons from one of the strong fields mix with one from the other strong field, to create either a Stokes or an anti-Stokes photon. In the third process, one photon each at Ω_1, Ω_2, and Ω_S (or Ω_A) combine to form a photon at Ω_A (or Ω_S).

Note that the first two of these processes are dominant because three of the fields involved are initially nonzero. For these processes, the phase mismatch is

$$\begin{aligned} \Delta k &= (k_2 + k_S - 2k_1 \text{ or } k_1 + k_A - 2k_2) \\ &= \left.\frac{\partial^2 k}{\partial \omega^2}\right|_{1,2} \Delta\omega^2 = -\frac{\lambda^2 D(\lambda_{1,2})}{2\pi c}\Delta\omega^2, \end{aligned} \tag{5.12}$$

where the subscripts 1,2 apply to the processes in Eqs. (5.11a) and (5.11b), respectively. It is important that Eq. (5.12) is completely independent of third-order dispersion and of the choice of zero frequency.

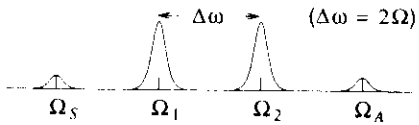

Fig. 12.38 Spectrum of source fields and their four-wave mixing products at Ω_S and Ω_A.

When the fields at Ω_1 and Ω_2 are continuous waves, the four-wave mixing products grow as

$$\frac{dE_i}{dz} \propto E_j^2 E_k^* \exp(i\,\Delta k z), \tag{5.13}$$

where the set of subscripts i,j,k on the field quantities E is either S,1,2 (process in Eq. [5.11a]) or A,2,1 (process in Eq. [5.11b]), and z is the distance along the fiber. Note that the phase of the generated product is periodic in z, with period $L_{res} = 2\pi/\Delta k$, as a result of the phase mismatch. For a lossless fiber with constant dispersion (i.e., where $E_{1,2}(z) = const$, and $\Delta k = const$), Eq. (5.13) is readily integrated to yield

$$E_i(z) \propto \frac{E_j^2 E_k^*}{i\,\Delta k}[\exp(i\,\Delta k z) - 1], \tag{5.14}$$

a field that merely oscillates between zero and a fixed maximum and never grows.

Nevertheless, if the transmission line has periodic perturbations with k_{pert} in resonance with the phase mismatch of the four-wave mixing, i.e., when

$$N k_{pert} = \Delta k, \qquad (N = 1, 2, 3, \ldots), \tag{5.15}$$

then one has pseudo phase matching, and the four-wave mixing product can grow steadily. The perturbations can correspond to the gain–loss cycle whose period is the amplifier spacing, L_{amp}, and/or to periodic variations of the fiber parameters (dispersion, mode area). For the case of lumped amplifiers, $k_{pert} = 2\pi/L_{amp}$, and the pseudo-phase-matching conditions are met when

$$L_{amp} = N L_{res} \equiv 2\pi N/\Delta k. \tag{5.16}$$

Although four-wave mixing generation during a soliton–soliton collision is more complicated than with continuous waves, the basic features remain the same. Figure 12.39 shows the numerically simulated growth in energy of the four-wave mixing products at $\omega_{A,S}$ during a single collision of two solitons. (The particular parameters represented in Fig. 12.39 are those of recent experiments [28, 29], viz., $\tau = 20$ ps, adjacent channel separation $\Delta f = 75$ GHz [$\Delta\lambda = 0.6$ nm at $\lambda = 1556$ nm], and where the path-average dispersion $\overline{D} = 0.5$ ps/nm-km.) For these parameters, $L_{res} = 44.4$ km. Note that for the case of lossless fiber of constant dispersion, and for the case of real fiber with exponentially tapered dispersion, the four-wave mixing energy disappears completely following the collision. Also note that because

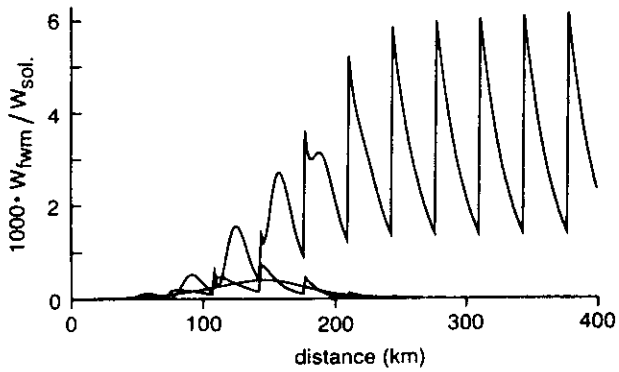

Fig. 12.39 Growth of four-wave mixing energy during a single soliton–soliton collision, for three conditions: lossless fiber with constant dispersion (*small, smooth curve*); real fiber with lumped amplifiers spaced 33.3 km apart and exponentially tapered dispersion (*small, jagged curve*); real fiber with lumped amplifiers spaced 33.3 km apart and constant dispersion (*large, jagged curve*). The four-wave mixing energy is for a single sideband and is normalized to the soliton pulse energy. Note that for the first two cases, the four-wave mixing energy disappears completely following the collision, whereas for the third case, where there is effective pseudo phase matching, the four-wave mixing energy builds to a large residual value.

the solitons have finite temporal and spectral envelopes, and because of the effect of cross-phase modulation (which shifts the pulses' carrier frequencies during the collision), the oscillations of the four-wave mixing energy with the period of L_{cell} are almost completely washed out. Finally, for the case of real fiber with constant dispersion, note that the collision produces a residual four-wave mixing energy several times larger than the (temporary) peak obtained with lossless fiber.

Although the residual energy from the pseudo-phase-matched collision of Fig. 12.39 may seem small, the fields from a succession of such collisions can easily build to a dangerously high value. Such uncontrolled growth of the four-wave mixing imposes penalties on the transmission by two mechanisms. First, because the energy represented by the four-wave mixing fields is not reabsorbed by the solitons, the solitons tend to lose energy with each collision. Because the net energy loss of a given soliton depends on the number of collisions it has suffered, and upon the addition of four-wave mixing fields with essentially random phases, it directly creates amplitude jitter. The energy loss leads to timing jitter as well, both through the intimate coupling between amplitude and frequency inherent in filtered

systems, and through its tendency to asymmetrize the collision, and hence to induce net velocity shifts. Finally, certain noise fields in the same band with the four-wave mixing products can influence the soliton's frequencies, in a kind of extended Gordon–Haus effect. Thus, even in a two-channel WDM, there can be serious penalties (see Fig. 12.40). Moreover, if the wavelengths of the four-wave mixing products coincide with the wavelengths of other WDM channels (possibly only when three or more channels exist), the runaway four-wave mixing becomes an additional source of noise fields to act on those channels. In that way, the well-known amplitude and timing jitter effects of spontaneous emission are enhanced.

The growth of four-wave mixing can often be controlled adequately with the use of one or another of the N-step approximations to the ideal exponential dispersion taper discussed in Section 5.4. Figure 12.41 plots the residual four-wave mixing intensity resulting from a single collision, as a function of L_{amp}, for various numbers of steps in D per L_{amp}, for the channel separation of 0.6 nm, and for the $\tau = 20$ ps solitons and $\overline{D} = 0.5$ ps/nm-km of Fig. 12.33. Figure 12.42 does the same, but for twice the channel separation (1.2 nm). First, note that the intensity scale in Fig. 12.41 is approximately a factor of $2^5 = 32$ times that of Fig. 12.42, just as implied by Eqs. (5.12) and (5.14) and by the fact that L_{coll} scales inversely as the channel spacing. This scaling is easily generalized; for channels spaced n

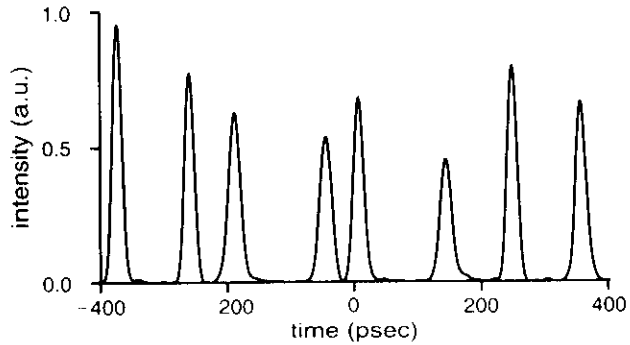

Fig. 12.40 Pulses that have traversed a 10-Mm transmission line with L_{amp} = 33 km and constant D = 0.5 ps/nm-km, and that have undergone collisions with an adjacent channel, 0.6 nm away, containing all ones. In this numerical simulation, there were no guiding filters. A small seed of noise was added, but only in the four-wave mixing sidebands; thus, the large amplitude and timing jitter seen here is from the uncontrolled growth of four-wave mixing alone.

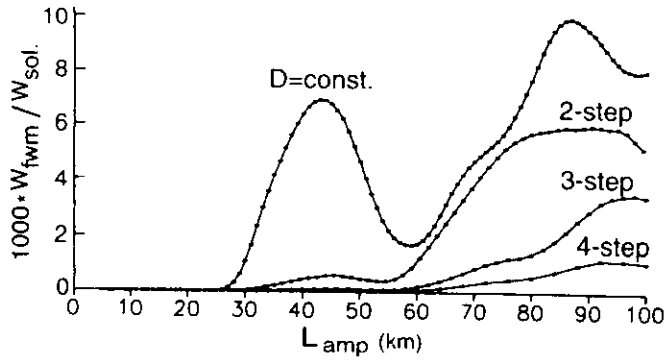

Fig. 12.41 Residual four-wave mixing energy following a single collision of 20-ps solitons in channels spaced 0.6 nm apart in a chain of fiber spans with $\overline{D} = 0.5$ ps/nm-km, as a function of the amplifier spacing, for constant D and for the optimal two-, three-, and four-step approximations to the ideal exponential taper. The four-wave mixing energy is for a single sideband and is normalized to the soliton pulse energy. No noise seed was used in these simulations.

times the adjacent channel spacing, the four-wave mixing intensity should scale as n^{-5}. This apparently rapid falloff in four-wave mixing effect is tempered somewhat by the fact that the number of collisions tends to increase as n, and that it is really the vector addition of residual field quantities from at least several successive collisions that is to be feared in this case. Also note that the number of steps required for total suppression

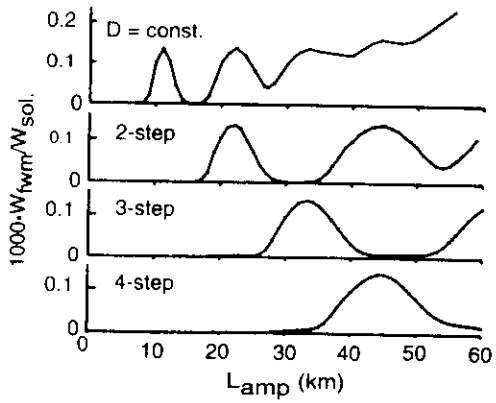

Fig. 12.42 The same setup as Fig. 12.41, except the channel spacing is twice as great; i.e., it is 1.2 nm.

of the four-wave mixing intensity increases with wider channel spacing. For example, in Fig. 12.41, just two steps are required for L_{amp} in the neighborhood of 30 km, whereas four steps are required for the same in Fig. 12.42. Finally, note that because of the finite nature of the pulse widths and collision lengths, the resonances in Figs. 12.41 and 12.42 are fairly broad.

5.6 *CONTROL OF COLLISION-INDUCED TIMING DISPLACEMENTS*

With the use of dispersion-tapered fiber spans, the only major penalty in WDM comes from the collision-induced timing displacements given by Eq. (5.7) or Eq. (5.8c). Because some pulses undergo dozens of collisions whereas others undergo nearly none in the course of a transoceanic transmission, the resultant timing jitter can be substantial, even when the time displacement from a single collision is no more than a picosecond or two. It so happens, however, that the frequency guiding filters nearly eliminate that jitter as well [30]. The argument can be made as follows.

First, to simplify the notation, let $\delta v_g^{-1} \to v$, and $\partial v_g^{-1}/\partial z \to a$. Without filtering, let the colliding solitons accelerate each other by $a_0(z)$, whose first z integral is $v_0(z)$, and whose second z integral is $t_0(z)$. We require only that the completed collision leave no residual velocity shift (see Fig. 12.35, for example). Thus,

$$v_0(\infty) = \int_{-\infty}^{\infty} a_0(z)\, dz = 0. \tag{5.17}$$

For simplicity, we assume that the filters are continuously distributed and that they provide a damping (acceleration) $a_d = -\gamma v = -v/\Delta$, where γ and Δ are the damping constant and characteristic damping length, respectively (see Eq. [4.8]). The equation of motion then becomes

$$\frac{dv}{dz} = a_0(z) - v(z)/\Delta. \tag{5.18}$$

Equation (5.17) can be rewritten as

$$v(z) = \left[a_0(z) - \frac{dv}{dz}\right]\Delta. \tag{5.18a}$$

To get t, we simply integrate Eq. (5.18a):

$$t(z) = \int_{-\infty}^{z} v(x)\,dx = \Delta \times \int_{-\infty}^{z} \left[a_0(x) - \frac{dv}{dx}\right] dx. \qquad (5.19)$$

We are primarily interested in $t(\infty)$:

$$t(\infty) = \Delta \times \int_{-\infty}^{\infty} a_0(x)\,dx - \Delta \times \int_{\infty}^{\infty} dv. \qquad (5.19a)$$

The first term on the right is equal to zero by virtue of Eq. (5.17). The second term is just $v(\infty)$, which for a filtered system with no excitation beyond a certain point must equal zero. Figure 12.43 shows the quantities $a_0(z)$, the δf corresponding to $-v(z)$, and $t(z)$, numerically simulated for the case of lumped filters. One can see from this figure how the timing displacement is nulled: the filters reduce the maximum frequency (velocity) shift, so that the acceleration in the second half of the collision causes an overshoot in frequency; the area under the long tail of the frequency curve thus produced just cancels the area under the main peak.

Real filters, such as etalons, do not always perform exactly as in the simplified model just discussed. First, with real filters the damping force is not always strictly proportional to $-v$, or, equivalently, to δf. Second, the time delay through the filters exhibits a certain dispersion as the signal frequency moves off the filter peak. Nevertheless, numerical simulation shows that the etalons used in the theoretical examples and in the experi-

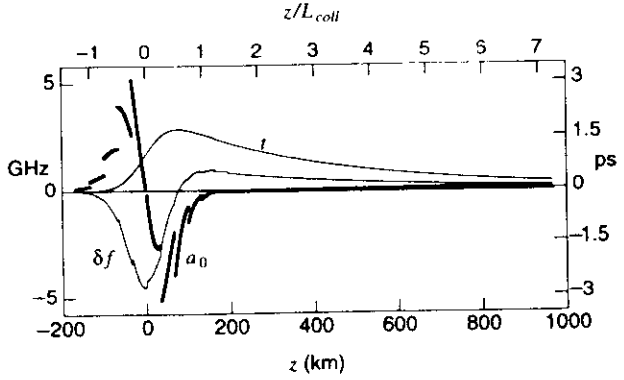

Fig. 12.43 The frequency and time shifts, as a function of distance, resulting from a collision in a transmission line with lumped amplifiers and lumped filters spaced 33.3 km apart. The other parameters are as follows: D = 0.5 ps/nm-km; τ = 20 ps; channel spacing, $\Delta\lambda$ = 0.6 nm; damping length, Δ = 400 km.

ments cited here tend to cancel out at least 80% of the timing displacements. That large improvement has turned out to be sufficient for most purposes.

5.7 EFFECTS OF POLARIZATION

Thus far in the discussion, we have assumed that the colliding pulses are copolarized. It is important to note, however, that all the effects discussed so far (cross-phase modulation and four-wave mixing) are significantly affected by polarization, and all in the same way. Although we defer a full-blown discussion of polarization until the following seciton, the state of affairs can be summarized as follows: First, just as for the path-average solitons (Section 2), the residual birefringence of even the highest quality transmission fibers available at present is large enough that over the (tens or hundreds of kilometers long) path of a single collision, the Stokes vectors representing the polarization states of the individual pulses tend to rotate, more or less at random, many times over and around the Poincaré sphere. Thus, in that way, the polarization tends to be well averaged over a representative sample of all possible states during a collision. On the other hand, the relative polarization — i.e., the angle between the Stokes vectors — of the colliding pulses tends to be only mildly affected. (The relative polarization is affected by two factors: the dispersion in the fiber's linear birefringence and, as is detailed in Section 6, a nonlinear birefringence induced by the collision itself.) Thus, even in the worst case, to first order at least, one can treat the relative polarization during a collision as a constant, so polarization does not significantly affect the symmetries of the collision. Nevertheless, under those conditions (of thorough averaging over absolute polarization states, while relative polarization states are preserved), the frequency shifts induced by cross-phase modulation and the intensities of four-wave mixing products are both just half as great for orthogonally polarized pulses as they are for copolarized pulses. This fact is of obvious practical importance.

5.8 GAIN EQUALIZATION WITH GUIDING FILTERS

The inevitable variation of amplifier gain with wavelength presents a problem for WDM, one that becomes ever more serious with increasing system length. In linear transmission (such as NRZ), where no self-stabilization of the pulse energies is possible, custom-designed, wavelength-dependent loss elements must be inserted periodically along the line to try to compensate for the variable amplifier gain. Even then, however, in practice it has

proven difficult to maintain even approximately equal signal levels among the various channels. For soliton transmission using guiding filters, however, the guiding filters themselves provide a powerful built-in feedback mechanism for controlling the relative strengths of the various signal channels in the face of variable amplifier gain. As should be evident from the discussion of guiding filters already presented (Section 4), the control stems from the fact that the guiding filters provide a loss that increases monotonically with the soliton bandwidth, and hence with the soliton energy. Thus, for a channel having excess amplifier gain, a modest increase in soliton energy quickly creates a compensating loss, and the signal growth is halted.

Because the soliton bandwidth scales as $\tau^{-1} \propto W/D$, where W is the soliton pulse energy (see Eq. [2.16]), the soliton's energy loss from the guiding filters can be written as a monotonically increasing function of (W/D). For Gaussian filters, the relation $f(W/D)$ is quadratic; for the shallow etalon filters used in practice, however, $f(W/D)$ is more nearly linear. The energy evolution of N WDM channels in a soliton transmission line with sliding filters can then be described by the following system of coupled nonlinear equations [31]:

$$\frac{1}{W_i}\frac{dW_i}{dz} = \frac{\alpha_i}{1 + mR(W_1 + W_2 + \ldots + W_N)/P_{sat}} - \alpha_{Li} - f(W_i/D_i). \tag{5.19}$$

The subscript $i = 1, \ldots, N$ identifies the particular channel, $W_i(z)$ is its energy, α_i is its small-signal gain coefficient, α_{Li} is its linear loss rate, m is the mark-to-space ratio (usually one-half), R is the per-channel bit rate, P_{sat} is the saturation power of the amplifiers, and $D_i(z)$ is the dispersion at the ith channel wavelength (the dispersion could change with distance z as a result of the combined action of the frequency sliding and third-order dispersion). Note that the Eq. (5.19) fixes the equilibrium values of W_i/D_i according to the various α_i. Thus, when the α_i are all nearly the same, the various channel energies will scale in direct proportion to $D(\lambda)$. In the usual situation where the third-order dispersion is essentially a constant, the channel energies will be in direct proportion to their separation in wavelength from λ_0, the wavelength of zero D. It should also be noted that Eq. (5.19) is essentially the same as Eq. (4.5a), with the frequency offset term omitted. (Recall that in soliton units, one has $W = A$ [not $W = A^2$], and recognize that the quantity α in Eq. [4.5a] is just a compact way of writing the sum of the first two terms on the right-hand side of Eq. [5.19]. Finally, for Gaussian filters, $f[W/D] = const. \times W^2$.) Thus, just as

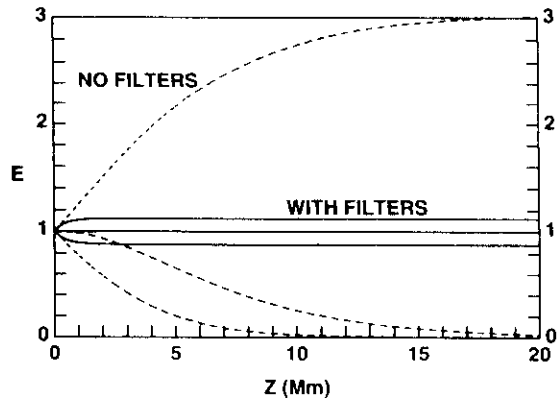

Fig. 12.44 Growth with distance of signal pulse energies in WDM channels having relative gain rates of ±1 and 0 dB/Mm, respectively, for a system using sliding-frequency filters (damping length Δ = 400 km), and for no filters at all.

a linearized version of Eq. (4.5a) was shown to be a damping equation, the linearized version of Eq. (5.19) is essentially the same damping equation, with $W\, df/dW$ as the damping constant. Thus, one has

$$W\frac{df}{dW} = \frac{1}{\Delta}, \tag{5.20}$$

where, at least for Gaussian filters, Δ is the same characteristic damping length as discussed in Section 4.3.

Figure 12.44 shows the solution to Eq. (5.19) for the case of three channels with significantly different small-signal gain rates, both with and without filters. Note how the filters quickly lock the signal energies to tightly clustered equilibrium values. By contrast, the large divergence in channel energies that occurs when no filters are used will clearly lead to large penalties and disastrous error rates. Thus, the ability of the guiding filters to regulate the relative channel energies constitutes a major and very important advantage for solitons over all other possible modes of WDM.

5.9 *EXPERIMENTAL CONFIRMATION*

Recently, the ideas in this section have been put to extensive test in transmission involving massive WDM at per-channel rates of 5 and 10 Gb/s (with the major emphasis on the greater rate) [28, 29]. Whereas many aspects of the transmissions were monitored, the ultimate criterion of success was

to achieve measured BER rates of 1×10^{-9} or less on all channels over at least the trans-Pacific distance of 9 Mm.

Figure 12.45 is an overall schematic of the signal source. The soliton pulse shaper, based on a $LiNbO_3$ Mach–Zehnder-type modulator, both carves out the pulses and provides them with a controlled and desired chirp [32]. (A simple phase modulator, driven sinusoidally at the bit rate, was also used successfully, as an alternative to the pulse shaper. The idea in this case is that whenever the upper or lower sidebands created by the phase modulator are selected by a suitable filter, one obtains a train of nearly sech-shaped pulses suitable for soliton transmission [33]. In this example, the filtering action of the transmission line itself provides the necessary sideband selection.) After a second modulator imposes the data (a 2^{15}-bit, random pattern), the 4-km length of standard fiber ($D \sim 17$ ps/nm-km at 1557 nm) compresses the pulses to about 20 ps; it also separates the bits of adjacent channels by 40 ps. This separation prevents the occurrence of half-collisions at the input to the transmission line for all but the most widely spaced channels. Finally, the 3.7-m length of polarization-maintaining fiber, used as a multiple half-wave plate, enables adjacent channels to be launched with orthogonal polarizations.

The orthogonal polarizations provide two significant benefits: First, they reduce the interchannel interaction by a factor of 2 over that obtaining with copolarization states. Second, at least where the number of channels is even, the net optical power in the transmission line is essentially unpolarized, so the amplifiers exhibit no significant polarization-dependent gain from polarization hole burning. Thus, there is no need for polarization scrambling of the individual channels. There is more here than just the

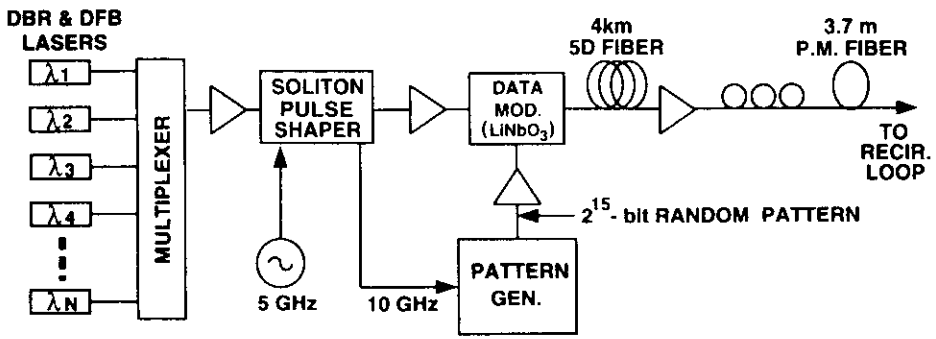

Fig. 12.45 Source for soliton WDM experiments at 10 Gb/s per channel. DBR, dis-

avoidance of unnecessary and expensive hardware, however, because the fiber's birefringence tends to convert polarization scrambling into timing jitter. Therefore, unless it is needed (as with NRZ) to avoid serious polarization hole burning, polarization scrambling is a detriment and is thus to be avoided.

It should also be noted that the order of the pulse shaper and the data modulator is of no consequence. In a real system, of course, prior to multiplexing, each continuous-wave (CW) laser source would be followed by its own individual data modulator. Thus, for soliton transmission, schematically one just has a WDM NRZ source, followed by a common soliton pulse shaper. In a source for true NRZ transmission, however, one must use expensive $LiNbO_3$, Mach–Zehnder-type modulators, symmetrically driven to avoid significant chirping at the transition points between ones and zeros. For soliton transmission, on the other hand, one could just as well use a set of semiconductor absorption modulators, with their absence of significant bias drift and their potentially much lower cost. This exchange is possible because in removing all but the center of each NRZ bit, the soliton pulse shaper also tends to get rid of all chirping induced by the data modulators. Thus, in this way the soliton transmission has an advantage over NRZ that is significant both economically and in the strictly technical sense.

The recirculating loop contains six spans of 33.3 km each between (Er fiber) amplifiers, each span dispersion-tapered typically in three or four steps, with span path-average value $\overline{D} = 0.5 \pm 0.05$ ps/nm-km at 1557 nm. Two of every three loop amplifiers are immediately followed by piezo-driven, Fabry–Perot etalon filters, each having a 75-GHz (0.6 nm at 1557 nm) free spectral range and mirror reflectivities of 9%; this combination provides the optimum path-average filter strength of $\eta \sim 0.4$ at 1557 nm (Fig. 12.46).

At the receiver, the desired 10-Gb/s channel is first selected by a wavelength filter and is then time-division demultiplexed to 2.5 Gb/s by a polarization-insensitive electrooptic modulator having a 3-dB bandwidth of 14 GHz [34] and driven by a locally recovered clock (Fig. 12.47) The demultiplexer provides a nearly square acceptance window in time, one bit period wide.

Figure 12.48 shows a typical set of BER data. Note the tight clustering of the BER performance for all channels.

Figure 12.49 plots the measured error-free distances versus the number, N, of 10-Gb/s channels. For each of these points, the BER was better than

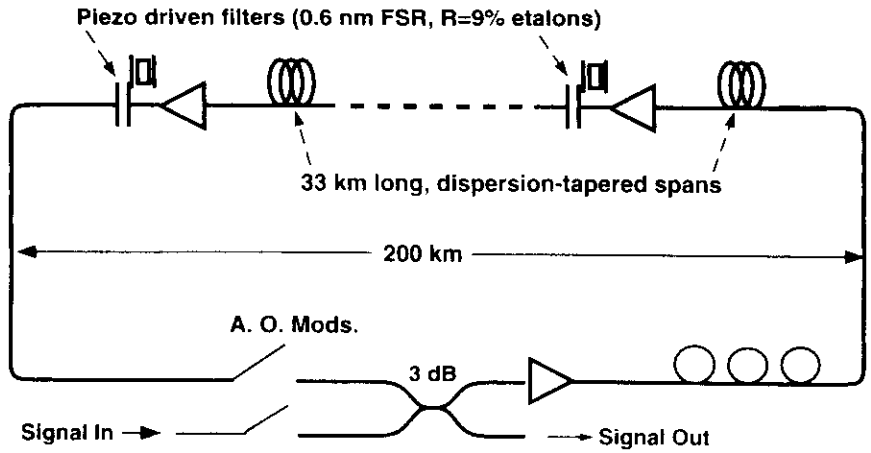

Fig. 12.46 Recirculating loop with sliding-frequency filters and dispersion-tapered fiber spans. The A.O. (acoustooptic) modulators act as optical switches with very large on–off ratios to control the sequencing of each transmission. That is, initially the lower switch is held closed and the upper switch open long enough for the source to fill the recirculating loop with data and to bring the amplifier chain to equilibrium. The conditions of the two switches are then simultaneously reversed, so that the loop is closed on itself, and there is no longer an external source. During each such transmission, a linear ramp voltage is applied to the piezo-driven filters to produce the desired sliding of the filter frequencies. Samples of the signal, corresponding to successive round-trips, emerge more or less continuously from the signal out port.

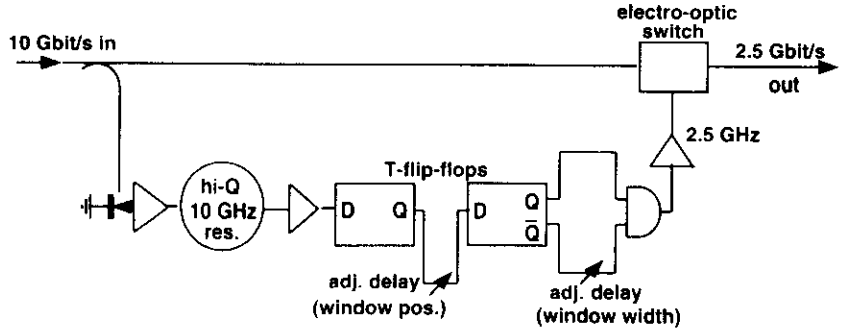

Fig. 12.47 Time-division demultiplexer.

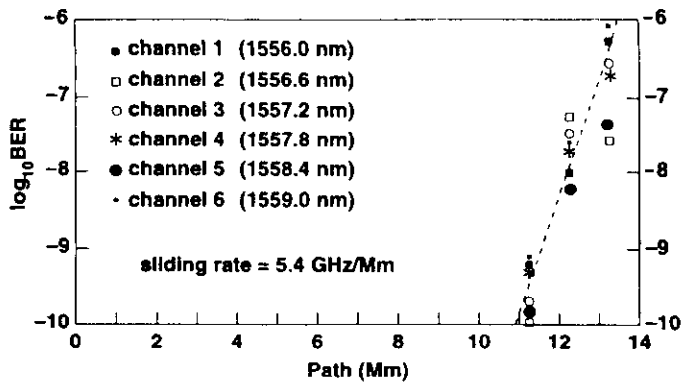

Fig. 12.48 Measured BER versus distance for a 6 × 10 Gb/s WDM transmission.

to loop amplifiers pumped at 1480 nm, with corresponding high noise figure (~6 dB) and narrow gain bandwidth. The last point corresponds to pumping at 980 nm, however, where the noise figure is much closer to 3 dB and the gain bandwidth is improved, at least toward shorter wavelengths. The error-free distances represented in Fig. 12.49 tend to be determined by a low-

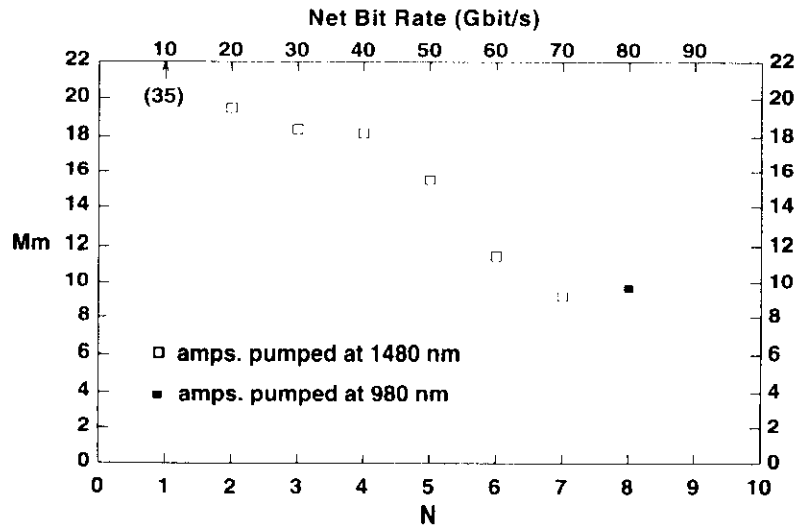

Fig. 12.49 Measured error-free distances versus the number, N, of channels at 10 Gb/s per channel.

level error floor, which is only very weakly dependent on distance. This dependence is especially noticeable for the largest values of N. Thus, even small future improvements should enable both the error-free distances and the maximum number of allowable channels to be increased.

An experiment was also performed at 5 Gb/s per channel (six channels), with the same apparatus, simply by programming the pattern generator to eliminate every second pulse of the otherwise 10-Gb/s data. As the only other substantial change, consistent with the lower bit rate, the time-acceptance window of the demultiplexer (Fig. 12.47) was opened up by a factor of 2. For that experiment, the error-free distance was greater than 40 Mm on all channels. The great increase in error-free distance was due primarily to two factors: First, at half the bit rate, the rate of collisions was decreased by half. Second, the doubled time-acceptance window greatly increased the tolerance to timing jitter.

Finally, Fig. 12.50 shows an example of the spectrum of the WDM transmission. Although the example corresponds to a particular distance (10 Mm), the spectrum looks the same at any other but the very shortest distances. In all the experiments carried out so far, regardless of the number of channels, the spectra all had the same feature, viz., that the spectral peaks could all be joined by a straight line that passed through the zero intensity axis at λ_0, the wavelength of zero dispersion. All this occurred in the face of considerable amplifier gain variation over the total wavelength span. Thus, in these spectra we have direct and complete confirmation of

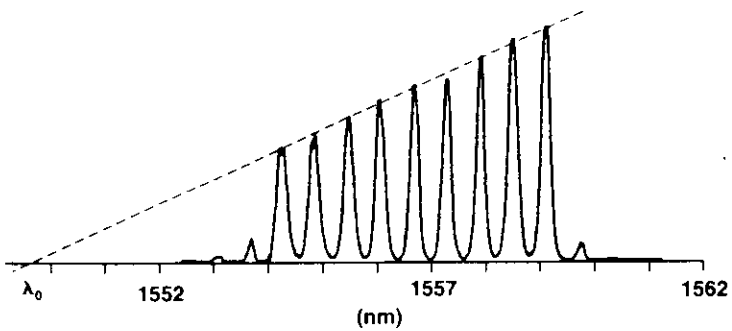

Fig. 12.50 Optical spectrum of 9 × 10 Gb/s WDM transmission, as measured at 10 Mm. Note that the *dashed line* connecting the spectral peaks of the individual channels passes through the wavelength of zero dispersion, λ_0. This behavior results from the strong regulation of the soliton pulse energies provided by the sliding-frequency filters. Following initial adjustment, it becomes independent of distance.

the ideas presented in Section 5.8, where the guiding filters were shown to provide a very tight control over the relative signal strengths of the various channels.

6. Polarization Effects

6.1 *APOLOGIA*

Thus far in this chapter, we have tended to gloss over polarization and effects of the fiber's birefringence on it. That is, for the most part we have been content to note the thorough polarization averaging, created by the fiber's random residual birefringence, over those distances for which the nonlinear term has significant effects. We have used that averaging to justify further neglect of polarization. Nevertheless, there are certain important polarization phenomena that require examination. One of these is called *polarization mode dispersion* (*PMD*), which makes the transit time for a pulse dependent on its polarization history and produces some dispersive-wave radiation in the process. The other is the fact that colliding solitons in WDM alter each other's polarization states. Therefore, we now examine the linear birefringence of fibers and its statistical properties, the birefringence induced nonlinearly by the pulse itself, and the effects of both on transmission.

6.2 *POLARIZATION STATES AND THE STOKES–POINCARÉ PICTURE*

If z is the propogation direction and $\hat{x}$ and $\hat{y}$ are unit vectors in the x and y directions, respectively, a unit normalized polarization vector can be written as $\hat{\mathbf{u}} = (r\hat{x} + s\hat{y})$, where r and s are complex numbers with $|r|^2 + |s|^2 = 1$, so that $\hat{\mathbf{u}}^* \cdot \hat{\mathbf{u}} = 1$. A corresponding normalized real field component at frequency ω has the form

$$\mathrm{Re}(\mathbf{u}) = \mathrm{Re}[(r\hat{x} + s\hat{y})e^{i\Psi}] \quad : \quad \Psi = kz - \omega t + \Phi. \tag{6.1}$$

If the phases of r and s are both changed by the same amount $\delta\Phi$, then Φ in Eq. (6.1) simply changes to $\Phi + \delta\Phi$. With no loss of generality we can therefore express r and s in polar form by $r = \cos(\theta)\exp(-i\phi)$ and $s = \sin(\theta)\exp(i\phi)$, where $0 \le \theta \le \pi/2$ so that $\cos(\theta) = |r|$ and $\sin(\theta) = |s|$. Thus, the real field can be written as

$$\mathrm{Re}(\mathbf{u}) = \hat{x}\cos(\theta)\cos(\Psi - \phi) + \hat{y}\sin(\theta)\cos(\Psi + \phi). \quad (6.1a)$$

One way to visualize the polarization state of the field is to plot the motion of the vector Re(**u**) in an x–y coordinate system as Ψ varies from 0 to 2π. The resulting figure is generally an ellipse. The state of polarization of the field is determined by the shape of the ellipse and by the direction of motion of the vector around the ellipse. It is independent of the constant Φ in the phase Ψ. In general, a change from ϕ to $-\phi$ reverses the direction of motion around the same ellipse. When $\phi = 0$ or $\phi = \pi/2$, the ellipse degenerates into a straight line making an angle θ or $-\theta$, respectively, with the x axis. This represents linear polarization. When $\phi = \pi/4$, the axes of the ellipse are the x and y axes, and they have lengths of $2\cos(\theta)$ and $2\sin(\theta)$, respectively. When $\theta = \pi/4$, so that $\cos(\theta) = \sin(\theta) = 1/\sqrt{2}$, the axes of the ellipse are rotated by $\pi/4$ from the x and y axes, and they have lengths of $2|\cos(\phi)|$ and $2|\sin(\phi)|$, respectively. When both ϕ and Ψ are equal to $\pi/4$, the ellipse degenerates to a circle and we have circular polarization.

A more useful tool for visualizing the state of polarization as it varies during transmission is the real three-dimensional Stokes vector. A Stokes vector $\hat{\mathbf{S}}$ of unit length is derived from the normalized polarization vector in Eq. (6.1) or Eq. (6.1a). It has the components

$$\begin{aligned} S_1 &= |r|^2 - |s|^2 = \cos(2\theta) \\ S_2 &= 2\mathrm{Re}(r^*s) = \sin(2\theta)\cos(2\phi) \\ S_3 &= 2\mathrm{Im}(r^*s) = \sin(2\theta)\sin(2\phi). \end{aligned} \quad (6.2)$$

We see that the angles 2θ and 2ϕ are, respectively, the polar and aximuthal angles representing the vector $\hat{\mathbf{S}}$ in a spherical coordinate system with the S_1 axis as the polar axis. It is worth noting that S_1 is proportional to the difference in the powers that would emerge from linear polarizers in the x and y directions, and that S_2 is likewise proportional to the difference in the powers that would emerge from linear polarizers rotated from the previous two by an angle of $\pi/4$, thus bisecting the x and y directions, whereas S_3 is the difference between the powers that would emerge from left and right circular polarizers. Hence, the Stokes vector can be measured directly, and such machines are now fairly common. One can verify that the (S_1, S_2) plane represents plane polarized fields ($2\phi = 0$ or π), whereas the S_3 axis represents circularly polarized fields. Note that the Stokes vectors corresponding to the orthogonal polarization states $\hat{x}$ ($r = 1$, $s = 0$) and $\hat{y}$ ($s = 1$, $r = 0$) lie antiparallel along the S_1 axis. More generally, two polarization vectors $\hat{\mathbf{u}}_a$ and $\hat{\mathbf{u}}_b$ are orthogonal if $\hat{\mathbf{u}}_a^* \cdot \hat{\mathbf{u}}_b = 0$. Thus $(s^*\hat{x} - r^*\hat{y})$ represents the state orthogonal to $(r\hat{x} + s\hat{y})$, and the Stokes vectors of these two polarization states always lie antiparallel along the same axis. Because the Stokes vectors of concern here have unit length, their ends always lie on a sphere of unit radius, the Poincaré sphere, as shown in Fig. 12.52.

6.3 LINEAR BIREFRINGENCE OF TRANSMISSION FIBERS

6.3.1 Birefringence Element and Its Effects

Consider the effect on $\hat{\mathbf{S}}$ of a short length dz of birefringent fiber (Fig. 12.51). There are many reasons for such birefringence, principal among them being a slight ellipticity of the fiber, or some strain on it. Suppose first that the principal states of the birefringence are the x and y linear polarizations ($\theta = 0$ in Fig. 12.51). If δk is the corresponding difference in wave number, then in the course of traversing the piece of fiber, a phase shift $\delta\phi = \delta k\, dz$ will develop in the quantity rs^*. Consequently, the Stokes vector precesses through the angle $\delta\phi$ around the S_1 axis, marking out a cone. The corresponding generalization is that for any birefringence, the Stokes vector precesses through an angle $\delta\phi = \delta k\, dz$ around the axis in Stokes space that corresponds to the two principal states of the birefringence. If $\boldsymbol{\beta}$ is a vector whose length is δk and that lies along this axis of birefringence, then $\hat{\mathbf{S}}$ precesses around $\boldsymbol{\beta}$ according to the equation

$$\frac{d\hat{\mathbf{S}}}{dz} = -\boldsymbol{\beta} \times \hat{\mathbf{S}}. \quad (6.3)$$

Figure 12.52 illustrates this behavior. When $\delta\phi$ reaches 2π, $\hat{\mathbf{S}}$ has swept out a complete cone. An optical element of this sort is called a *full-wave plate.*

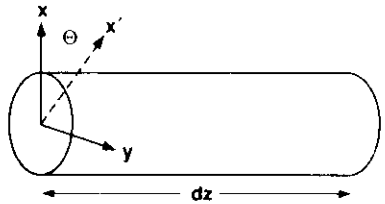

Fig. 12.51 Element of fiber with birefringence axis x'.

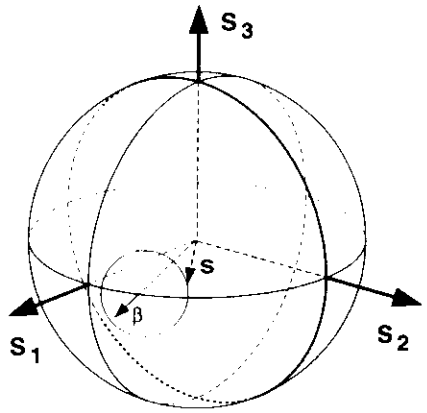

Fig. 12.52 The birefringence element β causes $\mathbf{S}$ to precess in a cone around it.

In a fiber, the needed length $2\pi/\delta k = \lambda(k/\delta k)$ is called the *beat length*. It is typically very short, a few meters to tens of meters. If the birefringence axis varies in a random way along the fiber, the Stokes vector soon comes to have a random direction on the Poincaré sphere.

Along with the wave-number birefringence just discussed comes a birefringence in the inverse group velocity. Let $\mathbf{b} = d\boldsymbol{\beta}/d\omega$. If $\boldsymbol{\beta}$ does not change direction with frequency (in practice the change tends to be negligibly small), then we have

$$b = \frac{d\beta}{d\omega} = \frac{d\delta k}{d\omega} = \delta v_g^{-1}, \tag{6.4}$$

where b, for example, is the magnitude (length) of the vector $\mathbf{b}$, and the last equality is so because $dk/d\omega = v_g^{-1}$ holds for each of the two principal states of polarization. If we refer again to our piece of fiber with x–y birefringence, we can determine that the average time delay for the energy of a field in the polarization state $(r\hat{x} + s\hat{y})$ is proportional to $(|r|^2 - |s|^2)$ and thus to S_1. In general, the time delay is proportional to the projection of $\hat{\mathbf{S}}$ on the birefringence axis, so we get

$$dt_d = \tfrac{1}{2}\,\hat{\mathbf{S}} \cdot \mathbf{b}\, dz. \tag{6.5}$$

6.3.2 Calculus for Long Fibers

In a typical transmission fiber, both the strength and the axis of the birefringence vary along the length of the fiber, which causes the Stokes vector to wander more or less randomly around the Poincaré sphere. The motion of

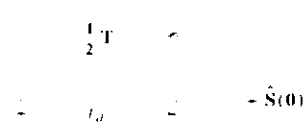

Fig. 12.53 Relative time delay, in a long fiber, of a pulse with polarization vector $\hat{\mathbf{S}}$.

$$\hat{\mathbf{S}}(z_2) = \mathbf{M}(z_2, z_1) \cdot \hat{\mathbf{S}}(z_1), \tag{6.6}$$

where $\mathbf{M}$ is a rotation matrix, a (3×3) form of a Mueller matrix, and $\mathbf{M}(z_1, z_2)$ is the inverse of $\mathbf{M}(z_2, z_1)$. For a long fiber, of length Z, the total delay caused by the birefringence can be written as

$$\begin{aligned} t_d &= \frac{1}{2}\int_0^Z \hat{\mathbf{S}}(z) \cdot \mathbf{b}(z)\, dz = \frac{1}{2}\,\hat{\mathbf{S}}(0) \cdot \int_0^Z [\mathbf{M}(0, z) \cdot \mathbf{b}(z)]\, dz \\ &= \tfrac{1}{2}\,\hat{\mathbf{S}}(0) \cdot \mathbf{T}, \end{aligned} \tag{6.7}$$

where we have used the inverse Mueller matrix to project the vector dot product at location z back to the input of the fiber, and the last equality defines the vector $\mathbf{T}$. We call $\mathbf{T}$ the *polarization time-dispersion vector* [35].* Its length is the difference between the maximum and minimum delay times, and the Stokes vectors pointing in its positive and negative directions represent the principal states of polarization for which the delay times are, respectively, longest and shortest. It behaves very much like the local birefringence, except its magnitude and direction on the Poincaré sphere are more rapidly frequency dependent (Fig. 12.53). In the case of linear propagation, any input pulse can be resolved into a linear combination of components in the two principal states, which have different delays. As a result, one sees the output pulse width vary as a function of the input polarization, its mean delay time being given by Eq. (6.7). In the case of soliton propagation, if the PMD is not too large, the nonlinear effects hold the pulse together, so that the pulse width does not change, but its mean delay time also obeys Eq. (6.7). Soliton propagation is discussed further later in this chapter.

6.3.3 Growth of T with Increasing Fiber Span Length

We can think of a long fiber as a concatenation of two shorter fibers, joined at some point $z = z_1$. Accordingly, the vector $\mathbf{T}$ for the whole fiber can be split into two pieces as

* Prior to the appearance of Ref. 35, however, the polarization dispersion vector and its statistical properties had already been thoroughly explored by Poole and coauthors; see, for example, Refs. 36 and 37. Note that the vector Ω in those papers is the same as $\mathbf{M}(Z, 0) \cdot \mathbf{T}$

$$\mathbf{T} = \int_0^{z_1} \mathbf{M}(0, z) \cdot \mathbf{b}(z)\, dz + \mathbf{M}(0, z_1) \cdot \int_{z_1}^{Z} \mathbf{M}(z_1, z) \cdot \mathbf{b}(z)\, dz \tag{6.8}$$
$$= \mathbf{T}_1 + \mathbf{M}(0, z_1) \cdot \mathbf{T}_2,$$

where $\mathbf{T}_1$ and $\mathbf{T}_2$ are the $\mathbf{T}$ vectors for the two sections taken individually. We are primarily interested in fiber spans that are long with respect to the characteristic distance (typically only a few meters) for the reorientation of $\mathbf{b}$. In that case, the direction of $\mathbf{T}_2$ is at random with respect to that of $\mathbf{T}_1$; furthermore, because there is no correlation between $\mathbf{M}(0, z_1)$ and $\mathbf{T}_2$, the second term in Eq. (6.8) is still oriented at random with respect to the first. This division can be iterated, giving

$$\mathbf{T} = \mathbf{T}_1 + \sum_{i=2}^{N-1} \mathbf{M}(0, z_i) \cdot \mathbf{T}_i, \tag{6.9}$$

until the $\mathbf{T}$ vectors of the individual sections cease being uncorrelated. From this exercise it should be obvious that the growth of T (the magnitude of $\mathbf{T}$) is a random walk process, where T is expected to grow as $z^{1/2}$. Another way of seeing this is to look at the quantity

$$T^2 = \mathbf{T} \cdot \mathbf{T} = \int_0^Z \int_0^Z [\mathbf{M}(0, z) \cdot \mathbf{b}(z)] \cdot [\mathbf{M}(0, z') \cdot \mathbf{b}(z')]\, dz'\, dz \tag{6.10}$$
$$= \int_0^Z \int_0^Z \mathbf{b}(z) \cdot \mathbf{M}(z, z') \cdot \mathbf{b}(z')\, dz\, dz'.$$

Beyond the length over which $\mathbf{b}(z)$ is correlated with $\mathbf{M}(z, z') \cdot \mathbf{b}(z')$ this double integral is expected to grow noisily but roughly linearly with Z. To take a simple example, imagine a fiber, initially with a constant linear birefringence, which is cut into short sections of length l_{sect} and put back together after each section has been rotated through a random angle around its cylindrical axis. Then, referring to Eq. (6.10), we can see that because $\mathbf{b}(z)$ is oriented along the local birefringence axis, $\mathbf{M}(z, z')$ reduces to the identity matrix as long as z and z' are both in the same section. There is no correlation between the directions of $\mathbf{b}(z)$ in the different sections, so in getting the expected value of T^2, the first integral over z' reduces simply to $b^2 l_{sect}$, and the second integral produces the factor Z.

An expected value of T is usually inferred from measurements made over a wide band of optical frequencies. As the fiber is cut back, the data [38] indeed tend to fit a curve of form

$$T(z) = D_p z^{1/2}. \tag{6.11}$$

D_p is known as the PMD parameter. For the highest quality transmission fibers available at present, $0.06 \le D_p \le 0.1$ ps/km$^{1/2}$.

6.3.4 Statistical Properties of T

The PMD parameter D_p for a length of fiber is found from averaging the values of T obtained over a rather broad range of frequencies. The distribution of T values so obtained tends to be Maxwellian. Changing the temperature of a fiber leads to similar results. This distribution can be understood as follows: The value of T is sensitive to the wave-number birefringence of the fiber, because this is what causes precession of the Stokes vector, and so determines the values of the Mueller matrices. We have seen that $\mathbf{T}$ can be considered to be the sum of a large number of independent vectors $\mathbf{T}_i$ from fiber sections, each projected to the beginning of the fiber by the appropriate Mueller matrix. As these Mueller matrices are changed by changing frequency, say, one would expect the components of $\mathbf{T}$ to have nearly independent Gaussian distributions.

If each of the three components of $\mathbf{T}$ in Stokes space (T_1, T_2, T_3) has an independent Gaussian distribution with standard deviation σ, then the distribution of $\mathbf{T}$ has spherical symmetry and the magnitude of $\mathbf{T}$ will have a Maxwellian distribution, as illustrated in Fig. 12.54. The probability that T lies between T and $T + dT$ is

$$p(T)\, dT = \sqrt{\frac{2}{\pi}} \frac{1}{\sigma^3} T^2 e^{-1/2(T/\sigma)^2}\, dT. \tag{6.12}$$

The most probable value of T/σ is $\sqrt{2} \approx 1.414$, its mean value is $\sqrt{8/\pi} \approx 1.596$, and its standard deviation is $\sqrt{3} \approx 1.732$. By definition, D_p is the mean value of T divided by the square root of the length of the fiber, so that $\sigma = D_p \sqrt{\pi Z/8}$. As an example, if $D_p \sim 0.1$ ps/km$^{1/2}$ and

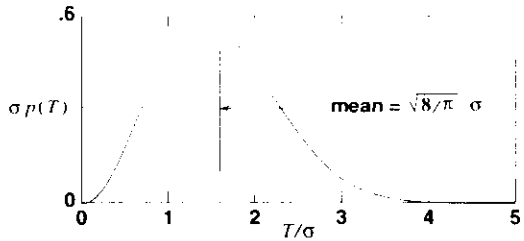

Fig. 12.54 Maxwellian probability distribution of T.

$Z = 10{,}000$ km, then $\sigma \sim 6.3$ ps. As a final bit of housekeeping here, note from Eq. (6.7) that the delay time for a pulse is half the component of $\mathbf{T}$ along the direction of $\hat{\mathbf{S}}(0)$. Thus the expected standard deviation of the pulse delay is $\sigma_{delay} = \sigma/2 = D_p\sqrt{\pi Z/32}$.

6.4 SOLITON PROPAGATION

We now consider soliton pulse propagation in a randomly birefringent fiber. First, it is known that the nonlinear coefficient n_2 is a function of polarization, varying, relative to its polarization average, from $\frac{8}{9}$ for linear polarization to $\frac{3}{4}$ for circular polarization (on average, linear polarization is twice as likely as circular polarization). The changes in n_2 as a soliton's polarization state varies during propagation cause some radiative loss of energy. However, this loss is much smaller than a similar loss due to PMD, and it may be ignored. To avoid unnecessary complication, we shall therefore continue to treat n_2 as though it were polarization independent.

We now come to consider the residual birefringence. On the often used assumption that the local form of the birefringence is not very important overall, we shall invoke a well-worn model similar to that used previously, in which the fiber is composed of short sections of constant linear birefringence, whose axes are assumed randomly directed, and whose magnitude may also have some random distribution. Consider the effect of one such section. We can denote the slow and fast axes of this piece of fiber by the orthogonal unit vectors $\hat{x}$ and $\hat{y}$. The entering soliton will be in some linear combination of these two polarization states and will in general have the form

$$\mathbf{u}(z, t) = (r\hat{x} + s\hat{y})\,\mathrm{sech}(t), \tag{6.13}$$

where the polarization state vector has unit length, as before, satisfying $(|r|^2 + |s|^2 = 1)$. After traversing the section of length l, this soliton will have changed to the form

$$\mathbf{u}(z + l, t) = e^{i\theta}[re^{i\phi}\hat{x}\,\mathrm{sech}(t - \varepsilon) + se^{-i\phi}\hat{y}\,\mathrm{sech}(t + \varepsilon)], \tag{6.14}$$

where the angle $\phi = (\frac{1}{2})\,\delta k l$ arises from the local wave-number birefringence δk, while $\varepsilon = (\frac{1}{2})\,bl$ is half the time delay birefringence of the fiber section. For good fibers, ε is a very small number. Using this, we can expand the sech functions to first order in ε [$d\,\mathrm{sech}(t)/dt = -\mathrm{sech}(t)\tanh(t)$], and with a bit of manipulation arrive at

$$\begin{aligned}\mathbf{u}(z + l, t) \approx e^{i\theta}[&(re^{i\phi}\hat{x} + se^{-i\phi}\hat{y})\mathrm{sech}(t - \varepsilon(|r|^2 - |s|^2)))\\ &+ \varepsilon\, 2rs(s^* e^{i\phi}\hat{x} - r^* e^{-i\phi}\hat{y})\mathrm{sech}(t)\tanh(t)].\end{aligned} \tag{6.15}$$

We have split the terms proportional to ε into two parts, one having the same polarization state as the soliton, which we put back together with the soliton, and the other having a polarization state orthogonal to the soliton. We see that the soliton's polarization state and PMD time delay have changed in accordance with our previous general discussion. The field scattered into the orthogonal polarization state, proportional to $\mathrm{sech}(t)\tanh(t)$, can be shown to be a dispersive field and so represents a loss mechanism for the soliton. The fractional energy loss due to this section of fiber is the ratio of the time integrals of $|u|^2$ in the two orthogonal polarization states, which yields $\delta E/E = (\frac{4}{3})|rs|^2\varepsilon^2$, independent of ϕ. If we assume that the birefringent time delay stays small with respect to the pulse width of the soliton, then the scattered fields will be uncorrelated, and the total loss will be the sum of the energies scattered from each section. To find the expected loss, it is appropriate to do an average over polarizations. From Eq. (6.2) one can see that $4|rs|^2$ is the sum of the squares of the S_2 and S_3 components of the unit Stokes vector $\hat{\mathbf{S}}$, and therefore its polarization average is $\frac{2}{3}$. Using this, and evaluating ε, we get

$$\alpha_{pmd} l = \frac{\delta E}{E} = \frac{1}{18} b^2 l^2, \tag{6.16}$$

where α_{pmd} is the exponential energy loss coefficient. In comparison, the time delay for this section, $\delta t_d = \varepsilon(|r|^2 - |s|^2)$, is proportional to the S_1 component of $\hat{\mathbf{S}}$, so its polarization average is zero, but its variance is

$$\sigma_d^2 = \tfrac{1}{3}\,\varepsilon^2 = \tfrac{1}{12}\,b^2 l^2. \tag{6.17}$$

The loss due to PMD is therefore related to the variance of the time delay by $\alpha_{pmd} l = (\frac{1}{3})\sigma_d^2$. Because the loss and the variance of the time delay both grow linearly with the number of sections, the loss for a length z of fiber will be given by

$$\alpha_{pmd} z = \frac{2}{3}\sigma_d^2(z) = \frac{\pi}{48} D_p^2 z. \tag{6.18}$$

This equation is written in soliton units. It can be made dimension free by dividing its right side by t_c^2, or $(\pi/1.7627)^2$; removing the common factor of z as well, one gets

$$\alpha_{pmd} = 0.2034 D_p^2/\tau^2. \tag{6.18a}$$

To take a good fiber as an example, with $D_p = 0.1$ ps/km$^{1/2}$, then a pulse with $\tau = 20$ ps yields $\alpha_{pmd} = 5 \times 10^{-6}$/km, or 0.005/Mm. Although the loss rate in soliton energy due to PMD appears small in this case, note that the total energy lost in 10 Mm is 5% of the soliton's energy. Because this lost energy is scattered into dispersive waves, it can add significantly to the total noise, especially in a broadband transmission line. On the other hand, sliding-frequency filters (see Section 4) control the growth of this noise just as effectively as they control the growth of spontaneous emission noise.

It should also be noted from Eq. (6.18a) that the loss rate from PMD increases rapidly with decreasing pulse width. For example, for the maximum pulse width ($\tau \approx 2$ ps) permitting a single-channel rate of 100 Gb/s, and again for $D_p = 0.1$ ps/km$^{1/2}$, α_{pmd} rises to 0.5/Mm, a value large enough to cause very serious problems. This is yet another reason why, for the attainment of very large net bit rates, massive WDM (as described in Section 5.9, for example) is by far the better choice.

If the value of D_p becomes too large, solitons can become unstable. For distances of the order of z_c, essentially linear propagation occurs, so a soliton has a chance of being split into its two principal state components. Some years ago, a criterion for stability was established by numerical simulation, using a kind of worst case scenario [39]. In soliton units, the result was simply

$$D_p \leq 0.27 t_c/z_c^{1/2}. \tag{6.19}$$

Using Eq. (6.19) with the equality sign to establish the largest allowable D_p, and setting $D_p z^{1/2} \approx t_c$, note that a linear pulse would split into two pieces spaced by t_c in a distance $(0.27^2 \approx 14) \times z_c$. Under those same conditions, however, nonlinear effects hold the soliton together over an indefinitely long distance of propagation. From Eq. (2.15a), we recall that $t_c/z_c^{1/2}$ scales with the dispersion constant D, so in standard units Eq. (6.19) becomes

$$D_p \leq 0.3 D^{1/2}. \tag{6.19a}$$

Note that for $D_p = 0.1$ ps/km$^{1/2}$, Eq. (6.19a) is satisfied for D as small as about 0.11 ps/nm-km. For an example of what can happen when the criterion of Eq. (6.19a) is violated, see Ref. 40.

It is interesting that even at the stability border, the loss calculated from Eq. (6.18) seems very small. If we use Eq. (6.19) with an equals sign, then from Eq. (6.18) we get $\alpha_{pmd} = 0.048/z_c$, which does not seem large enough to signal impending doom for the soliton. The answer to this conundrum is probably in the statistics. The loss was calculated on the basis of polarization averaging, while the split-up of a soliton can occur in any section of the transmission fiber a few z_c long if the **T** vector for that section is large enough. Simulations also support this conclusion. As long as the soliton transmission is stable, the loss (per z_c) is small.

6.5 *POLARIZATION SCATTERING BY SOLITON–SOLITON COLLISIONS*

As already noted in the introduction to this section, colliding solitons in WDM alter each other's polarization states. Although this polarization scattering was described in 1973 by Manakov [41], its consequences were not generally appreciated until they became manifest in a fairly recent experiment [42]. In the experiment, each of several 10-Gb/s WDM channels was subdivided into two polarization- (and time-) division multiplexed, 5-Gb/s subchannels. As had been known for some time [43], such polarization-division multiplexing works well, at least in the absence of WDM. Indeed, in the experiment, with only one such polarization-multiplexed, 10-Gb/s channel present, the orthogonality of the 5-Gb/s subchannels was well maintained over transoceanic distances, and the transmission was error free. As soon as a second WDM channel was added, however, polarization scattering from the collisions destroyed the orthogonality of the subchannels, and the error rate became high for all but very short distances. To confirm that polarization scattering was to blame, the degree of polarization of each 10-Gb/s channel (this time with all pulses initially copolarized) was measured as a function of distance. The results are summarized in Fig. 12.55. With only one channel present (no WDM), as expected, the degree of polarization (DOP) was only slightly reduced in 10 Mm, from the mild effects of spontaneous emission [43]. With just one other channel present, however, the degree of polarization of either channel was reduced nearly to zero in the same distance.

The origin of the polarization scattering in WDM transmission is not difficult to understand. It comes about because the magnitude of the cross-phase modulation between waves of different frequencies is dependent on their relative polarizations, being twice as large for copolarized waves as for orthogonally polarized waves. One can think of this as a nonlinearly induced effective birefringence, keeping in mind that the birefringence seen

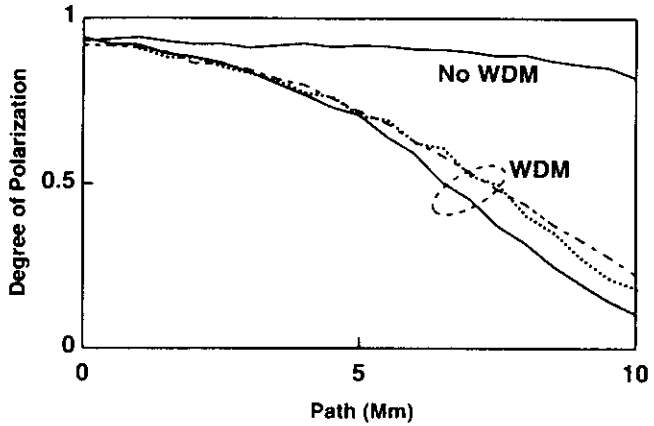

Fig. 12.55 Experimentally measured degree of polarization for a given wavelength channel as a function of distance. *No WDM*: Only one channel is present on the transmission line. *WDM*: Two channels are present on the line. Channel separations: 0.6 nm (*solid line*); 1.2 nm (*dashed line*); 1.8 nm (*dotted line*). In all cases, the channels were initially copolarized.

by each of the waves is different from that seen by the other. We discuss this effect in more detail later. Consider now a collision between solitons in two frequency channels of a WDM system. Label the solitons a and b. The cross-phase modulation phase shift given to the component of soliton a copolarized with soliton b is twice as large as that given to the component of soliton a orthogonal to soliton b. The result is a change in the polarization state of soliton a. In terms of the three-dimensional Stokes vector representation of a soliton's polarization state, the first-order result is a precession of soliton a's Stokes vector around that of soliton b. Soliton b is similarly influenced by soliton a, so their Stokes vectors precess around each other. The cross-phase modulation occurs only while the solitons overlap, and after a completed collision the differential phase shift (which, as we shall show, equals the precision angle of the Stokes vectors) is approximately equal to $L_{coll}/(1.76z_c)$. Note that there is no change in the polarizations of either soliton if they are in the same or orthogonal polarization states.

To analyze the polarization scattering in detail, we describe the optical field envelope in a fiber, in the manner of Eq. (6.13), using

$$\mathbf{u} = u_x\hat{x} + u_y\hat{y}. \tag{6.20}$$

Here u_x and u_y are the x and y components of the field, normalized so that $\mathbf{u}^* \cdot \mathbf{u} = |u_x|^2 + |u_y|^2$ is the optical power in the fiber. Instead of the Stokes vector of unit length used in Section 6.2, we shall here use an instantaneous Stokes vector with the components $(S_1, S_2, S_3) = [|u_x|^2 - |u_y|^2, 2\mathrm{Re}(u_x^* u_y), 2\mathrm{Im})u_x^* u_y)]$, so that the length of the Stokes vector is the optical power. Using a unitary transformation (the Jones matrix), we can mathematically eliminate the rapid motion of the polarization of the optical field caused by the fiber's wave-number birefringence. Then, taking into account that the collision length for the solitons of interest here is short enough ($L_{coll} \leq 200$ km), that the effects of polarization dispersion on the relative polarizations of the two fields can be neglected, and that the nonlinear term is averaged over all polarizations, we are left with a much simplified version of the propagation equation, known as the Manakov equation [41]:

$$-i\frac{\partial \mathbf{u}}{\partial z} = \frac{1}{2}\frac{\partial^2 \mathbf{u}}{\partial t^2} + (\mathbf{u}^* \cdot \mathbf{u})\mathbf{u}. \tag{6.21}$$

Now if $\mathbf{u}$ is composed of two fields with distinctly separable frequency ranges (e.g., pulses in a WDM system), we can isolate the terms of Eq. (6.21) in each frequency range. If the two frequencies are identified by subscripts a and b, then for the frequency of $\mathbf{u}_a$, we find the equation

$$-i\frac{\partial \mathbf{u}_a}{\partial z} = \frac{1}{2}\frac{\partial^2 \mathbf{u}_a}{\partial t^2} + (\mathbf{u}_a^* \cdot \mathbf{u}_a)\mathbf{u}_a + (\mathbf{u}_b^* \cdot \mathbf{u}_b)\mathbf{u}_a + (\mathbf{u}_b^* \cdot \mathbf{u}_a)\mathbf{u}_b. \tag{6.22}$$

The equation for the frequency of $\mathbf{u}_b$ is obtained by interchanging indices. There are three nonlinear terms on the right-hand side of Eq. (6.22). The first is the self-phase modulation term, while the second and third constitute the polarization-dependent cross-phase modulation. For copolarized fields, the second and third terms become identical (compare with Eq. [5.3]), while for orthogonally polarized fields, the third term goes to zero.

If we expand Eq. (6.22) into its field components, it is straightforward to show that the cross-phase modulation terms of Eq. (6.22) modify the Stokes vector of the a field according to the equation

$$\frac{\partial \mathbf{S}_a}{\partial z} = \mathbf{S}_a \times \mathbf{S}_b. \tag{6.23}$$

This equation and that for $\mathbf{S}_b$ (exchange subscripts) show that the nonlinear term causes the Stokes vectors of the two fields to precess around each other, so that $\partial(\mathbf{S}_a + \mathbf{S}_b)/\partial z = 0$. It is important to note from Eq. (6.23) that when the pulses are either exactly copolarized or exactly orthogonally

polarized, there is no scattering. Thus, for example, in the experiment of Fig. 12.55, there was no scattering between the initially copolarized channels until the fiber's PMD gradually opened up the angle between their Stokes vectors.

To apply Eq. (6.23) to solitons, we have only to integrate it over the course of a collision. In first order, if we neglect the simultaneous precession of soliton b, then the integration of Eq. (6.23) gives an effective precession angle of $\mathbf{S}_a$ around $\mathbf{S}_b$. Single solitons of Eq. (6.21) have the general form

$$\mathbf{u}(z, t) = \hat{\mathbf{u}} A \operatorname{sech}[A(t + \Omega z)] \exp[iz(A^2 - \Omega^2)/2 - i\Omega t], \quad (6.24)$$

where $\hat{\mathbf{u}}$ is a unit normalized polarization vector ($\hat{\mathbf{u}}^* \cdot \hat{\mathbf{u}} = 1$). To evaluate the precession angle most easily, let $\mathbf{u}_a$ be a stationary soliton ($\Omega_a = 0$), and let $\mathbf{u}_b$ be a soliton substantially displaced in frequency ($|\Omega_b| \gg 1$). Then the integration over the collision involves the integration over z of $A_b^2 \operatorname{sech}^2[A_b(t + \Omega_b z)]$, which gives a precession angle of $2A_b/\Omega_b$. This formula uses soliton units. Noting that the full spectral width of the soliton in Eq. (6.24) is $\Delta\omega = (2/\pi) \times 1.763\, A$, we can reexpress the polarization angle in the dimensionally independent form

$$\Delta\theta_a \simeq 1.78 \frac{\Delta\nu_b}{\Delta\nu_{ab}}, \quad (6.25)$$

where $\Delta\theta_a$ is the precession angle for the stationary solition, $\Delta\nu_b$ is the full (spectral) width at half maximum of the passing soliton, and $\Delta\nu_{ab}$ is the frequency separation of the two solitons. Note the inverse dependence of the change in polarization angle on channel separation ($\Delta\nu_{ab}$). Because the number of collisions in a given distance is in direct proportion to $\Delta\nu_{ab}$, however, the net spread in polarization vectors tends to be independent of channel separation, as observed experimentally (Fig. 12.55). Note also that Eq. (6.25) is valid whether or not the colliding solitons are equal in amplitude. Because the bandwidth of a soliton is proportional to its amplitude, the collision of two unequal solitons will yield unequal precessions for the two. In the WDM experiments described in Section 5, the ratio of the channel spacing to the soliton's spectral FWHM was about 5, which would make the precession angle per collision about 0.35 radians. This is a small enough angle to make the previously described theory applicable, and yet is large enough that just a few collisions are enough to prohibit the use of polarization-division multiplexing.

The argument just presented gives results applicable to a WDM communications system, where the channel spacing is much greater than the soliton

bandwidth, so that the precession angle in a collision is small. Manakov [41] was able to show that Eq. (6.21) supports polarized solitons in the strict sense. A collision of two solitons therefore does not give rise to any scattered radiation. The solitons emerge from the collision with their energies and velocities unchanged, but their polarizations change as well as their positions and phases. A translation of Manakov's result gives the following Stokes–Poincaré picture. If colliding solitons a and b have amplitudes A_a and A_b, and normalized Stokes vectors $\hat{\mathbf{S}}_a$ and $\hat{\mathbf{S}}_b$, then the vector $\mathbf{A} \equiv A_a\hat{\mathbf{S}}_a + A_b\hat{\mathbf{S}}_b$ remains the same before and after the collision. As a result of the collision, the two Stokes vectors $\hat{\mathbf{S}}_a$ and $\hat{\mathbf{S}}_b$ precess around the axis defined by $\mathbf{A}$ through an angle ϕ whose tangent is given by $\tan\phi = 2A\Omega/(\Omega^2 - A^2)$, where Ω is the difference between the solitons' frequencies and A is the length of the vector $\mathbf{A}$. With a little practice in geometry, one can show that when $\Omega^2 \gg A^2$, the exact result reduces to the approximate one given previously.

Another consequence of the polarization scattering from collisions, more fundamental than the simple prohibition of polarization-division multiplexing, is a jitter in pulse arrival times, mediated by the fiber birefringence. Reference 35 describes a qualitatively similar birefringence-mediated jitter, as initiated by the (relatively small) noise-induced scatter in polarization states. Because the spread in polarization states from collisions tends to be much larger (note that it eventually tends to spread the Stokes vectors over a large fraction of the Poincaré sphere), the jitter is correspondingly greater, and in a typical case can easily add at least a few tens of picoseconds to the total spread in arrival times over transoceanic distances. This represents a significant reduction in safety margin for individual channel rates of 10 Gb/s or more. Nevertheless, note that in the WDM results reported in Section 5.9, that reduction, although undoubtedly present, was not fatal.

References

[1] Mollenauer, L. F., J. P. Gordon, and M. N. Islam. 1986. Soliton propagation in long fibers with periodically compensated loss. *IEEE J. Quantum Electron.* QE-22:157–173.

[2] Mollenauer, L. F., M. J. Neubelt, S. G. Evangelides, J. P. Gordon, J. R. Simpson, and L. G. Cohen. 1990. Experimental study of soliton transmission over more than 10,000 km in dispersion shifted fiber. *Opt. Lett.* 15:1203–1205.

[3] Mollenauer, L. F., S. G. Evangelides, and H. A. Haus. 1991. Long distance solition propagation using lumped amplifiers and dispersion shifted fiber. *J. Lightwave Tech.* 9:194–197.

[4] Blow, K. J., and N. J. Doran. 1991. Average soliton dynamics and the operation of soliton systems with lumped amplifiers. *Photon. Tech. Lett.* 3:369–371.

[5] Hasegawa, A., and Y. Kodama. 1990. Guiding-center soliton in optical fibers. *Opt. Lett.* 15:1443–1445.

[6] Gordon, J. P., and L. F. Mollenauer. 1991. Effects of fiber nonlinearities and amplifier spacing on ultra long distance transmission. *J. Lightwave Tech.* 9:170–173.

[7] Gordon, J. P., and L. F. Mollenauer. 1990. Phase noise in photonic communications systems using linear amplifiers. *Opt. Lett.* 15:1351–1353.

[8] Gordon, J. P., and H. A. Haus. 1986. Random walk of coherently amplified solitons in optical fiber. *Opt. Lett.* 11:665–667.

[9] Smith, K., and L. F. Mollenauer. 1989. Experimental observation of soliton interaction over long fiber paths: Discovery of a long-range interaction. *Opt. Lett.* 14:1284–1286.

[10] Dianov, E. M., A. V. Luchnikov, A.N. Pilipetskii, and A. N. Starodumov. 1990. Electrostriction mechanism of soliton interaction in optical fibers. *Opt. Lett.* 15:314–316.

[11] Dianov, E. M., A. V. Luchnikov, A. N. Pilipetskii, and A. M. Prokhorov. 1991. Long-range interaction of solitons in ultra-long communication systems. *Soviet Lightwave Commun.* 1:235–246.

[12] Dianov, E. M., A. V. Luchnikov, A. N. Pilipetskii, and A. M. Prokhorov. 1992. Long-range interaction of picosecond solitons through excitation of acoustic waves in optical fibers. *Appl. Phys. B* 54:175–180.

[13] Mollenauer, L. F., E. Lichtman, G. T. Harvey, M. J. Neubelt, and B. M. Nyman. 1992. Demonstration of error-free soliton transmission over more than 15,000 km at 5 Gbit/s, single-channel, and over 11,000 km at 10 Gbit/s in a two-channel WDM. *Electron. Lett.* 28:792–794.

[14] Mecozzi, A., J. D. Moores, H. A. Haus, and Y. Lai. 1991. Soliton transmission control. *Opt. Lett.* 16:1841–1843.

[15] Kodama, Y., and A. Hasegawa. 1992. Generation of asymptotically stable optical solitons and suppression of the Gordon–Haus effect. *Opt. Lett.* 17:31–33.

[16] Mollenauer, L. F., J. P. Gordon, and S. G. Evangelides. 1992. The sliding-frequency guiding filter: An improved form of soliton jitter control. *Opt. Lett.* 17:1575–1577.

[17] Golovchenko, E. A., A. N. Pilipetskii, C. R. Menyuk, J. P. Gordon, and L. F. Mollenauer. 1995. Soliton propagation with up- and down-sliding-frequency guiding filters. *Opt. Lett.* 20:539–541.

[18] Mamyshev, P. V., and L. F. Mollenauer. 1994. Stability of soliton propagation with sliding frequency guiding filters. *Opt. Lett.* 19:2083–2085.

[19] Mollenauer, L. F., P. V. Mamyshev, and M. J. Neubelt. 1994. Measurement of timing jitter in soliton transmission at 10 Gbits/s and achievement of 375 Gbits/s-Mm, error-free, at 12.5 and 15 Gbits/s. *Opt. Lett.* 19:704–706.

[20] Mecozzi, A. 1995. Soliton transmission control by Butterworth filters. *Opt. Lett.* 20:1859–1861.

[21] LeGuen, D., F. Fave, R. Boittin, J. Debeau, F. Devaux, M. Henry, C. Thebault, and T. Georges. 1995. Demonstration of sliding-filter-controlled soliton transmission at 20 Gbit/s over 14 Mm. *Electron. Lett.* 31:301–302.

[22] Nakazawa, M., E. Yamada, H. Kubotra, and K. Suzuki. 1991. 10 Gbit/s soliton transmission over one million kilometers. *Electron. Lett.* 27:1270–1271.

[23] Widdowson, T., and A. D. Ellis. 20 Gbit/s soliton transmission over 125 Mm. *Electron. Lett.* 30:1866–1867.

[24] Forysiak, W., K. J. Blow, and N. J. Doran. 1993. Reduction of Gordon–Haus jitter by post-transmission dispersion compensation. *Electron. Lett.* 29:1225–1226.

[25] Suzuki, M., I. Morita, N. Edagawa, S. Yamamoto, H. Taga, and S. Akiba. 1995. Reduction of Gordon–Haus timing jitter by periodic dispersion compensation in soliton transmission. *Electron. Lett.* 31:2027–2028.

[26] Mollenauer, L. F., S. G. Evangelides, and J. P. Gordon. 1991. Wavelength division multiplexing with solitons in ultra long distance transmission using lumped amplifiers. *J. Lightwave Tech.* 9:362–367.

[27] Mamyshev, P. V., and L. F. Mollenauer. 1996. Pseudo-phase-matched four-wave mixing in soliton WDM transmission. *Opt. Lett.* 21:396–398.

[28] Mollenauer, L. F., P. V. Mamyshev, and M. J. Neubelt. 1996. Demonstration of soliton WDM transmission at 6 and 7 × 10 GBit/s, error-free over transoceanic distances. *Electron. Lett.* 32:471–473.

[29] Mollenauer, L. F., P. V. Mamyshev, and M. J. Neubelt. 1996. Demonstration of soliton WDM transmission at up to 8 × 10 GBit/s, error-free over transoceanic distances. In *OFC '96, San Jose, CA*, Postdeadline paper PD-22, PD22-2–PD22-5.

[30] Mecozzi, A., and H. A. Haus. 1992. Effect of filters on soliton interactions in wavelength-division-multiplexing systems. *Opt. Lett.* 17:988–990.

[31] Mamyshev, P. V., and L. F. Mollenauer. 1996. WDM channel energy self-equalization in a soliton transmission line using guiding filters. *Opt. Lett.* 21:1658–1660.

[32] Veselka, J. J., and S. K. Korotky. 1994. Optical soliton generator based on a single Mach–Zehnder generator. In *Technical Digest 1994 OSA & IEEE integrated photonics research topical meeting, San Francisco, CA, 17–19 February*, 190–192.

[33] Mamyshev, P. V., 1994. Dual-wavelength source of high-repetition-rate, transform-limited optical pulses for soliton transmission. *Opt. Lett.* 19:2074–2076.

[34] Yamada, K., H. Murai, K. Nakamura, H. Satoh, Y. Ozeki, and Y. Ogawa. 1995. 10-Gbit/s EA modulator with a polarization dependence of less than

0.3 dB. In *Technical Digest 1995 OSA & IEEE Optical Fiber Conference, San Diego, CA, 26 February–3 March*, 24–25.

[35] Mollenauer, L. F., and J. P. Gordon. 1994. Birefringence-mediated timing jitter in soliton transmission. *Opt. Lett.* 19:375–377.

[36] Poole, C. D. 1988. Statistical treatment of polarization dispersion in single-mode fiber. *Opt. Lett.* 13:687–689.

[37] Foschini, G. J., and C. D. Poole. 1991. Statistical theory of polarization dispersion in single mode fibers. *J. Lightwave Tech.* 9:1439–1456.

[38] Poole, C. D. 1989. Measurement of polarization-mode dispersion in single-mode fibers with random mode coupling. *Opt. Lett.* 14:523–525.

[39] Mollenauer, L. F., K. Smith, J. P. Gordon, and C. R. Menyuk. 1989. Resistance of solitons to the effects of polarization dispersion in optical fibers. *Opt. Lett.* 14:1219–1221.

[40] Wai, P. K. A., C. R. Menyuk, and H. H. Chen. 1991. Stability of solitons in randomly varying birefringent fibers. *Opt. Lett.* 16:1231–1233.

[41] Manakov, S. V. 1973. On the theory of two-dimensional stationary self-focusing of electromagnetic waves. *Zh. Eksp. Teor. Fiz.* 65:505. Also published in 1974 in *Sov. Phys. JETP* 38:248–263.

[42] Mollenauer, L. F., J. P. Gordon, and F. Heismann. 1995. Polarization scattering by soliton–soliton collisions. *Opt. Lett.* 20:2060–2062.

[43] Evangelides, S. G., L. F. Mollenauer, J. P. Gordon, and N. S. Bergano. 1992. Polarization division multiplexing with solitons. *J. Lightwave Tech.* 10:28–35.

Lecture #1:

THE NONLINEAR SCHRÖDINGER EQUATION AND THE SOLITON

Linn F. Mollenauer
Photonics Systems Research
Bell Labs
Lucent Technologies
Holmdel, NJ
USA

Winter College on Optics, Trieste, Italy
February 9, 1998

ELECTRONIC REGENERATION VS OPTICAL AMPLIFIERS

Regenerated System:

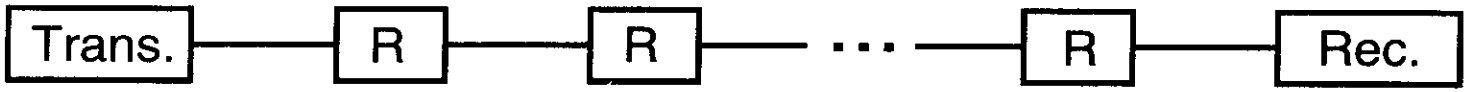

Disadvantages:

Cost increases rapidly with increasing bit rate.

Each wavelength channel requires its own set of regenerators

Complexity increases probability of failure.

System Using Optical Amplifiers:

Advantages:

Amplifier bandwidth does not limit single-channel bit rates.

Many channels can be amplified simultaneously.

Simple, reliable, and inexpensive.

Erbium - Doped Fiber Amplifier

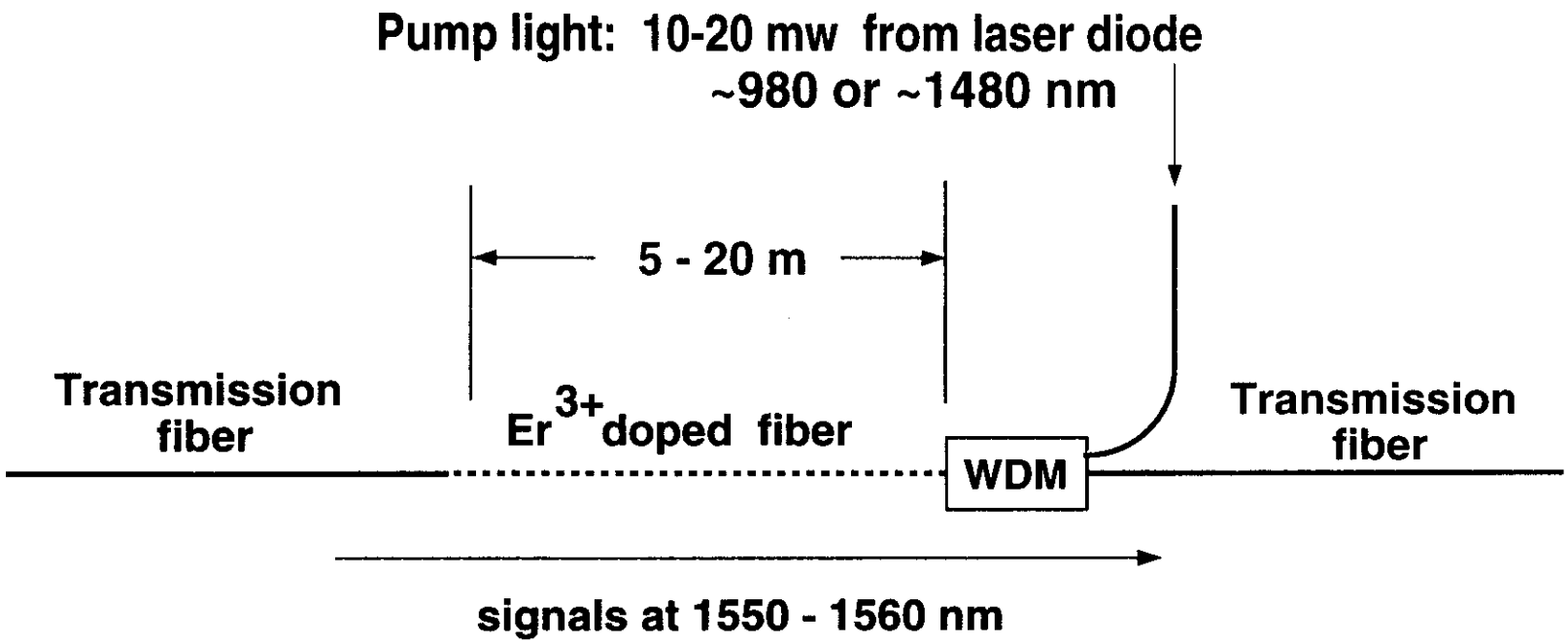

ERBIUM FIBER AMPLIFIER GAIN VERSUS WAVELENGTH

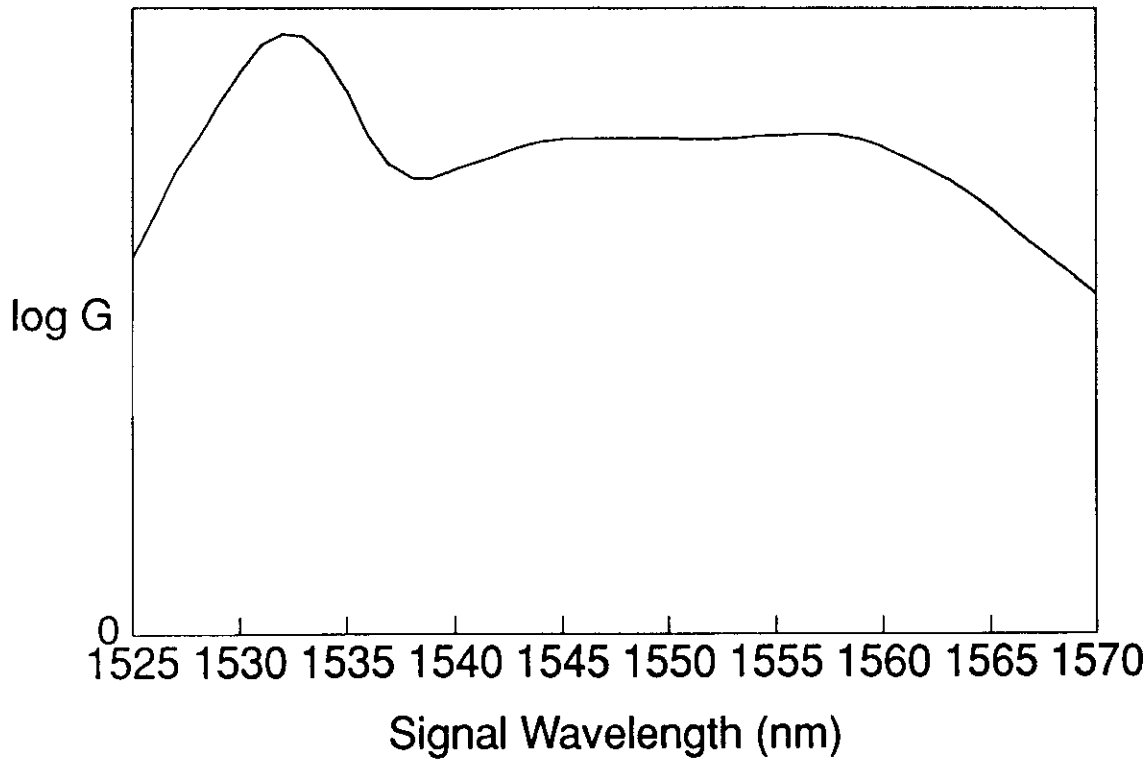

THE NONLINEAR SCHRÖDINGER EQN:

$$-i\frac{\partial u}{\partial z} = \frac{1}{2}\frac{\partial^2 u}{\partial t^2} + |u|^2 u - i(\alpha/2)u$$

ordinary dispersion

based on $n = n_0 + n_2 I$

SOLITON:

$$u(z,t) = \text{sech}(t)\, e^{iz/2}$$

SOLITON UNITS:

Length	*Time*	*Power*
$z_c = 0.322\frac{2\pi c}{\lambda^2}\frac{\tau^2}{D}$	$\frac{\tau}{1.763}$	$P_{sol} = \frac{A_{eff}}{2\pi n_2}\frac{\lambda}{z_c} \propto \frac{D}{\tau^2}$

(For τ=20 ps, D= 0.5 ps/nm-km, and λ= 1556 nm, z_c~200 km.)

A BRIEF (AND SELECTIVE) HISTORY OF SOLTIONS

1834 John Scott Russell observes "solitary" wave in the Union canal near Edinburgh, Scotland.

1895 Kortweg and deVries derive the equation of Russell's solitary wave.

1965 N. Zabusky (then at Bell Labs) and M. Kruskal observe that solitary waves survive collisions with one another. Rename them *solitons.*

1971 Zhakarov and Shabat (USSR) develop the inverse scattering theory and use it to explore solitons of the nonlinear Schrödinger equation.

1973 Hasegawa and Tappert (Bell Labs) predict that fibers can support solitons.

1980 Mollenauer, Stolen, and Gordon (Bell Labs) make first experimental observation in fibers.

1988 Mollenauer and Smith (Bell Labs) demonstrate first long distance (4000 km) all-optical transmission, by using solitons and Raman gain.

1987 Erbium fiber amplifier invented (Mears et al., Desurvire et al.).

FIBER NONLINEARITY

The induced polarization in a nonlinear dielectric takes the form:

$$\mathbf{P} = \varepsilon_0 \left[\chi^{(1)} \cdot \mathbf{E} + \chi^{(2)} : \mathbf{EE} + \chi^{(3)} \vdots \mathbf{EEE} + \cdots \right]$$

For (isotropic) fibers, $\chi^{(1)} = n^2 - 1$ (n is the index of refraction), while $\chi^{(2)} = 0$.

$\chi^{(3)}$ yields third harmonic generation (ordinarily negligibly weak in silica glass fibers), four-wave mixing, and nonlinear refraction; only the later two are of interest here.

In silica glass fibers, the index can be written, with great accuracy, as:

$$n(\omega, |\mathbf{E}|^2) = n(\omega) + n_2 |\mathbf{E}|^2$$

where n_2 is related to $\chi^{(3)}$ by

$$n_2 = \frac{3}{8n} \chi^{(3)}_{xxxx}$$

($\chi^{(3)}_{xxxx}$ is a scalar component of $\chi^{(3)}$, appropriate to the polarization.)

In silica glass fibers, if we write the nonlinear index as $n_2 I$, where I is the intensity, then n_2 has the polarization-averaged value of 2.8×10^{-16} cm^2/W.

PHASE AND GROUP VELOCITIES

Consider a medium characterized by the dispersion relation $\omega(k)$.
The phase of any frequency component is

$$\phi(z,t) = \omega t - kz$$

For an observer in a frame moving at velocity v

$$\frac{d\phi}{dt} = \omega - kv$$

For stationary ϕ, the terms in the above equation are zero.
The corresponding solution, $v_p = \omega/k$, is the phase velocity.

A pulse's peak occurs where its Fourier components add most constructively.
Thus, in a frame moving at the group velocity, v_g, one must have:

$$\frac{d}{dk}\left(\frac{d\phi}{dt}\right) = \frac{d\omega}{dk} - v_g = 0$$

The solution is the well-known result $v_g = d\omega/dk$.

INVERSE PHASE AND GROUP VELOCITIES

Let the dispersion relation be written as $k(\omega)$.
Let the phase of any frequency component be written as

$$\phi(z,t) = kz - \omega t$$

For an observer in a time frame moving at reciprocal velocity v^{-1},

$$\frac{d\phi}{dz} = k - \omega v^{-1}$$

For stationary ϕ, the terms in the above equation are zero.
The corresponding solution, $v_p^{-1} = k/\omega$, is the reciprocal phase velocity.
A pulse's peak occurs where its Fourier components add most constructively.
Thus, in a time frame moving with reciprocal group velocity v_g^{-1}, one must have:

$$\frac{d}{d\omega}\left(\frac{d\phi}{dz}\right) = \frac{dk}{d\omega} - v_g^{-1} = 0$$

The solution is $v_g^{-1} = dk/d\omega$

DERIVATION OF THE NONLINEAR SCHRODINGER EQN
Method of J. P. Gordon

Represent the complex field amplitudes with a scalar, dimensionless fn. $U(z,t)$, where $P = P_c \mid U \mid^2$, and let $k(\omega,P)$ be the dispersion relation of monochromatic waves $U(z,t) = u_0 e^{i(kz-\omega t)}$

Expand $k(\omega,P)$ in a Taylor series about $(\omega_0,0)$:

$$k = k_0 + k'(\omega-\omega_0) + \tfrac{1}{2}k''(\omega-\omega_0)^2 + k_2 P \qquad (1)$$

Reciprocal group velocity (time per unit distance):

$$v_g^{-1} = \frac{\partial k}{\partial \omega} = k' + k''(\omega-\omega_0)$$

i.e., $k' = v_g^{-1}(\omega_0)$ and k'' is the dispersion constant.

Note: Dispersion is often quoted as a wavelength derivative:

$$D \equiv \frac{\partial k'}{\partial \lambda} = -\frac{2\pi c}{\lambda^2} k''$$

DISPERSION PARAMETER OF SINGLE MODE FIBERS

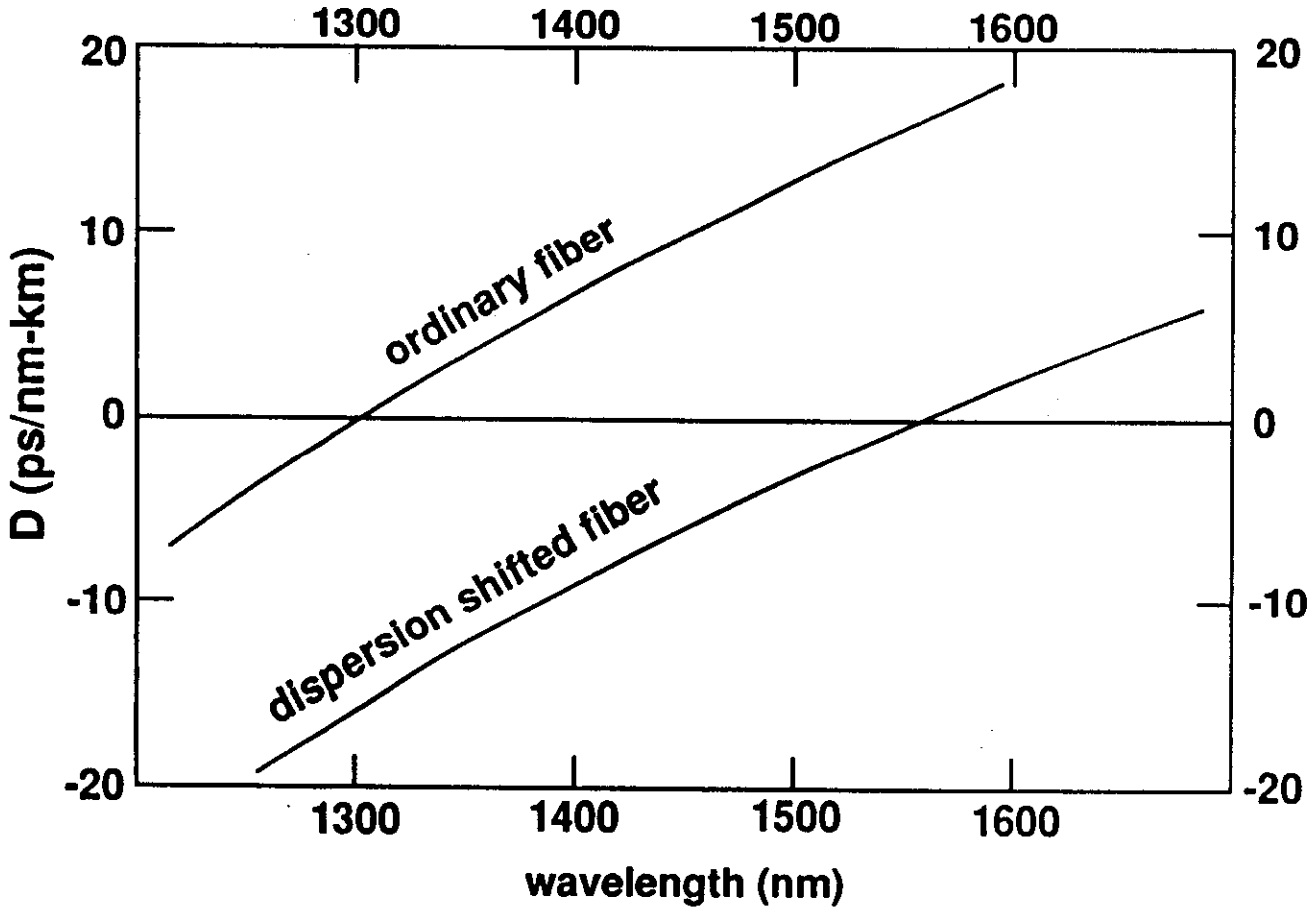

DERIVATION OF THE NONLINEAR SCHRODINGER EQN
Step II: Shift to zero frequency and retarded time.

Remove ω_0 and k_0 from $U(z,t)$ by defining

$$u(z,t) = U(z,t)\, e^{i(\omega_0 t - k_0 z)} = u_0\, e^{i[(k-k_0)z - (\omega-\omega_0)t]}$$

The equation for u that reproduces the dispersion relation (1) is clearly

$$-i\frac{\partial u}{\partial z} = i\,k'\frac{\partial u}{\partial t} - \tfrac{1}{2}k''\frac{\partial^2 u}{\partial t^2} + k_2 P_c\, |u|^2 u \qquad (2)$$

To make the time-frame for representing a pulse ind. of z, transform to retarded time:

$$t_{ret} = t - k'z$$

Since the eqn. of motion for a pulse at ω_0 is $t_{ret} = const.$, we have:

$$k'_{ret} = \frac{dt_{ret}}{dz} = \frac{dt}{dz} - k' = 0,$$

Thus, the (coefficient of the) $\frac{\partial u}{\partial t}$ term in (2) is eliminated.

DERIVATION OF THE NONLINEAR SCHRODINGER EQN

Step III: Rescale the independent variables

Choose unit values t_c, z_c, and P_c for time, distance, and power, respectively, such that the rescaled coefficients k'' and $k_2 P_c$ in (2) each become unity. That is, we have the new, "dimensionless" variables

$$t' = t_{ret}/t_c = (t - k'z)/t_c$$

$$z' = z/z_c$$

where the new unit values must obey the relations

$$-t_c^2/z_c = k''$$

$$(z_c P_c)^{-1} = k_2$$

Rewriting eqn. (2) in terms of the new variables, and dropping the primes, we get

$$-i\frac{\partial u}{\partial z} = \frac{1}{2}\frac{\partial^2 u}{\partial t^2} + |u|^2 u$$

FOURIER TRANSFORMS

Let $u(t)$ and $\tilde{u}(\omega)$ be Fourier transforms of each other, i.e.,

$$u(t) = \frac{1}{\sqrt{2\pi}} \int_{-\infty}^{+\infty} \tilde{u}(\omega)\, e^{-i\omega t} d\omega \quad \longleftrightarrow \quad \tilde{u}(\omega) = \frac{1}{\sqrt{2\pi}} \int_{-\infty}^{+\infty} u(t)\, e^{i\omega t} dt$$

Note that

$$\frac{\partial u(t)}{\partial t} = \frac{1}{\sqrt{2\pi}} \int_{-\infty}^{+\infty} -i\omega \tilde{u}(\omega)\, e^{-i\omega t} d\omega$$

$$\text{i.e.,} \quad \frac{\partial u(t)}{\partial t} \quad \longleftrightarrow \quad -i\omega \tilde{u}(\omega)$$

$$\text{similarly,} \quad \frac{\partial^2 u(t)}{\partial t^2} \quad \longleftrightarrow \quad -\omega^2 \tilde{u}(\omega)$$

THE NLS EQN: ACTION OF THE DISPERSIVE TERM

To get action of dispersive term alone, turn off NL term, so eqn. becomes:

$$\frac{\partial u}{\partial z} = \frac{i}{2}\frac{\partial^2 u}{\partial t^2}$$

The problem is most naturally solved in the frequency domain, where eqn. becomes:

$$\frac{\partial \tilde{u}}{\partial z} = -\frac{i}{2}\omega^2 \tilde{u}$$

and where the general solution is:

$$\tilde{u}(z,\omega) = \tilde{u}(0,\omega)\, e^{-i\frac{\omega^2 z}{2}}$$

Thus, the dispersive term merely rearranges the phase relations among existing frequency components; it adds no new ones.

To get the spreading of the pulse, must transform back to the time domain.

Example: Let $u(0,t) = e^{-t^2/2}$ for which $\tilde{u}(0,\omega) = e^{-\omega^2/2}$.

$$u(z,t) = \frac{1}{\sqrt{2\pi}}\int_{-\infty}^{\infty} \tilde{u}(0,\omega)\, e^{-i\frac{\omega^2 z}{2}}\, e^{-i\omega t}\, d\omega = \frac{1}{\sqrt{2\pi}}\int_{-\infty}^{\infty} e^{-\frac{\omega^2}{2}(1+iz)}\, e^{-i\omega t}\, d\omega \propto e^{-\frac{t^2}{2(1+iz)}}$$

Thus, intensity envelope $|u|^2 \propto e^{-t^2/(1+z^2)} = e^{-(2t/\delta t)^2}$, where $\delta t/2 = \sqrt{1+z^2}$.

DISPERSIVE BROADENING OF GAUSSIAN PULSE WITH DISTANCE

(Minimum spectral width at origin)

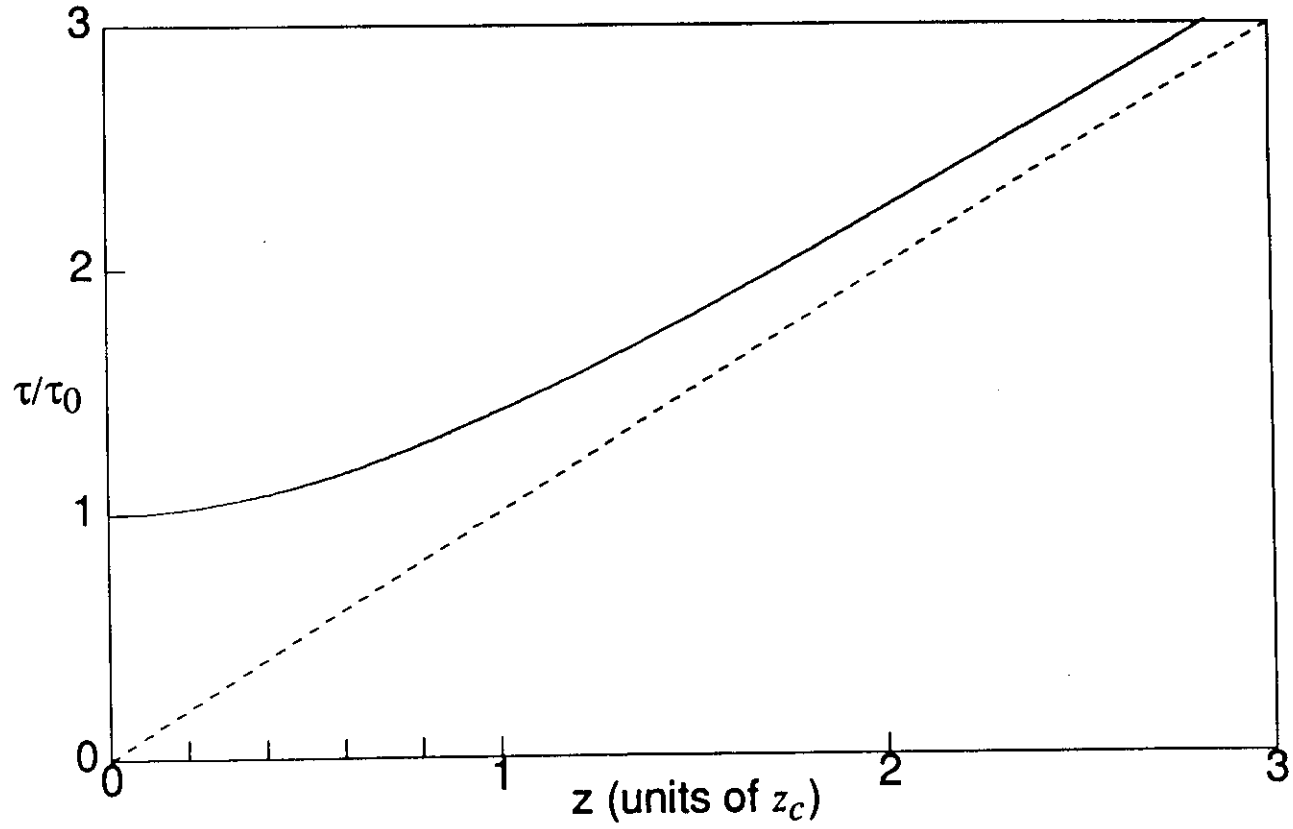

THE NLS EQN: ACTION OF THE NONLINEAR TERM

To get action of NL term alone, turn off dispersive term, so eqn. becomes:

$$\frac{\partial u}{\partial z} = i\,|u|^2 u$$

The problem is most naturally solved in the time domain, where gen. soln. is:

$$u(z,t) = u(0,t)\,e^{i|u|^2 z}$$

The NL term modifies $\phi(t)$, but not the intensity envelope.

Thus, it only adds new frequency components.

To get spectral spreading, must transform back to the frequency domain.

Example: Again, let $u(0,t) = e^{-t^2/2}$.

$$\tilde{u}(z,\omega) = \frac{1}{\sqrt{2\pi}} \int_{-\infty}^{\infty} u(0,t)\,e^{i|u|^2 z}\,e^{i\omega t}\,dt = \frac{1}{\sqrt{2\pi}} \int_{-\infty}^{\infty} e^{-t^2/2}\,e^{iz e^{-t^2}}\,e^{i\omega t}\,d\omega$$

For $z>>1$, this integral produces a multi-peaked spectrum, where the number of peaks and the over-all spectral width increase directly with z.

However, for $z<<1$, the integral is approximately

$$\frac{1}{\sqrt{2\pi}} \int_{-\infty}^{\infty} e^{-t^2/2}(1+iz\,e^{-t^2})\,e^{i\omega t}\,dt = \tilde{u}(0,\omega) + iz\,\tilde{v}(\omega)$$

Note that once again, the new component is in quadrature with the original pulse.

Thus, the increase in net spectral width scales only as z^2.

SPECTRAL BROADENING OF GAUSSIAN PULSE AT ZERO DISPERSION†

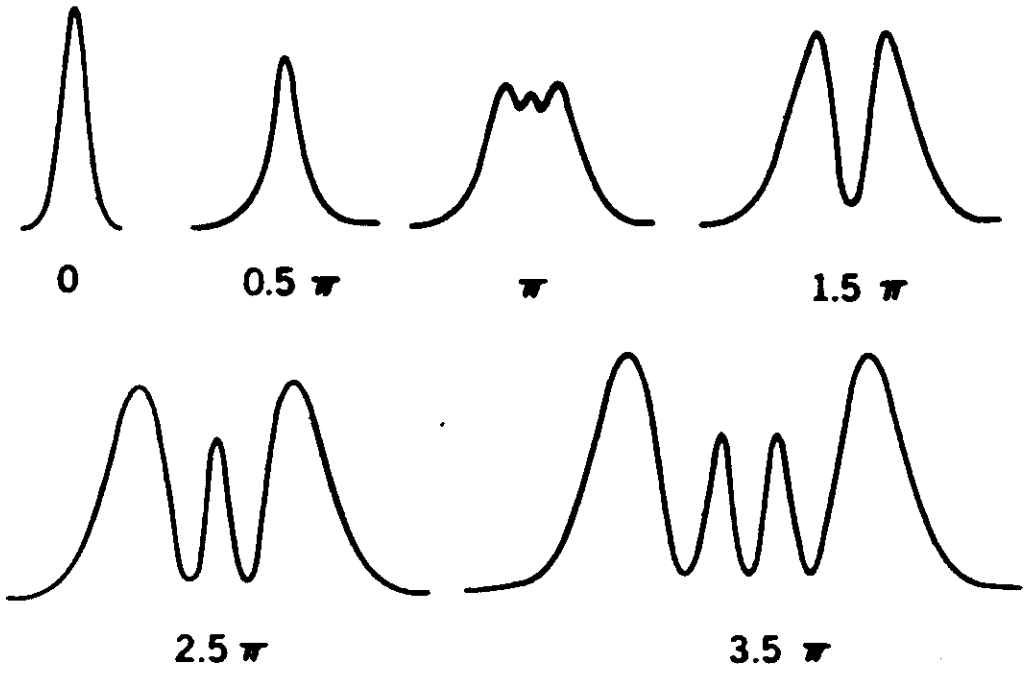

Nonlinear Φ shift ($\propto$'distance) shown under each spectrum.

† From Stolen and Lin, *Phys. Rev. A* **17** (1978)

ORIGIN OF THE SOLITON

For the soliton, the NL and dispersive terms cancel each other's effects.
But, how can the tendancies to spectral and temporal broadening cancel one another?
Ans: There is no broadening of either kind to first order in dz!
The first order effects of both terms are just complementary phase shifts $d\phi(t)$.

Proof: If $f(z,t)$ is real, then the general eqn.

$$\frac{\partial u}{\partial z} = if(z,t)u$$

simply generates the phase change $d\phi(t) = f(0,t)\,dz$ in dz.
We have already seen how the NL term generates $d\phi(t) = |u(t)|^2 dz$
For the dispersive effect, write the eqn. in the form

$$\frac{\partial u}{\partial z} = \left(\frac{i}{2u}\frac{\partial^2 u}{\partial t^2}\right)u$$

Thus, the dispersive term generates $d\phi = \left(\frac{1}{2u}\frac{\partial^2 u}{\partial t^2}\right)dz$

For $u = \text{sech}(t)$, these terms are, respectively,

$$d\phi_{NL} = \text{sech}^2(t)\,dz \quad \text{and} \quad d\phi_{disp.} = [\tfrac{1}{2} - \text{sech}^2(t)]\,dz.$$

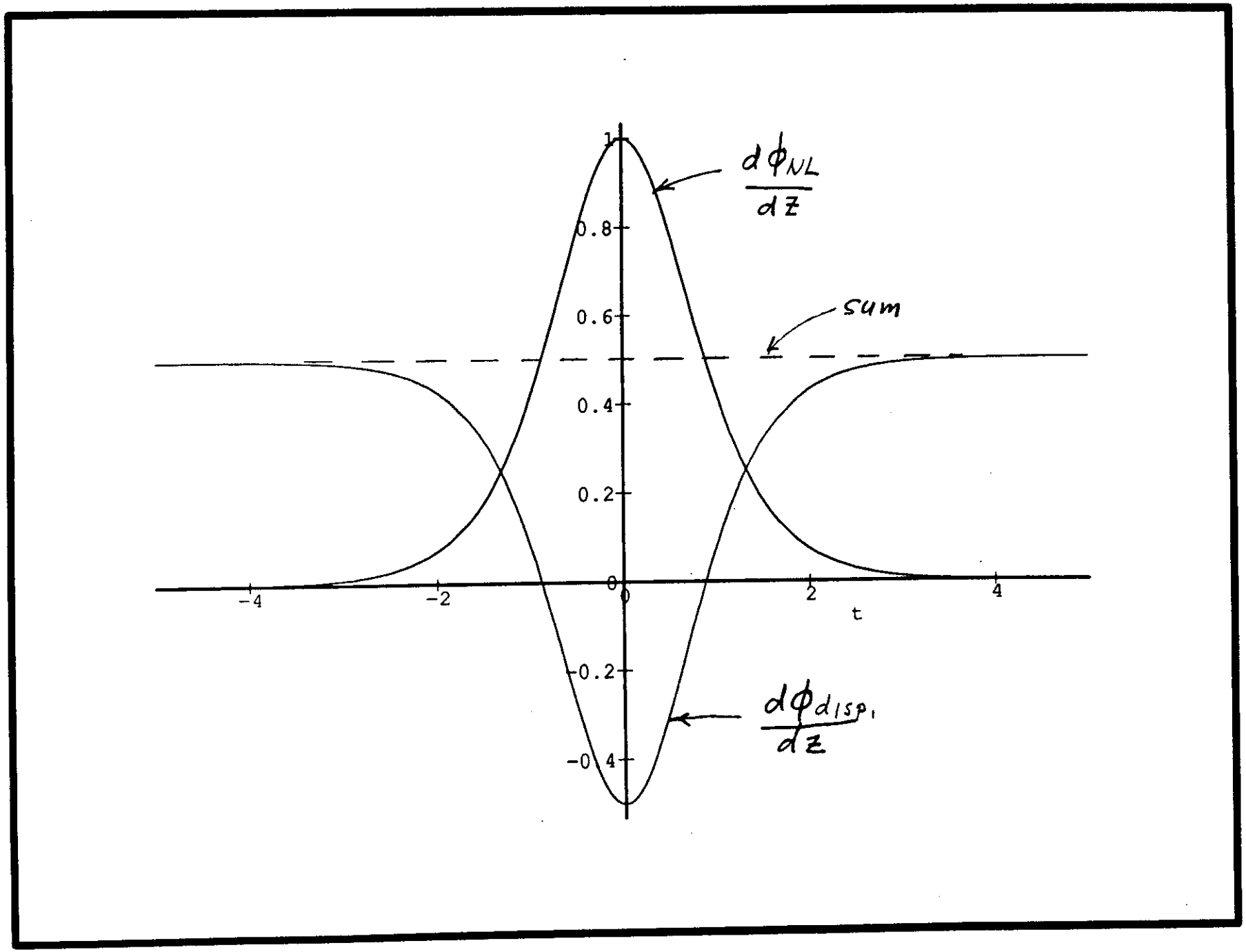
1
0.8
0.6
0.4
0.2
0
-0.2
-0.4
-4
-2
0
2
4
t
$\frac{d\phi_{NL}}{dz}$
sum
$\frac{d\phi_{disp}}{dz}$

SEGMENT OF "HYBRID" SYSTEM FOR TEST OF SOLITON PROPAGATION THROUGH CHAIN OF LUMPED AMPS AND D.S. FIBER

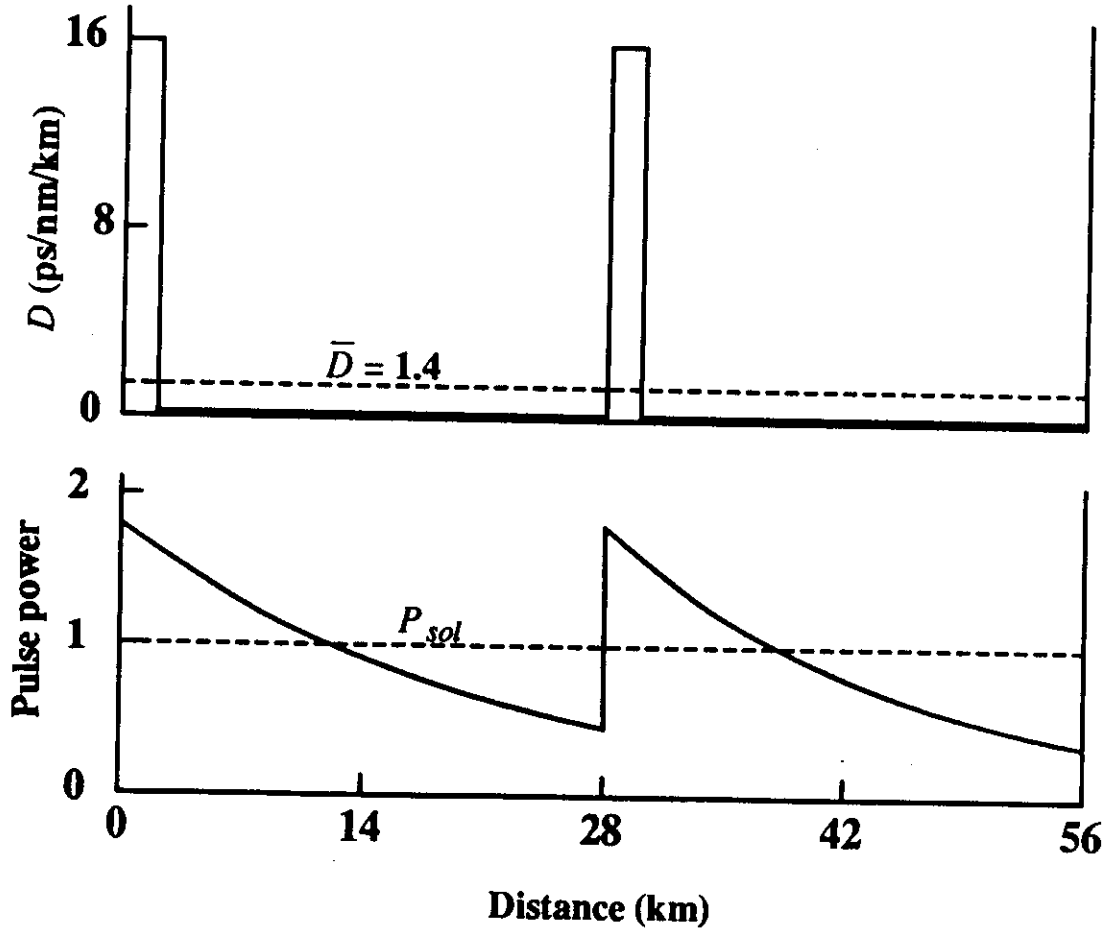

PERIODIC PULSE ENERGY AND FIBER DISPERSION IN SEGMENT OF TRANSMISSION LINE USED FOR TEST OF "PATH-AVERAGE" SOLITONS

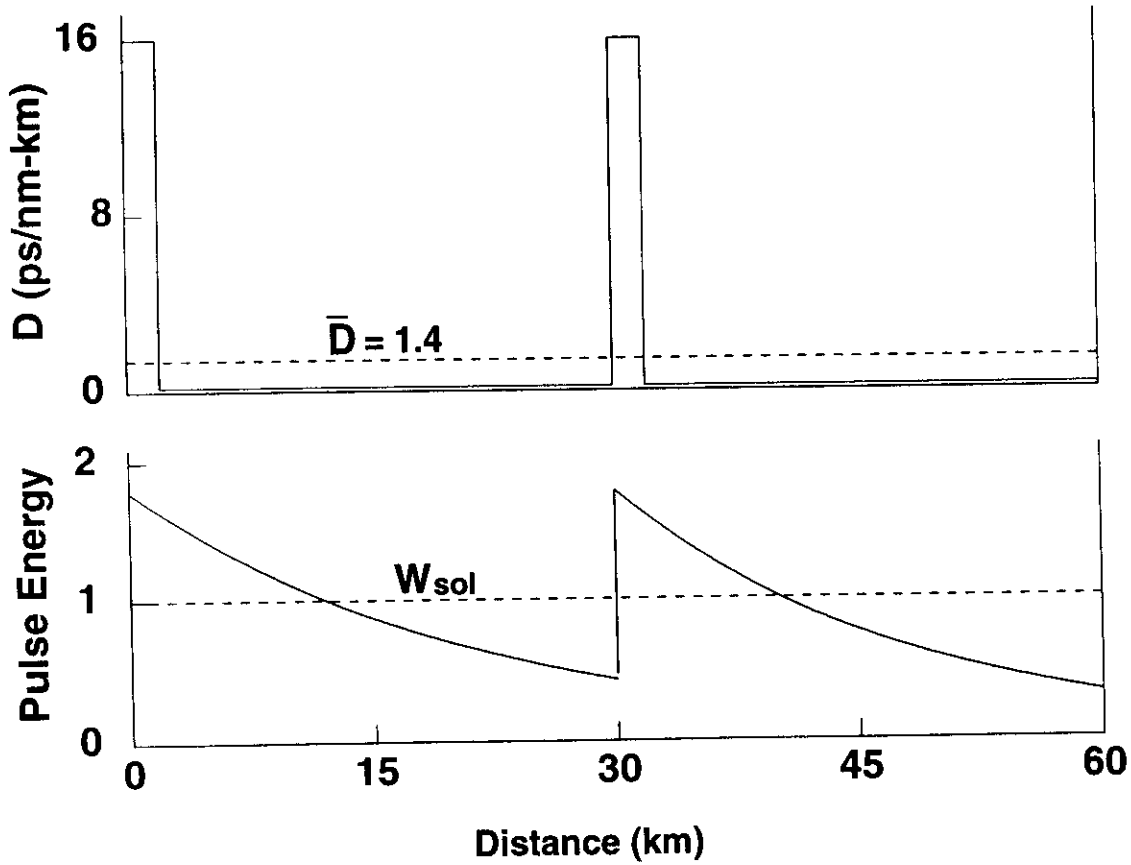

SIMULATED TRANSMISSION THROUGH SYSTEM WITH LUMPED AMPLIFIERS AND PERIODICALLY VARYING DISPERSION

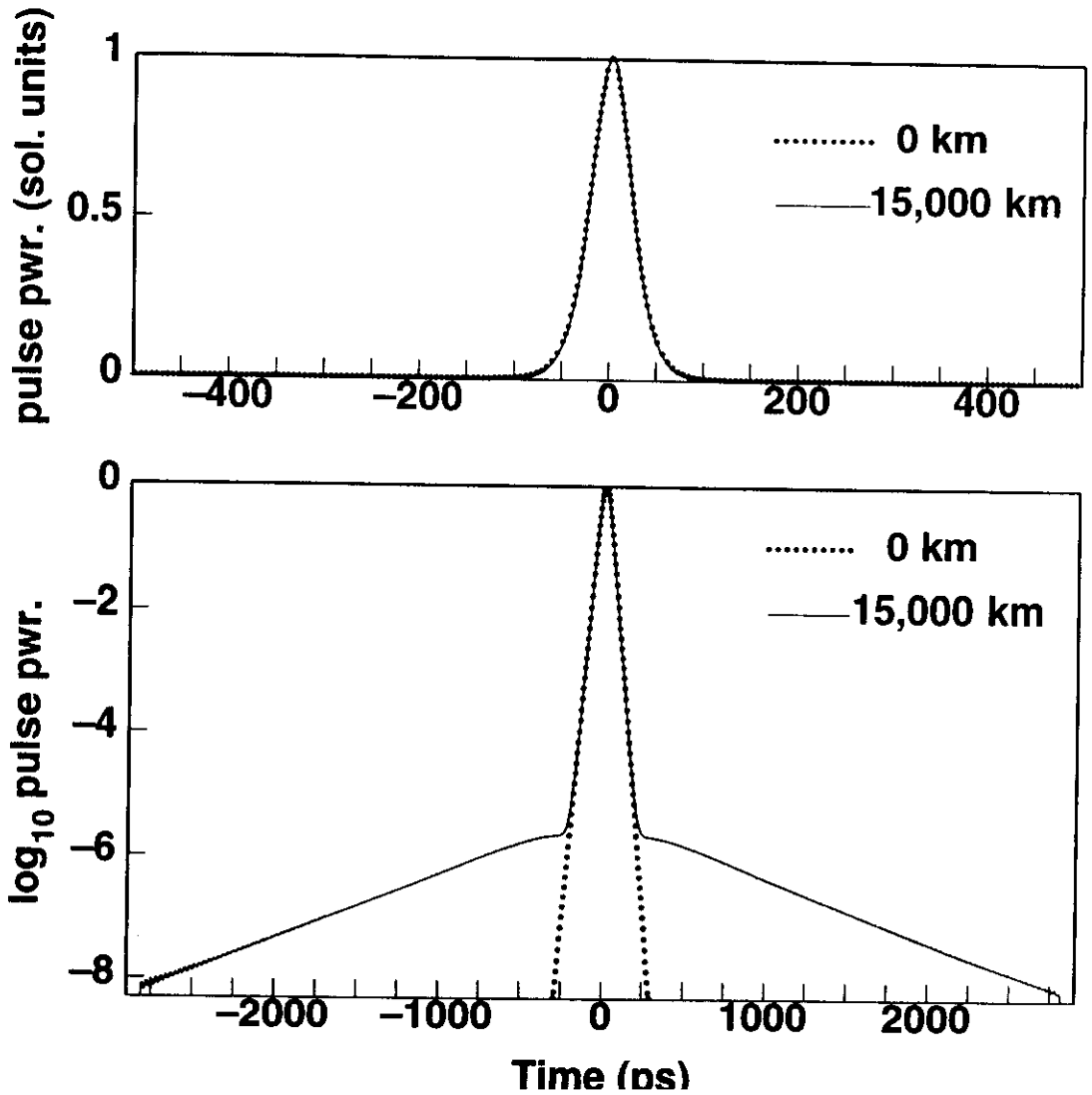

Dispersion Relation for Solitons and Linear Waves
Soliton Spectral Density Also Shown

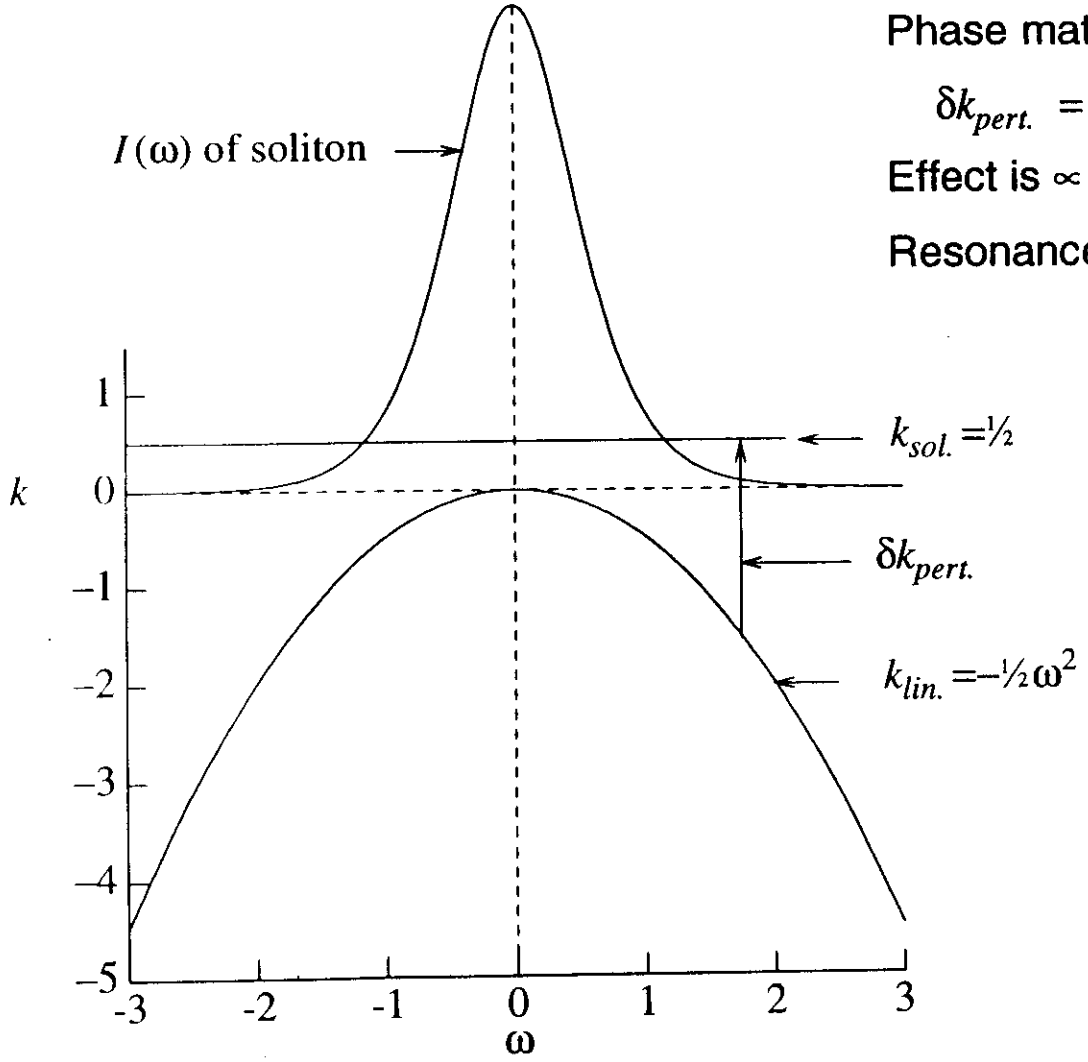

Phase matching condition:

$\delta k_{pert.} = k_{sol.} - k_{lin.}$

Effect is $\propto I(\omega_{match})$.

Resonance $\rightarrow \delta k_{pert.} = ½$.

NUMERICAL SOLUTION OF THE NLS EQN: THE SPLIT-STEP FOURIER METHOD

The NLS equation is generally difficult to solve analytically. Numerical solution, however, can be remarkably efficient, when it is based on the "split-step Fourier" method:

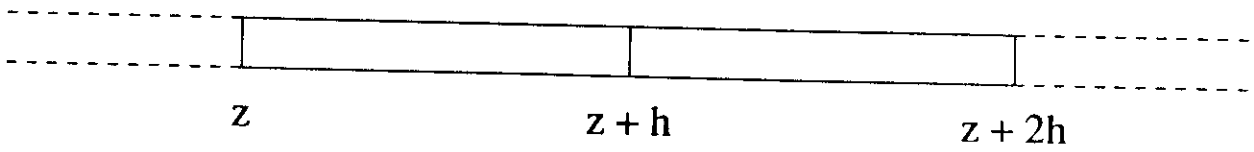

The method is based on the fact that the effects of the dispersive term are most naturally dealt with in the frequency domain, while those of the non-linear term are best handled in the time domain. Thus, each increment h in z is treated in two consecutive steps, as follows:

$$u(z,t) \rightarrow \tilde{u}(z,\omega); \qquad \tilde{u}(z,\omega)\, e^{-i(\omega^2/2)h} = \tilde{u}(z+h,\omega)$$

$$\tilde{u}(z+h,\omega) \rightarrow u_{new}(z,t); \qquad u_{new}(z,t) e^{i|u|^2 h} = u(z+h,t)$$

Based on the ideas just discussed with respect to path-average solitons, reasonable accuracy can often be maintained with relatively large step sizes. Fiber loss and amplifier gain are simulated by appropiate scale factors on $u(z)$. Filter response functions and other frequency dependent factors are most easily applied in the frequency domain.

Lecture #2:

RATE LIMITING EFFECTS OF AMPLIFIER SPONTANEOUS EMISSION AND AMELIORATION WITH "GUIDING" FILTERS

Linn F. Mollenauer
Photonics Systems Research
Bell Labs
Lucent Technologies
Holmdel, NJ
USA

Winter College on Optics, Trieste, Italy
February 9, 1998

SPONTANEOUS EMISSION NOISE: GROWTH AND EFFECTS

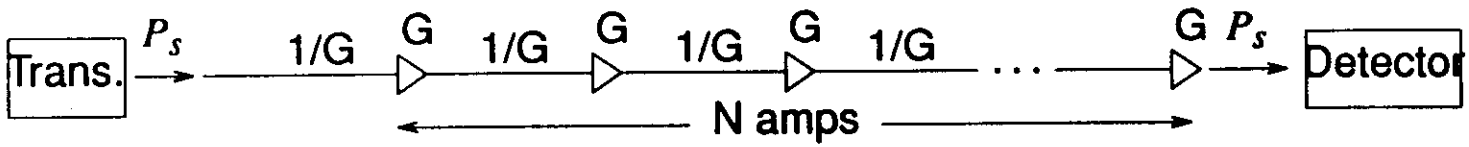

Noise Power/Unit Bandwidth

Each amplifier contributes $P(\nu) = (G-1)\, h\nu\, n_{sp}$.

Noise at system output is:

$$P(\nu) = N(G-1)\, h\nu\, n_{sp} = \frac{\alpha Z}{\ln G}(G-1)\, h\nu\, n_{sp}$$

Path average value in final segment of the line:

$$P(\nu) = \alpha Z\, h\nu\, n_{sp}\, \frac{(G-1)^2}{G(lnG)^2}$$

The quantity $F(G) = \dfrac{(G-1)^2}{G(lnG)^2}$ is a penalty function.

NOISE PENALTY VS AMPLIFIER GAIN

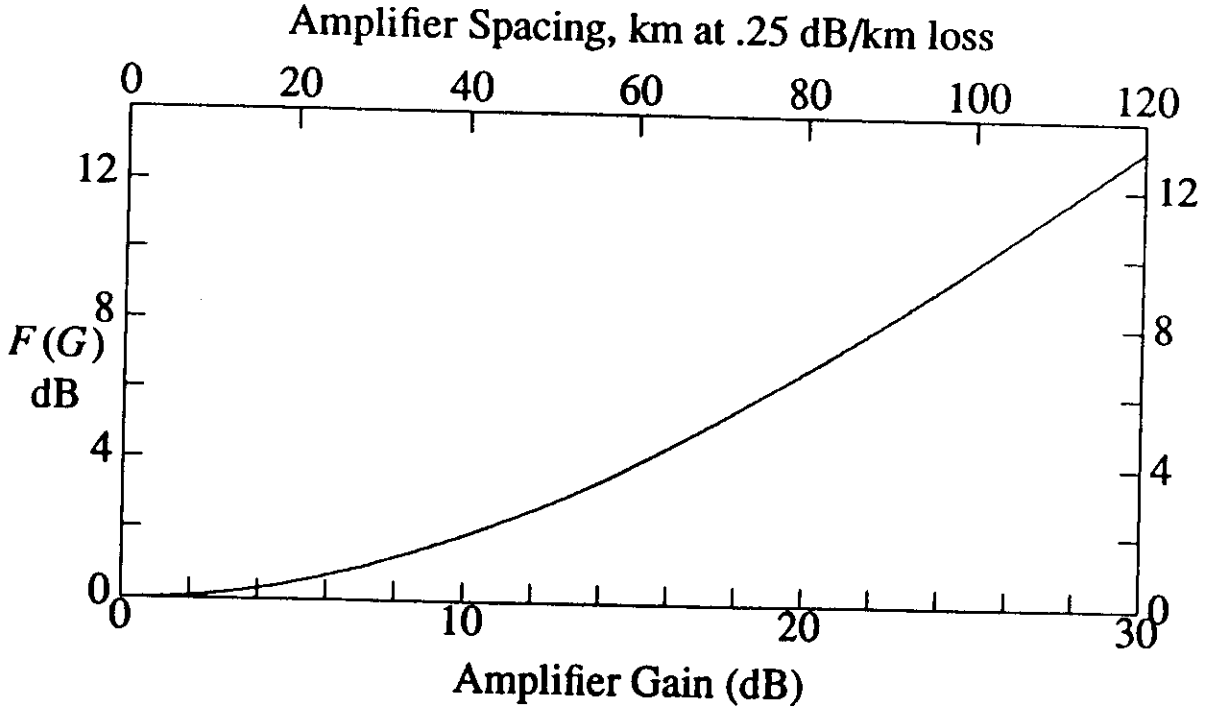

THE GORDON-HAUS EFFECT: OUTLINE OF PROOF

At each amplifier, addition of the noise field component $\delta u = i a u_{sol} \tanh(t)$ shifts the soliton's frequency by

$$\delta\Omega = \frac{2}{3} a$$

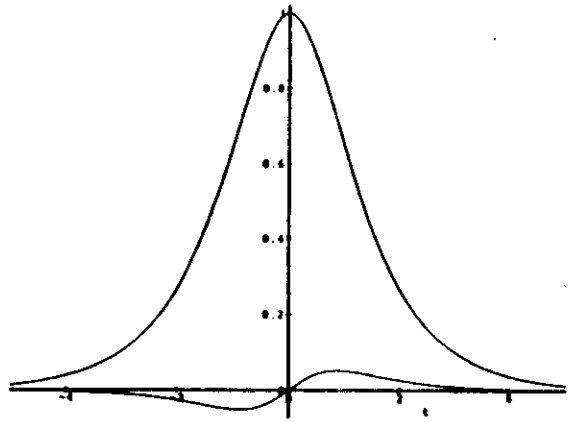

The net time shift of a given pulse is:

$$\delta t = \sum_{amps} \delta\Omega_n z_n$$

where z_n is distance from nth amp. to the end.

Get variance of δt by summing variances of the (independent) δt_n:

$$\langle \delta t^2 \rangle = \langle \delta\Omega^2 \rangle_{amp} \sum_{amps} z_n^2 = \langle \delta\Omega^2 \rangle_{amp} \frac{Z^3}{3L_{amp}}$$

(It can be shown that $\langle \delta\Omega^2 \rangle_{amp} = \frac{1}{3} \frac{(G-1) n_{sp} h\nu}{W_{sol}}$.)

THE GORDON-HAUS EFFECT: VARIANCE IN PULSE ARRIVAL TIMES FROM AMPLIFIED SPONTANEOUS EMISSION

In a broad-band transmission line, spontaneous emission modulates the soliton frequencies (velocities) at random.

Resultant variance of Gaussian distribution in arrival times at Z is:

$$\sigma^2 = 4138\, n_{sp} F(G) \frac{\alpha_{loss}}{A_{eff}} \frac{D}{\tau} Z^3$$

where α_{loss} is in km^{-1}, D in ps/nm-km, Z in Mm, τ in ps, A_{eff} in $\mu\mathrm{m}^2$.

Example: Let τ=20 ps, D=0.5 ps/nm-km, A_{eff}=50 $\mu\mathrm{m}^2$, α_{loss}=0.048/km (0.21 dB/km), F =1.19 (span between amplifiers = 30 km), and n_{sp} ~1.4.
Then, for 9,000 km, one obtains:

$$\sigma = 11 \text{ ps}$$

BIT ERROR RATES IN SOLITON TRANSMISSION AT 9000 km
BROADBAND TRANSMISSION LINE, 30 km AMPLIFIER SPACING

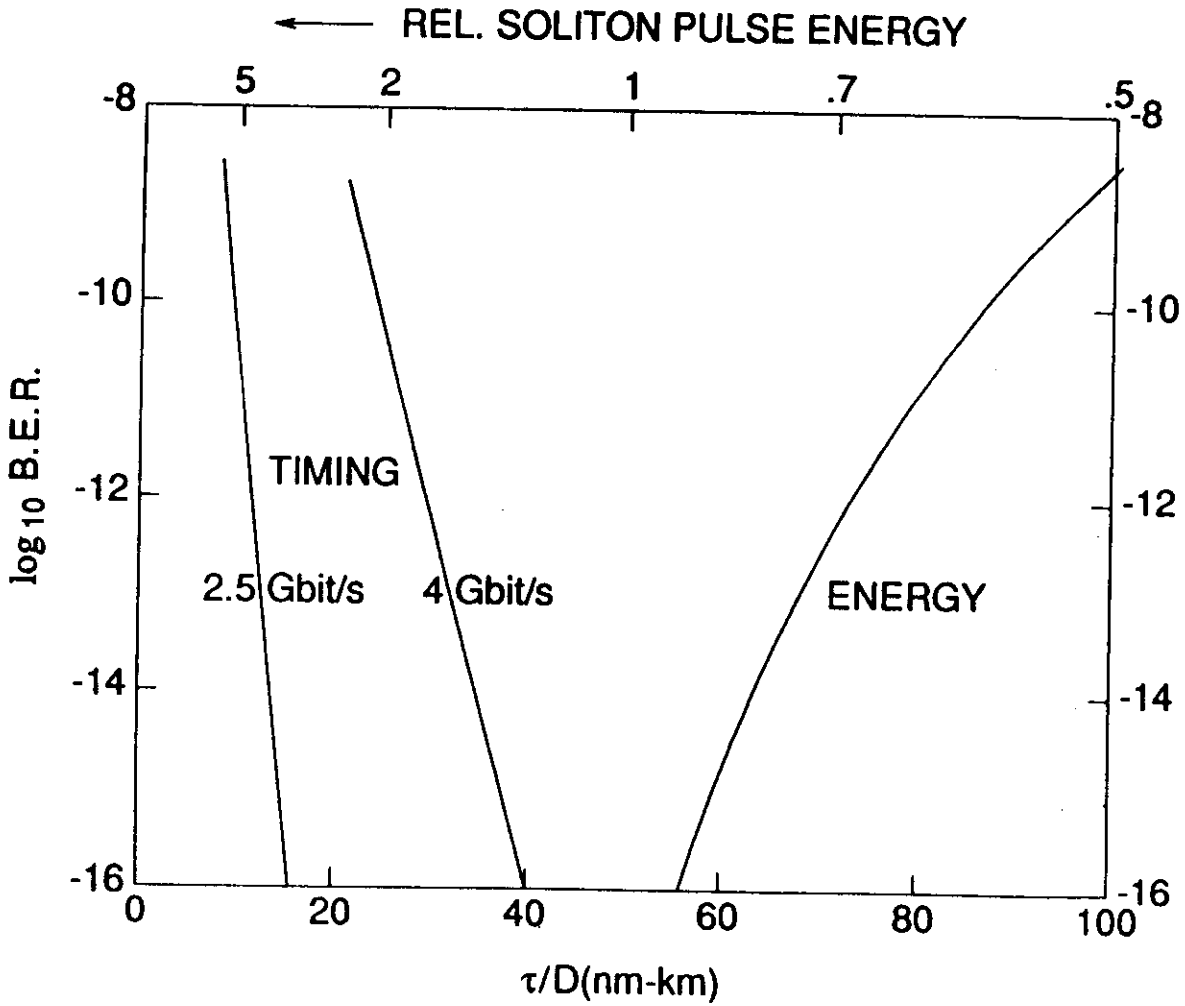

FREQUENCY-GUIDING FILTERS
(Typically, low-finesse FP etalons, one per amplifier)

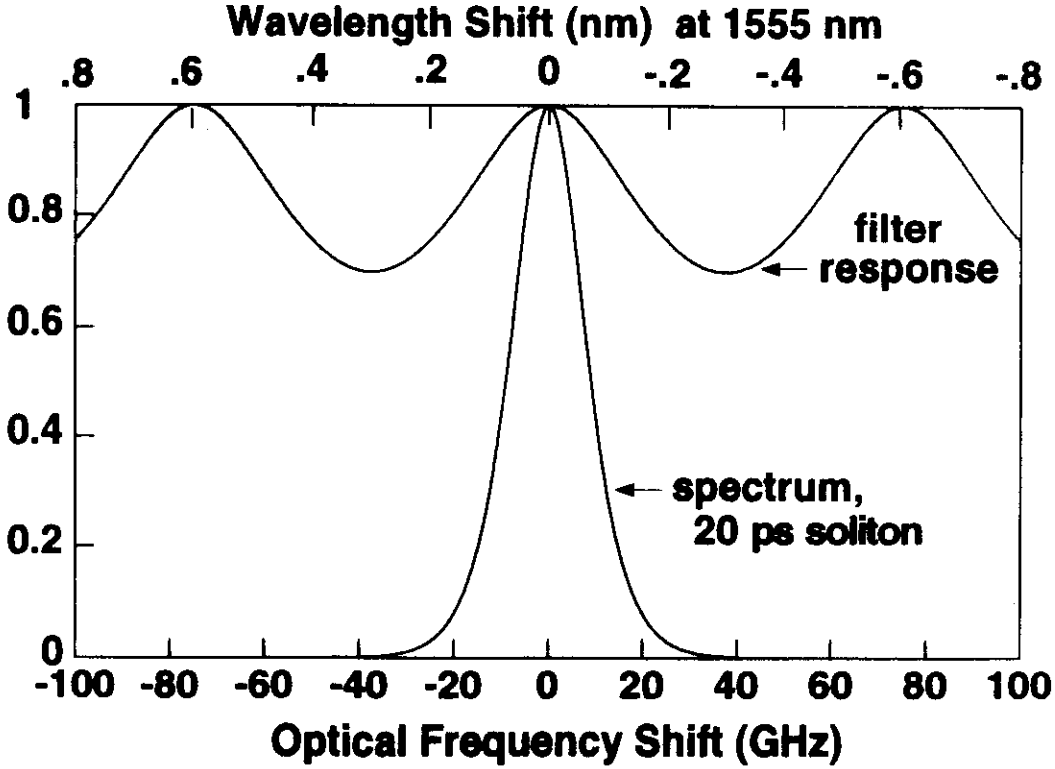

Filters:

- Reduce GH jitter by "guiding" soliton specta back to filter peaks.
- Reduce amplitude jitter because filter loss increases as soliton BW ($\propto W_{sol.}$)
- Are compatible with extensive WDM.
- Work only with solitons!

DECREASE OF JITTER IN PULSE ARRIVAL TIMES WITH OPTIMUM STRENGTH, FIXED-FREQUENCY FILTERS

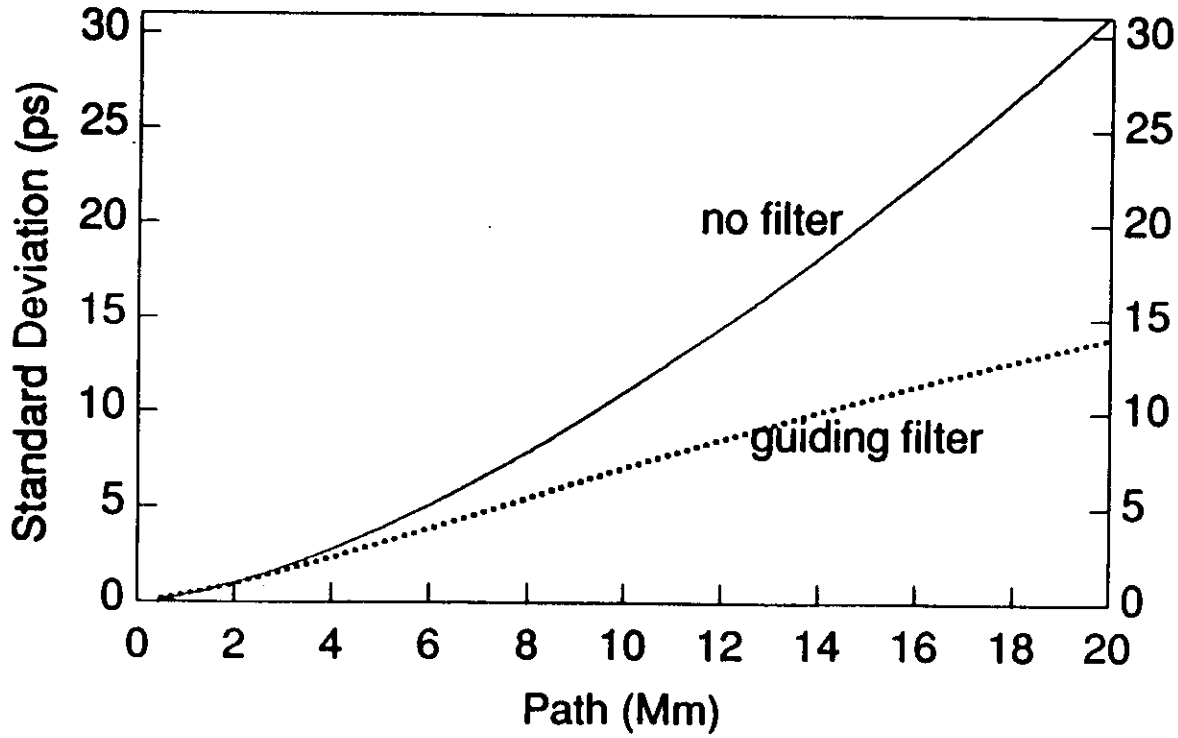

SLIDING-FREQUENCY GUIDING FILTERS:
Filter Frequency Response vs Distance

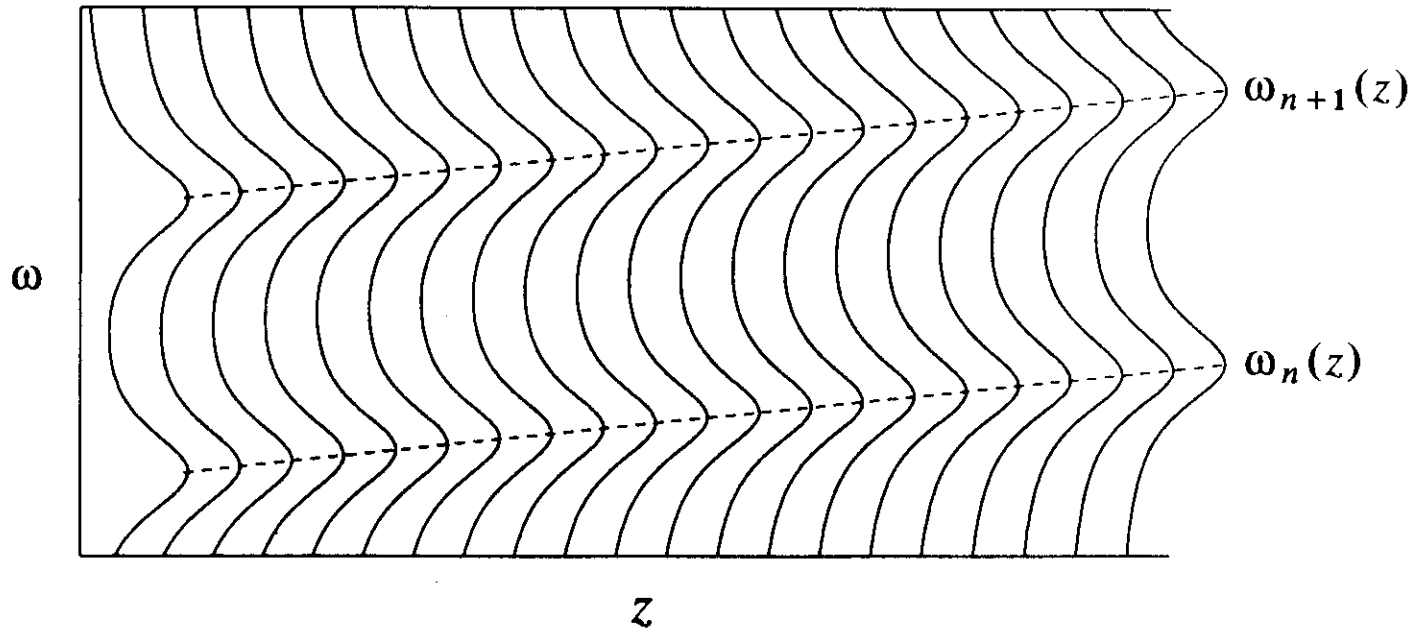

- **Solitons can follow the filter frequency sliding; noise cannot.**
- **Sliding allows filters to be many times stronger.**

SLIDING FREQUENCY FILTERS:
NOISE SPECTRAL DENSITY VS. FREQUENCY AND DISTANCE

One R=9%, 75 GHz FSR Etalon Filter per 50 km

Sliding Rate = 13 GHz/Mm; excess In gain = 1.4/Mm

Density normalized to value at 10 Mm with no filtering.

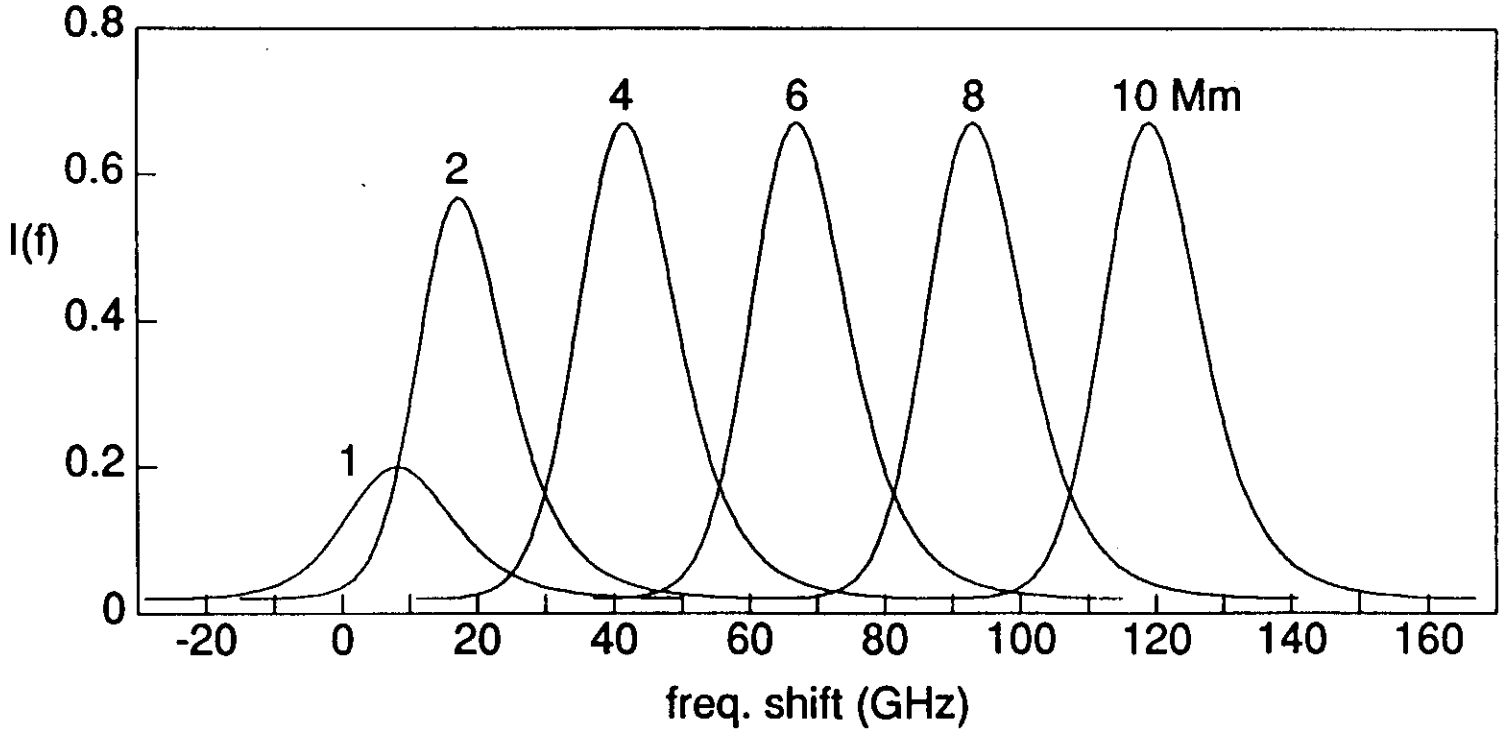

NLS EQUATION WITH FILTERING:

$$\frac{\partial u}{\partial z} = i\left[\frac{1}{2}\frac{\partial^2 u}{\partial t^2} + u^* u^2\right] + \frac{1}{2}\left[\alpha - \eta(i\frac{\partial}{\partial t} - \omega_f)^2\right] u$$

$\eta \equiv 2\zeta_2$ = curvature at filter peak; ω_f = filter frequency; α = excess gain

Exact Solution (no sliding; $\omega_f = 0$):

$$u = \sqrt{P}\,\mathrm{sech}(t)\exp(i\phi), \text{ where } \phi = Kz - \nu \ln\cosh(t)$$

$$\nu = \frac{3}{2\eta}\left[\sqrt{1+\frac{8\eta^2}{9}} - 1\right] = \frac{2}{3}\eta - \frac{4}{27}\eta^3 + \cdots$$

$$\alpha = (\eta/3)(1+\nu^2)$$

$$P = (1+\eta^2)(1-\nu^2/2)$$

$$K = (1/2)(1-\nu^2) + (\nu^2/3)(2-\nu^2)$$

(Pulse is chirped, i.e., $\frac{\partial \phi}{\partial t} = -\nu \tanh(t)$; rms BW increased by $\sqrt{1+\nu^2}$)

STD. DEV. OF SOLITON ENERGY ("ONES") AND OF "ZEROS"

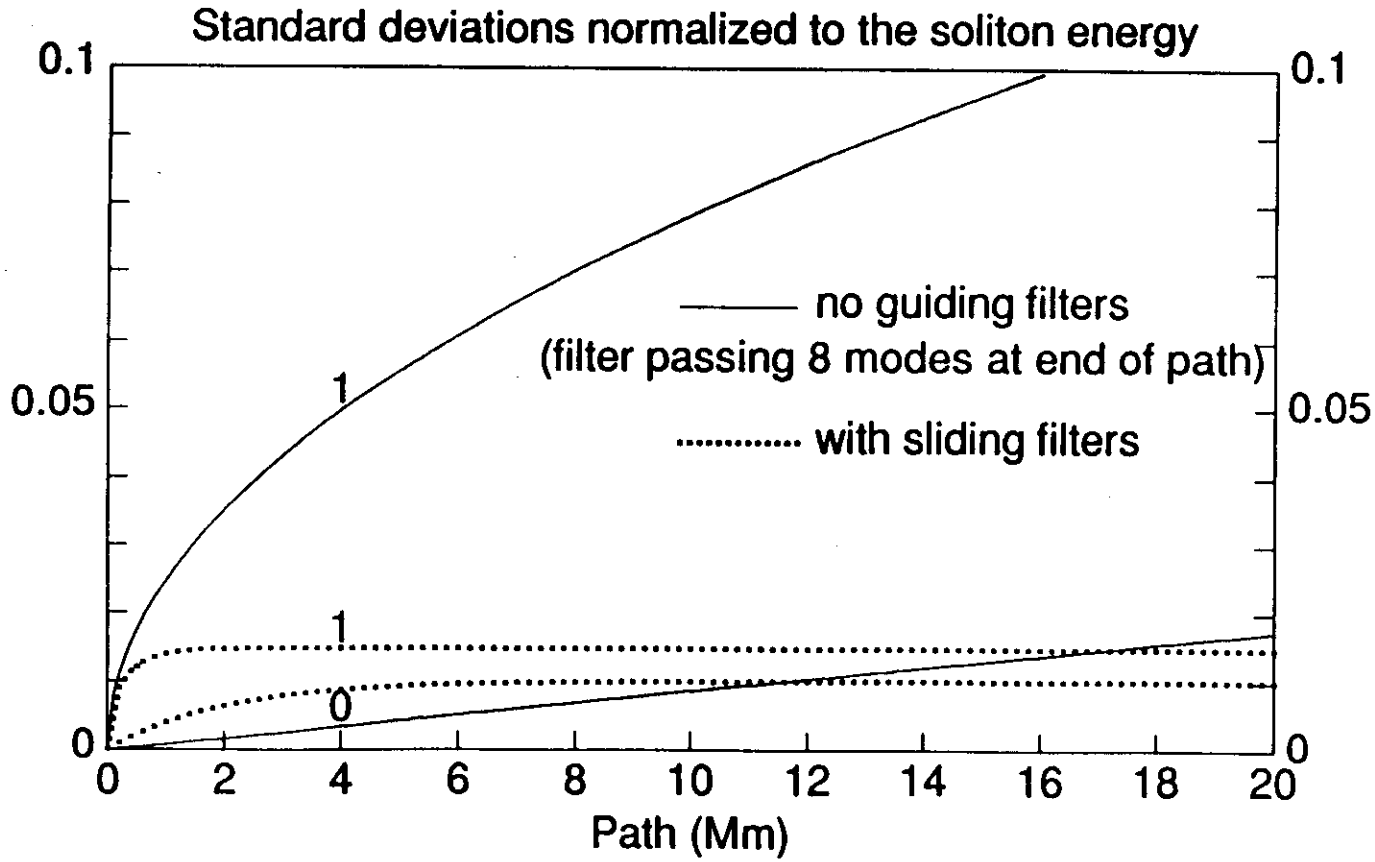

THE GORDON-HAUS EFFECT:
BROAD-BAND VS FILTERED TRANSMISSION LINES

Get variance of δt by summing variances of the (independent) δt_n:

For broad-band transmission line, one has:

$$\langle \delta t^2 \rangle = \langle \delta \Omega^2 \rangle_{amp} \sum_{amps} z_n^2 = \langle \delta \Omega^2 \rangle_{amp} \frac{Z^3}{3L_{amp}}$$

where z_n is the distance from the nth amp. to the end.

Filters reduce the z_n to the filter-damping length, γ^{-1}, so one then has:

$$\langle \delta t^2 \rangle = \langle \delta \Omega^2 \rangle_{amp} \sum_{amps} \gamma_n^{-2} = \langle \delta \Omega^2 \rangle_{amp} \frac{\gamma^{-2} Z}{L_{amp}}$$

Ex: For 10,000 km line, root mean square value of z_n ~7000 km.

But typical value for γ^{-1} is ~500 km.

STANDARD DEVIATION OF JITTER IN PULSE ARRIVAL TIMES

16 ps pulse, D = 0.5 ps/nm-km, n_{sp} = 1.6

Effective damping length ≈400 km

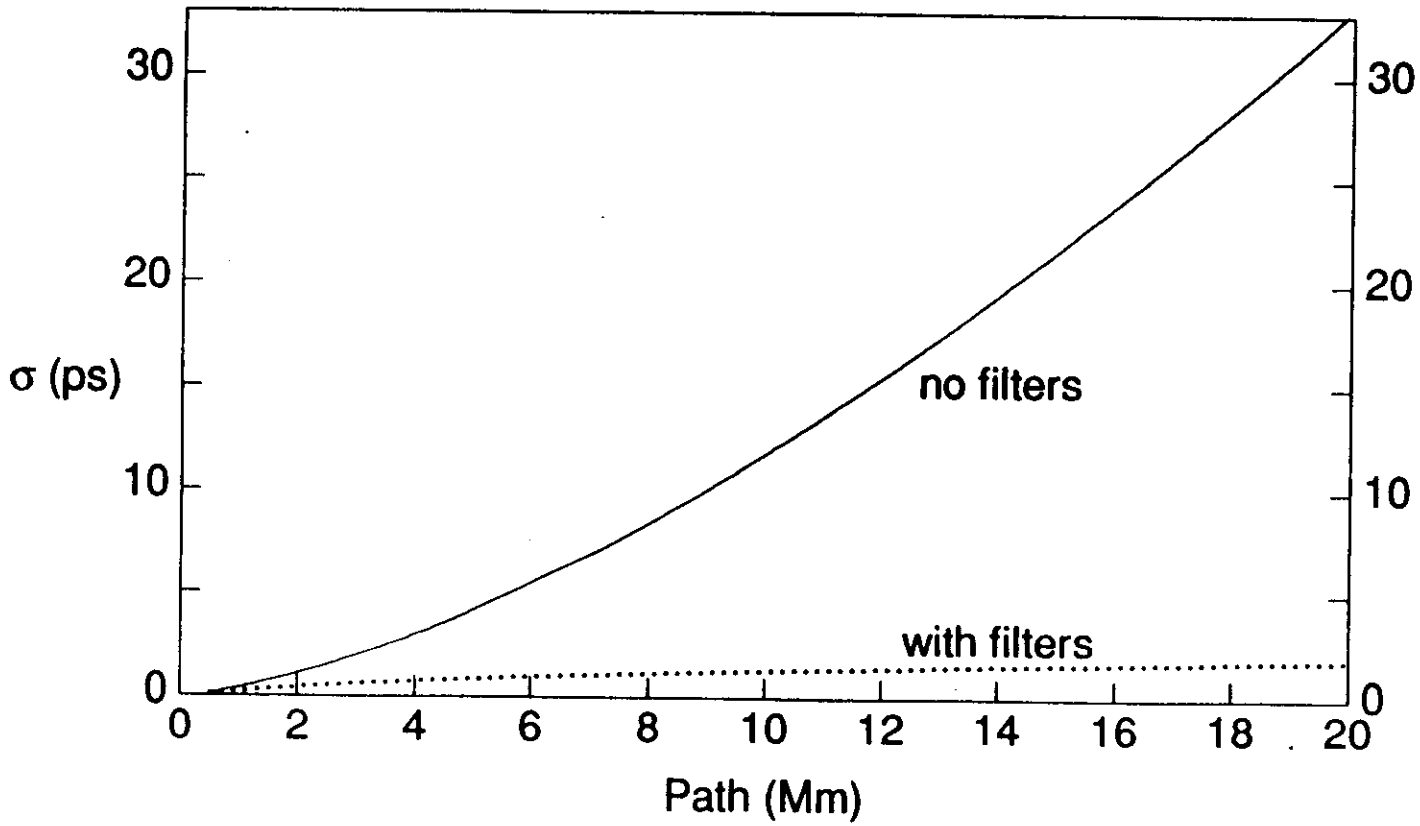

PRACTICAL EXAMPLE

Filters: one 1.5(2) mm gap, R = 9% etalon every 33(50) km

Pulse width	16 ps
D	0.5 ps/nm-km
z_c	130 km
Sliding rate	~7-14 GHz/Mm

Soliton pwr.	3.6 mW(path av.)
Time av. pwr.	0.6 mW(span input, 10 Gbit/s)

Recirculating Loop with Sliding -Frequency Filters
(Filters are 75 GHz FSR etalons with R=9%)

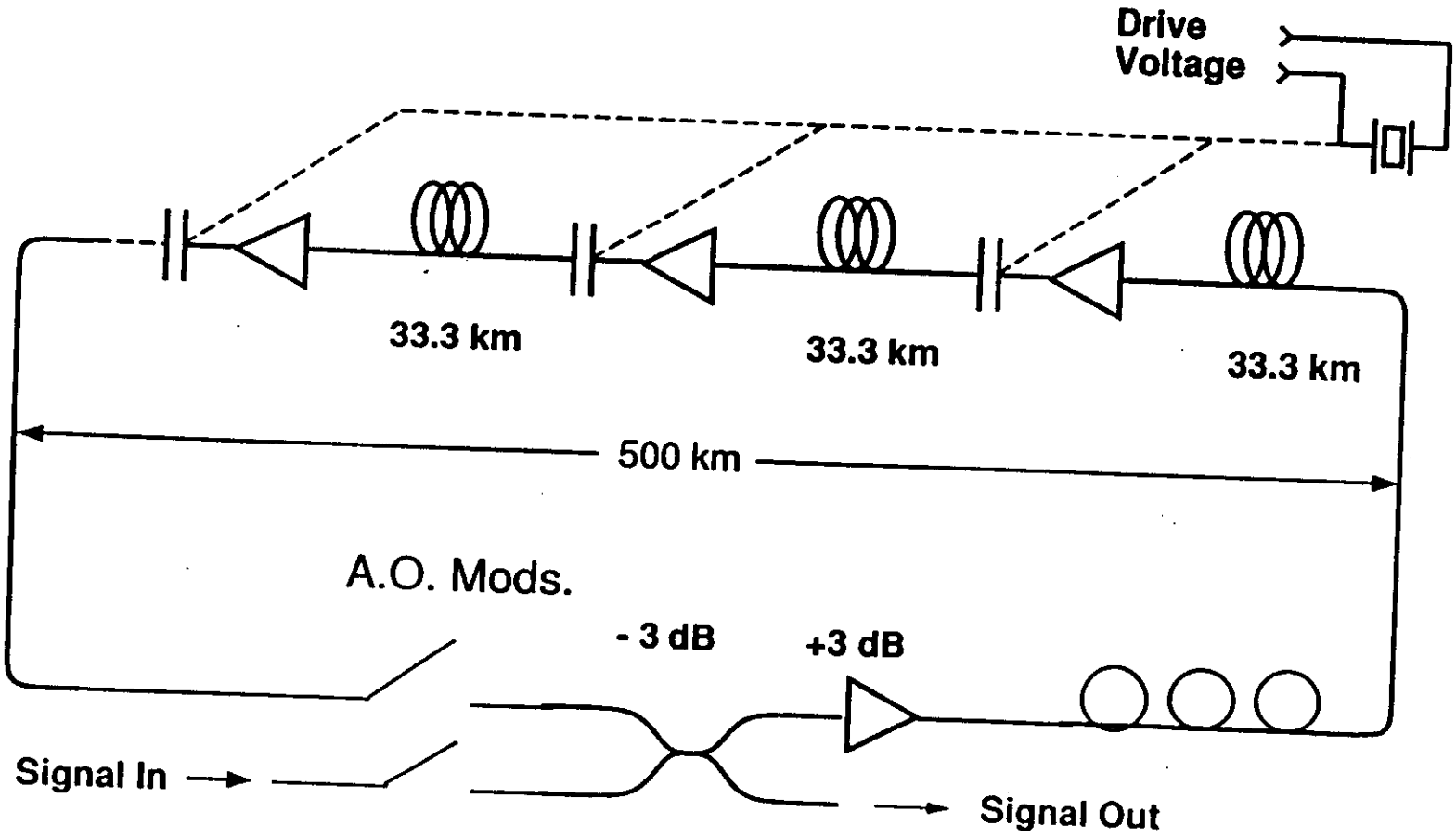

TIME-AVERAGE SIGNAL AND NOISE VS. DISTANCE WITH SLIDING-FREQUENCY FILTERS

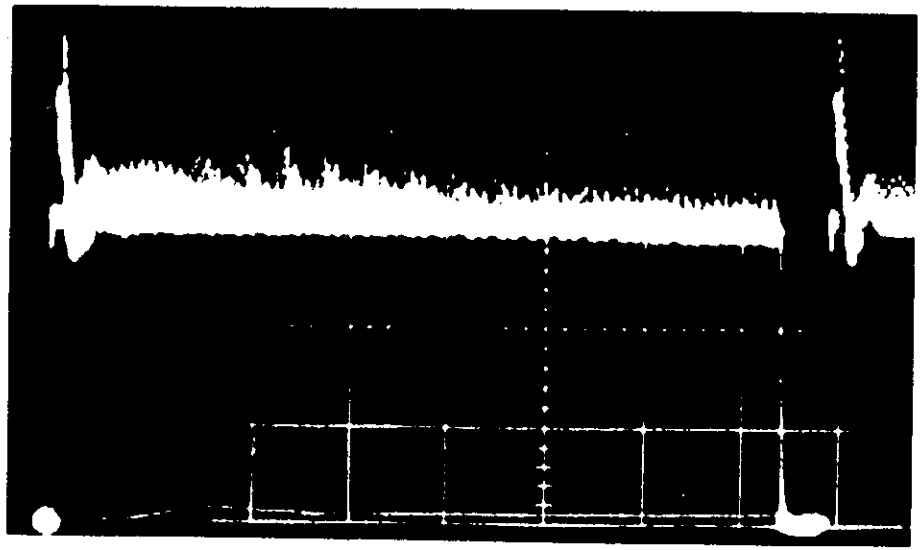

15 Mm

SLIDING-FREQUENCY GUIDING FILTERS AS AMPLITUDE NOISE EATERS

NOTE GREAT REDUCTION IN SOURCE AMPLITUDE NOISE AFTER ONLY ~6 ROUND TRIPS (PASSAGE THROUGH 18 FILTERS):

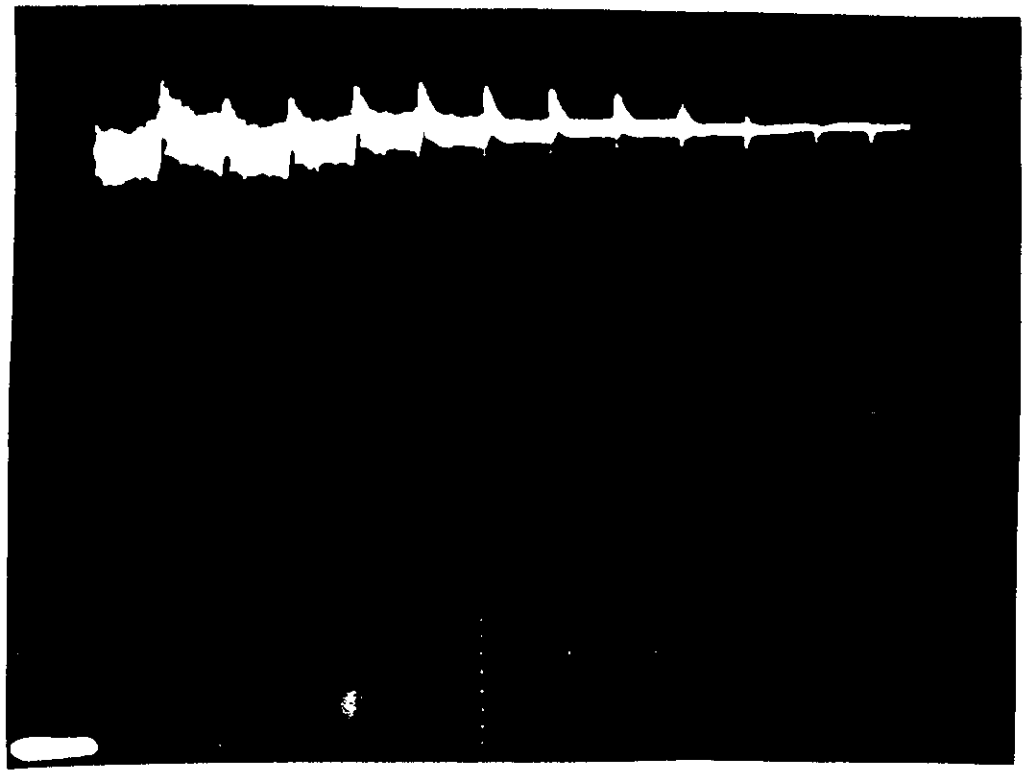

1000 km

IMPLIED DAMPING LENGTH = 380 km.

EYE DIAGRAM OF 20 ps SOLITONS AFTER 10 Mm TRANSMISSION USING SLIDING-FREQUENCY, GUIDING FILTERS

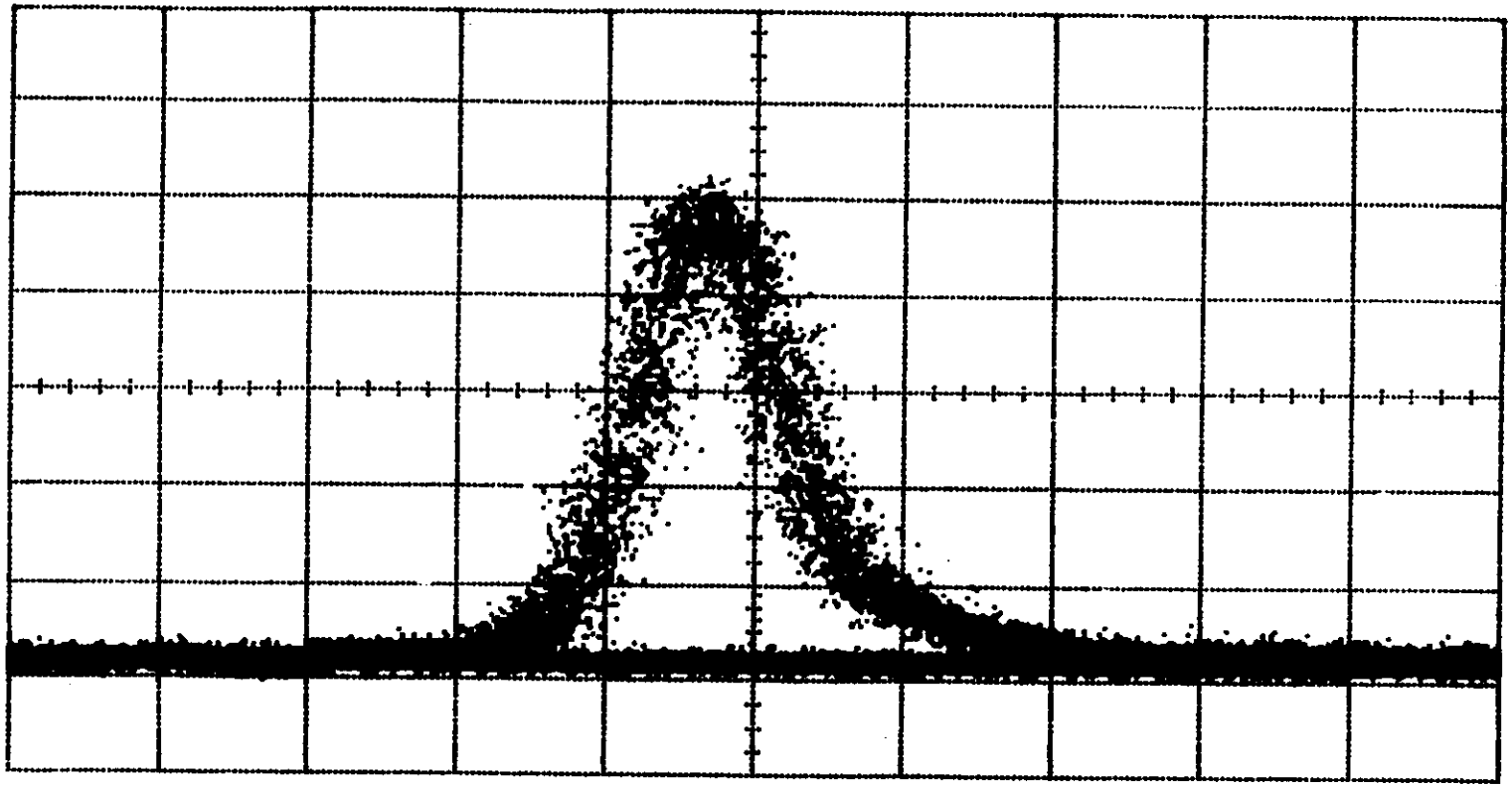

20 ps per division

TIME-DIVISION DEMULTIPLEXER

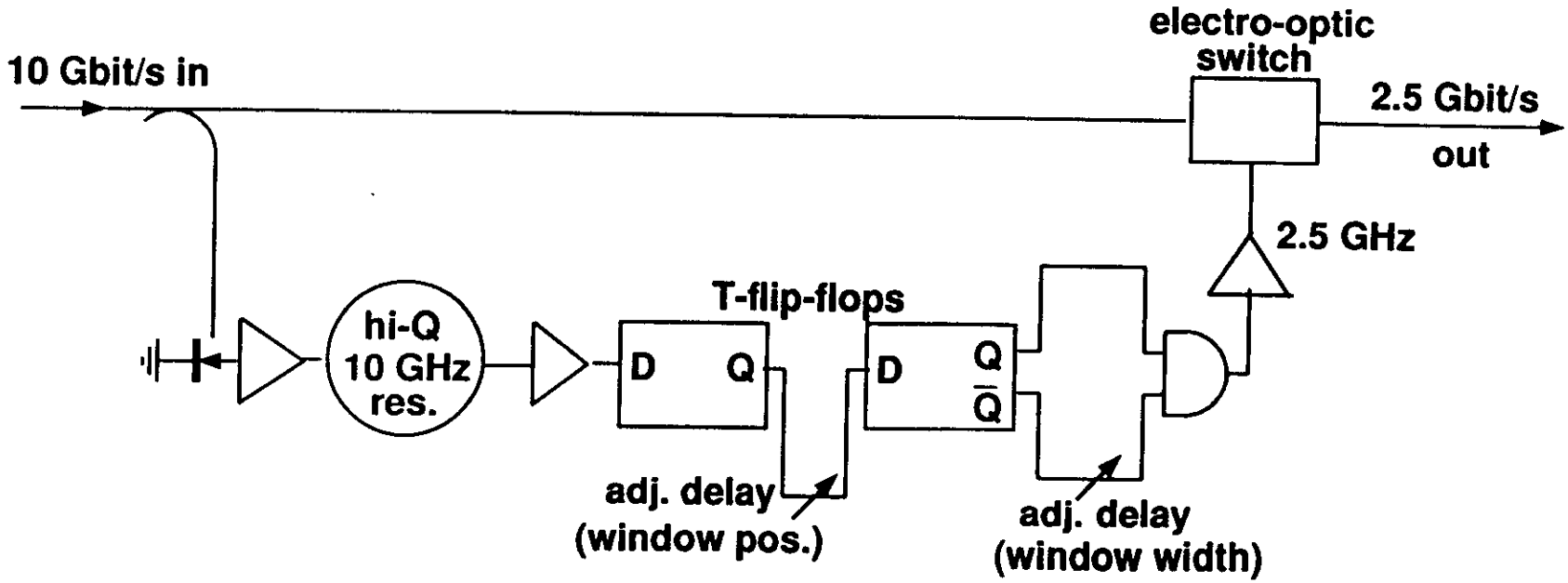

PHASE MARGIN AT 10^{-10} BER VS Z

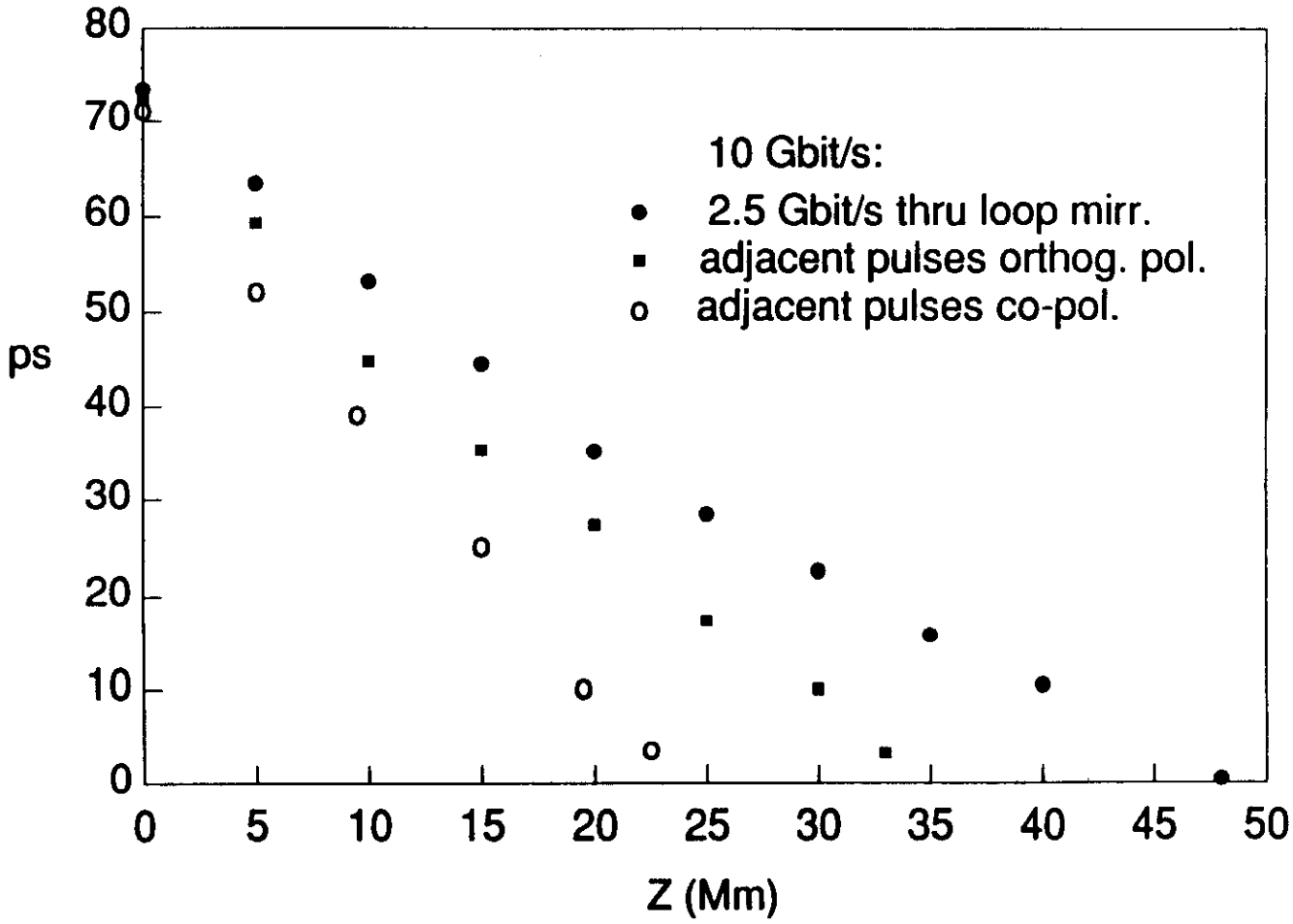

STD. DEV. OF JITTER USING SLIDING FREQ. FILTERS

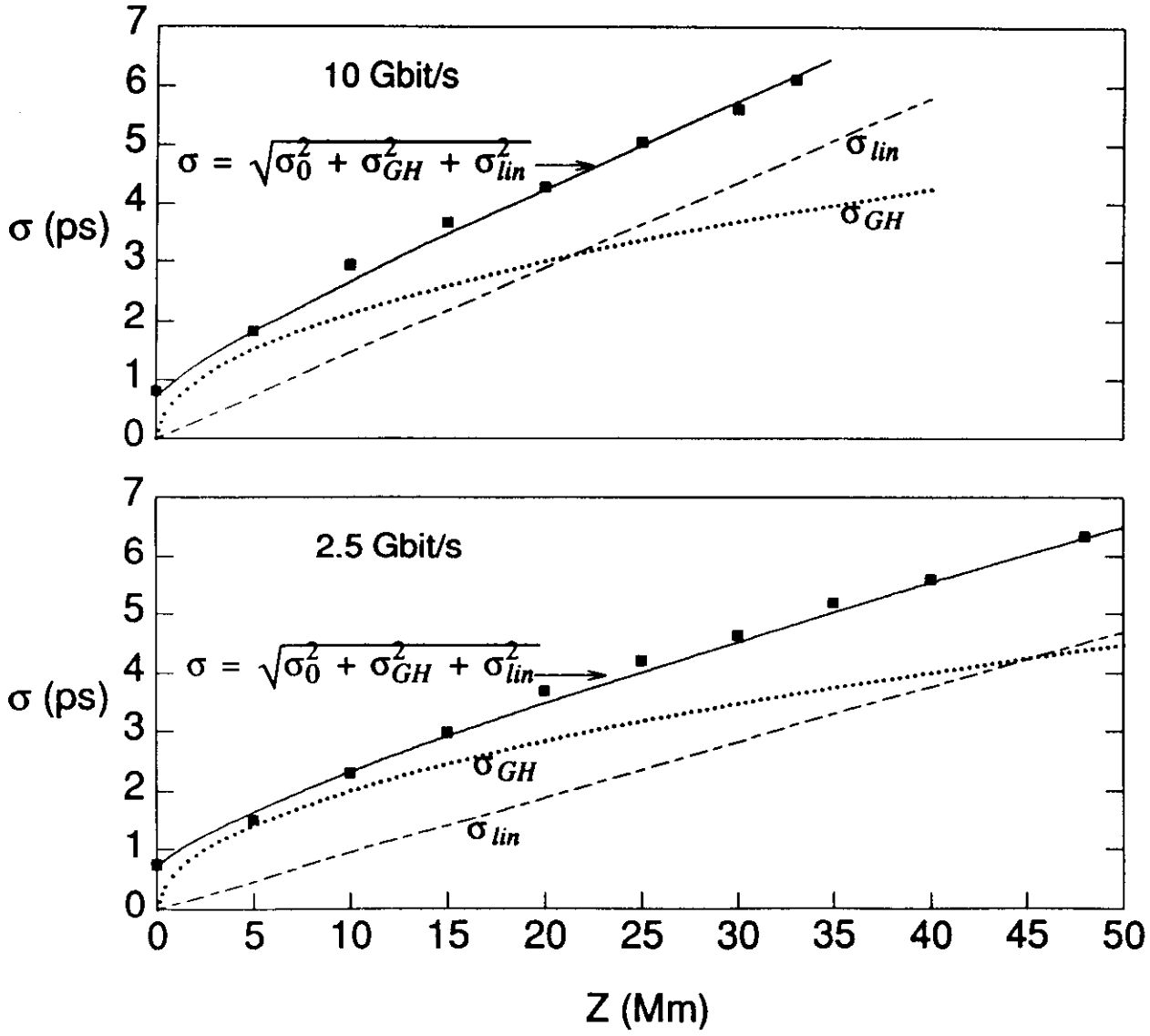

ACOUSTIC RESPONSE FOLLOWING PASSAGE OF SOLITON AT t = 0, AND REL. FREQUENCY SHIFTS INDUCED ON FOLLOWING SOLITONS†

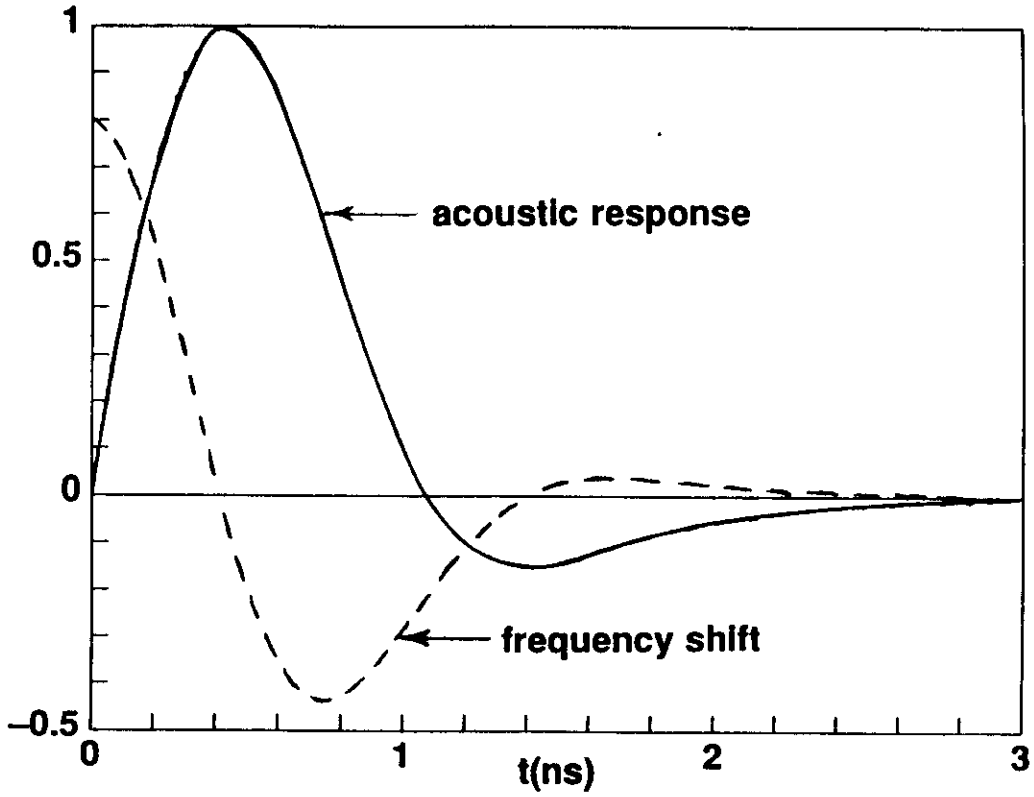

This leads to the jitter term: $\sigma_a = 8.6 \frac{D^2}{\tau} \sqrt{R - 0.99}\ \Delta^* Z$

where R is the bit rate and Δ is the filter damping length.

† from Dianov, Luchnikov, Pilipetskii, and Starodumov, *Opt. Lett.* 15 314 (1990)

BIT-ERROR-RATE IN SOLITON TRANSMISSION PASSIVILY REGENERATED BY "SLIDING-FREQUENCY GUIDING FILTERS"

Capacities shown can be multiplied many times by WDM

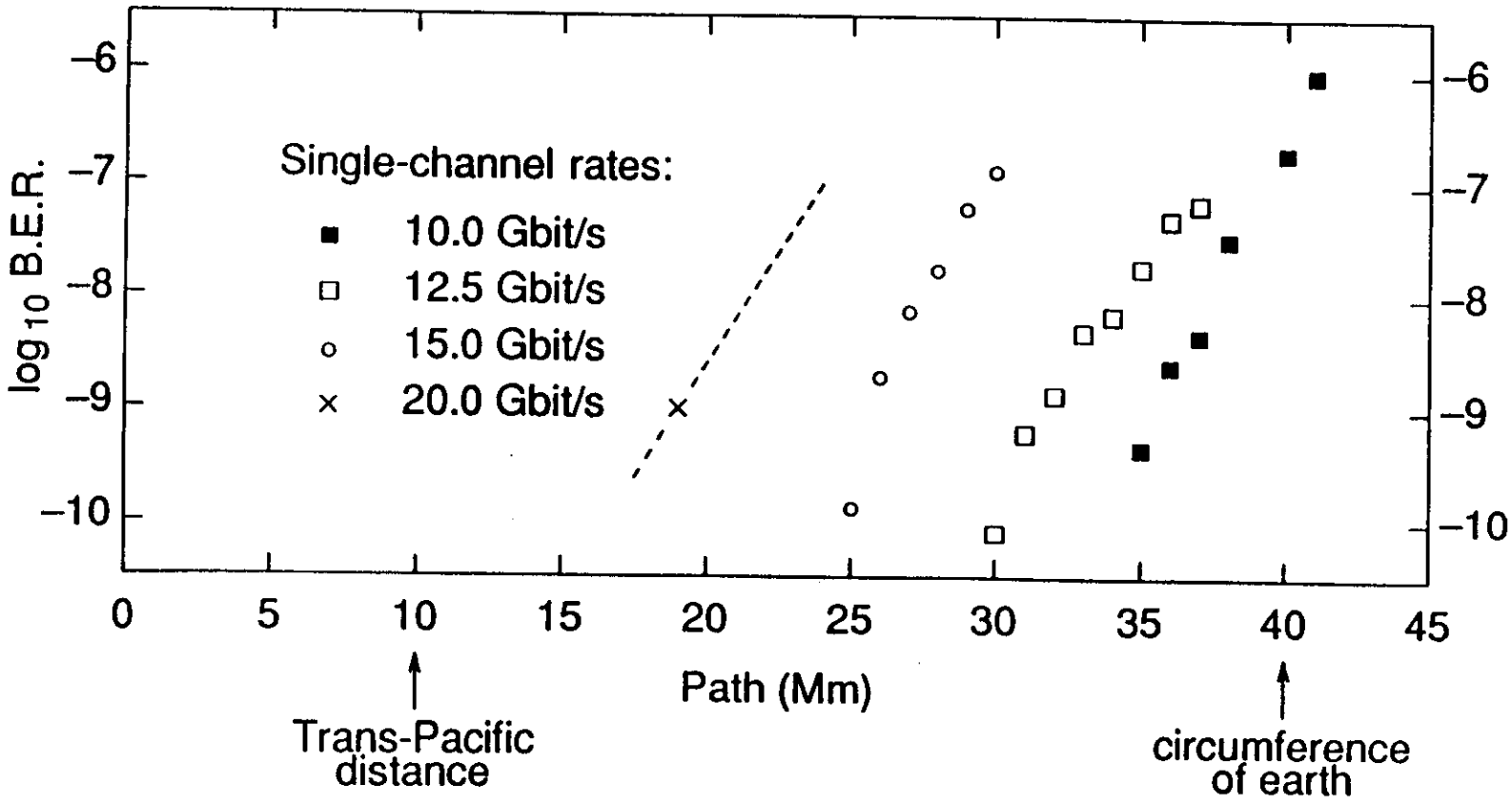

COMPUTATION OF "DIMENSIONLESS" FILTER STRENGTH, SLIDING RATE, AND EXCESS GAIN PARAMETERS FROM REAL WORLD QUANTITIES

With filters, the simplified propagation equation in soliton units is:

$$\frac{\partial u}{\partial z} = i\left(\frac{1}{2}\frac{\partial^2 u}{\partial t^2} + |u|^2 u\right) + \frac{1}{2}\left[\alpha - \eta\left(i\frac{\partial}{\partial t} - \omega_f\right)^2\right]u$$

When using etalon filters with mirror spacing d, reflectivity R, spaced L_f apart, η, ω'_f and α are computed as:

$$\eta = \frac{8\pi R}{(1-R)^2}\left(\frac{d}{\lambda}\right)^2 \frac{1}{DL_f}$$

$$\omega'_f = 4\pi^2 f' c t_c^3/(\lambda^2 D)$$

$$\alpha = \alpha_R t_c^2 2\pi c/(\lambda^2 D)$$

SOLITON PULSE ENERGY RANGE FOR ERROR FREE TRANSMISSION
SLIDING RATE = 13 GHz/Mm (OPTIMUM RATE)

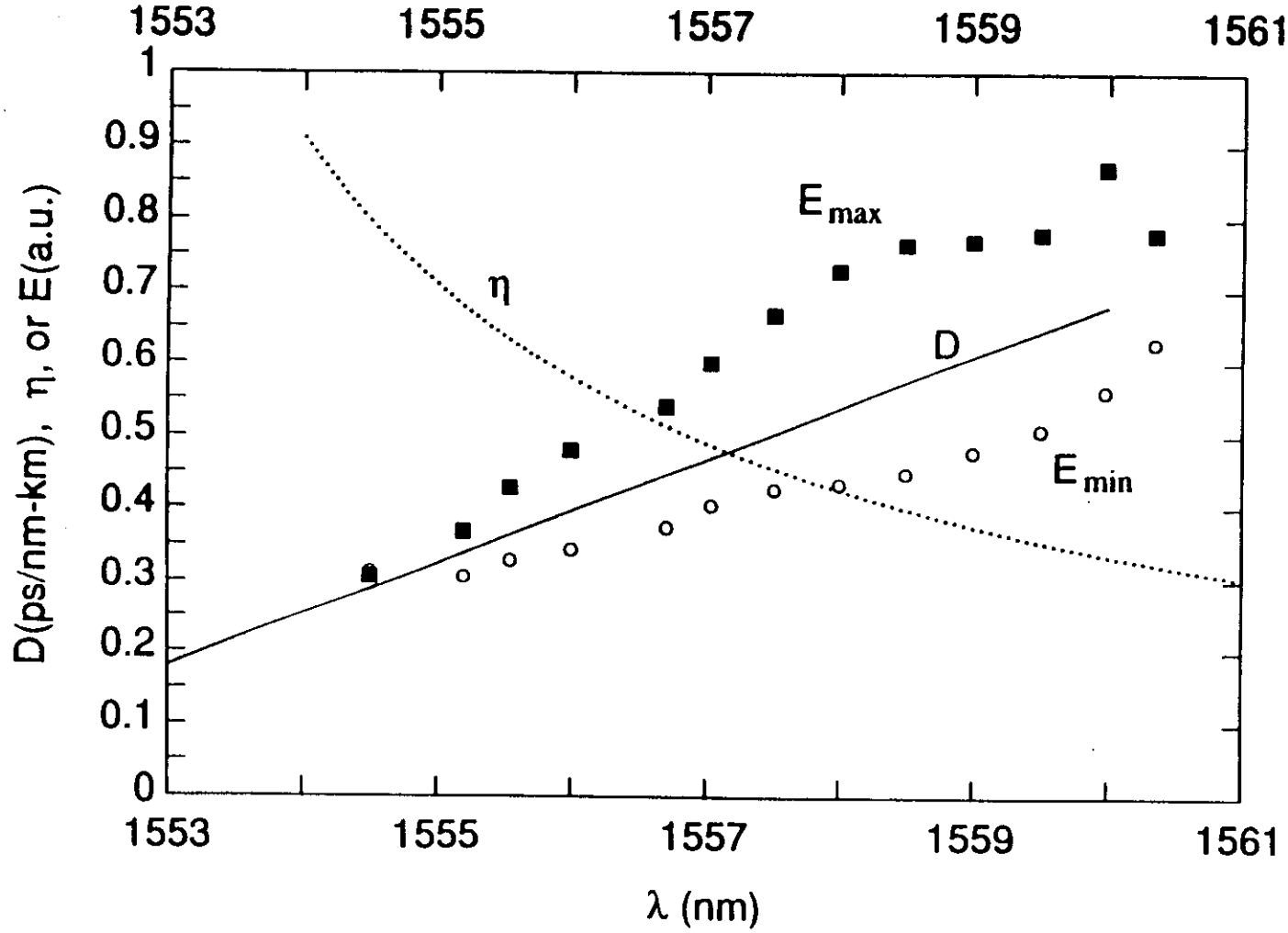

SOLITON ENERGY RANGE FOR ERROR FREE TRANS. VS SLIDING RATE FILTER STRENGTH PARAMETER $\eta = 0.4$ (OPTIMUM VALUE)

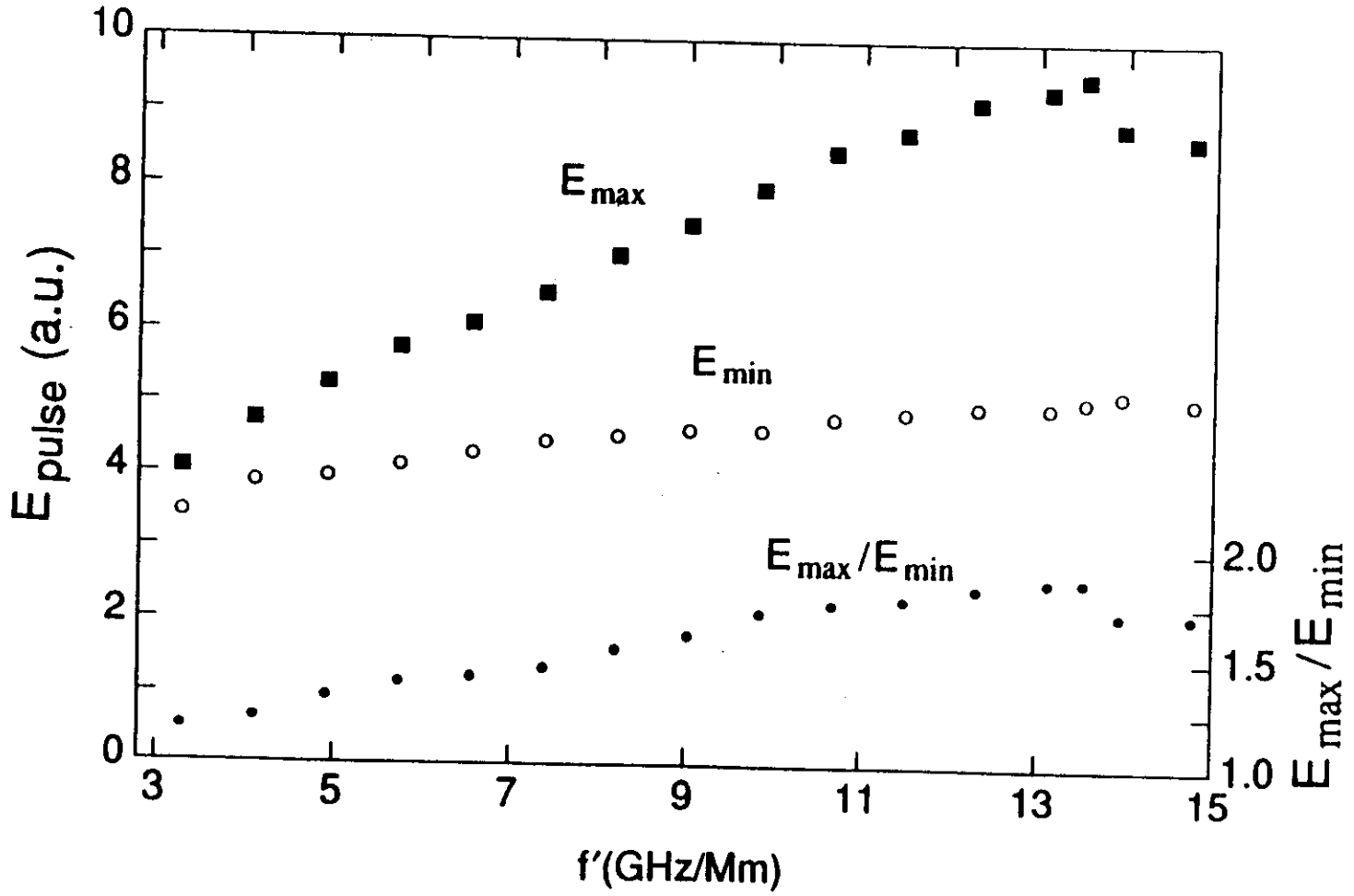

SOLITON PEAK INTENS. VS. PATH FOR VARIOUS EXCESS GAINS

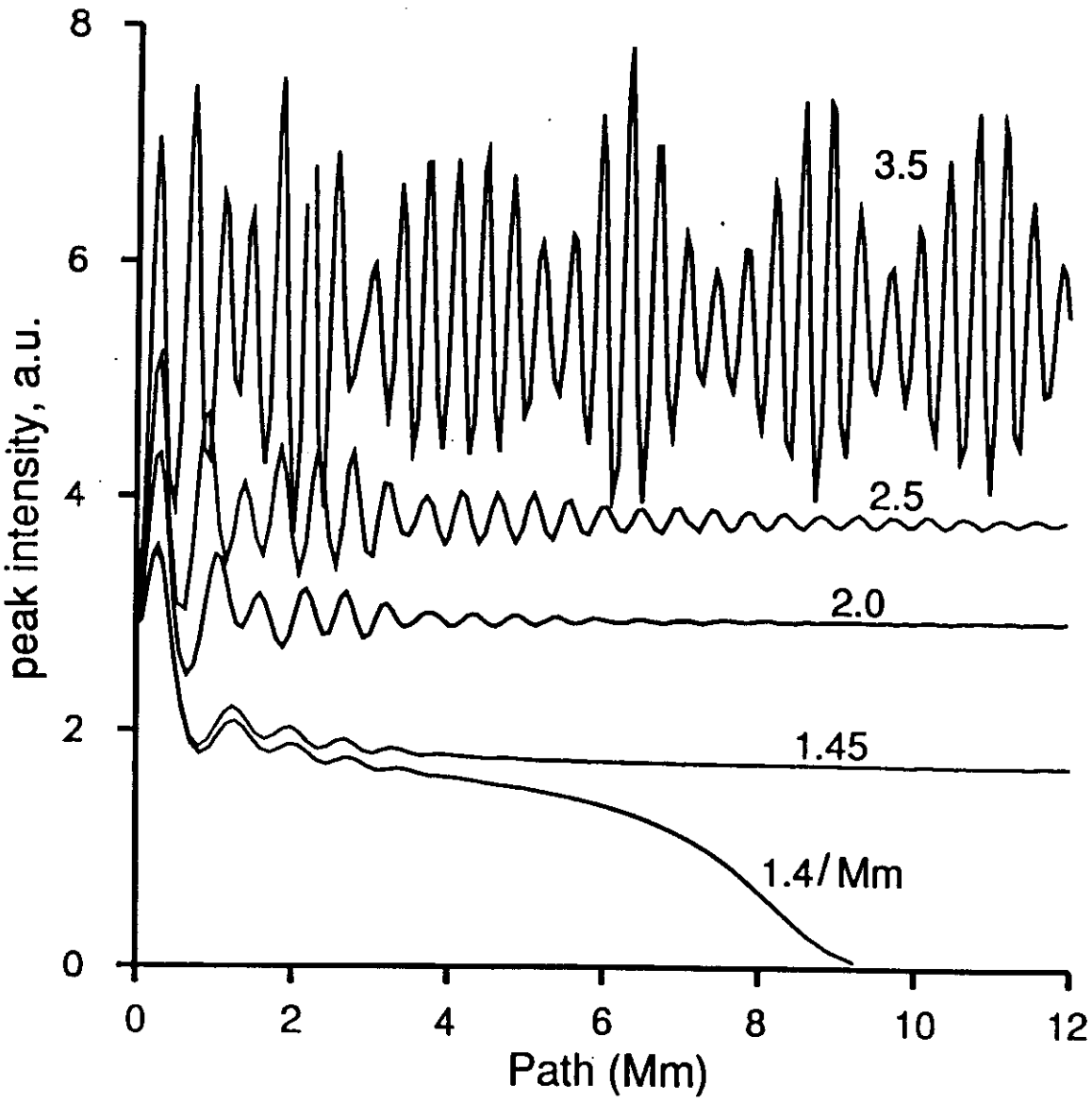

TRANSFER FUNCTION

OF A TRANSMISSION LINE WITH SLIDING FILTERS

(sliding rate 13 GHz/Mm, excess gain 2/Mm, τ_{in} = 15 ps)

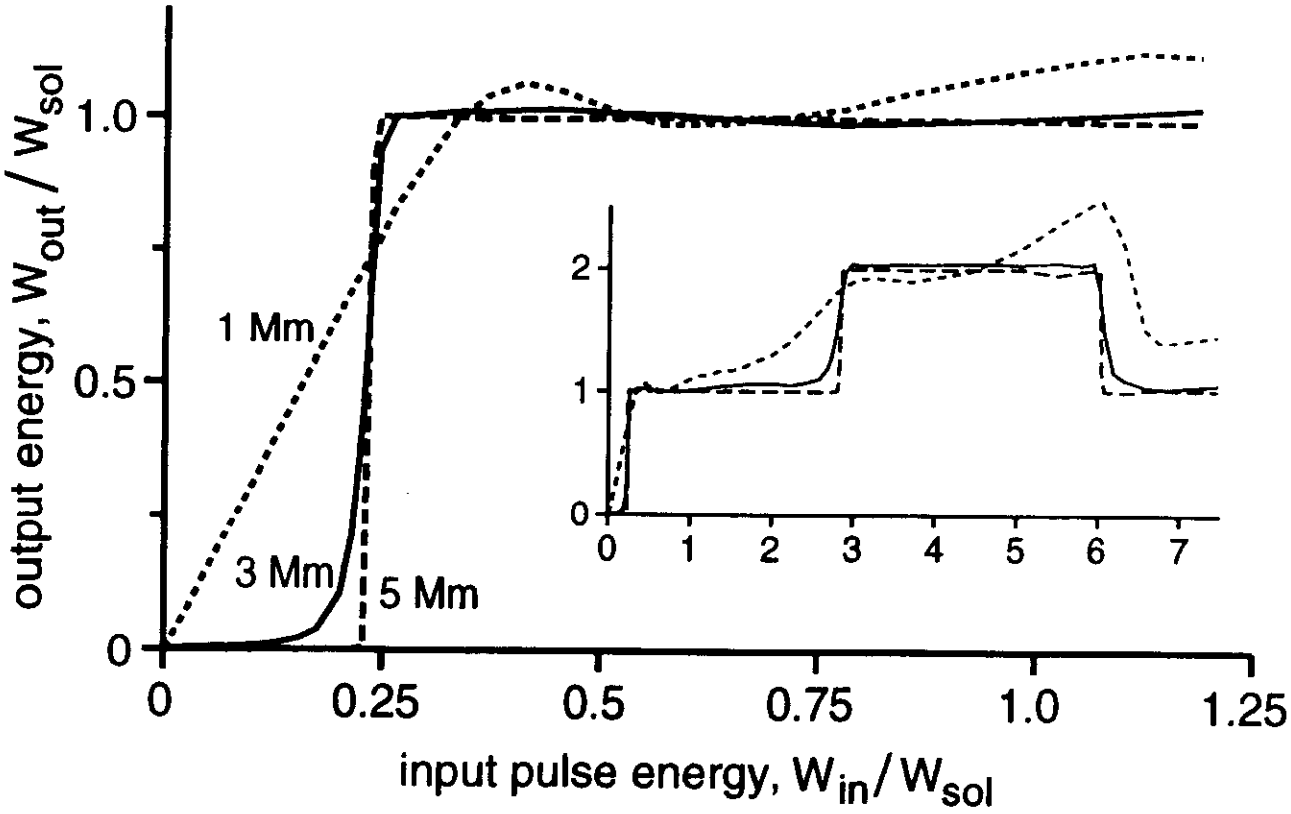

Dual-wavelength source of high-repetition-rate, transform-limited optical pulses for soliton transmission

Inventor: Pavel V. Mamyshev

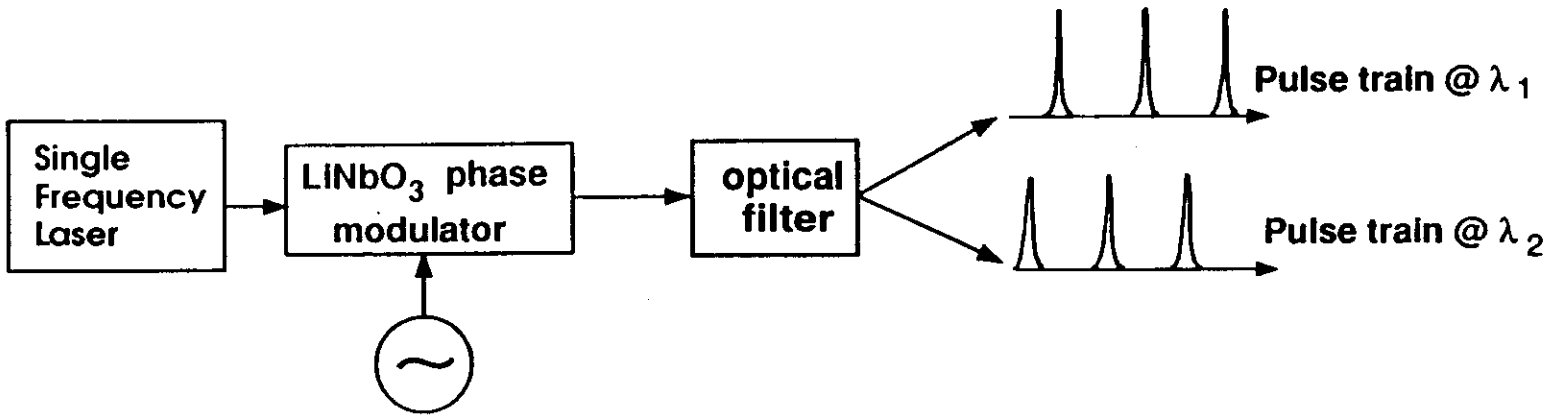

$$\Phi(t) = A\sin(\Omega t) + \Phi_0$$

$$\delta\omega(t) \equiv \omega(t) - \omega_0 = \frac{\partial \Phi}{\partial t} = A\Omega\cos(\Omega t)$$

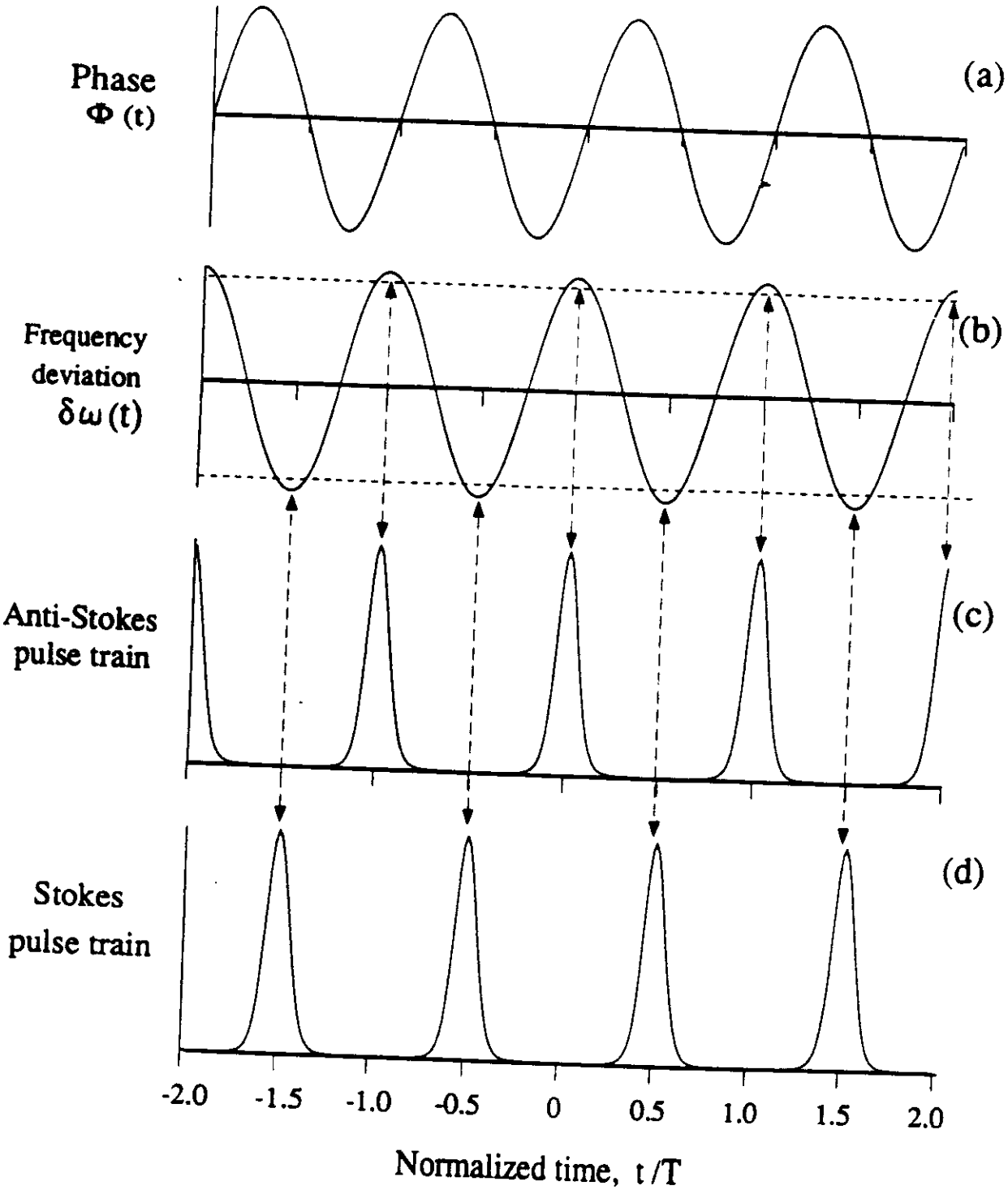

Experimental test at 10 GHz:

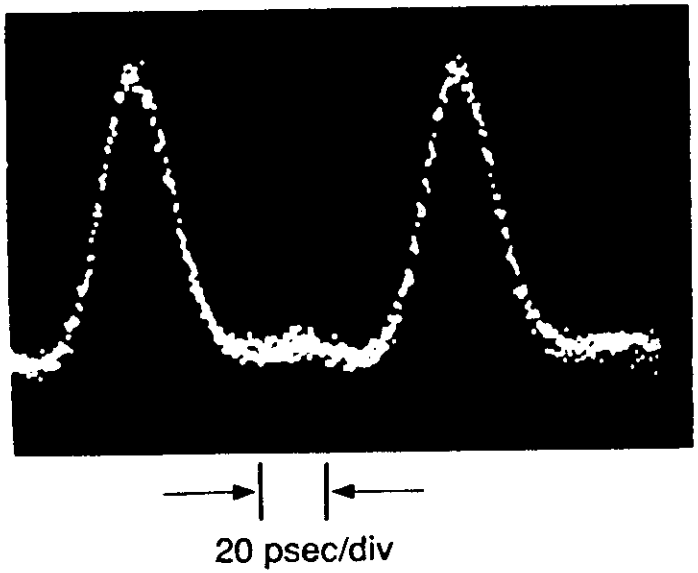

Pulses

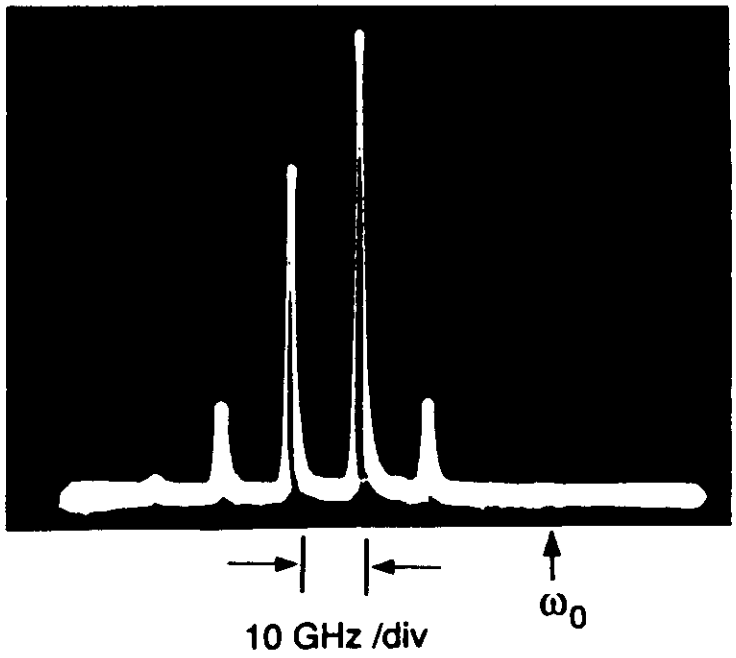

Spectrum

"NRZ" soliton source

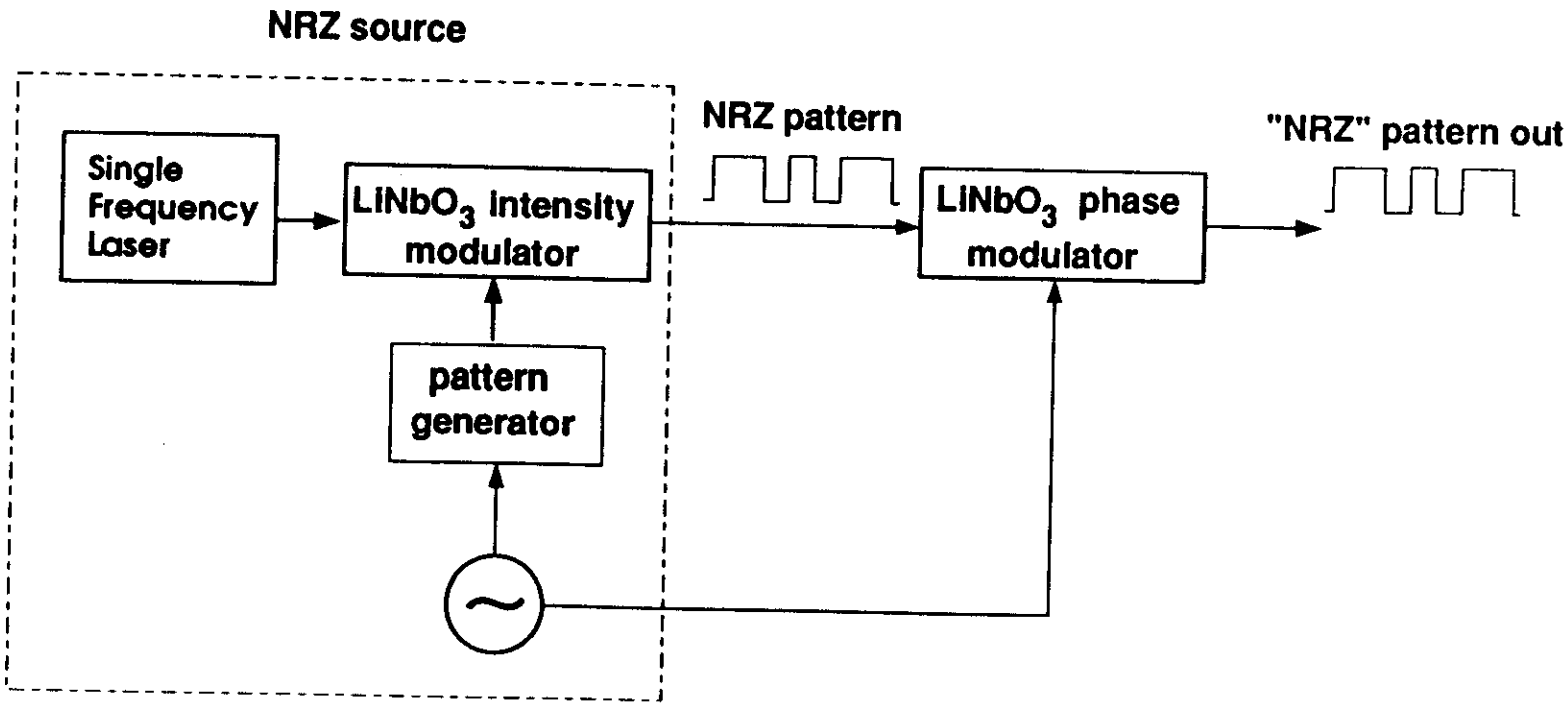

"NRZ" TO SOLITON CONVERSION BY FILTERED TRANS. LINE

"NRZ" DATA IN

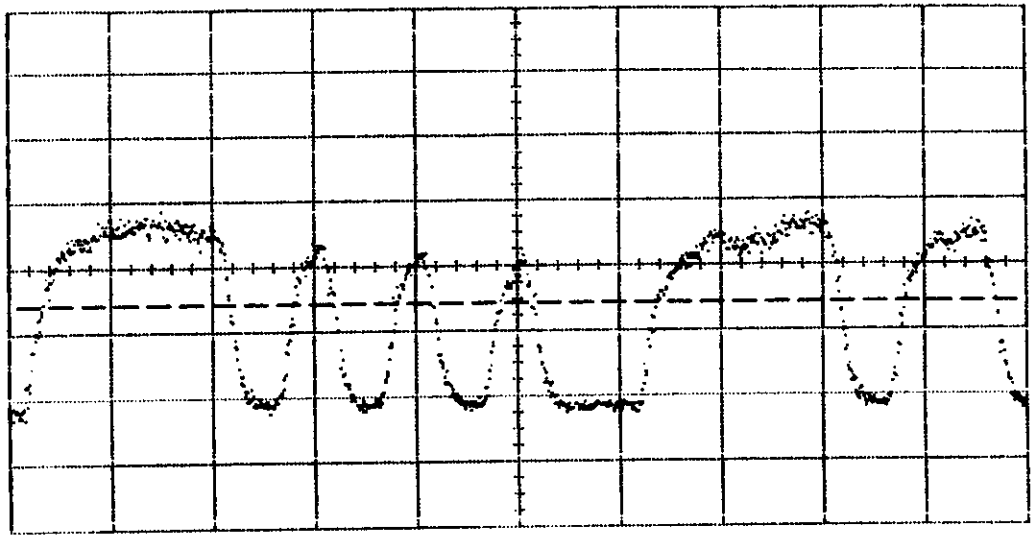

DATA OUT AT 10 Mm
(EYE DIAGRAM)

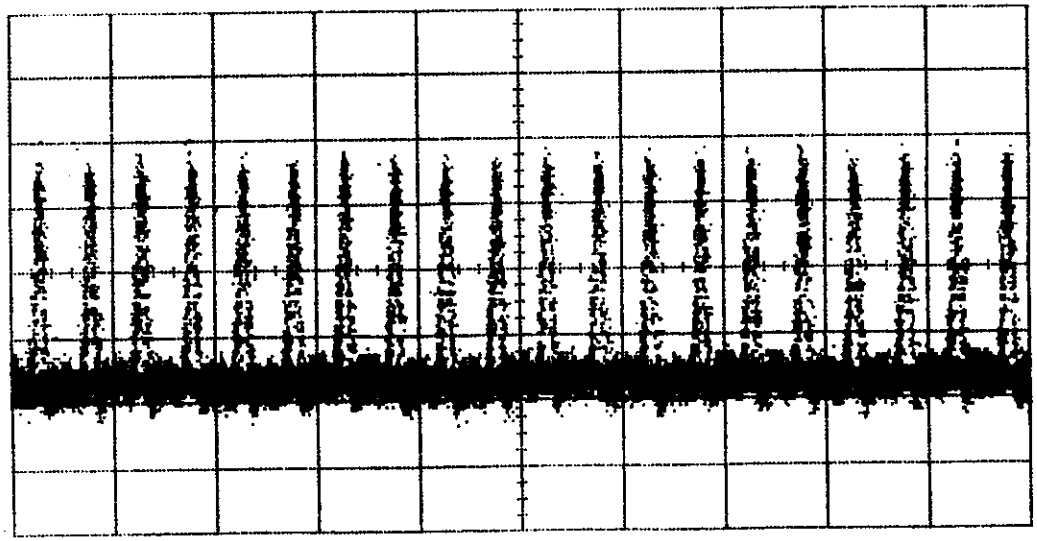

200 ps/div

ERROR FREE DISTANCES IN SINGLE CHANNEL TRANSMISSION

SOLITONS VS NRZ

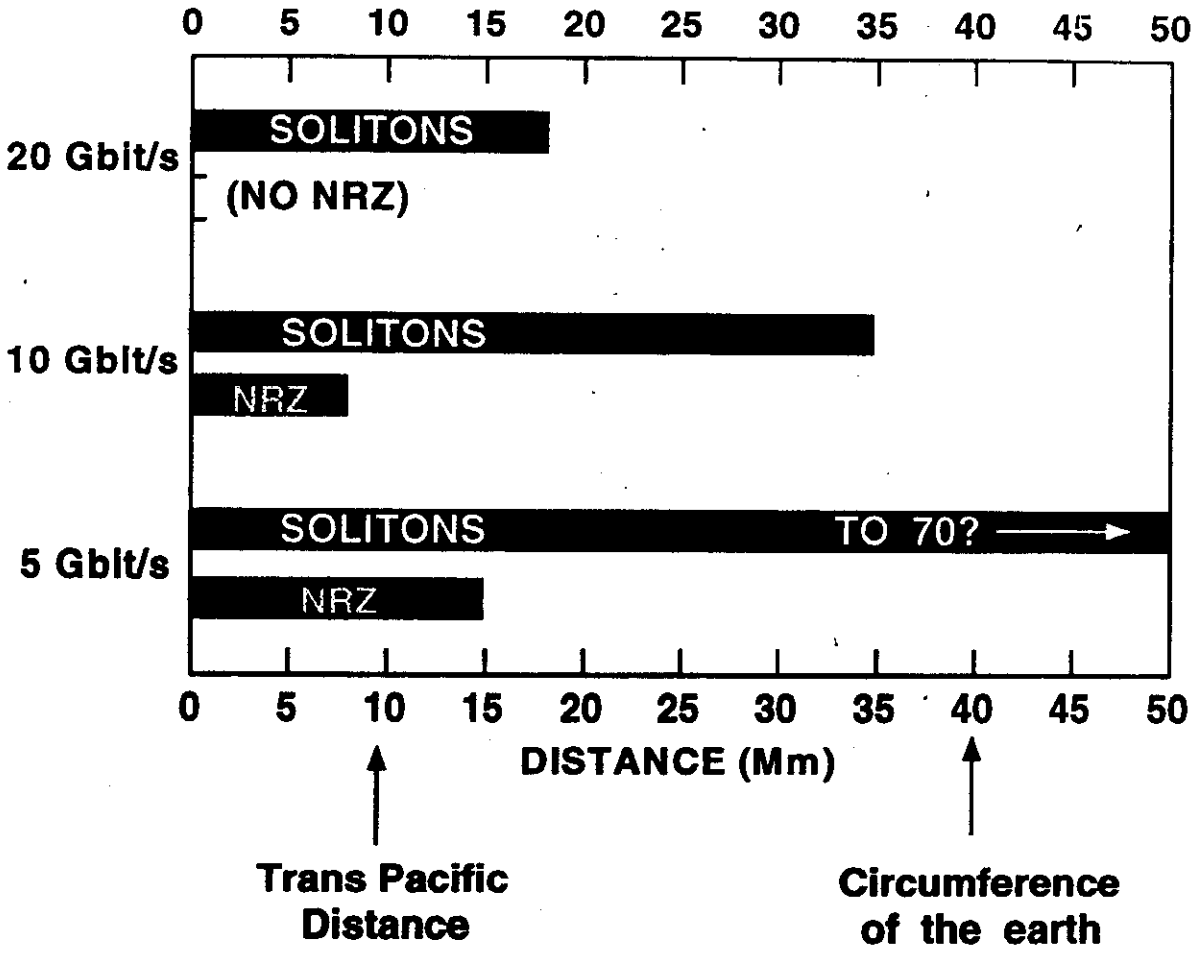

Lecture #3:

WAVELENGTH DIVISION MULTIPLEXING

Linn F. Mollenauer
Photonics Systems Research
Bell Labs
Lucent Technologies
Holmdel, NJ
USA

Winter College on Optics, Trieste, Italy
February 10, 1998

POTENTIAL CAPACITY OF ERBIUM AMPLIFIERS FOR WDM

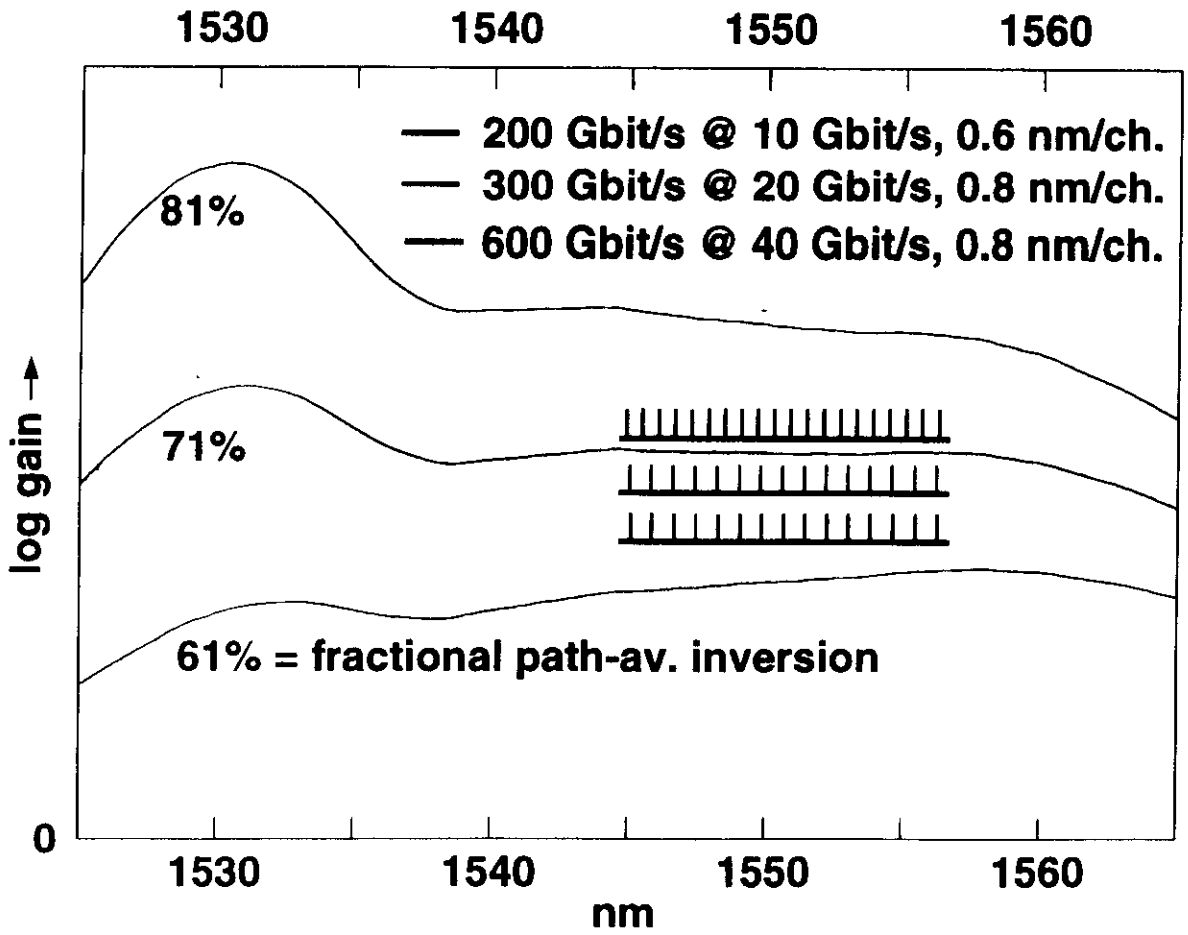

SOLITON-SOLITON COLLISIONS IN WDM

In WDM, solitons of different channels overtake and pass through ("collide" with) each other:

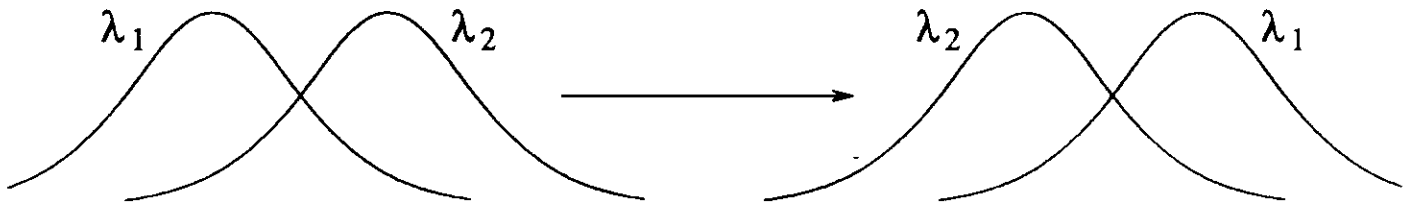

Let L_{coll} begin and end with overlap at the half power points:

$$L_{coll} = \frac{2\tau}{D\,\Delta\lambda}$$

Example: for $\tau = 20$ ps, $D = 0.5$ ps/nm-km and $\Delta\lambda = 0.6$ nm,

$$L_{coll} = 133 \text{ km}$$

SOLITON-SOLITON COLLISION IN A LOSSLESS FIBER

ACCELERATION, VELOCITY, AND TIME SHIFTS OF THE SLOWER PULSE

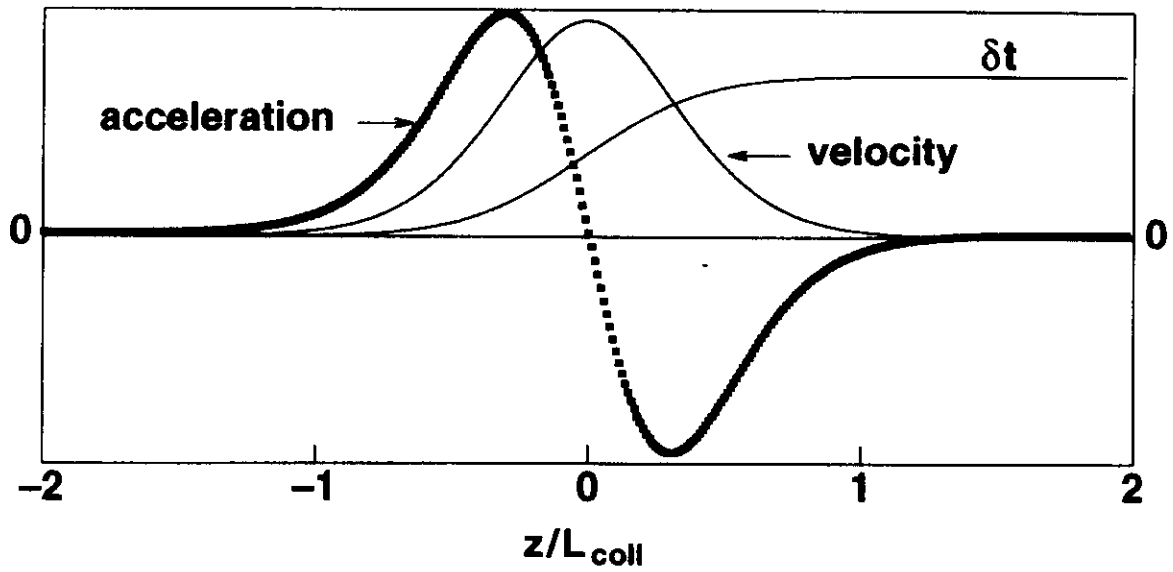

Note that there has been no net exchange of energy or momentum. Thus, the solitons are perfectly transparent to one another.

SOLITON-SOLITON COLLISIONS IN A SYSTEM WITH LUMPED AMPS.

L_{coll} = 2.5× AMPLIFIER SPACING

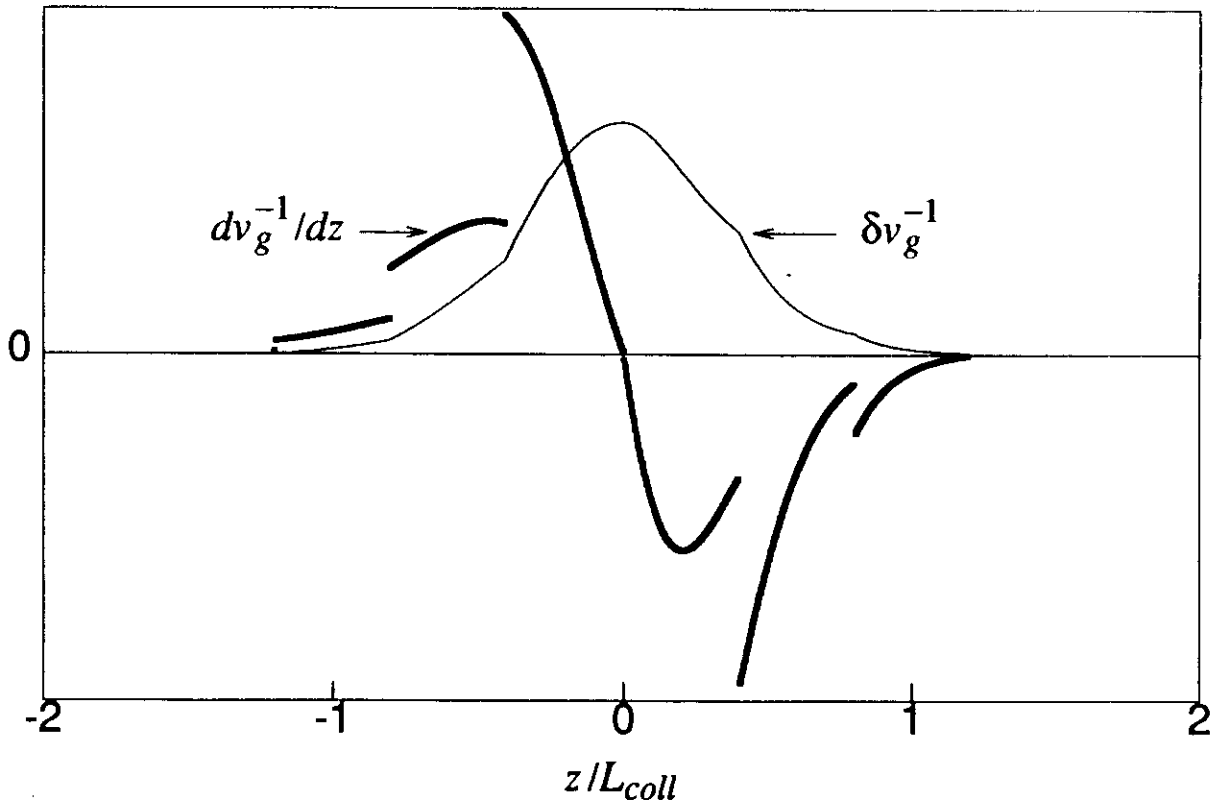

Four-Wave Mixing in Soliton-Soliton Collisions

Collisions between solitons at optical frequencies ω_1 and ω_2 produce the following four-wave mixing processes:

$$2\omega_1 - \omega_2 \rightarrow \omega_S$$

$$2\omega_2 - \omega_1 \rightarrow \omega_A$$

$$\omega_1 + \omega_2 - \omega_S \rightarrow \omega_A$$

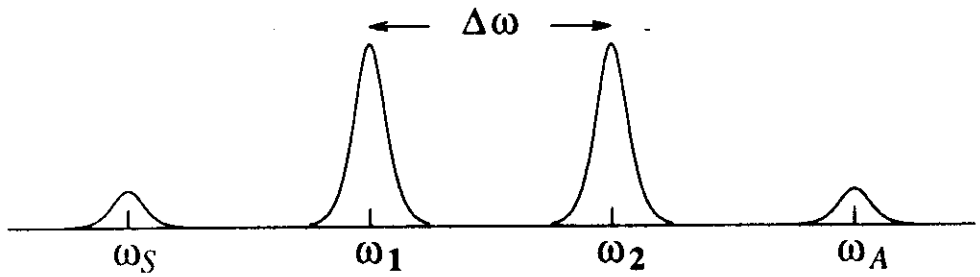

Note that the first two of the above processes are dominant, since three of the fields involved there are initially non-zero. For these processes the phase mismatch is

$$\Delta k = (k_2 + k_s - 2k_1 \text{ or } k_1 + k_a - 2k_2)$$

$$= \frac{\partial^2 k}{\partial \omega^2}\Delta\omega^2 = -\frac{\lambda^2 D}{2\pi c}\Delta\omega^2$$

GROWTH OF FWM ENERGY DURING A SOLITON-SOLITON COLLISION

0.6 nm channel spacing, D = 0.5 ps/nm/km, 20 ps solitons.

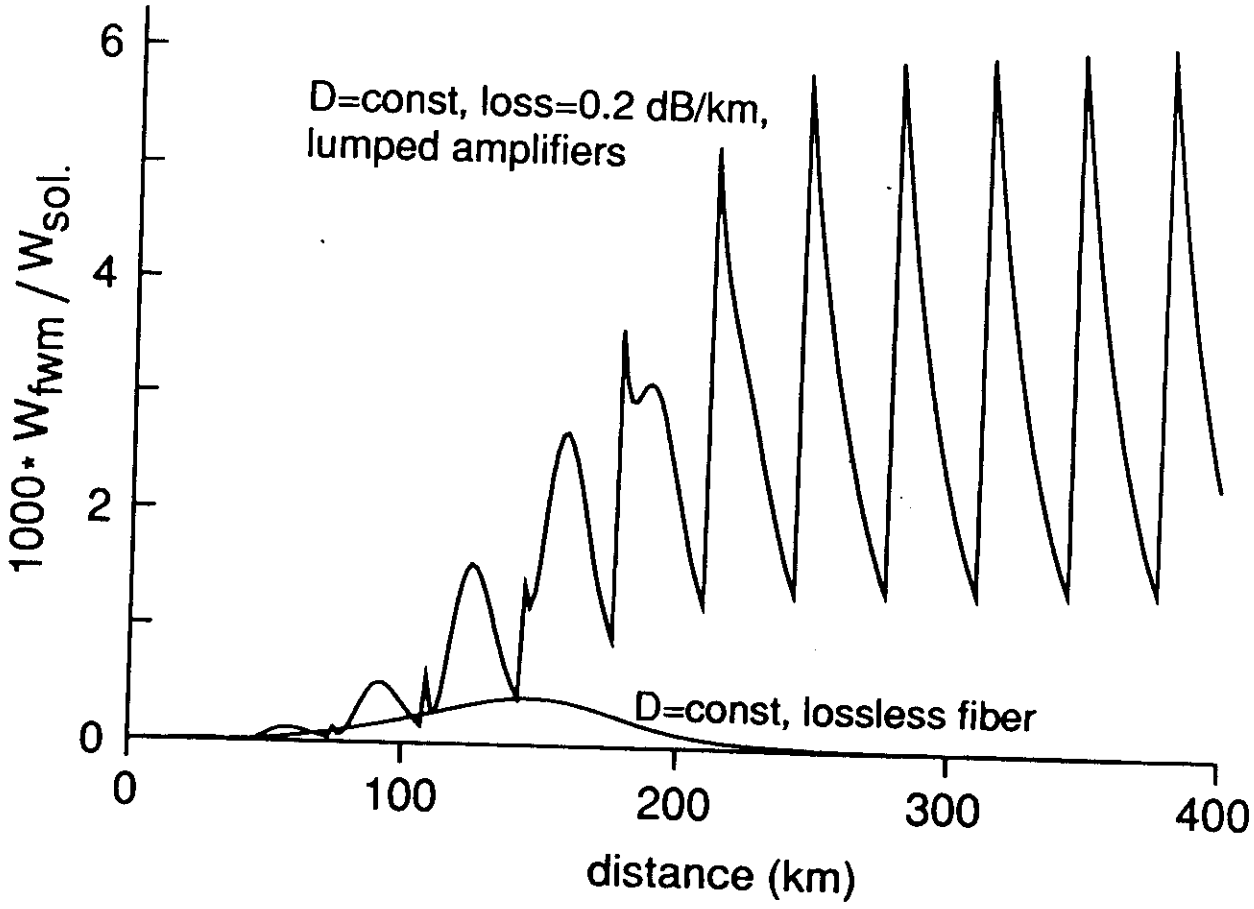

AMPLITUDE AND TIMING JITTER INDUCED BY PSEUDO-PHASE-MATCHED FWM IN A TWO-CHANNEL SOLITON WDM TRANSMISSION

Stokes channel; Z=10 Mm; channel spacing 0.6 nm; Z_{amp}=33.3 km, D=const.=0.5 psec/nm/km

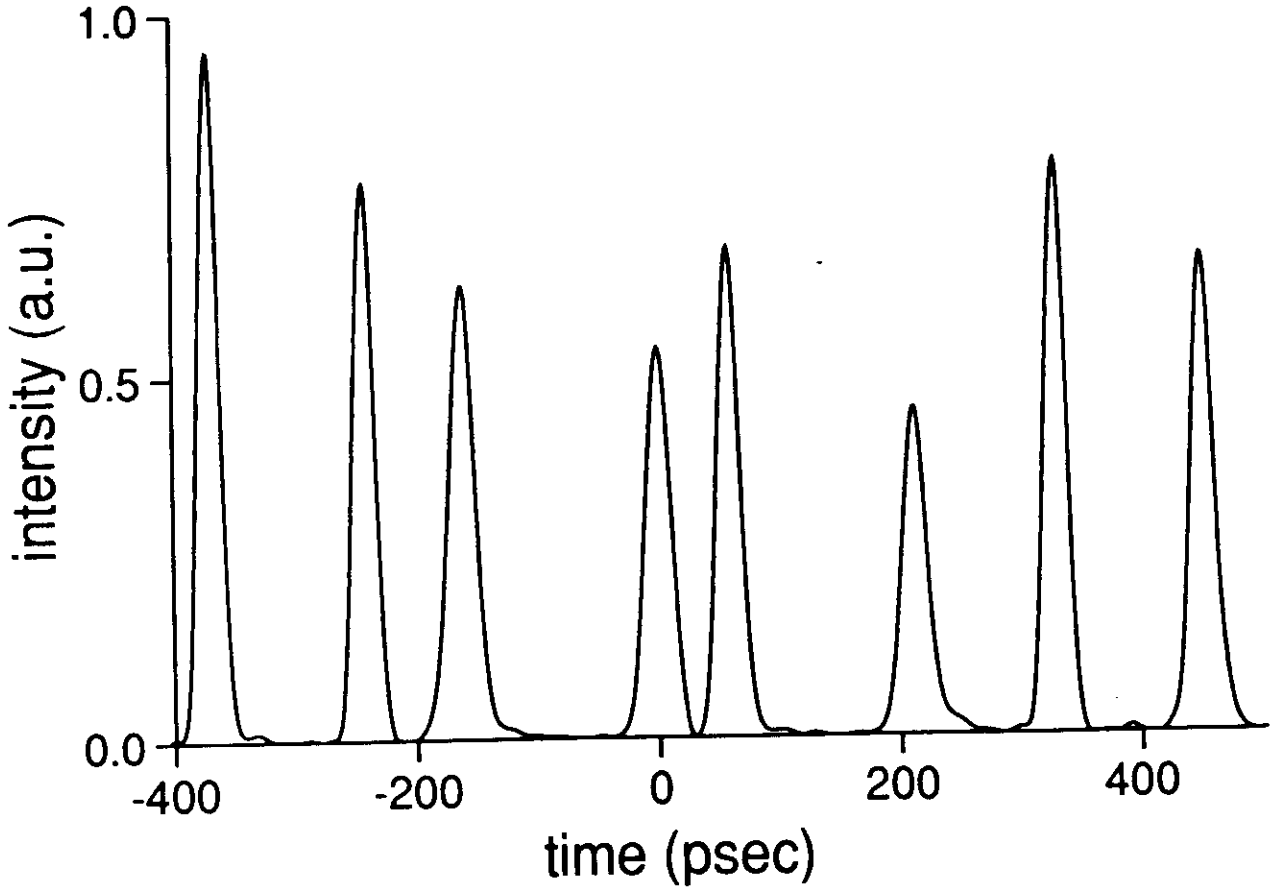

DISPERSION-TAPERED FIBER SPANS

Let D(z) in each fiber span decay exactly as the intensity:

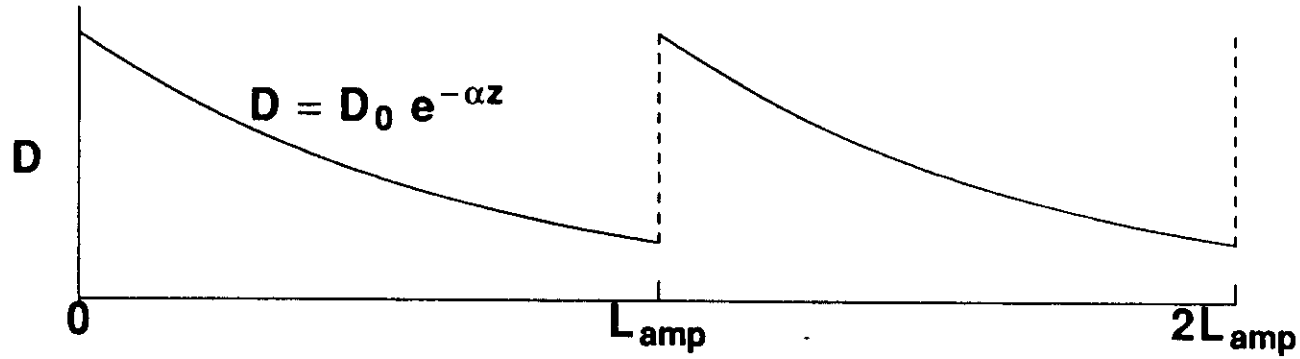

Behaves just like lossless, constant-D fiber.

So, all perturbations stemming from the use of lumped amplifiers disappear.
In particular, for WDM:

- Pseudo phase matching of Four Wave Mixing disappears.
- The symmetry of XPM in soliton soliton collisions is restored.
  Thus, the requirement $L_{coll} > 2L_{amp}$ is lifted,
  so no longer have limit on maximum channel spacing.

Recirculating Loop

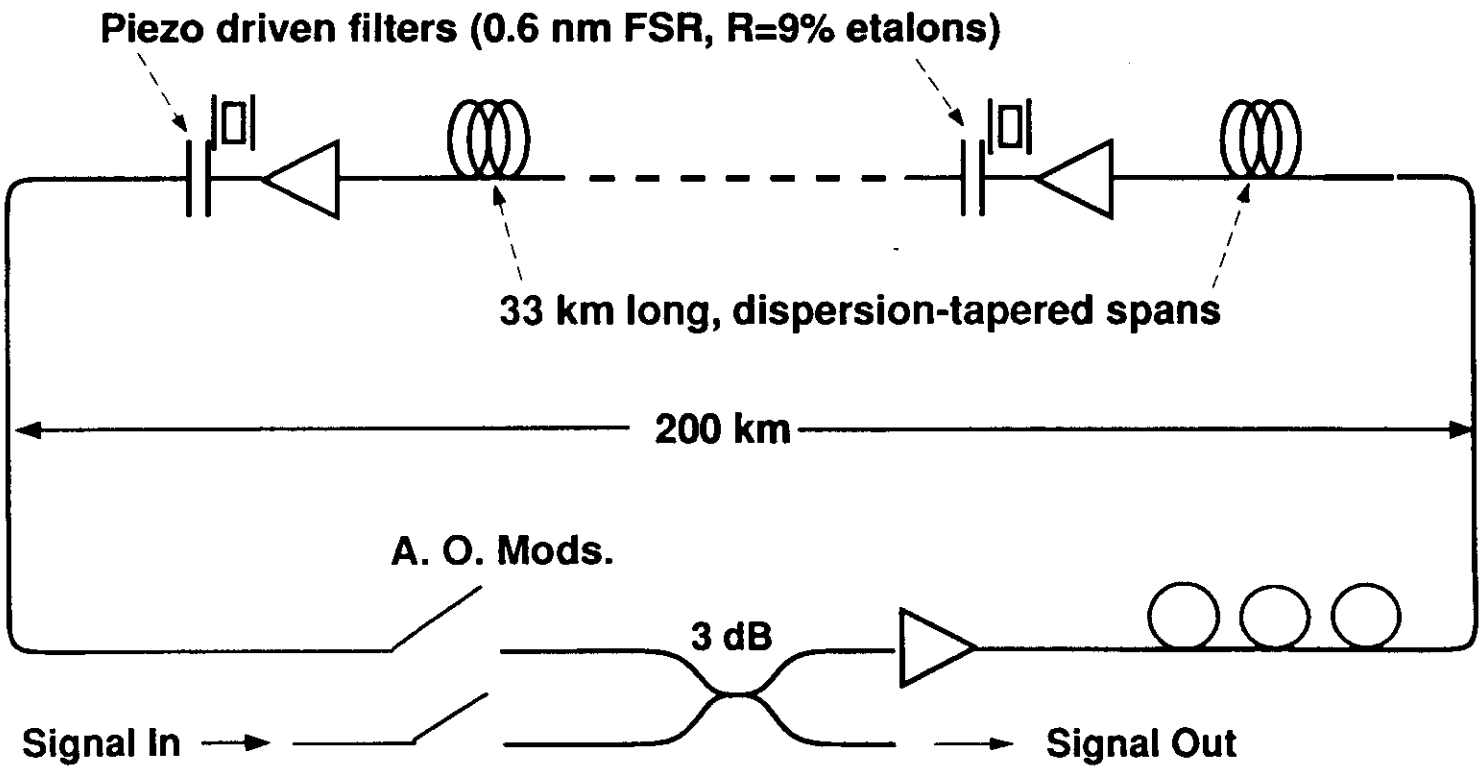

BEST 3-STEP APPROXIMATION TO THE IDEAL EXPONENTIAL TAPER OF D

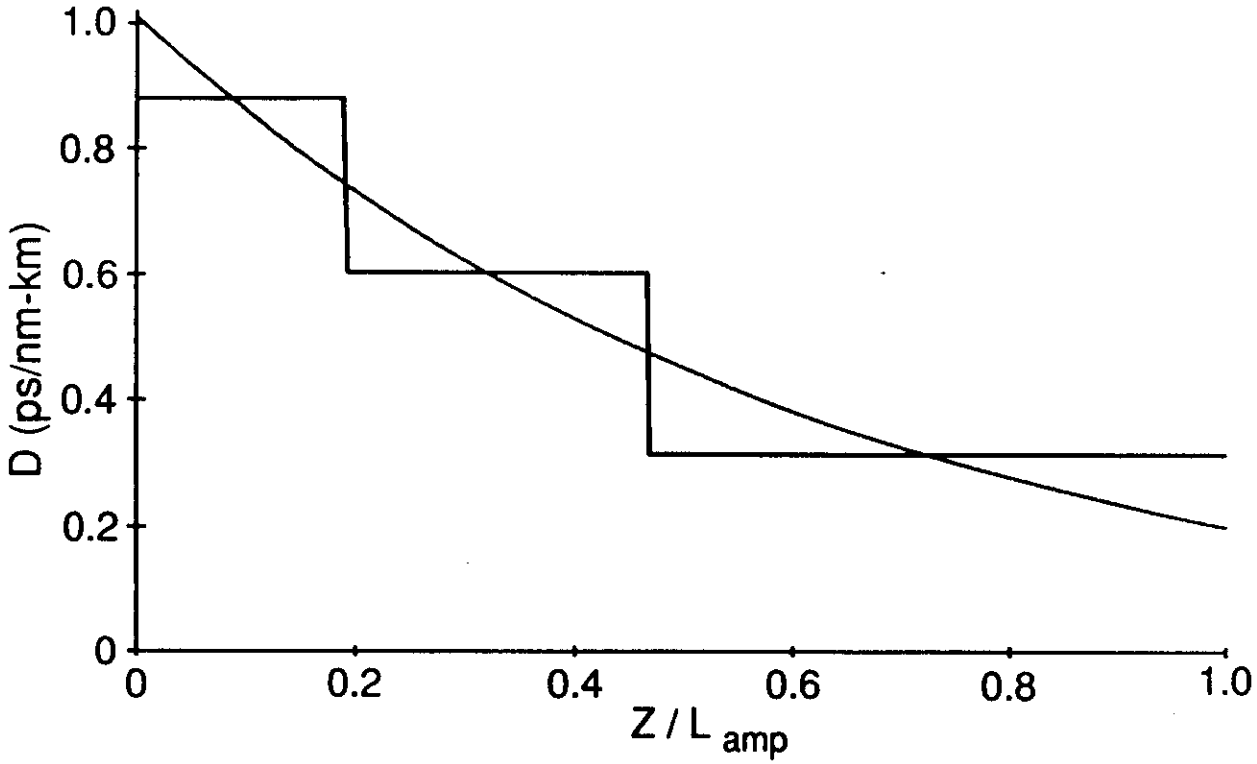

RESIDUAL FWM ENERGY PER SOLITON COLLISION VS AMPLIFIER SPACING

Constant D and 2, 3 and 4-step approximation
to ideal exponential taper of D

0.6 nm channel spacing, $D_{av.}$= 0.5 ps/nm/km, 20 ps solitons.

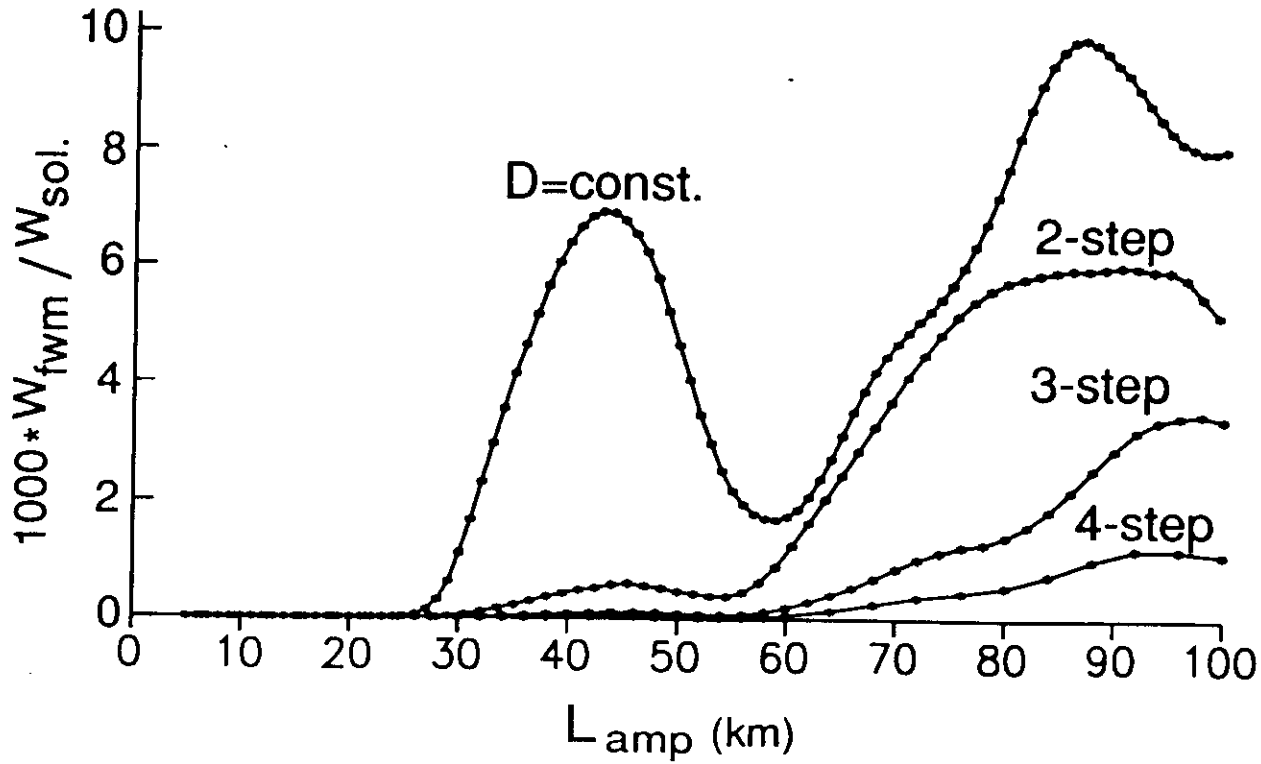

SOURCE FOR
N x 10 Gbit/s SOLITON WDM TRANSMISSION

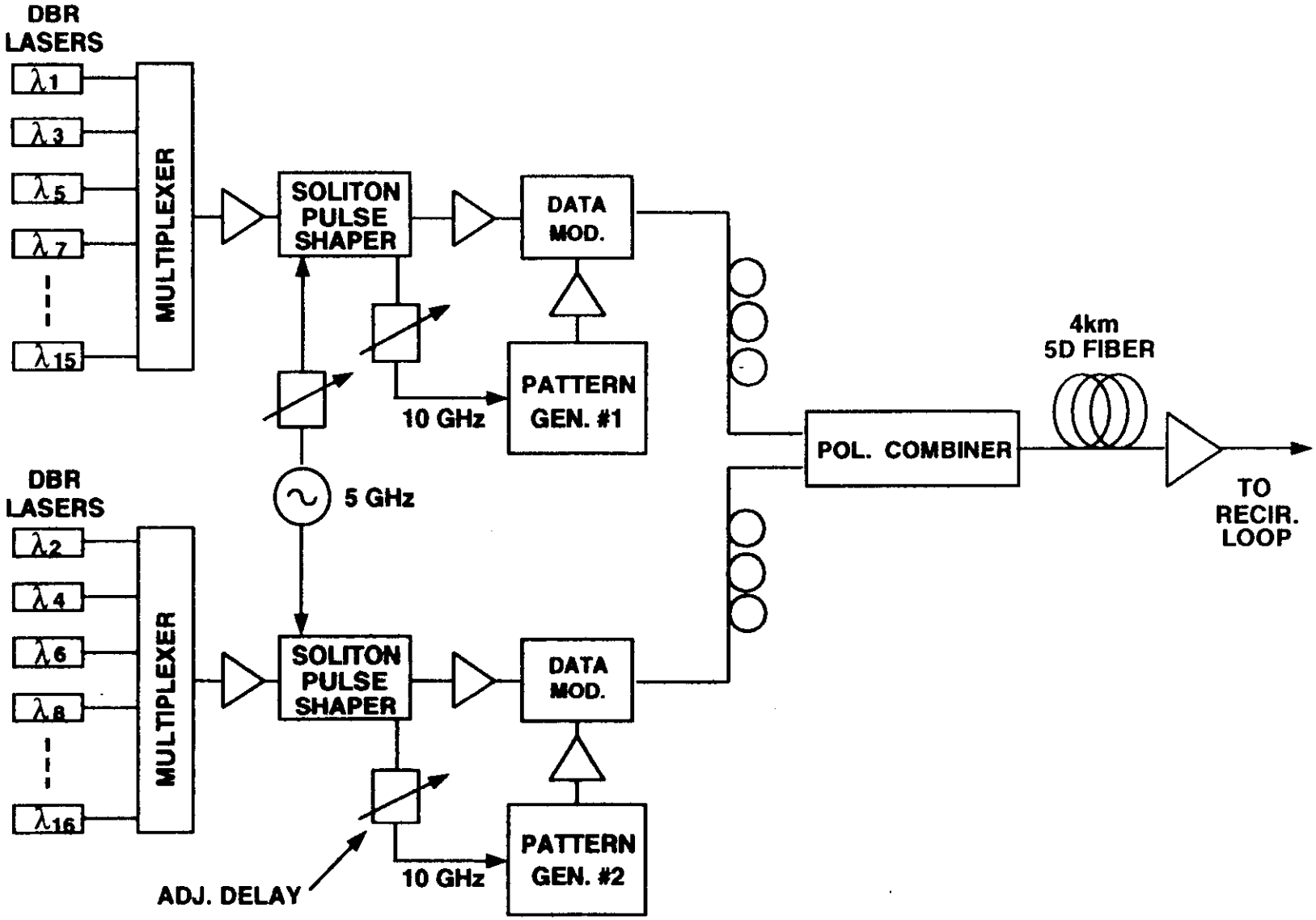

Error-free distances in soliton WDM at N X 10 Gbit/s.

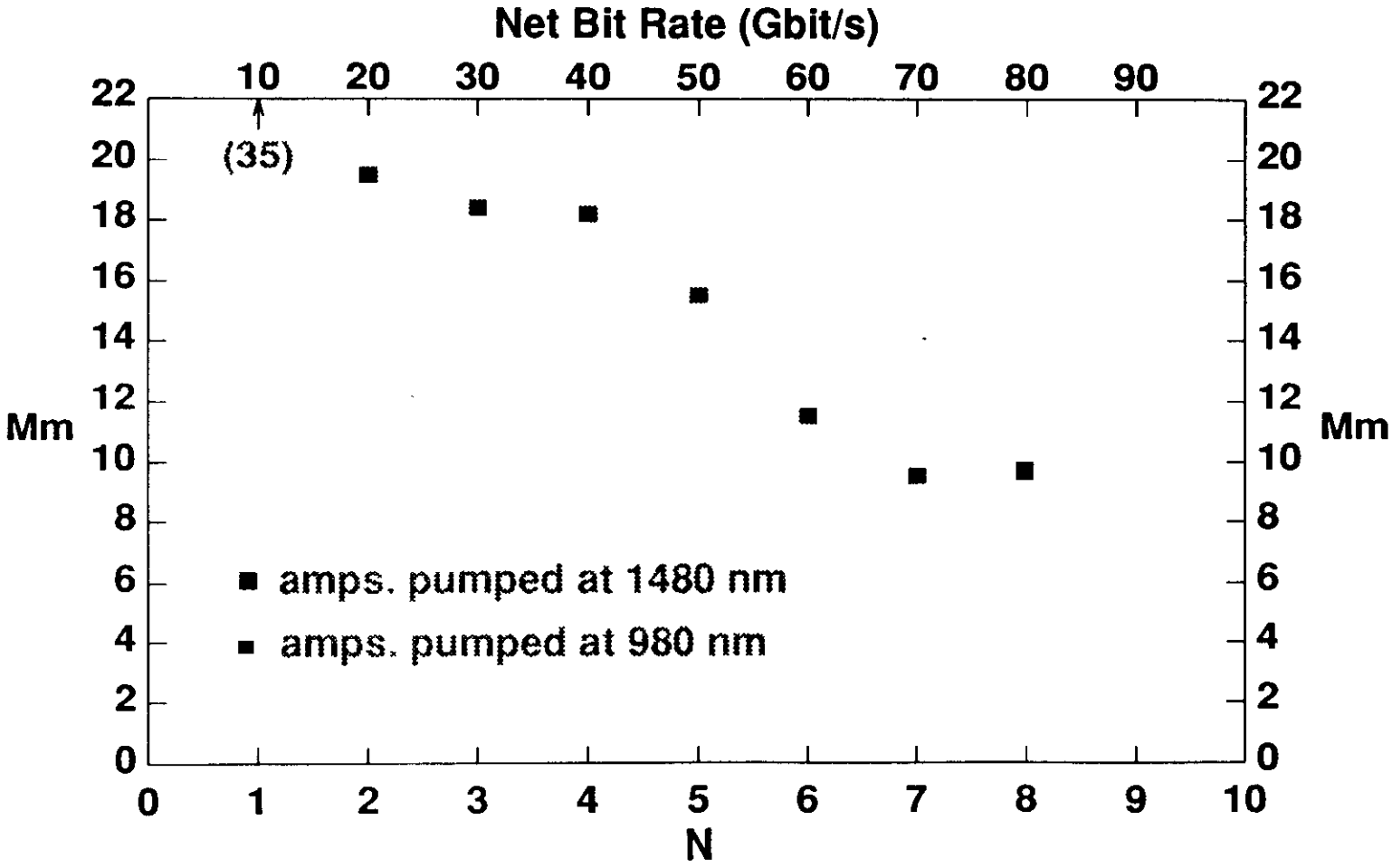

FILTERING CAN DAMPEN OUT THE TIME DISPLACEMENTS OF SOLITON-SOLITON COLLISIONS

Without filtering, colliding solitons accelerate each other by $a_0(z)$, whose first integral is $v_0(z)$, and whose second integral is $t_0(z)$. We require only that:

$$v_0(\infty) = \int_{-\infty}^{\infty} a_0(z)\,dz = 0 \tag{1}$$

That is, the completed collision must leave no residual velocity shift. Filters provide a damping, i.e., an accel. towards $v=0$. When the filter response function is parabolic, $a_d = -\gamma v$, where γ is the damping constant. Eqn. of motion then becomes:

$$\frac{dv}{dz} = a_0(z) - \gamma v(z) \tag{2}$$

Eq. (2) can be rewritten as:

$$v(z) = \frac{1}{\gamma}\left[a_0(z) - \frac{dv}{dz}\right] \tag{2a}$$

To get t, we simply integrate Eq. (2a):

$$t(z) = \int_{-\infty}^{z} v(x)\,dx = \frac{1}{\gamma}\int_{-\infty}^{z}\left[a_0(x) - \frac{dv}{dx}\right]dx \tag{3}$$

We are primarily interested in $t(\infty)$:

$$t(\infty) = \frac{1}{\gamma}\int_{-\infty}^{\infty} a_0(x)\,dx - \frac{1}{\gamma}\int_{-\infty}^{\infty} dv \tag{3a}$$

The first term on the right = 0 by virtue of Eq. (1). The second term is just $v(\infty)$, which for a filtered system with no excitation beyond a certain point, must = 0.

Velocity and time shifts caused by soliton-soliton collision in fiber with lumped amps and with Parabolic filters Filters lumped at each amplifier.

$D = 0.5$ ps/nm-km; $\tau = 20$ ps; $\Delta\lambda = 0.6$ nm ($\Omega = 2.6729$);
$L_{coll} = 133$ km; $L_{amp} = 33.3$ km; Δ=400 km.

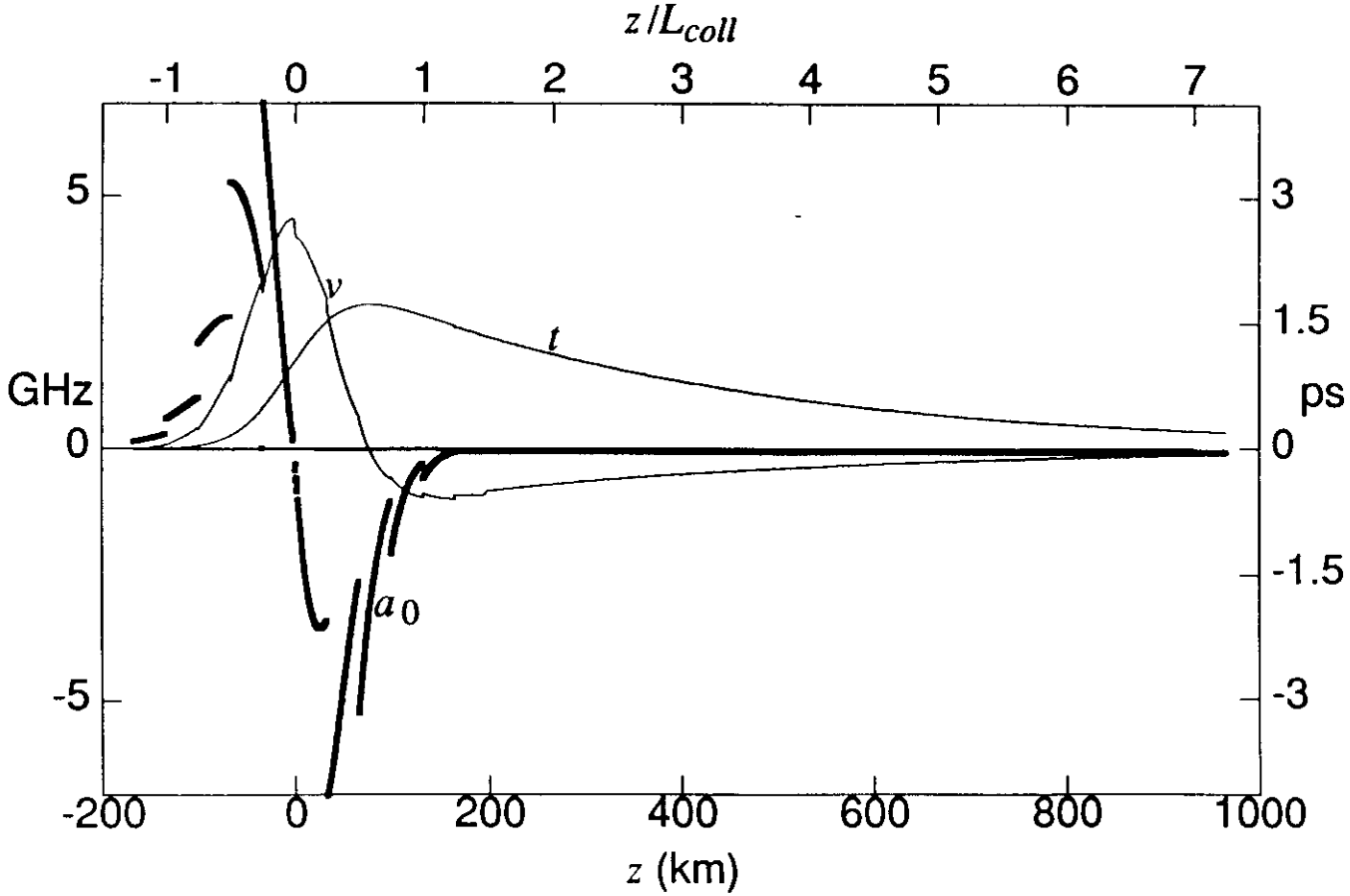

WDM CHANNEL STRENGTHS VS DISTANCE WITH AND WITHOUT FILTERS

THREE CHANNELS WITH RELATIVE GAINS OF +1, 0, AND -1 dB/Mm.

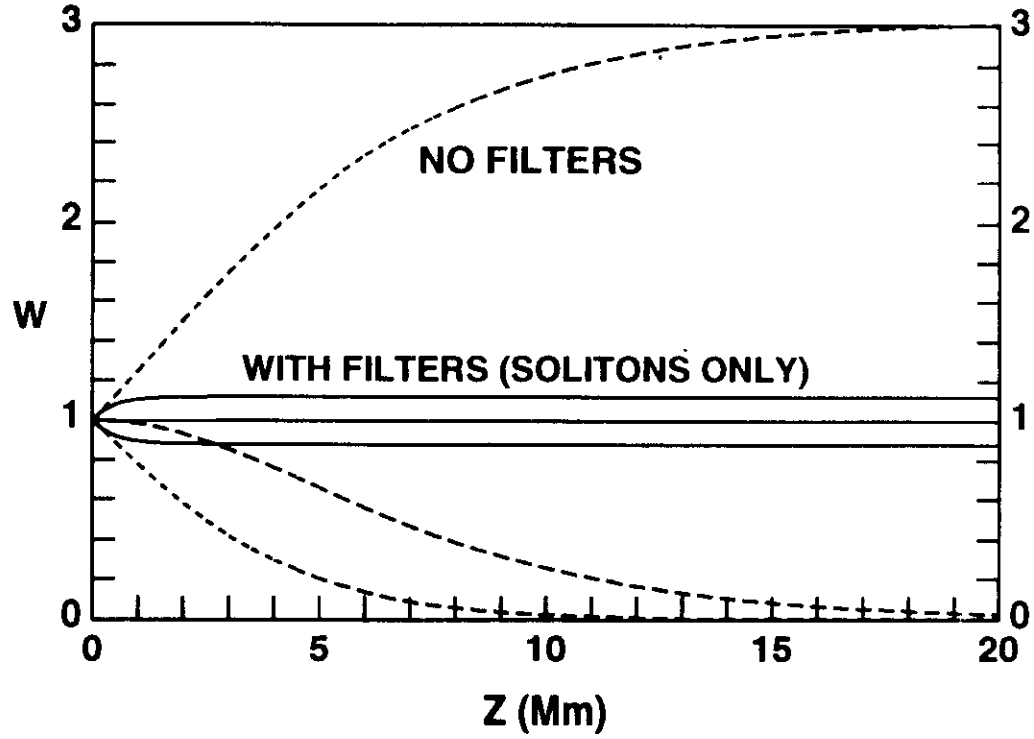

FILTERS PROVIDE AUTOMATIC GAIN LEVELING AMONG THE CHANNELS.

OPTICAL SPECTRUM AT 10 Mm OF 9-CHANNEL WDM TRANSMISSION

FILTERS PROVIDE STRONG REGULATION OF SOLITON ENERGIES.

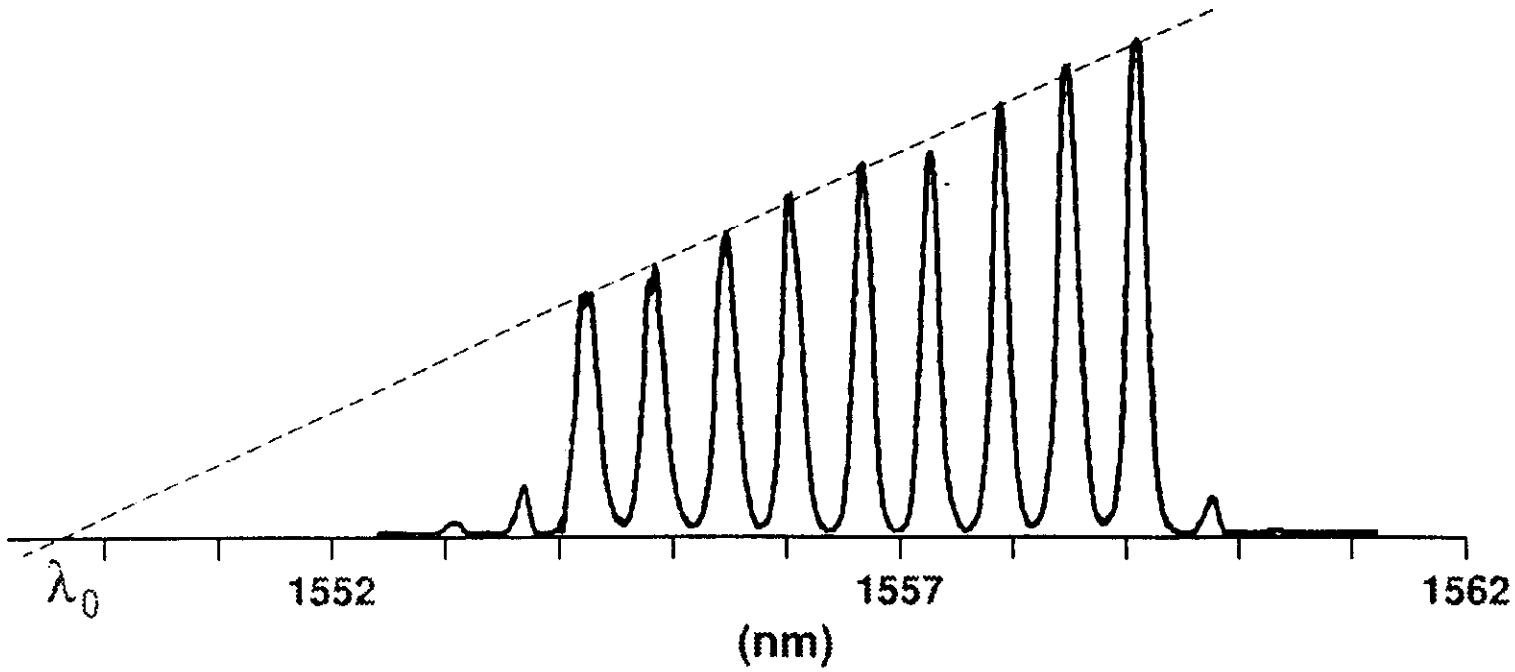

PEAK SPECTRAL DENSITIES ARE IN DIRECT PROPORTION TO D.

GUIDING FILTER STRENGTH PARAMETER η

- For good stability range, must maintain $\eta \approx 0.4$ (Stability range $\rightarrow$ 0 for $\eta \geq 0.8$.)

- But, for shallow etalons, $\eta \propto R/D$.

- Thus, to compensate for D-slope, must make etalons with compensating variation in $R(\lambda)$.

TRANSMISSION OF VARIABLE-R ETALON FILTER MADE FROM BRAGG GRATING MIRRORS IN FIBER. YIELDS NEARLY CONSTANT FILTER STRENGTH IN THE FACE OF DISPERSION SLOPE OF 0.07 ps/nm^2-km.

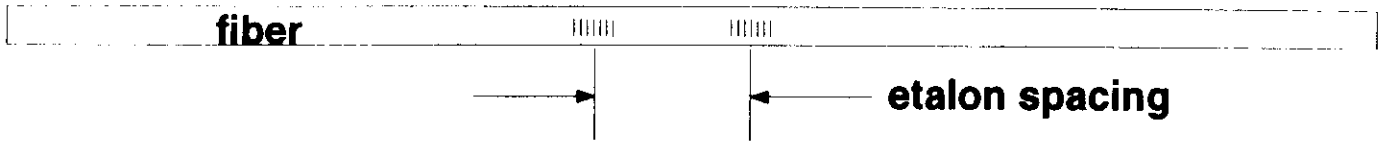

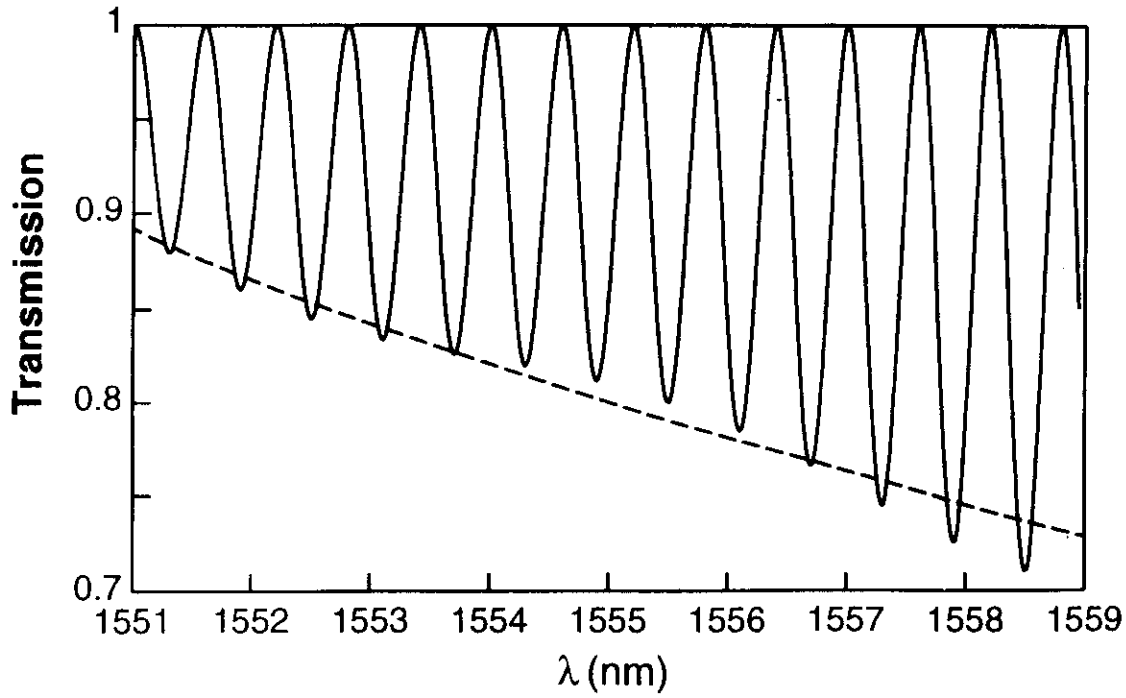

MEASURED STRENGTH (BW^{-2}) OF GRATING-IN-FIBER ETALON FILTER AS A FUNCTION OF WAVELENGTH

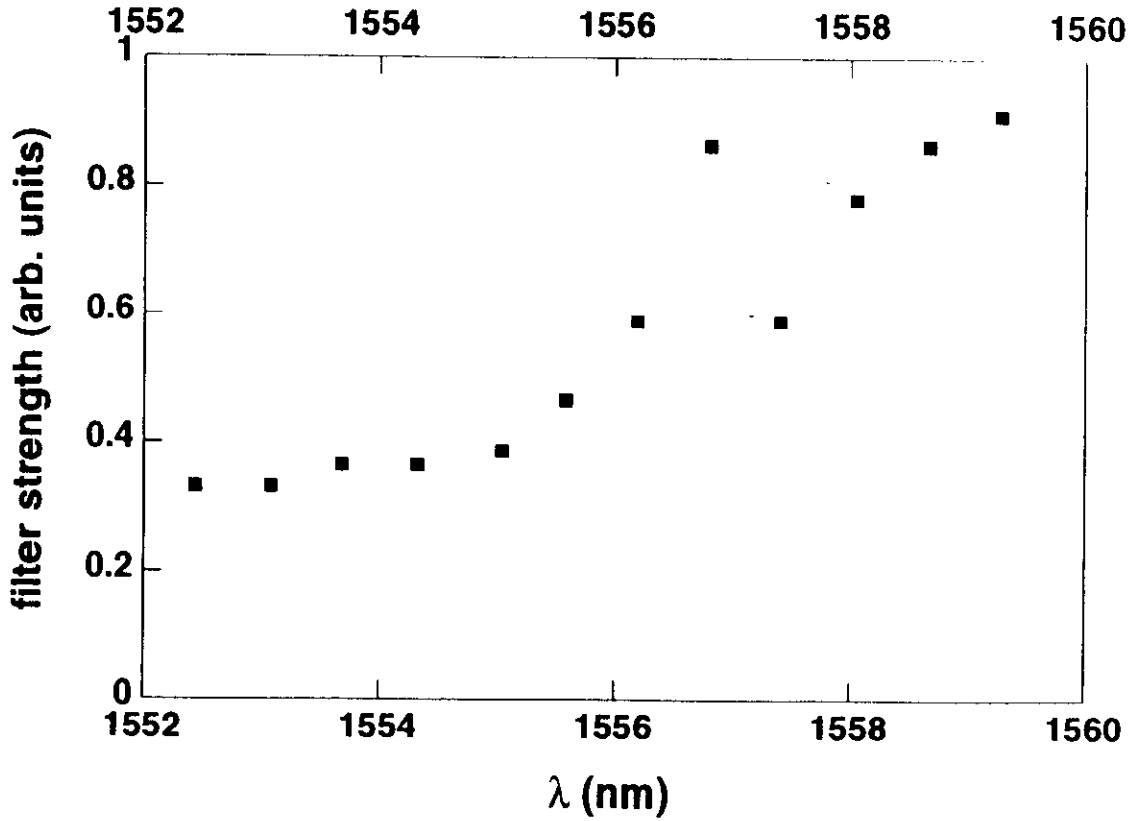

PATH OF 4-WAVE MIXING VECTOR IN THE COMPLEX PLANE

FUNDAMENTAL RESONANCE ($\int_{\text{D-map}} \delta k \, dz = 2\pi$)

(CHANNEL SPACING ≅ 0.63 nm)

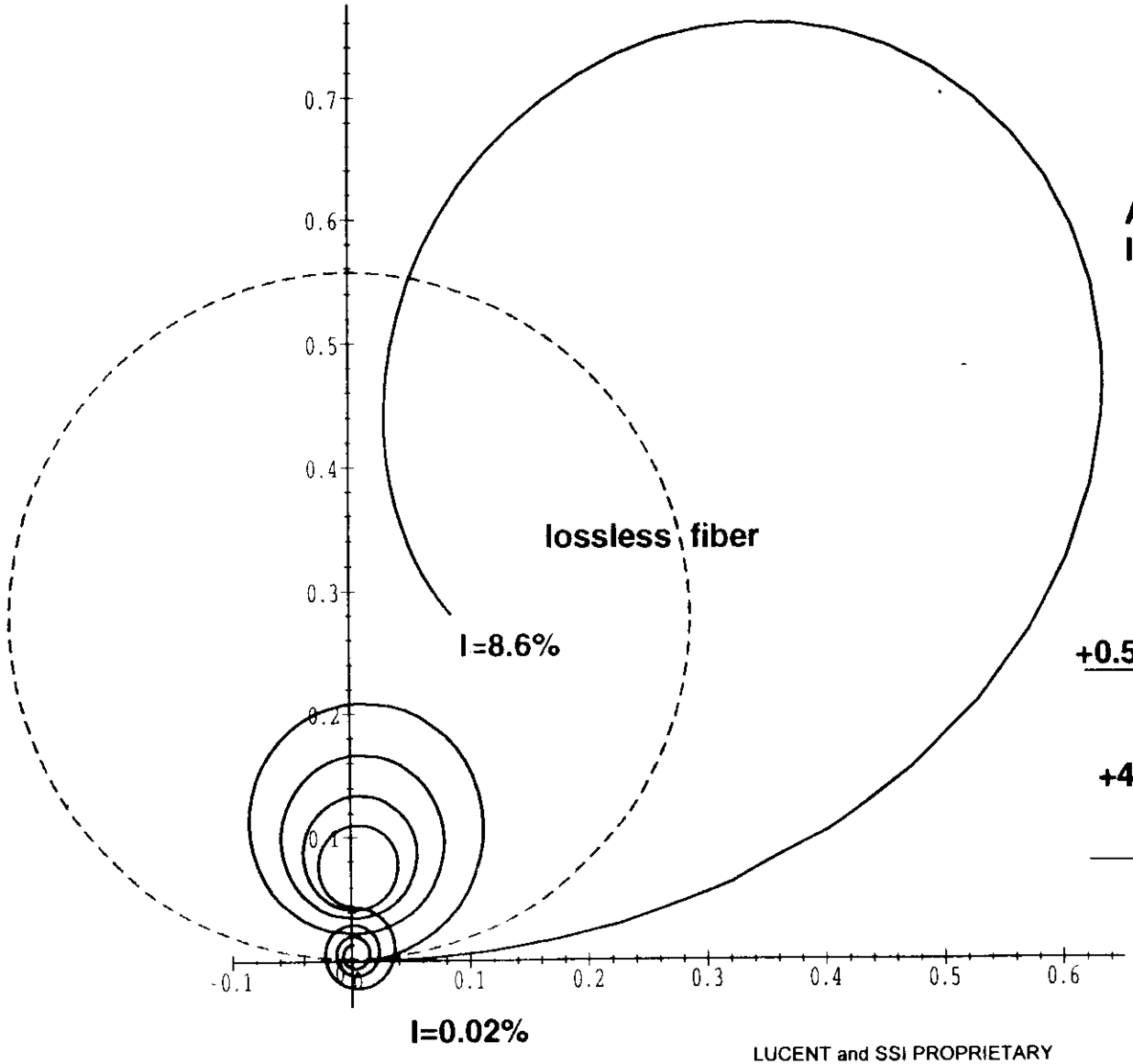

All final intensities normalized to I=1 for the phase-matched case.

D-maps (D in ps/nm-km):

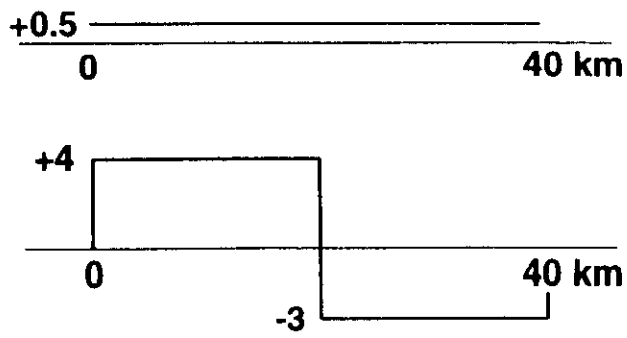

DISPERSION MANAGED SOLITONS IN A NUTSHELL

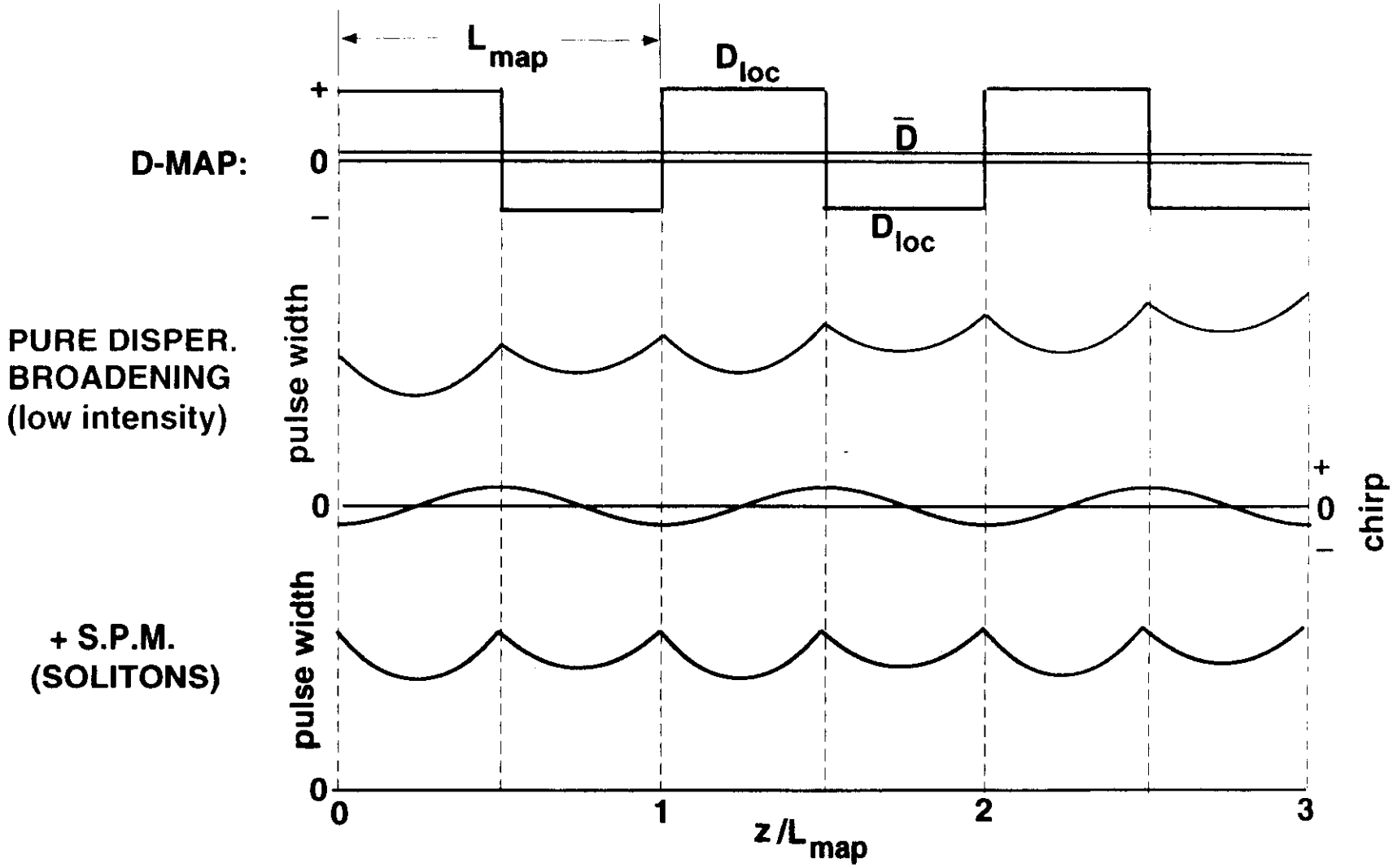

Path-av. SPM and $\bar{D}$ cancel each other's effects exactly over each L_{map}.

Pulse shape, however, is largely determined by D_{loc} (the dominant term).
Thus, pulse shape is essentially Gaussian.

COLLIDING SOLITONS:
RELATIVE MOTION IN RETARDED TIME

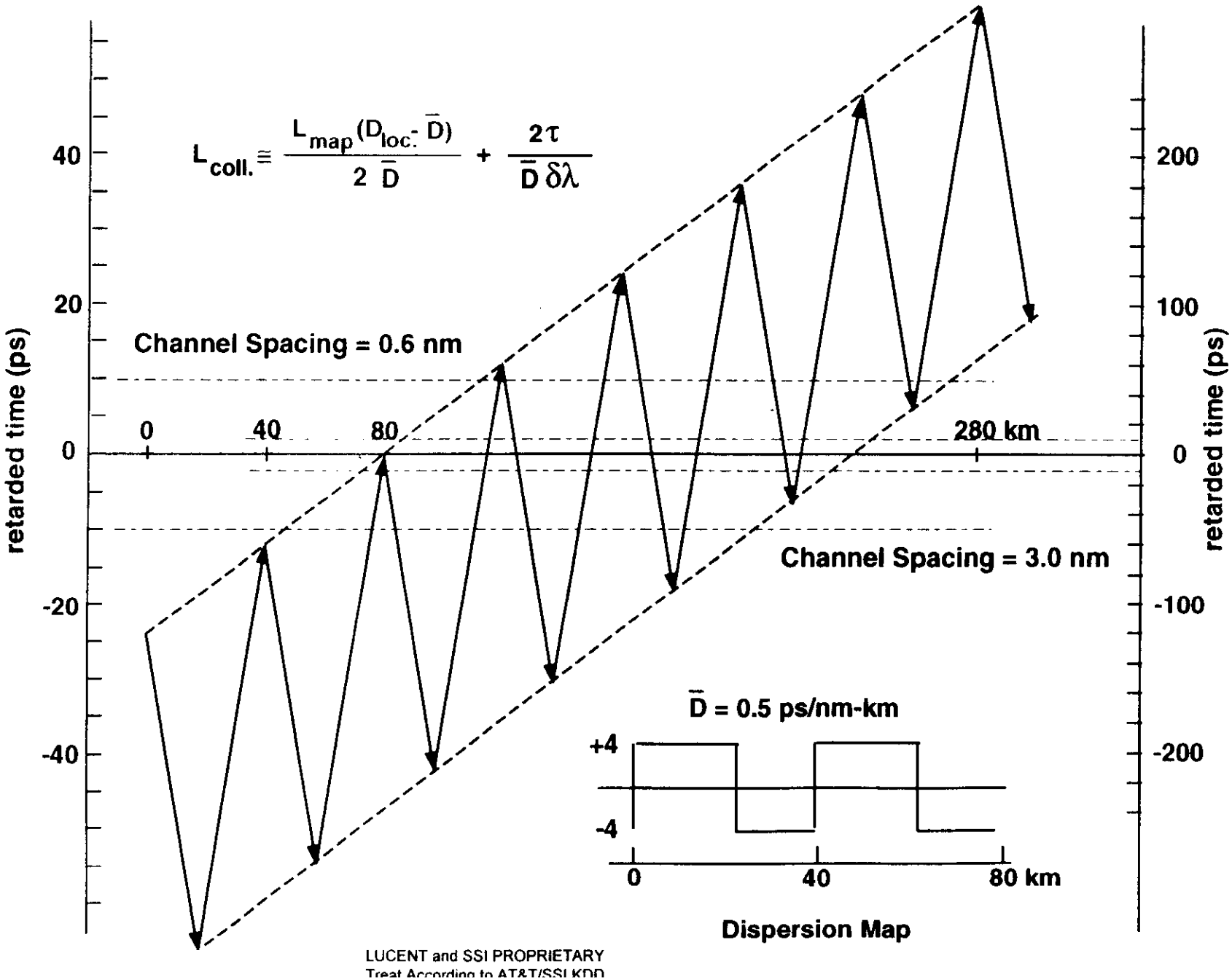

SOLITON - SOLITON COLLISION LENGTH VS. CHANNEL SEPARATION

τ = 20 ps; L_{map} = 40 km ; $\overline{D}$ = 0.5 ps/nm-km

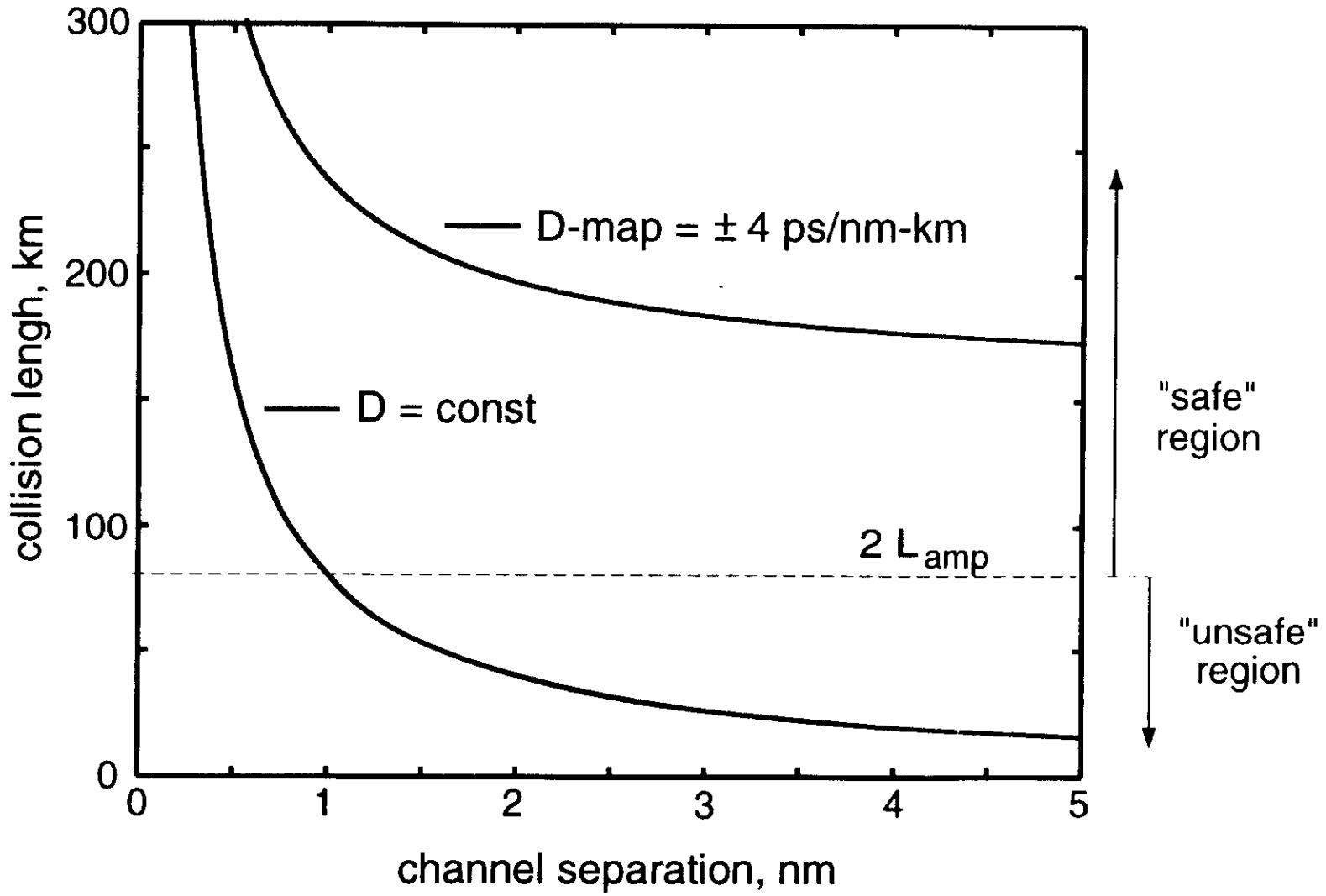

INSTANTANEOUS FREQUENCY SHIFTS OF COLLIDING SOLITONS

CHANNELS SEPARATED BY 75 GHz (0.6 nm)

$L_{map} = L_{amp} = 40$ km; $\bar{D} = 0.5$ ps/nm-km

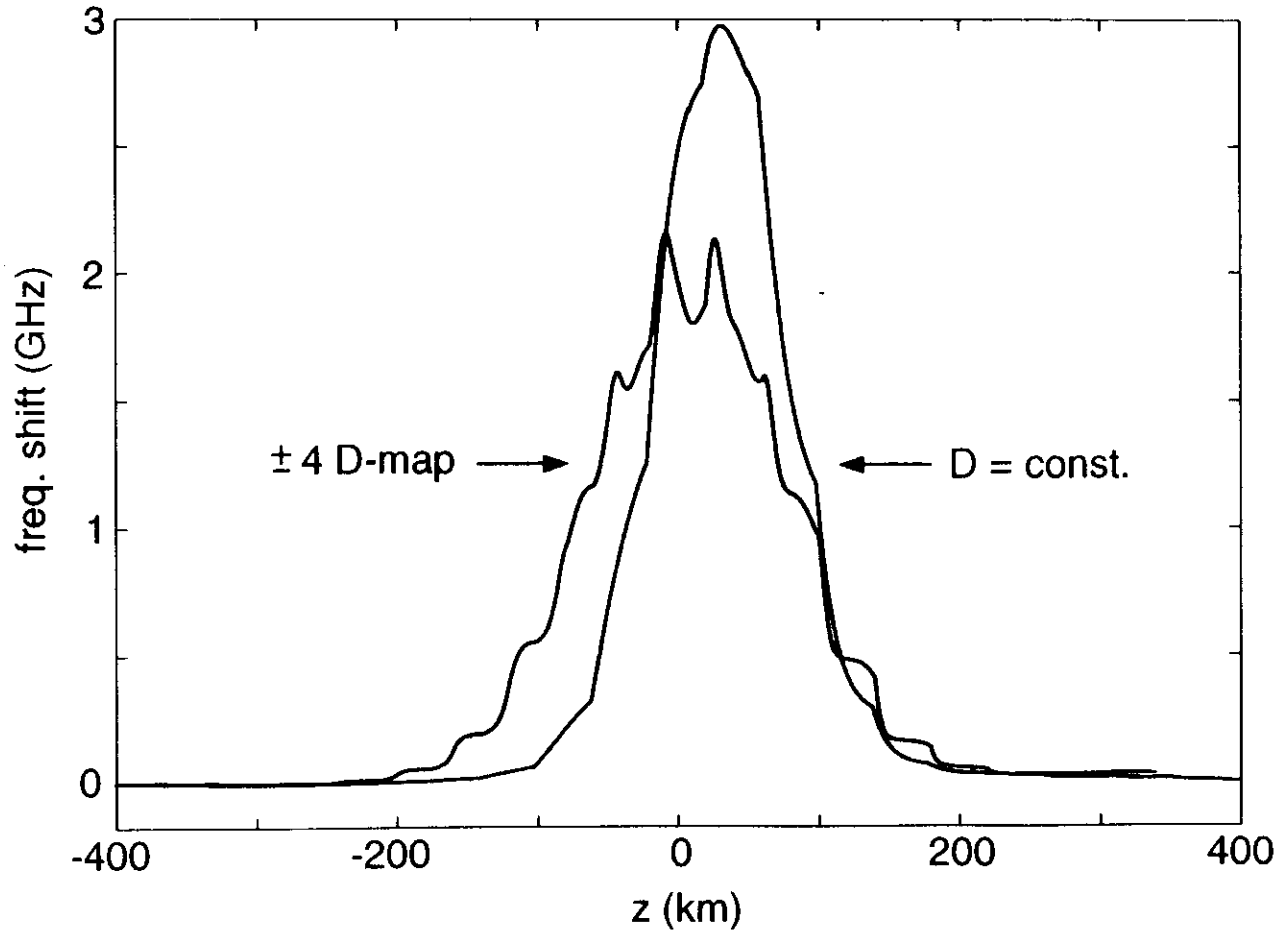

INSTANTANEOUS FREQUENCY SHIFTS OF COLLIDING SOLITONS

$L_{map} = L_{amp} = 40$ km; $\bar{D} = 0.5$ ps/nm-km

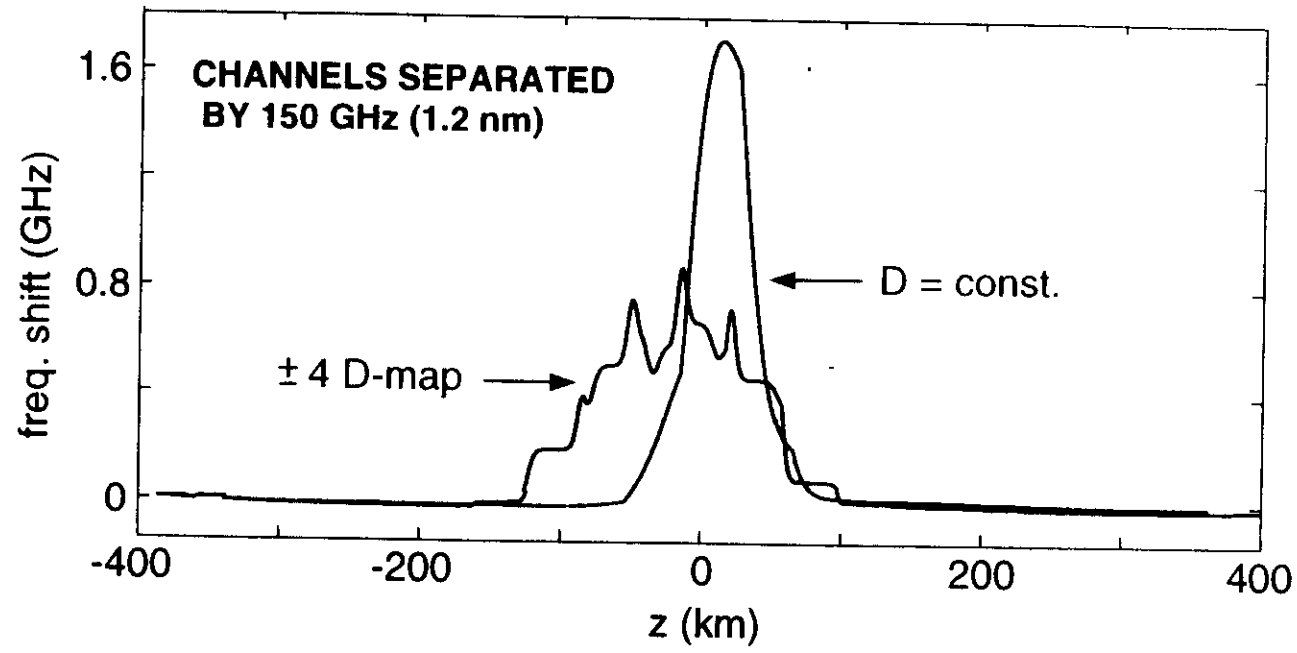

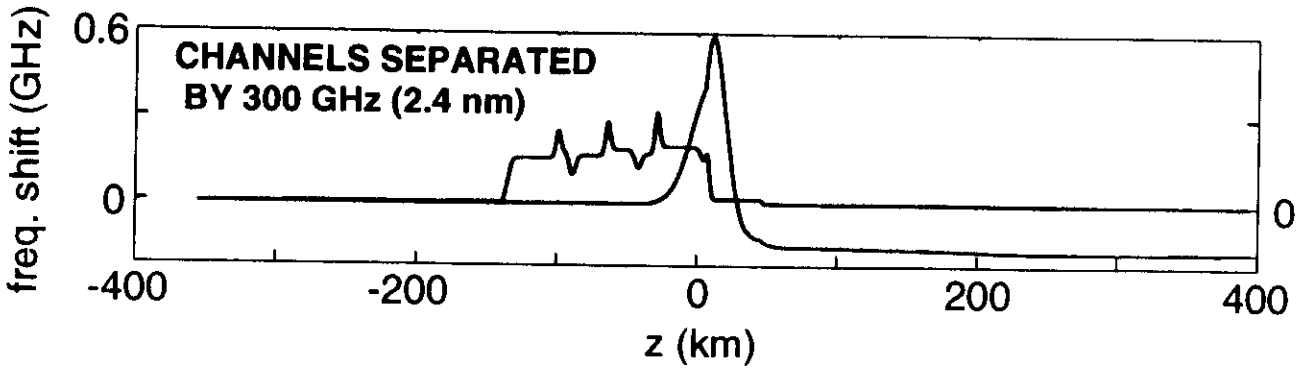

"±4" D-MAP: FEATURES AND REQUIREMENTS

"Ideal" map:

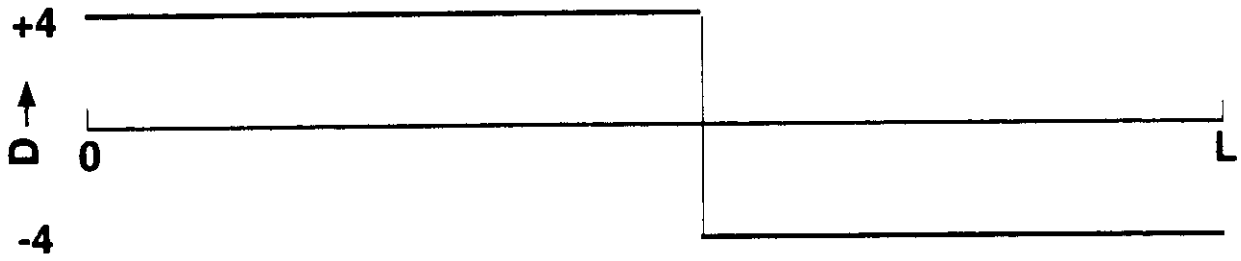

Real map:

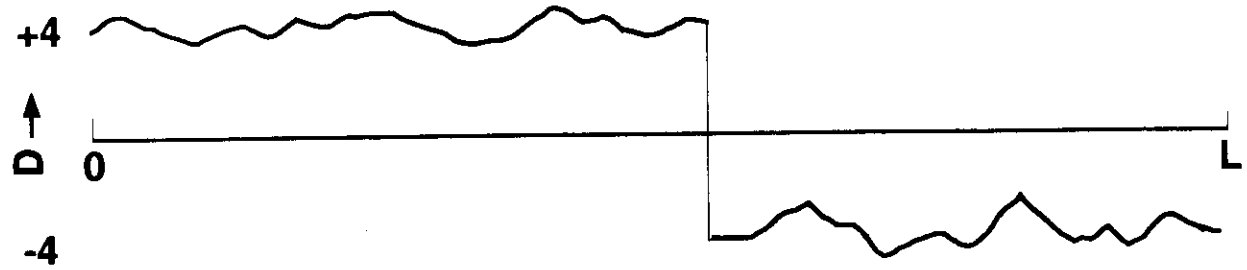

Variation of ~±1 ps/nm-km within each segment is not important.

Only $\bar{D} = (1/L) \int_0^L D(z)\, dz$ needs to be accurate.

OTDR-LIKE TECHNIQUE FOR MEASURING D-MAPS

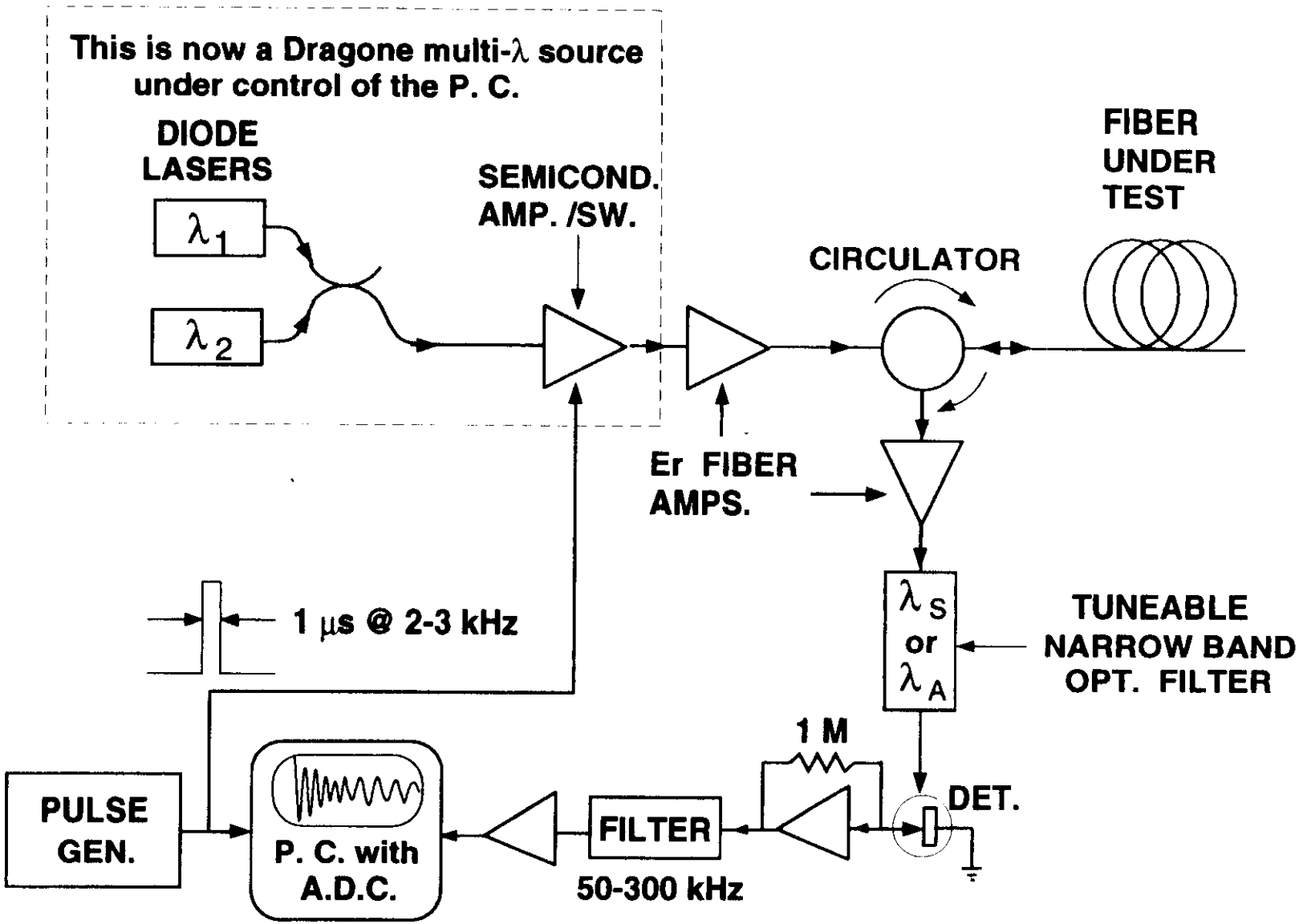

(A.D.C. = analog-to-digital converter)

OTDR-LIKE METHOD FOR D-MAP MEASUREMENT

- **Principal features:**
  - **Requires access to only one end of the fiber span.**
  - **Fast: Produces accurate D-map and its integral in seconds.**
  - **Long range: Measures spans of up to 50 km without gain; with Raman gain, should extend to 80 km.**
  - **Accurate: Measures D to within <0.05 ps/nm-km and with spatial resolution of 1 km or better.**
- **Major uses:**
  - **To characterize installed fiber spans in the field.**
  - **To create spans with precisely controlled path-average D.**